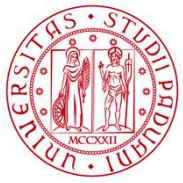

UNIVERSITÀ
DEGLI STUDI
DI PADOVA

Head Office: Università degli Studi di Padova

Department of Cardiac, Thoracic and Vascular Sciences and Public Health

Ph.D. Course in: Translational Specialistic Medicine "G. B. Morgagni"

Curriculum: Cardiothoracic and Vascular Sciences

Series XXXI

TOWARDS AN INCREASED BIOCOMPATIBILITY IN TOTAL HEART REPLACEMENTS:

A NEW HYBRID MEMBRANE FOR ARTIFICIAL BLOOD PUMPS AND THE WHOLE BIOENGINEERED HEART

Coordinator: Ch.mo Prof. Annalisa Angelini

Supervisor: Ch.mo Prof. Gino Gerosa

Ph.D. student: Eleonora Dal Sasso

A Michele Bellucci, dal cuore invincibile.

"Does there not exist a high ridge
where the mountainside of 'scientific' knowledge
joins the opposite slope of 'artistic' imagination?"

Vladimir Nabokov

Abstract

The only definitive treatment currently used for end-stage heart failure (HF) is cardiac transplantation. However, the procedure is limited by organ shortage and the side-effects of life-long immunosuppression. The need for new therapeutic strategies paved the way for the development of mechanical circulatory supports (*e.g.*, total artificial hearts, TAHs) and the whole bioengineered heart. Although the two approaches may appear to be in conflict, TAHs are intended for short- to middle-term applications and can be developed and clinically applied relatively faster; the bioengineered heart approaches a definitive solution but, although current results are promising, a full organ equivalent has not yet been achieved.

The creation of a novel TAH internal lining and the generation of a decellularized matrix for total heart bioengineering were the aim of this doctoral thesis, in order to improve the common goal of biocompatibility in formulating whole heart replacements.

The TAH approach was investigated by coupling a TriCol-decellularized bovine pericardial scaffold (DBP) with a medical-grade polycarbonate urethane. This combination gave rise to a hybrid membrane (HM) capable of overcoming materials' reciprocal limitations. The DBP was assessed by histology, two-photon microscopy (TPM)-combined immunofluorescence and TPM-mediated morphometric quantifications. Following HM assembly, surface analyses showed that the polymer penetrated the DBP scaffold. *In vitro* cytocompatibility was performed according to ISO 10993-5 with human umbilical vein endothelial cells (HUVECs) and human bone marrow-derived mesenchymal stem cells (hBM-MSCs). All tests confirmed unaltered morphology, proliferation, viability, and absence of cytotoxicity. No activation of the complement system, part of ISO 10993-4, was reported for HM.

The poor endothelialization and occurrence of thromboembolism in TAH may be prevented by accelerating endothelial adhesion through immobilization of short synthetic peptides. TriCol DBP scaffolds were selectively and covalently linked by Arg-Glu-Asp-Val (REDV) and rhodamine-conjugated REDV (RhodREDV) at different concentrations. After functionalization, the amount of bound RhodREDV was quantified with a TPM. The bioactivity of REDV was evaluated by *in vitro* static seeding of HUVECs. Live/dead staining and MTS reduction quantification demonstrated improved early adhesion, viability and proliferation of HUVECs on 10^{-5} M REDV-functionalized DBP at 24 hours. The LDH assay reported negligible levels of cytotoxicity. Histological evaluations revealed a near-continuous type of cell lining.

The first step towards whole heart bioengineering was performed by developing a preservative decellularization protocol for cardiac organs. Rat hearts were decellularized by a combination of myorelaxant, protease inhibitors, sodium dodecyl sulfate (SDS) and Triton X-100. All solutions were administered by retrograde coronary perfusion. The effectiveness of the protocol was evaluated by histology, TPM-combined immunofluorescence, DNA quantification, and proteomic analysis. Cytocompatibility was assessed according to ISO 10993-5 by static seeding of hBM-MSCs on isolated ventricles. The results confirmed unaltered morphology, maintained proliferation and the absence of cytotoxicity. Histology showed continuous monolayer of hBM-MSCs at 24 hours, whereas cell penetration was visible at days 7 and 14.

Concluding, this doctoral thesis describes the progresses towards the biocompatibility of heart replacements. A first generation of HM, based on DBP and polyurethane, was created and demonstrated its suitability for TAH internal lining. The covalent and selective functionalization of 10^{-5} M REDV peptide on DBP proved its efficacy in accelerating endothelial adhesion and promoting cell proliferation. A more preservative and cytocompatible protocol for whole heart decellularization was developed and achieved complete cell removal well-maintaining cardiac matrix.

Sommario

Il trapianto di cuore è l'unico trattamento dell'insufficienza cardiaca terminale, ma la sua applicazione è limitata dalla carenza di organi e dagli effetti collaterali delle terapie immunosoppressive. La necessità di nuove strategie terapeutiche ha portato allo sviluppo delle assistenze meccaniche ed al cuore bioingegnerizzato. Sebbene possano sembrare in contrasto, i cuori artificiali totali (TAH) sono impiantati a breve/medio termine e possono essere sviluppati ed introdotti nella clinica più rapidamente, mentre il cuore bioingegnerizzato si avvicina ad una soluzione definitiva, ma nonostante i risultati promettenti non è ancora stato prodotto un organo equivalente completo.

La creazione di un nuovo rivestimento interno per i TAH e la generazione di una matrice decellularizzata per la bioingegnerizzazione del cuore sono stati l'obiettivo di questa tesi di dottorato al fine di migliorare la biocompatibilità dei sostituti cardiaci.

Il rivestimento per i TAH è stato realizzato accoppiando pericardio bovino decellularizzato TriCol (DBP) ad un poliuretano, producendo una membrana ibrida (HM). Il DBP è stato valutato con istologie, immunofluorescenza combinata con microscopia a due fotoni (TPM) e quantificazione morfometrica. Le analisi superficiali della HM hanno mostrato la penetrazione del polimero. La citocompatibilità *in vitro* (ISO 10993-5) è stata valutata con cellule endoteliali di vena ombelicale umana (HUVEC) e mesenchimali staminali derivate da midollo osseo umano (hBM-MSC). I test hanno confermato inalterate morfologia, proliferazione, vitalità ed assenza di citotossicità. Nessuna attivazione del sistema del complemento (ISO 10993-4) è stata segnalata per HM.

La scarsa endotelizzazione ed il verificarsi di tromboembolia nei TAH possono essere prevenuti accelerando l'adesione endoteliale con brevi peptidi sintetici. Gli scaffold TriCol DBP sono stati selettivamente e covalentemente legati ad Arg-Glu-Asp-Val (REDV) e REDV coniugato con rodamina (RhodREDV). Dopo la funzionalizzazione, la quantità di RhodREDV legato è stata quantificata con il TPM. La bioattività di REDV è stata valutata mediante semina statica di HUVEC *in vitro*. Il live/dead staining e la quantificazione della riduzione di MTS hanno dimostrato adesione precoce e migliore vitalità e proliferazione delle cellule nei DBP funzionalizzati con 10-5 M di REDV a 24 ore. Il saggio LDH ha riportato livelli trascurabili di citotossicità. Le valutazioni istologiche hanno rivelato un rivestimento cellulare quasi continuo.

Il primo passo verso la bioingegnerizzazione del cuore è stato eseguito sviluppando un protocollo di decellularizzazione più conservativo. I cuori di ratto sono stati decellularizzati con miorilassante, inibitori delle proteasi, sodio dodecil solfato e Triton X-100. Le soluzioni sono state somministrate mediante perfusione coronarica retrograda. L'efficienza del protocollo è stata valutata con istologie, immunofluorescenza combinata con TPM, quantificazione del DNA e analisi proteomica. La citocompatibilità è stata eseguita mediante semina statica di hBM-MSC in ventricoli isolati (ISO 10993-5). I risultati hanno confermato morfologia inalterata, mantenimento della proliferazione e assenza di citotossicità. Le hBM-MSC hanno formato un monolayer continuo a 24 ore, mentre a 7 e 14 giorni era visibile la penetrazione.

Concludendo, questa tesi di dottorato descrive i progressi verso la biocompatibilità dei sostituti cardiaci. La prima generazione di HM, basata su DBP e poliuretano, ha dimostrato la sua idoneità per il rivestimento interno dei TAH. La funzionalizzazione covalente e selettiva di DBP con 10-5 M di REDV ha provato la sua efficacia nell'accelerare l'adesione e proliferazione endoteliale. Un protocollo più conservativo e citocompatibile per la decellularizzazione del cuore totale è stato sviluppato e ha determinato la completa rimozione delle cellule endogene, preservando la matrice cardiaca.

List of contents

1 Introduction

1.1 Embryological and anatomical background

The circulatory system provides living tissues with oxygen and nourishing elements, whereas eliminating cellular metabolites and waste. The concentration of these substances is maintained stable (homeostasis) by a continual exchange between interstitial fluids and the bloodstream. The functionality of the cardiovascular apparatus is closely correlated with the performance of the cardiac pump, the organ located at the center of the two which maintains blood flow to all body districts.

1.1.1 Cardiac embryogenesis

The cardiovascular system is the first working system in the embryo, in which the cells of the atria and ventricles can contract spontaneously even before the development of the conducting elements (Armato et al. 2012).

The increased nutritional needs of the embryo serve as stimuli for the development of the vascular system (Sadler 2012). The embryonic development of the human heart starts at the third week of gestation and requires an extremely complex sequence of time-sensitive phases. The order of all these steps is finely regulated, in order to prevent the morphogenesis of structural and functional defects (Kloesel, Dinardo, and Body 2016).

1.1.1.1 Gastrulation

The most important event of the third week after fertilization is gastrulation, which gives rise to three germ layers.

On day 16, the endoderm and mesoderm originate from migrant cells of the primitive streak, whereas the cells in the original cell layer become the ectoderm (Sadler 2012). Mesodermal cells, in turns, differentiate into four different populations, among which there is the cardiogenic mesoderm, *i.e.*, the specific region from which the heart originates (Kloesel et al. 2016).

1.1.1.2 Establishment of the first and second heart fields

At about day 16-17, cardiogenic mesodermal progenitors migrate from the cranial side of the primitive streak, to form the primary heart field by surrounding the cranial neural fold with a horseshoe-shaped cellular cluster (

Figure 1.1). The first heart field is mainly composed of cardiomyocyte progenitors and endothelial cells (ECs) (Armato et al. 2012). This region is destined to constitute the atria, left ventricle, and part of the right ventricle, whereas the underlying endoderm promotes the formation of cardiac myoblasts and structures that will after form the blood and blood vessels, *i.e.*, the blood islands (Sadler 2012).

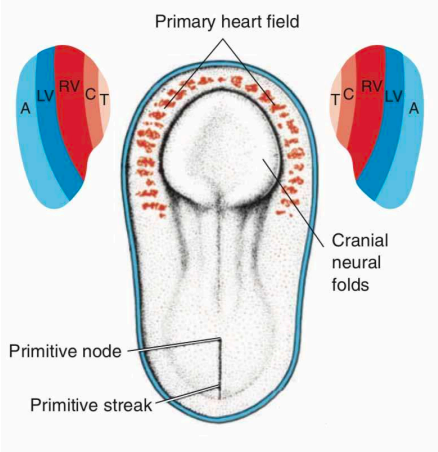

Figure 1.1 Dorsal view of embryo at 18 days. *Primary heart field surrounds cranial neural fold, to form atria, left ventricle and part of right ventricle(Sadler 2012).*

At day 20-21, a second heart field forms in the pharyngeal mesoderm and will give rise to the remaining parts of the right ventricle and outflow tract (Kloesel et al. 2016; Sadler 2012).

1.1.1.3 Formation of the heart tube

Migrant cells from the endothelial plexus of the first heart field produce two structures called right and left endocardial heart tubes. These elements are cranially connected to the region from which the ventricles and outflow regions will develop and caudally with the inflow region (Armato et al. 2012).

At about day 21, the progressive folding of the embryo induces the fusion of the endocardial tubes into a horseshoe-shaped structure, the heart tube, which progressively expands and bulges into the pericardial cavity. At day 24-25, the primitive heart starts pumping blood (Armato et al. 2012; Kloesel et al. 2016; Sadler 2012).

The endocardial tube is lined by ECs (endocardium) and surrounded by myocardial progenitors (myocardium). These two layers are separated by a loose mesenchyme, called cardiac jelly, rich in hyaluronic acid (Armato et al. 2012; Kloesel et al. 2016).

The epicardial layer forms due to the migration of proepicardial precursor cells. These cells penetrate the myocardium and are responsible for the formation of vascular endothelium, smooth muscle, and fibroblasts of the coronary tree (Armato et al. 2012; Kloesel et al. 2016; Sadler 2012).

At this stage, the heart is located in the pericardial cavity and possesses an inverted Y-like shape, in which the upper part becomes the left ventricle and the bottom will become the atrial region of the heart. The development of grooves on the tube surface identifies the *bulbus cordis*, where the two aortas originate, the primitive ventricle, the primitive atrium and lastly the venous sinus, where veins from the embryo, placenta and yolk sac flow (Armato et al. 2012).

1.1.1.4 Cardiac looping, convergence, and wedging

Most of the cardiac components (musculature and cardiac chambers with the exception of the left ventricle) are formed of the migrant precursor cells present

in the second heart field, which promotes the further elongation of the heart tube and is regulated by the neural crest (Kloesel et al. 2016; Sadler 2012).

From days 23 to 28, the cells of the cardiac tube start to change their shape and promote the bending of the structure, resulting in a looped configuration (Figure 1.2).

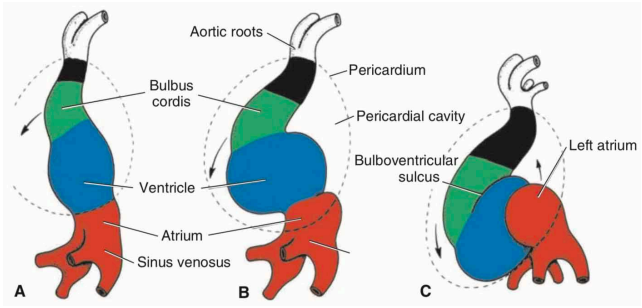

Figure 1.2 Cardiac looping. *Progressive lengthening of cardiac tube into pericardial cavity causes bending of structure at day 23 (Sadler 2012).*

In the meantime, local expansions of the cardiac tube form the common atrium incorporated in the pericardial cavity, whereas the atrioventricular canal and the distal part of the *bulbus cordis*, which will give rise to the ventricular outflow tract, narrows. The remaining part of the *bulbus cordis* then forms the right ventricular trabeculae and the *truncus arteriosus*. The end of this process also sees the formation of the primitive *trabeculae* in the heart tube, corresponding to the primitive left ventricle (Sadler 2012).

The outflow tract and atrioventricular canal then become more aligned in a process called convergence (Kloesel et al. 2016), causing the dilation of the atria on each side of the *bulbus cordis* (Sadler 2012).

The aortic outflow tract and pulmonary trunks develop by counterclockwise rotation of the outflow tract itself (wedging) and the formation of the conotruncal region (Kloesel et al. 2016).

1.1.1.5 Septation and formation of the cardiac chambers

Septation of the cardiac chambers is induced by the growth of one or two tissue agglomerates, called endocardial cushions, which progressively enlarge and fuse with the other side of the tube lumen or together. The endocardial cushions

are generated by the myocardium and are composed of extracellular matrix and proliferating mesenchymal cells (Sadler 2012).

- *Atria and sinus venosus*

The generation of the two atria involves the division of the atrioventricular canal and the formation of the atrial septum. The process starts at 4 weeks with the formation of four endocardial cushions (anterior, posterior, and two lateral). The latter fuse together at week 5, giving rise to the right and left atrioventricular canals, which separate the primitive atrium from the primitive ventricle (Figure 1.3). The formation of the *septum intermedium* reveals the openings of the future atrioventricular valves, where migration of epicardial cells from the cushions and the proliferation of mesenchymal tissue lead to the development of the mitral and tricuspid leaflets (Armato et al. 2012; Kloesel et al. 2016; Sadler 2012).

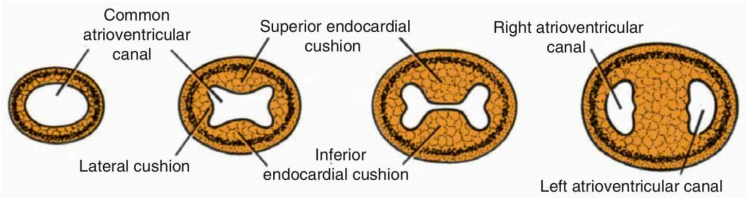

Figure 1.3 Formation of right and left atrioventricular canal. *Four endocardial cushions project into common atrioventricular canal and fuse together forming right and left canals (Sadler 2012).*

The *sinus venosus* opens on the dorsal wall of the primitive atrium and is supplied by the umbilical vein from the placenta, yolk sac veins, and cardinal veins (Figure 1.4). The opening of the *sinus venosus* progressively moves towards the right side of the primitive atrium, increases in dimension, and fuses with the right atrium, forming the smooth part of the right atrial wall at 4 weeks. The right vein of the yolk sac and the right cardinal vein become the inferior and superior *vena cava*, respectively, whereas the right umbilical vein closes. On the opposite side, the left part of the inflow decreases to form the coronary sinus, or progressively closes (Armato et al. 2012).

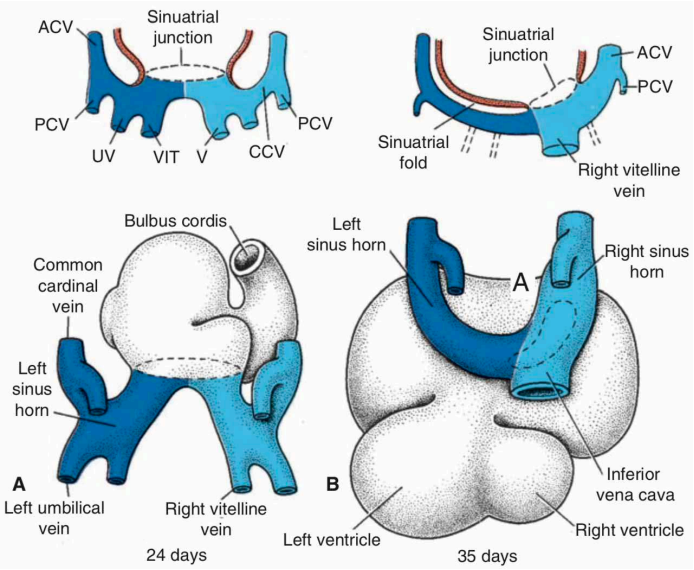

Figure 1.4 Development of sinus venous at days 24 (A) and 35 (B). (Sadler 2012).

The formation of the left atrium is secondary to the development of the lungs and their relative circulation. The pulmonary vein rises from the left-inferior part of the primitive atrium and, following atrial septation, bifurcates twice to originate the four final veins (Armato et al. 2012).

In the meantime, the lateral-superior part of the primitive atrium bulges, creating the two auriculae with the pectinate muscles (Armato et al. 2012).

At the end of the fourth week, septation of the atria starts with the formation of the *septum primum*, a membranous structure which divides the two atria, with the exception of the *ostium primum*, which allows right-left shunting of placental and systemic blood during gestation. This opening gradually closes but, in the superior portion, apoptosis of the its constituting cells produces the *ostium secundum*. At day 33, a second muscular septum forms in the right atrium, abutting the *ostium secundum* and generating a valve, the *foramen ovale*, which allows maintenance of the right-left shunt. After birth, the activity of the lungs produces an increase in the left atrial pressure, causing the adhesion and fusion of the *septum primum* and the *septum secundum*, with the formation of the interatrial septum (Armato et al. 2012; Kloesel et al. 2016).

- *Ventricles and conus and truncus arteriosus*

Tube elongation and looping cause the fusion of the *bulbus cordis*, *i.e.*, the future right ventricle, with the primitive ventricle. The proliferation of neural crest mesenchymal cells leads to the formation of the bulbar ridges in the *bulbus cordis*. The base of the ventricle has a muscular crest which, due to the proliferation of populating fibroblasts and dilatation of the two sides of the ventricle, creates the atrioventricular septum (Figure 1.5). This is completely closed by the end of the seventh week, when the interventricular foramen is sealed due to the fusion of bulbar ridges and endocardial cushions (membranous parts of the interventricular septum) (Armato et al. 2012).

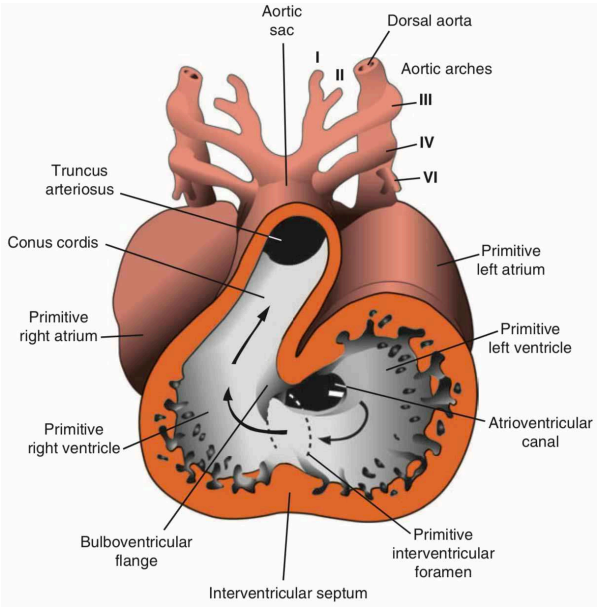

Figure 1.5 Section of primitive ventricle at 35 days. *At this stage, blood from atria passes into left and right ventricles through a primitive interventricular septum (Sadler 2012).*

The ventricular trabeculation gradually develops and gives the ventricular wall characteristic aspect. The blood filling the ventricles thins the ventricular surface and mesenchymal tissue composing the atrioventricular valves (Figure 1.6). Therefore, the cusps remain attached to the ventricular wall with muscular cords (papillary muscles). Lastly, parts of these cords degenerate into dense connective tissue, the *chordae tendinae* (Armato et al. 2012; Sadler 2012).

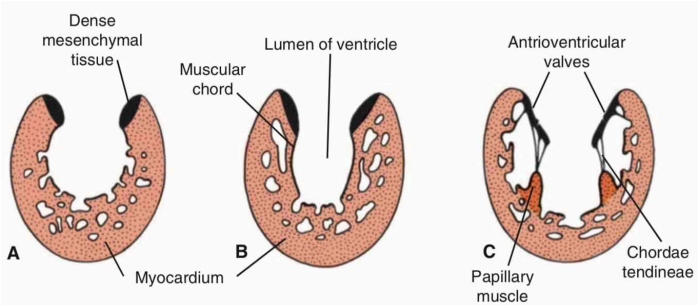

Figure 1.6 Development of anchoring system of atrioventricular valves. *Blood erodes ventricular walls and mesenchymal tissue of primitive valve, leaving papillary muscles and chordae tendinae to anchor leaflets to walls (Sadler 2012).*

The bulbar ridges undergo a rotation of 180° and fuse with each other, in order to originate the helical aortopulmonary septum inserted into the *conus* and *truncus arteriosus*. This transformation produces the aorta and pulmonary artery (Armato et al. 2012). The semilunar valve cusps are generated by the epithelial-to-mesenchymal transformation and migration of endocardial cells on the endocardial cushions located in the proximal ventricular outflow tract (Figure 1.7). These cells also contribute to the development of the vascular smooth musculature and fibroblast population of the cardiac interstitial connective tissue (Kloesel et al. 2016).

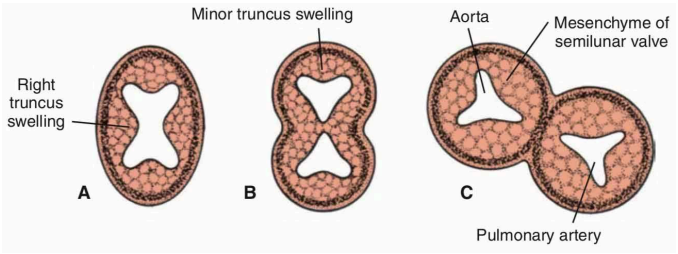

Figure 1.7 Development of semilunar valves (Sadler 2012).

The coronary tree originates from proepicardial progenitor cells, which undergo epithelial-to-mesenchymal transition, and venous endothelial angioblasts from the *sinus venosus*. The connection between the aorta and the coronary vasculature is induced by the invasion of the arterial ECs into the aorta (Armato et al. 2012).

1.1.1.6 The pericardium

The heart and pericardium develop independently, and their inclusion in the celomic cavity is a process of cavitation of the embryonic body wall (Gray 2008).

1.1.2 Macroscopic anatomy

Not unexpectedly, defining the cardiac organ is more about Engineering Science than Medicine. Indeed, the simplest and most effective description reports the heart as a valved, muscular organ composed of a series of two-chambered volumetric pumps, called the right and left hearts.

1.1.2.1 Physiological role

The right and left hearts represent the central components of the circulatory system, in which they play two completely separate physiological roles. Pulmonary circulation originates in the right part of the heart and collects deoxygenated blood, whereas the systemic circulation begins in the left part and distributes oxygenated blood (Figure 1.8). Each of the circuits originates and terminates into the heart (Martini, Timmons, and Tallitsch 2012)

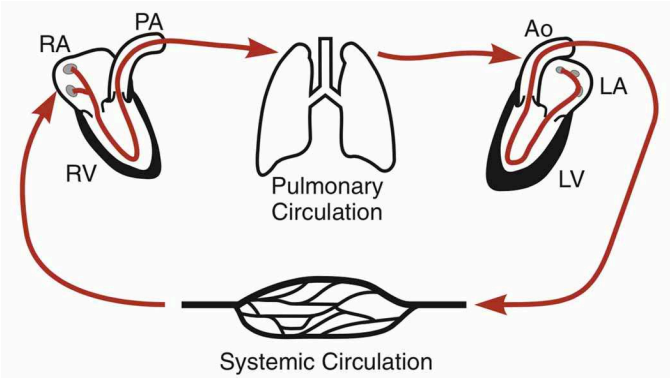

Figure 1.8 Right and left hearts and their relationship with pulmonary and systemic circulations. *Pulmonary circulation originates in right ventricle and ends in left atrium, whereas systemic circulation starts in left ventricle and terminates in right atrium* (Klabunde 2012)*.*

1.1.2.2 Location and general characteristics

The heart lies in the mediastinum, immediately behind the sternum, and is surrounded by the lungs and enveloped in the pericardial sac (Figure 1.9). It is characterized by conical geometry, in which the base and apex are respectively located at the top and bottom of the organ. It is also oriented obliquely in the thorax at an angle of 45° with respect to the sagittal plane (Anastasi et al. 2006; Gray 2008; Martini et al. 2012).

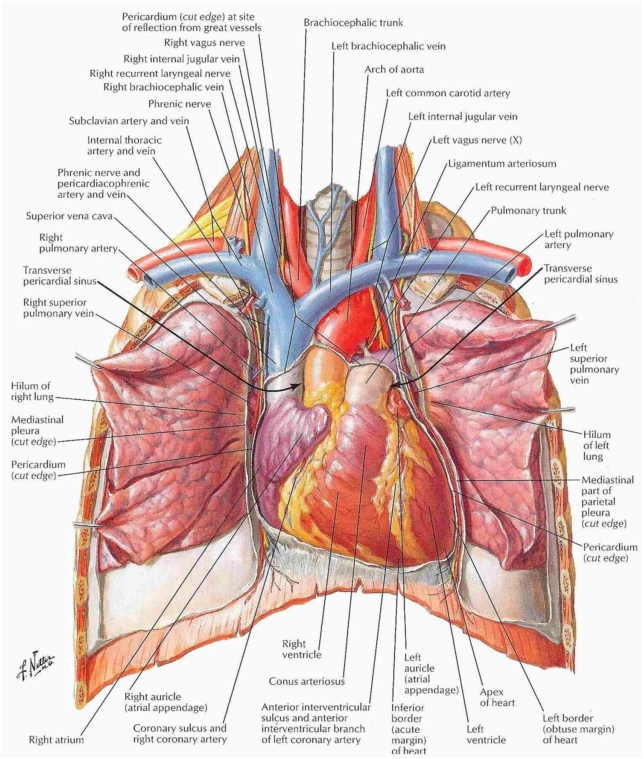

Figure 1.9 Heart in situ. *Heart is located into pericardial sac (not shown) in mediastinum between lungs* (Netter 2014).

As regards average dimensions, the cardiac pump is approximately the size of a closed fist: the distance between the base and the apex is about 12 cm, the transverse diameter is 8-9 cm, and the anteroposterior diameter is 6 cm. It weighs about 300 g in males and 250 g in females on average, and its capacity is about 500 ml (Anastasi et al. 2006; Cattaneo 2005; Gray 2008).

1.1.2.3 Surface anatomy

From the exterior of the heart, it is easy to locate the position of the internal chambers by identifying anatomical structures, called *sulci*, visible as depressions on the surface.

The division between the atria is marked by the coronary sulcus. The atrioventricular sulcus is present on both anterior and posterior surfaces and separates the two ventricles (Figure 1.9). These grooves usually contain adipose tissue and blood vessels (coronary arteries and coronary sinus) responsible for supply to the heart itself (Gray 2008; Martini et al. 2012).

1.1.2.4 Internal chambers

Based on their relative positions, the four chambers of a normal heart are distinguished into posterosuperior, or atria, and anteroinferior, named ventricles. Internally, the interatrial and interventricular septa separate the atria and ventricles, respectively (Figure 1.10) (Cattaneo 2005; Gray 2008).

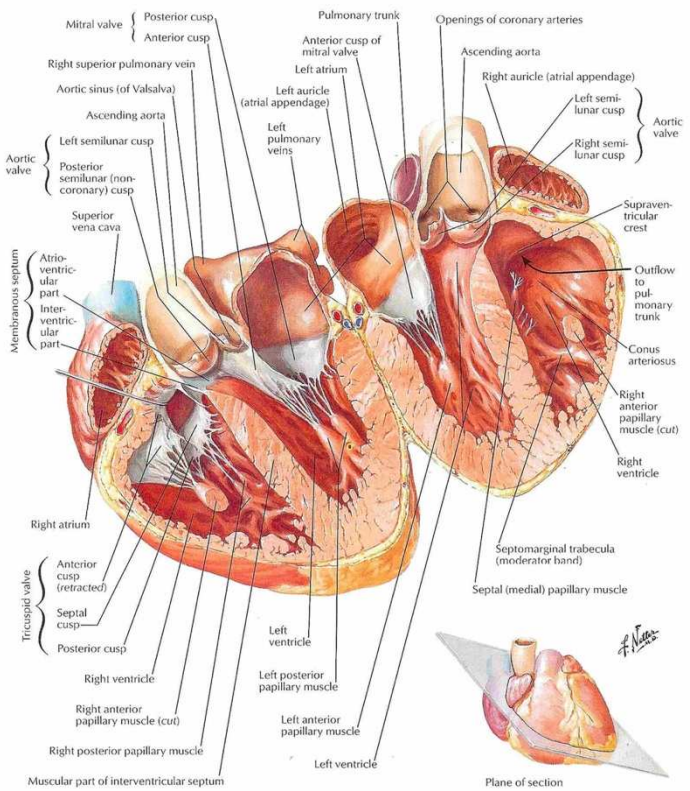

Figure 1.10 View of cardiac chambers. *Atria are located in posterosuperior region of heart, and ventricles in anteroinferior part (Netter 2014).*

- *Right atrium*

The right atrium collects deoxygenated venous blood from the coronary circuit and the upper parts (head, neck, upper limbs, and chest) and bottom (abdominal and pelvic regions, and lower limbs) of the body through the superior and inferior *vena cava*, respectively (Martini et al. 2012). Figure 1.11 shows the right atrial wall decorated with muscular structures, disposed vertically and parallel to each other, called pectinate muscles (Gray 2008).

During the fetal life, the lungs are not functional. For this reason, the interatrial septum presents an opening, the *foramen ovale*, which allows blood flow between the right and left atria. After birth, this opening closes, leaving in place a small depression, called the *fossa ovalis*. The right atrium has an appendage, the right auricle, which deflates when it is not filled with blood (Martini et al. 2012).

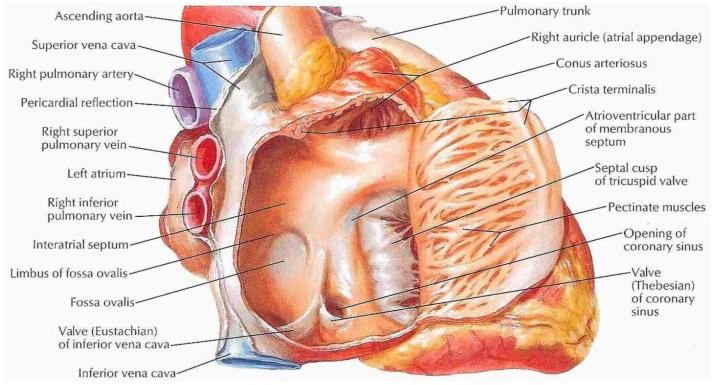

Figure 1.11 Right lateral view of right atrium (Netter 2014)**.**

- *Right ventricle*

The deoxygenated blood passes from the right atrium to the right ventricle through the right atrioventricular valve.

The wall of the right ventricle possesses irregular muscular cylindrical structures called *trabeculae carneae* (Figure 1.12). These include a characteristic band which projects from the free ventricular wall to the interventricular septum, called the moderator band. The right ventricle outflow tract consists of a smooth cone-shaped structure, the *conus arteriosus*, which terminates with the arterial valve of the pulmonary artery (Martini et al. 2012).

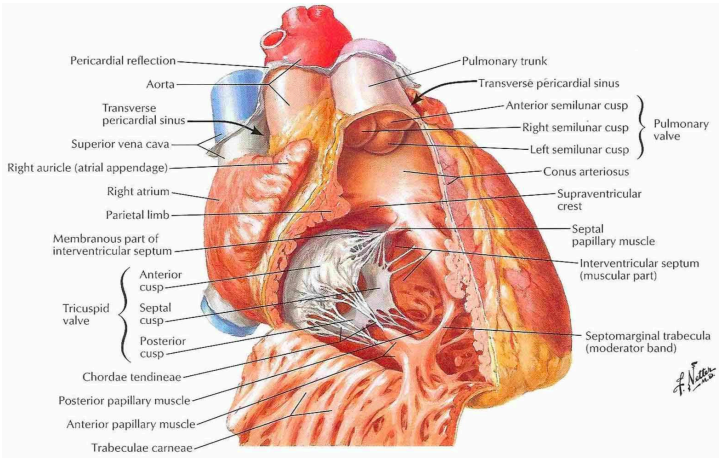

Figure 1.12 Anterior view of right ventricle *(Netter 2014).*

- *Left atrium*

The oxygenated blood reaches the left atrium from the lungs by flowing into the pulmonary veins. There are no pectinate muscles in the left atrium (Figure 1.13). The appendage, *i.e.*, the left auricle, is still present (Martini et al. 2012).

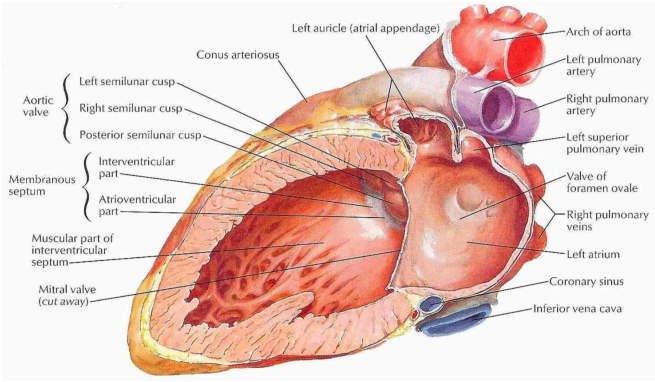

Figure 1.13 Lateral view of left atrium and ventricle *(Netter 2014).*

- *Left ventricle*

Lastly, oxygenated blood flows into the left ventricle by passing through the left atrioventricular valve. The organization of the *trabeculae carneae,* thriving the left cardiac walls, closely reflects the function of these chambers, as shown in Figure 1.14. The need to develop enough pressure to move the blood into the systemic circuit is responsible for the evolution of a thick wall with strong, prominent muscular bundles (Gray 2008).

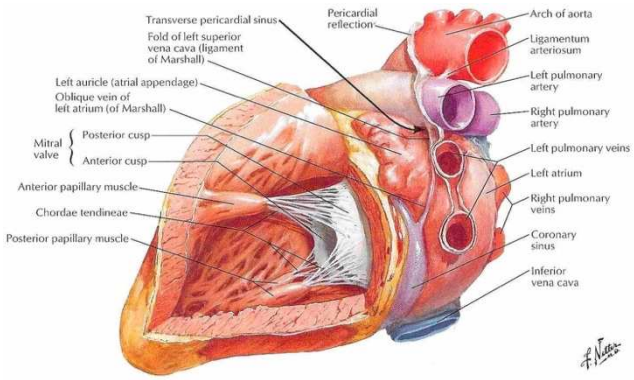

Figure 1.14 Posterolateral view of left ventricle *(Netter 2014).*

1.1.2.5 Valve apparatus

The unidirectionality of the blood flow is guaranteed by folds of endocardium, *i.e.*, the cardiac valves, which protrude into the openings between atria and ventricles and between ventricles and the arterial connections, preventing backflow. The cardiac valve apparatus is composed of two atrioventricular valves (tricuspid and mitral valves), which separate the atria from the ventricles, and by two semilunar valves (pulmonary and aortic valves), which separate the ventricles from the respective arteries (Cattaneo 2005; Martini et al. 2012).

During the systolic phase of the cardiac cycle, blood fills the ventricles and move against the tricuspid and mitral leaflets, causing the atrioventricular valves to close, while the semilunar ones open. The opposite happens during the diastolic phase (Figure 1.15).

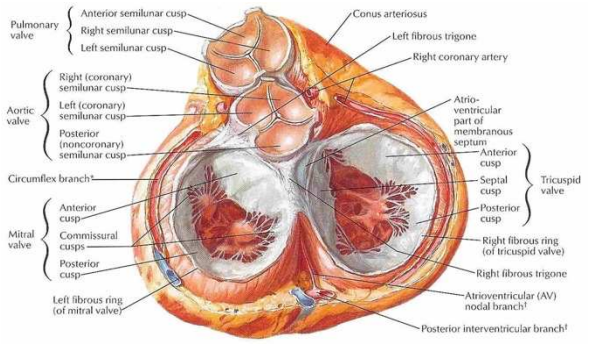

Figure 1.15 Diastolic atrial view of valve apparatus. *Tricuspid and mitral valves are atrioventricular, and separate atria from respective ventricles; pulmonary and aortic valves are arterial, and separate ventricles from corresponding outflow arteries (Netter 2014).*

For a more detailed anatomical description, the atrioventricular valves have a funnel-like shape protruding into the ventricles. They are composed of a ring of connective tissue inserted into the fibrous skeleton (*annulus*), a variable number of connective tissue leaflets (three for the tricuspid valve and two for the mitral valve), and a sophisticated supporting system, comprising the *chordae tendinae* and the papillary muscles, responsible for limiting movement of the leaflets into the atria (Figure 1.16). The *chordae tendinae* are bundles of collagen fibers connecting the free edges of the atrioventricular valves to cone-shaped muscular projections of the ventricular wall (Cattaneo 2005; Martini et al. 2012).

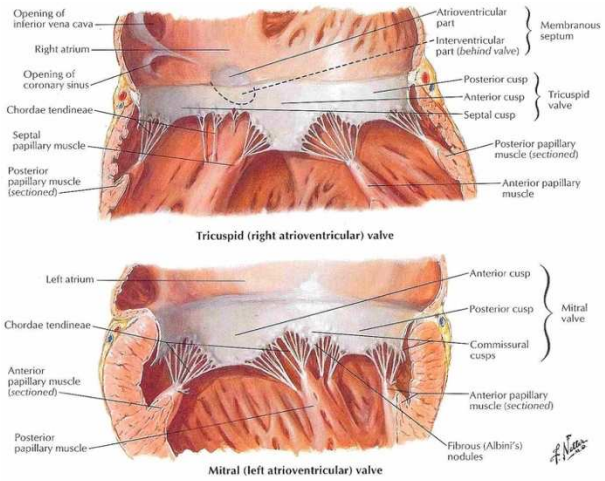

Figure 1.16 Anatomy of atrioventricular valves. *Tricuspid and mitral valves are composed of annulus, three or two cusps respectively, chordae tendinae, and papillary muscles (Netter 2014).*

The structure of the semilunar valve cusps is simpler and recalls a swallow's nest protruding from the wall of the respective artery (Figure 1.17). They are composed of three thick membranous folds, the cusps. The arterial valves present dilatation of the wall adjacent to each cusp, the sinuses. Their function is to prevent the cusps from adhering to the wall when the valves open. (Anastasi et al. 2006; Cattaneo 2005; Martini et al. 2012).

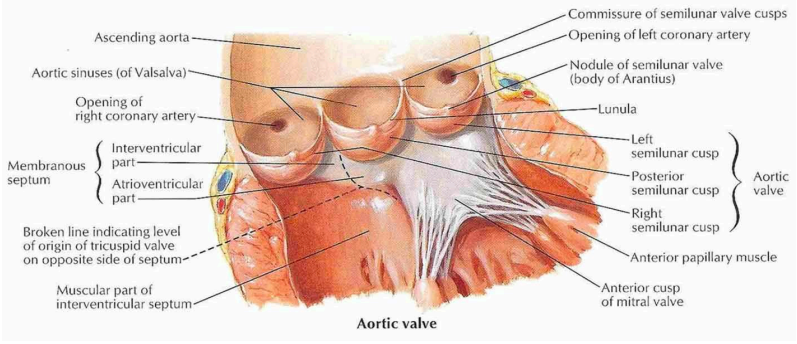

Figure 1.17 Anatomy of semilunar valves. *Aortic and pulmonary valves are composed of three cusps inserted in respective arterial walls (Netter 2014).*

Each cusp has a free margin with a fibrous nodule, the Morgagni and Aranzio *noduli* of the pulmonary and aortic valves, respectively, which mark the coaptation area (Anastasi et al. 2006; Cattaneo 2005).

1.1.2.6 Cardiac vascular supply

The continual work of the cardiac muscle is sustained by the coronary circulation, an intricate network of arteries and veins that originates at the base of the aorta and ends in the right atrium. The coronary flow is about 5% of the cardiac output and the highest blood pressure of the systemic circulation is found in the coronary circuit (Guyton et al. 2012; Martini et al. 2012).

The coronary arteries are defined as right and left according to their origin from the aortic sinuses. The supply territory of the two coronaries is reciprocal: the first provides blood mainly from the right atrium and ventricle, interatrial septum, part of the left ventricle, the posteroinferior region of interventricular septum, and part of the conduction system; the second from left atrium and remaining ventricle, part of the right ventricle, and the anterior side of the septum (Martini, Timmons, and Tallitsch 2012).

Seventy-five percent of the total venous coronary blood is collected in the great and middle cardiac veins and then converges into the coronary sinus of the right atrium. The rest arrives in small veins which rise directly in the four cardiac chambers (Cattaneo 2005; Martini et al. 2012; Netter 2014).

1.1.2.7 Conduction system

The cardiac impulse originates from highly specialized cells which compose the conduction system and is transmitted by fibers connecting the atria and the ventricles. Because of the reduced number of myofibers, the excitatory (nodal cells) and conduction fibers are less tense than the working myocardium. However, they control the cardiac contraction of working cardiomyocytes by developing and transmitting the action potentials to regenerate spontaneously, without the need for any neural or hormonal stimulation (Gray 2008; Guyton et al. 2012; Martini et al. 2012).

The events of the cardiac cycle are very precise and follow a specific order. During systole, blood is ejected into the subsequent cardiac compartment (ventricle or artery) due to cardiac contraction; during diastole, cardiac relaxation allows the chambers to fill with blood. In each cardiac cycle, the atria contract before the ventricles and these events are controlled by the conduction system (Martini et al. 2012) .

The conduction system comprises the sinoatrial and atrioventricular nodes, the bundle of His, the right and left atrioventricular bundles, and the Purkinje fibers (Figure 1.18).

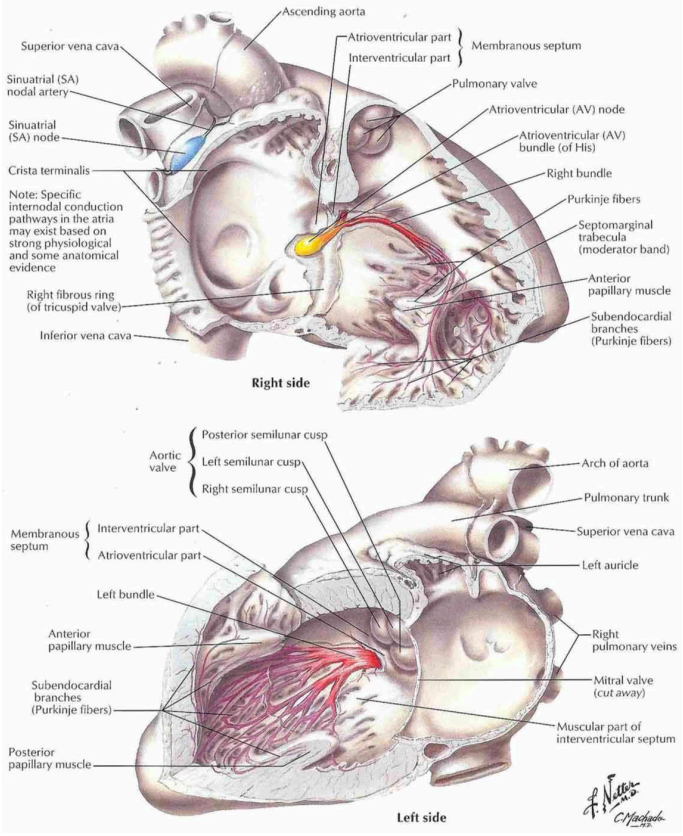

Figure 1.18 Conduction system *Conduction system is composed of sinoatrial and atrioventricular nodes, atrioventricular fibers (bundle of His), left and right bundles, and Purkinje fibers (Netter 2014).*

The sinoatrial node is located in the right atrium, near the superior *vena cava*, and is directly connected with its muscle fibers through thinner ones. The cells of the sinoatrial node are known as the heart's natural pacemaker, because of their ability to generate action potentials spontaneously at higher frequency. The impulse is propagated from the sinoatrial to the atrioventricular node, also located in the right atrium, with a delay which gives the atria the time to be filled with blood before ventricular contraction. Once the electric signal enters the atrioventricular bundles, it is conducted very rapidly across the working myocardium of the ventricles by the thick Purkinje fibers. Transmission from the ventricular endocardium to the epicardium is not immediate, due to the specific spiral-like organization of the ventricular muscle planes, which are separated by connective septa (Figure 1.19). Therefore, the electric stimulus does not propagate perpendicularly, but follows an angular vector (Gray 2008; Martini et al. 2012).

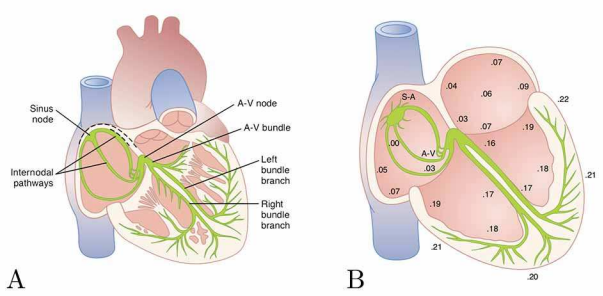

Figure 1.19 Transmission speed of electric impulse across heart. *Conduction of electric impulse between elements of conducting system (A) is not uniform: it is slower in atria than in ventricles (B) (Guyton et al. 2012).*

1.1.2.8 Pericardium

The pericardium is the fibrous sac which contains the heart (Figure 1.20). It has two components, the fibrous and the serosal pericardium. The pericardial cavity is filled with a thin film of lubricant fluid (about 10-20 ml) (Gray 2008; Martini et al. 2012).

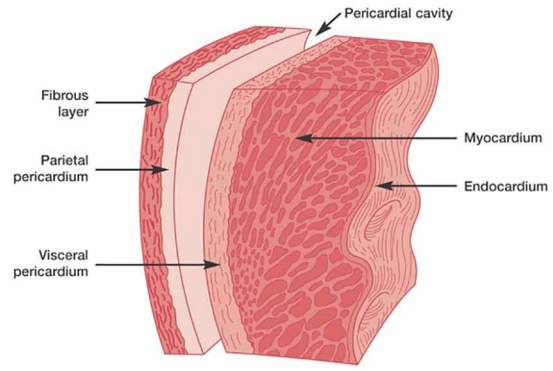

Figure 1.20 Structure of pericardial sac. *Parietal pericardium is composed of serosa and fibrosa, inner and outer layers, respectively.*

The fibrous pericardium, or *fibrosa*, has a rough appearance. Spatially, it blends with the *adventitia* of the great vessels located in the upper part of the heart; it is anchored to the diaphragm and the posterior surface of the sternum.

The visceral pericardium adheres to the heart, forming the epicardium, and covers the great vessels. This layer is reflected into the parietal pericardium (or *serosa*) which lines the fibrous pericardium internally (Gray 2008).

1.1.3 Microscopic anatomy

1.1.3.1 Cardiac wall

The cardiac wall is composed of three *tunicae*, called epicardium, myocardium, and endocardium.

- *The epicardium*

The outer *tunica* of the cardiac wall is composed of the visceral layer of the serosal pericardium which reflects into the parietal layer at the base of the heart. It is composed of epithelial cells (mesothelium) lying on a thin layer of loose connective tissue rich in elastic fibers (a *lamina propria,* called basal lamina). It is connected to the underlying myocardial connective tissue by a loose subepicardial layer enriched by elastic fibers, coronary branches surrounded by adipose tissue, lymphatic vessels, and nerve fibers (Anastasi et al. 2006; Cattaneo 2005; Krstic 1992).

- *The myocardium*

From a functional point of view, the myocardium is the most important layer of the cardiac wall. It can be subdivided into the working myocardium (90% of the whole musculature) and the fibers of the conduction system. The working myocardium constitutes the muscle fibers of the atria and ventricles, which are independent and separated by the fibrous skeleton of the heart (Anastasi et al. 2006; Cattaneo 2005).

The working myocardium is composed of multiple planes of cardiac muscles which originate and end on the fibrous skeleton and are interposed by connective tissue, blood vessels, and nerves. The atrial and ventricular myocardial tissues are very different and constitute two separate systems of fibers (Anastasi et al. 2006). The atrial myocardium is thinner and forms a figure-of-eight shape around the atria; the ventricular myocardium is thicker and the constituting plane orientation changes between consecutive layers (Martini et al. 2012).

In the atria, the bundles are distinguished into proper and common. The proper atrial bundles are disposed circularly around the inflow tracts; the common ones are organized transversally and vertically (Anastasi et al. 2006).

Bundles organization is more complicated in the ventricles. Three different layers compose the ventricular wall. In the latter, pocket-like muscular bundles, specific to each ventricle, are enveloped in a common layer which, from the subepicardium, becomes deeper and surrounds the proper bundles internally (Anastasi et al. 2006).

- *The endocardium*

The inner layer of the cardiac wall covers the internal surfaces of the heart chambers and valves, between 20 and 500 µm thick, being less variable in the atria (Anastasi et al. 2006).

The endocardium is composed of ECs lying on a connective *lamina propria* (basal lamina), rich in elastic fibers but lacking blood vessels, and in continuity with the endothelium of the arteries and veins. The basal lamina lies on a myoelastic layer composed of dense connective tissue made of collagen and elastin, and smooth muscle cells. The connective subendocardial layer, not present in the papillary muscles, is continuous with the myocardial endomysium and possesses vessels, nerves and the terminal part of the Purkinje fibers (Anastasi et al. 2006; Cattaneo 2005; Krstic 1992; Martini et al. 2012).

1.1.3.2 Cardiac muscle tissue

Cardiac muscle tissue has unique functional properties; it is similar to its skeletal counterpart but with substantial differences in terms of cell organization, vascular supply, absence of nervous system to support contraction, and poor resistence to ischemia (Guyton et al. 2012).

- *Cardiomyocytes*

Cardiac muscle cells, or cardiomyocytes, are relatively small cells with average dimensions of 10-20 µm in diameter and 50-100 µm in length (Anastasi et al. 2006; Martini et al. 2012). They have a single central nucleus and contain extended organized myofibrils of actin and myosin and aligned sarcomeres responsible for the typical microscopically visible striation. Cardiomyocytes have an extremely high energy demand for contraction, which means that the sarcoplasm is rich in hundreds of mitochondria and myoglobin reserve to store oxygen (Anastasi et al. 2006; Krstic 1985; Martini et al. 2012).

The cardiac muscle fibers are composed of several cardiomyocytes associated in series and parallel by highly specialized cell-to-cell junctions. Cells are joined by desmosomes binding the contiguous *sarcolemmae*. The connection between adjacent cells is achieved with specialized junctions (intercalated discs) and gap junctions which are highly permeable to ions and allow the rapid transmission of action potentials. This peculiar type of mechanical, chemical and electrical connection is responsible for transmission of impulses to the whole organ and thus for its contraction, and is the reason why cardiac tissue is defined as a functional syncytium (Anastasi et al. 2006; Guyton et al. 2012; Krstic 1985; Martini et al. 2012).

The cardiomyocytes of the atria are characterized by more developed Golgi apparatus and rough endoplasmic reticulum. They also have granular structures which produce a hormone, the natriuretic atrial factor, which has renal and vascular functions (Anastasi et al. 2006).

- *Cells of the conduction system*

As mentioned above, due to their function of producing and transmitting electric stimuli, the cells of the conducting system contain a reduced number of contractile elements. They are subdivided into nodal, transmission, and Purkinje cells.

The first are spindle-like in shape and smaller than the working cardiomyocytes. Their myofibers have an irregular pattern and the sarcoplasm contains many mitochondria and glycogen reserves.

The transmission cells are an intermediate phenotype between specific and working cardiomyocytes.

Purkinje cells are binucleate, larger than cardiomyocytes (100 µm x 50 µm) and contain high levels of glycogen. Their myofibers are rare and mainly distributed in the periphery. They are connected to each other by a different type of intercalary disc and separated from the surrounding working myocardium by a connective envelope (Anastasi et al. 2006; Krstic 1985).

- *Cardiac ECM*

Each cardiomyocyte is enveloped in a connective sheath of reticular collagen microfibrils and is connected to neighboring cells by a fibrous cross-link (Borg and Caulfield 1981; Krstic 1985; Martini et al. 2012).

This type of organization is the same as that of the muscle layers, which have a fibrous wrapping and fibrous sheets separating adjacent muscle layers. The connective tissue is continuous with the fibrous skeleton surrounding the valve annuli and the origin of the pulmonary trunk and aorta. The ECM is also enriched by coronaries, lymphatic vessels, and elements of the nervous system (Martini et al. 2012).

1.1.3.3 Heart valves

The atrioventricular valves have a fibrous *lamina*, in continuity with the fibrous skeleton of the heart and the *chordae tendinae*, covered by endocardium. On the axial face of the atrioventricular cusp, between the lamina and the endocardium, is a layer of loose connective tissue, the *spongiosa*, which contains rare myocardial muscle fibers. In humans, these leaflets are not vascularized and receive nourishing elements directly from blood and by diffusion (Anastasi et al. 2006).

The arterial valves have a similar structure. A *lamina fibrosa* is covered by the ventricular endocardium (on the convex side) and the arterial endothelium in continuity with the pulmonary or aortic *tunica intima* (on the concave side). The *lamina fibrosa* has a thickened knot-like structure located in the middle of the free margin, and called Morgagni and Aranzio *noduli*, for the pulmonary and aortic valves, respectively. In the setting of human physiology, the cusps are not vascularized (Anastasi et al. 2006).

1.1.3.4 Pericardium

The serosal layer of the parietal pericardium is composed of a mesothelial cell layer, lying on a thin submesothelial space constituted of the basal lamina (Figure 1.21). The fibrosa is made by dense connective tissue organized in bundles and enriched with elastic fibers, blood and lymphatic vessels, and nerve

elements. The elastic fibers, thinner in the *serosa* layer, are usually oriented in parallel to the collagen bundles (Krstic 1992; Rodriguez and Tan 2017).

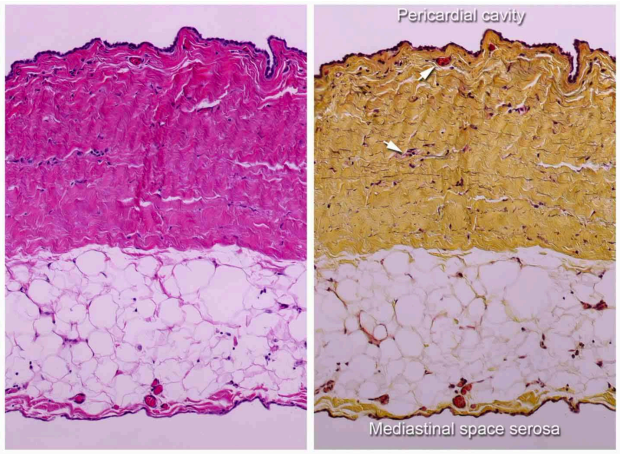

Figure 1.21 Human parietal pericardium. *Cross-sections of human pericardium, showing two constituting layers: serosa, populated by mesothelial cells lying on a basal lamina, and fibrosa, composed of collagen bundles with the typical periodic wavy pattern (Rodriguez and Tan 2017).*

1.2 Heart failure and therapeutic treatments

The most powerful and effective definition of heart failure (HF) was given in 2014, when it was addressed as a "global pandemic". In that year, 26 millions of people were affected worldwide (Ambrosy et al. 2014). Despite recent advances, treatment has not greatly improved the condition of patients and the disease is now spreading in both industrialized and developing countries (Tanai and Frantz 2016).

HF can also be defined as a systemic disease, because the pathophysiological mechanisms activated to compensate impaired heart function progressively affect the lungs, kidneys, gastrointestinal tract, and peripheral vascular system. Therefore, high mortality is often associated with debilitating comorbidities, poor quality of life, and frequent and prolonged hospital admissions (Tanai and Frantz 2016).

HF involves enormous medical costs for health services. The American Heart Association reports that, in 2030, the total costs for HF will increase by 127% with respect to 2012 (Benjamin et al. 2018).

1.2.1 Definition

HF is a severe pathophysiological condition, with an evolving nature and characterized by functional and/or structural cardiac impairment.

In this complex clinical picture, the capacity of the ventricle to fill and eject blood is severely compromised. Therefore, the heart is no longer able to pump an adequate volume, nor can it withstand a normal pumping efficiency by increasing the ventricular filling pressure. In both situations, the primary cardiac function of supporting the metabolism of peripheral tissues and lungs is dramatically compromised.

1.2.2 Classifications

HF is classified by the following criteria based on type of onset, impaired cardiac location, variation in cardiac output, and cardiac phase (Damiani 2014).

- *Type of onset*

Considering the rapidity of onset, HF is distinguished into acute or chronic. In the first case, an adverse acute event compromises the functionality of the cardiac pump without previous alterations. In the majority of acute cases, appropriate and effective medical therapies lead to full patient recovery. Conversely, chronic HF might be the common outcome of all cardiovascular diseases as a consequence of remodeling activated in order to withstand functional and structural adjustments, induced by the underlying primary pathology (Damiani 2014).

- *Location*

When primary underlying pathologies affect one of the two sides of the heart (*e.g.*, valve disease), HF may only involve the left or right ventricle. Otherwise, it may compromise the whole heart (Damiani 2014).

- *Cardiac output*

Reduced cardiac output is the axiom of HF. However, it may be less than or more than to 5 l/min. In the first case, HF is defined as low cardiac output; in

the second, with high cardiac output, which cannot satisfy the needs of the peripheral regions of the body (Damiani 2014).

- *Cardiac phase*

HF may affect the systolic or diastolic phase of the cardiac cycle and lead to different structural and functional consequences (Figure 1.22).

In the first case, cardiac failure is indicated as systolic HF or HF due to reduced ejection fraction (HFrEF). The phenotype is characterized by reduced sarcomere shortening responsible for the reduced ventricular ejection fraction (below 50%), ventricular dilatation, eccentric remodeling with reduction of the cardiac mass/volume ratio, or volume overload followed by forward HF (Damiani 2014; Tanai and Frantz 2016).

In the second case, cardiac failure is called diastolic HF or HF with preserved ejection fraction (HFpEF). The contractility of the heart is not affected but relaxation is reduced. The phenotype is characterized by an ejection fraction higher than 50%, ventricular stiffness, ventricular hypertrophy and absence of dilatation, concentric remodeling with increase of the cardiac mass/volume ratio, and backward failure due to pressure overload (Damiani 2014; Tanai and Frantz 2016). The impaired diastolic phase is caused by several factors involving calcium-handling processes, depression of beta-adrenergic signaling, and reduced recoil of elastic elements (titin) not sufficiently compressed during systole (Sharma and Kass 2014).

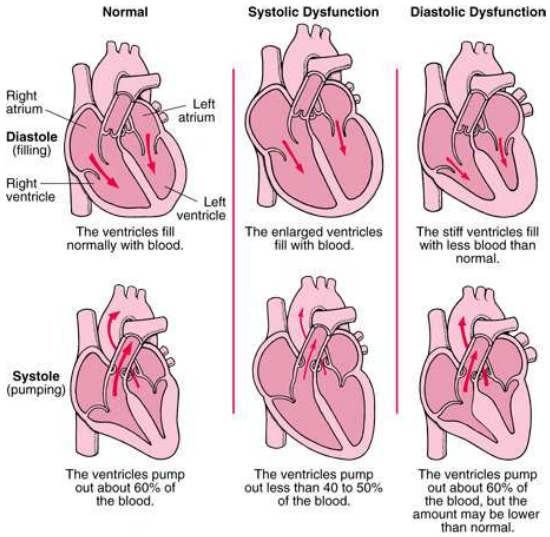

Figure 1.22 Structural and functional alterations in HFrEF and HFpEF. *HFrEF is characterized by an ejection fraction of less than 50%; in HFpEF, ejection fraction is preserved (Porter, 2018).*

1.2.3 Epidemiology

It is well-known that cardiovascular diseases are the primary cause of death worldwide, accounting for 50% of deaths in Europe and the US, and 25% in developing countries (Lopez 1993; Lopez et al. 2006). Among the cardiovascular diseases, HF is one of the most common (Figure 1.23).

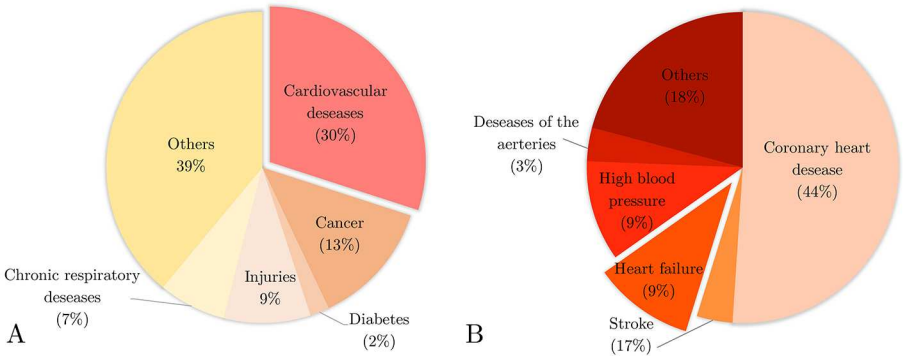

Figure 1.23 Percentage of deaths associated with cardiovascular diseases. *Cardiovascular diseases are leading cause of death (A) and HF is one of the most common (B). Adapted from* (World Health Organization 2018) *and (Benjamin et al. 2018).*

In the westernized world, HF prevalence is around 1-2% of the population (Mosterd and Hoes 2007). The estimation for developing countries is uncertain because of the poor reliability of monitoring and data (Lopez 1993). The latest

report of the American Heart Association announced that the rapid and unexpected increase in HF prevalence was due to population aging and improved survival from other cardiovascular pathologies. This growth will lead to 8 million affected people, only in the US by 2030 (Benjamin et al. 2018).

HF incidence is closely correlated with age, gender, and ethnic group. The incidence in men is higher and associated with the worst outcome. Conversely, the Framingham Heart Study reported its decline between 1950 and 1999 in women, who generally survive longer despite later onset (Adams et al. 1999; Benjamin et al. 2018; Levy et al. 2002).

HF is a fatal condition, associated with poor long-term prognosis for both systolic and diastolic impairment (Udelson 2011). In 1993, following a 40-year-long observation period, the Framingham Heart Study attributed a survival of 57% and 64% after one year and 25% and 38% after five years, respectively for men and women (Ho et al. 1993). Mortality is still high, despite improvements in pharmacological therapies (use of angiotensin-converting enzyme inhibitors and β-blockers) and surgery (coronary revascularization, implantable cardioverter-defibrillators, and cardiac resynchronization) (Benjamin et al. 2018).

1.2.4 Etiology

The risk factors for HF vary substantially between world regions and nations, due to economic and cultural aspects.

In industrialized countries, coronary heart disease (CAD) due to acute or chronic myocardial ischemia is the first cause of HF, and is followed by arterial hypertension, valve diseases, diabetes mellitus, familiar or congenital heart disease, use of cardiotoxins, connective tissue disorders, and arrhythmias (Tanai and Frantz 2016). In more detail, CAD, uncontrolled hypertension leading to pressure overload, volume overload due to valve disease, conduction abnormalities, and altered contractility induced by cardiotoxins and cardiotoxic drugs are responsible for the loss of myocardial function leading to HFrEF. Atrial fibrillation, chronic hypertension and cardiomyopathies are more prone to develop into HFpEF (Kemp and Conte 2012; Tanai and Frantz 2016; Udelson 2011). Lifestyle also plays a key role. Cardiovascular diseases,

together with hypertension, diabetes, obesity and smoking account for 52% of deaths due to HF (Benjamin et al. 2018).

In poor countries, the most common causes are rheumatic heart disease or rare diseases, like Chagas' disease and malaria; in developing areas, changes in lifestyle are progressively increasing the occurrence of coronary pathologies and hypertension (Celermajer et al. 2012; Mendez et al. 2001).

1.2.5 Signs and symptoms

As HF is associated with a wide spectrum of multifactorial signs and symptoms, due to the presence of underlying primary pathologies, diagnosis is often challenging, especially in the case of HFpEF (Piepoli 1999; Tanai and Frantz 2016).

In general, in the case of left ventricular impairment, symptoms are mainly due to pulmonary hypertension; in the cases of right-side impairment, they are due to systemic hypertension. Common symptoms include (Tanai and Frantz 2016):

- Pulmonary congestion and dyspnea, caused by increased capillary and arterial pressure and pulmonary resistence;
- Cardiomegaly and cardiac cachexia;
- Activation of adaptive vascular mechanisms, such as regulation of vascular tone and increased production of vasoactive molecules, performed by the vascular endothelium;
- Dilation of the jugular vein caused by increased abdominal pressure;
- Renal failure, gastrointestinal complications (hepatomegaly) and cerebral symptoms due to hypoperfusion;
- Peripheral edema and muscle mass reduction in limbs;
- Cyanosis and paleness cause by vasoconstriction and centralization.

1.2.6 Pathophysiology

Reduced pumping ability has consequences in terms of mechanical alterations and leads to the activation of compensatory biological mechanisms, with potential deleterious side-effects.

Briefly, acute damage to the heart lead immediately to reduced cardiac performances, in terms of cardiac output, and increased venous pressure due to stasis. Immediately, low cardiac output activates the sympathetic nervous system, while inhibiting the parasympathetic system, which causes enhanced contraction and venous return. Reduced cardiac output also has consequences on renal functions. In the short term, initial liquid retention leads to increased blood volume, which has favorable effects on venous blood, and reduces venous resistence. However, when cardiac damage is extensive, renal blood flow is drastically reduced, and the kidneys stop eliminating liquids. The accumulation leads to edema, prevalently located in the lungs, due to excess of filtration in the pulmonary system. When HF is severe, the compensatory mechanisms of the sympathetic system and liquid retention are not effective (Guyton et al. 2012).

1.2.6.1 Compensated HF

The occurrence of HF implies, by definition, reduced cardiac output. However, this reduction can initially be compensated by a few mechanisms aimed at maintaining the arterial pressure and cardiac output. These processes take advantage of the cardiac reserve and are subdivided into acute and chronic (Damiani 2014).

- *Starling mechanism*

When systolic volume falls, telediastolic volume is necessarily increased. In this situation, the cardiac fibers are more elongated than normal because the heart is fuller. Consequently, the myocardial fibers are longer, the ventricular wall appears to be dilated, and systolic contraction is increased due to the relationship between ventricular volume and pressure (Figure 1.24) (Damiani 2014).

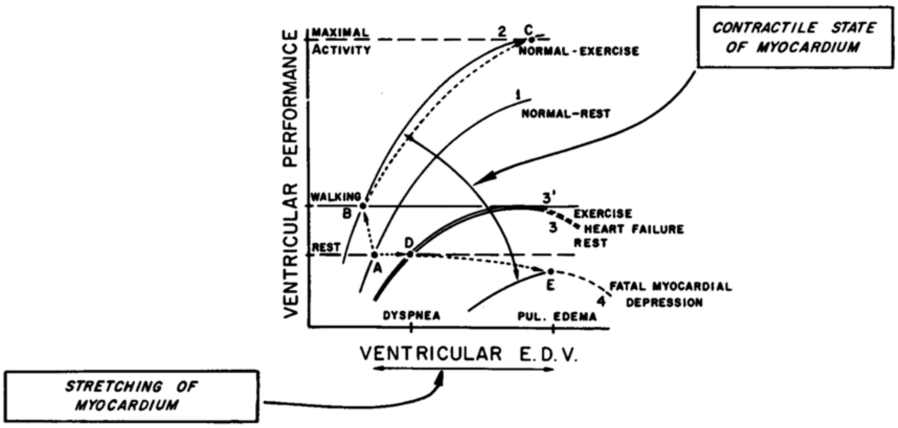

Figure 1.24 Frank-Starling's law. *Increased ventricular end-diastolic volume (EDV) allows initial preservation of ventricular performance (Braunwald, Ross, and Sonnenblick 1967).*

Progressive HF causes flattening of pressure/volume curves, since compensatory mechanisms become ineffective and the heart decompensates (Kemp and Conte 2012).

- *Adrenergic neurohormonal stimulation I: sympathetic system*

Reduction of arterial pressure activates the sympathetic nervous system (SNS), which can induce vasoconstriction and maintain the pressure of vital organs (heart, brain, kidney). Its activity is mediated by β (for heart) and α (for vessels) receptors. It is a fast-compensatory mechanism responsible for increased cardiac frequency and contractility.

The activation of the SNS induces fibrotic ventricular hypertrophy which increases the risk of ischemia due to the elevated request for oxygen and shortened diastolic myocardial perfusion. The phenotype of cardiomyocytes is modified by the shift of myosin from alpha (responsible for fast contractility) to beta (slower but stronger). Release of catecholamines also induces myocardial apoptosis.

The activated receptors might give rise to myocardial toxicity, and overstimulation of the SNS may cause tachycardia, arrhythmias, and receptor downregulation. It also leads to the release of renin (Damiani 2014; Kemp and Conte 2012).

- *Adrenergic neurohormonal stimulation II: renin-angiotensin-aldosterone system*

The production of renin is caused by SNS stimulation, renal hypoperfusion, and reduced re-uptake of sodium in the renal tubules. This enzyme acts on hepatic angiotensinogen to produce angiotensin I which is converted, by the angiotensin converter enzyme (ACE), in angiotensin II. Angiotensin II is a powerful vasoconstrictor. The consequent increase of peripheral resistence causes increased arterial pressure and positively affects cardiac output.

However, angiotensin II also promotes myocardial hypertrophy and stimulates the production of aldosterone, with consequent production of cardiac fibrosis. The latter is responsible for alterations in myocardial conduction properties, which lead to electrical instability and a higher risk of sudden death (Damiani 2014; Jessup and Brozena 2003; Kemp and Conte 2012).

- *Adrenergic neurohormonal stimulation III: activation of natriuretic peptides*

Variations in cardiac blood volume causes stretching of cardiomyocytes and the consequent production of three types of natriuretic peptides: brain natriuretic peptides (BNP, released and found in the ventricles), atrial natriuretic peptides (ANP, released and found in the atria), and c-type natriuretic peptides (CNP, in central nervous system). The main roles of these molecules are to contrast vasoconstriction, support the elimination of water and sodium, and inhibit the secretion of renin and aldosterone (Damiani 2014; Kemp and Conte 2012).

- *Cardiac remodeling*

Cardiac remodeling is a chronic compensatory mechanism, eventually detrimental, implemented to contrast the reduced ejection fraction. It is regulated by mechanical, neurohormonal and genetic factors, and involves the production of new fibrous tissue, with consequent alteration of ventricular size, shape and functionality. However, these modifications are not followed by any increase of cellular components (Damiani 2014; Jessup and Brozena 2003).

In HFpEF, cardiomyocytes are thicker, shorter, and have a higher passive force with respect to HFrEF (Borlaug 2014; Ouzounian, Lee, and Liu 2008).

HFpEF promotes the onset of fibrotic hypertrophy, with concentric remodeling and absence of chamber dilatation (Ouzounian et al. 2008). Myocardial stiffening, typical of HFpEF, is caused by the intrinsic characteristics of the diastolic phase of the heart. Diastole is the result of active and passive actions: the former is responsible for the stress relaxation of the myocardial wall due to myofilament dissociation and calcium uptake, and the latter depends on the viscoelastic relationships between sarcomeres and the ECM, ventricular chambers, and pericardial sac. In HFpEF, relaxation time is reduced and contributes to high pressure in the left ventricle and atrium. The myocardium also stiffens due to the elevated expression of collagen I and III (myocyte growth is coupled with increased connective tissue), shifting of the collagen phenotype, increased of the cross-linking, reduced collagenase, and the unbalanced pattern of matrix metalloproteinases (MMP-1) and their respective tissue inhibitors (Borlaug 2014; Norton et al. 1997; Sharma and Kass 2014; Yamamoto et al. 2002). There is also the influence of infiltration of inflammatory cells and amyloid proteins (Sharma and Kass 2014).

HFrEF induces gradual expansion of the ventricle and its remodeling, with elongation of cardiomyocytes and reorganization of the matrix (Ouzounian et al. 2008). Ventricular dilatation is characterized by increased cardiac volume and mass, whereas the mass/volume ratio is reduced. However, contractile activity is reduced, the geometry of the ventricular chambers is altered, and a secondary mitral insufficiency may develop.

1.2.6.2 Decompensated HF

The progression of HF eventually culminates in a decompensated phase. This transition may be caused by deterioration of the primary underlying pathology, side-effects of compensatory mechanisms, and cardiac remodeling (Damiani 2014). This condition, independently of its cause, represents the final stage of HF.

1.2.7 Diagnostics

The diagnosis of HF may include (Dalla Volta, Daliento, and Razzolini 1996):

1. instrumental examinations:

- electrocardiography is useful to investigate alterations caused by the primary underlying pathology;
- thoracic radiography is used to evaluate the degree of involvement of the lungs;
- echocardiography can evaluate ventricular geometry and contractility;

2. laboratory tests based on biological biomarkers (Sharma and Kass 2014; Zile et al. 2011):
   - BNPs;
   - biomarkers for ECM turnover and fibrosis;
   - renal biomarkers;
   - cardiac troponins;
   - inflammatory biomarkers.

1.2.8 Therapies

Chronic HF requires lifelong clinical care to eliminate or slow down the underlying disease, and improve the quality of life, by treating the signs and symptoms and reducing the risk of death.

1.2.8.1 Pharmacological treatment

The pharmacological treatment for systolic HF includes ACE inhibitors, β-blockers, and mineralocorticoid/aldosterone receptor antagonist. Other recommended therapies include angiotensin receptor blockers, drugs inhibiting the channels of the sinus node, drugs acting on the ATPase pump (inotropic agents), vasodilators, and diuretics.

In the case of diastolic HF, the situation is more complicated. There is no therapy effective in decreasing mortality. In general, diuretics are combined with treatments to reduce the effects of the primary pathology (Guyton et al. 2012; McMurray et al. 2012).

1.2.8.2 Electric therapy

Most of the patients suffering from HF die suddenly. These deaths may be prevented by implants (*e.g.*, implanted cardioverter-defibrillators), with the aim of preventing the risks associated with cardiac arrhythmia.

In those patients presenting severe symptoms, the strategy of cardiac resynchronization is usually followed (McMurray et al. 2012).

1.2.8.3 Surgical treatments

- *Cardiac transplantation*

Heart transplantation is the only definitive treatment for end-stage HF, representing the gold standard and the therapy of choice for this condition.

In June of this year, the United Network for Organ Sharing reported almost 4,000 patients waiting for a new heart in the US, against the 1,300 transplants performed so far in 2018 (UNOS 2018). Despite these tragic data, the number of heart transplants is increasing (Figure 1.25) and reached 5'000 operations worldwide in 2015 (Lund et al. 2017).

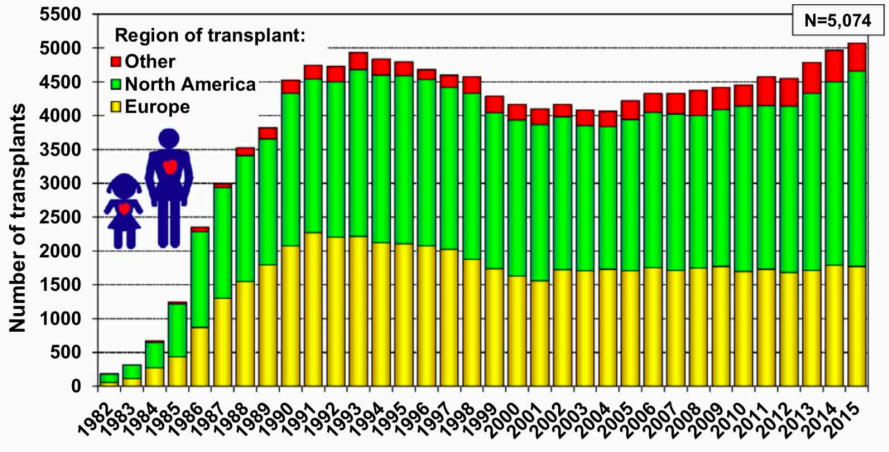

Figure 1.25 Number of adult and pediatric heart transplants from 1962 to 2015. *The number permanently increased from 2000 and is now around 5,000 (Lund et al. 2017).*

Short-term prognosis is very positive, with 75% of survival after 3 years, but it decreases to 50% after 10 years and is around 20% after 20 years (Figure 1.26) (Lund et al. 2017).

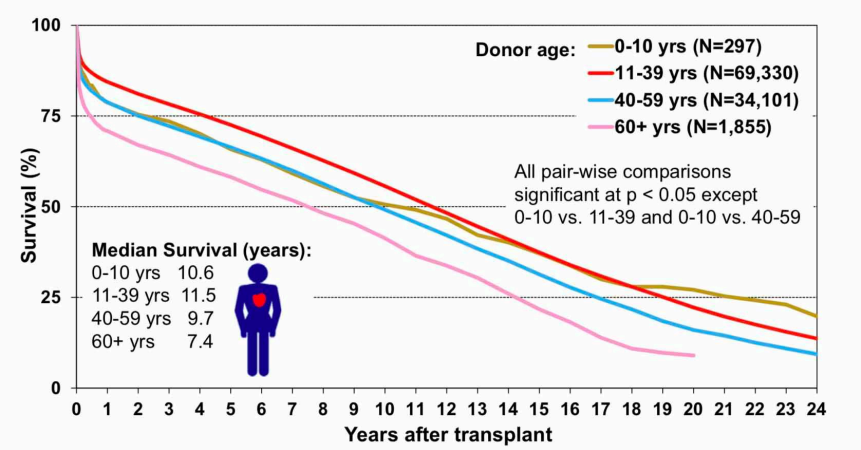

Figure 1.26 Kaplan-Mayer survival curves by donor age group. *Survival of transplanted patients progressively decreases over time (Lund et al. 2017).*

The causes of death are mainly related to graft failure (acute or chronic), infections, and multiple organ failure (Lund et al. 2017). Other complications are induced by preexisting donor pathologies, perioperative ischemic injury of the graft, side-effects of immunosuppressive therapies, neoplasia, and allograft vasculopathy (Halushka, Mitchell, and Padera 2016). In particular, allograft vasculopathy, driven by immunologic mechanisms, is one of the most important factors unfavorably affecting the long-term survival (Costello, Mohanakumar, and Nath 2013; Ramzy et al. 2005).

- *Mechanical circulatory support*

The term "mechanical circulatory support" (MCS) describes a wide class of medical devices adopted to lessen the dramatic deficiency of hearts suitable for transplantation (Figure 1.27).

In general, these devices can be used as bridges to decision (BTD), bridges to myocardial recovery to restore cardiac functionality (BTR), to candidacy for transplantation (BTC), to transplantation in patients with life-threatening conditions (BTT), and as destination therapy for patients not eligible for heart transplant but requiring long-term support (DT) (Timms 2011).

The classification of MCS is generally based on the type of circulatory assistance. When the device supports the function of one of the two ventricles, it is defined as ventricular assist device (VAD) or more in detail left ventricular assist device (LVAD), right ventricular assist device (RVAD), or biventricular

ventricular assist device (BiVAD) in the case of a LVAD and RVAD coupled together. VADs are characterized by different types of outflow (pulsatile or volume displacement and continuous or rotatory pumps) and are subdivided into generations (from first to third) (Timms 2011). These generations are characterized by progressive miniaturization of devices and less use is now made of the pulsatile flow (Spiliopoulos et al. 2012).

End-stage HF is characterized by the irreversible impairment of both ventricles. In such cases, BiVADs can be replaced by substituting the whole heart with a single mechanical pump defined as total artificial heart (TAH; for more detail see, Chapter 2).

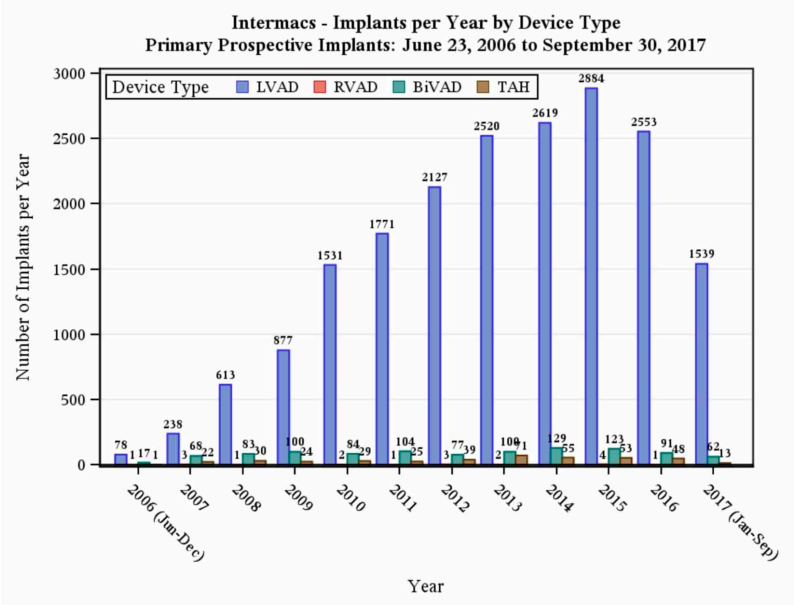

Figure 1.27 INTERMACS implants by year and device. *The number of implanted LVADs significantly exceeds the number of TAHs* (INTERMACS 2016)

2 Total artificial hearts: a journey from mechanical pumps to a novel hybrid membrane to increase the biocompatibility

2.1 Introduction

The requirements for the development of a functioning and efficient TAH have been specified since the very beginning of the mechanical heart era, when the first implantations revealed the weaknesses of these promising devices. A low-weight pump must fit into the human middle mediastinum (enclosed by the lungs, sternum, and coastal ribs) and to move the blood through the two circulations by avoiding hemolysis and ensuring inert contact surfaces to it and the biological environment. Careful choice of the materials involved may play a key role in the blood compatibility of the whole device by influencing the occurrence of thrombosis and embolism. The fully sterilizable TAH should function with minimal production of heat, noise and vibrations. Its design should also carefully considerate fatigue stress, to prevent early deterioration and, thus, the *locus minoris resistentiae* must be eliminated. These basic conditions must be accompanied by opportune physiologic specifications. The device must be composed of two pumps for the right and left hearts, and must guarantee adequate cardiac output, arterial pressure in the aorta and pulmonary trunk, and sensitivity to venous return (Cheng et al. 1977; Hall et al. 1961; Jarvik 1981; Morris and Couves 1971).

The story of TAHs has been told by a huge number of prototypes, sometimes even at the boundaries of science fiction, which have taken place tirelessly from the 1920's. Rollers, pistons and diaphragms have been activated pneumatically, hydraulically and electro-mechanically. Many solutions for transcutaneous drivelines and power supplies have been proposed. Their early failure was due to technical complications and poor implantation performance. Short-term survivals were already a success, considering that, very often, the animals could not be wakened after the surgical procedure. The most severe complications were also due to inadequate pump fitting and supplying (Jarvik 1981). Despite 90 years of research, innovations in this field are still limited and eventually resulted in only one device being admitted to clinical routine.

2.1.1 Historical Overview

The possibility of substituting the heart totally with a mechanical system was hypothesized for the first time in 1812 by J. J. C. LeGallois, a French scientist, philosopher and physician (Hogness and Van Antwerp 1991). While working on the mechanism of respiration, he demonstrated that organ perfusion was fundamental in order to guarantee its viability:

> *"But if the place of the heart could be supplied by injection—and if, for the regular continuance of this injection, there could be furnished a quantity of arterial blood, whether natural, or artificially formed, supposing such a formation possible—then life might be indefinitely maintained in any portion; and consequently, after decapitation, even in the head itself, without destroying any functions peculiar to the brain."* (Le Gallois 1813)

This visionary intuition laid the foundations for the unforeseen collaboration between A. Carrel and C. Lindbergh, respectively surgeon and aviator. Their combined efforts eventually culminated in the invention of the first apparatus for *ex vivo* long-term "culture" of organs (Malinin 1996). The pump-oxygenator was designed to work outside the body but a "Time" reporter improperly baptized it as an "artificial heart" (Ehrlich 1985). This primitive TAH aimed at preserving the organs intended for transplantations or surgical corrections alive by the perfusion of an appropriate oxygenated culture media

and was composed of a sterile single-piece Pyrex glass chamber, as shown in Figure 2.1 (Carrel and Lindbergh 1938; Lindbergh 1935; Lindbergh et al. 1966). The studies of Carrel and Lindbergh contributed to the development of the heart-lung machine.

Figure 2.1 Carrel-Lindbergh perfusion pump. *(A) Cover of TIME magazine of June 1938 showing the two scientists (B) and a picture of the pump (Malinin 1996).*

De facto, the very first attempt to replace the whole heart has been performed some years before in 1928. H. H. Dale and E. H. J. Schuster described a double pump able to bypass the heart when submitted to surgical procedures. However, the device was never used fully implanted as a closed circuit, but only to perfuse lungs or limbs of animals selectively with defibrinated blood drawn from external reservoirs (Dale and Schuster 1928).

In 1929, O. S. Gibbs was able to support the double circulation of heartless cats for a limited period of time (one to three hours). This extracorporeal pump was composed of two different circuits, pulmonary and systemic, with valved rubber sacs hydraulically compressed and released to allow blood flow (Gibbs 1930).

The first intrathoracic device was developed in Russia in 1937 by V. Demikhov, a biology student. The pump was implanted in dogs in the following year (Figure 2.2). Information regarding the materials and working principle is lacking but it was supposed to be made of steel and rubber, equipped with two diaphragms and electromechanically activated by an extracorporeal motor connected to transcutaneous drivelines (Glyantsev, Tchantchaleishvili, and Bockeria 2016). After several years of improvements, the machine was able to maintain a dog alive for five hours (Demikhov 1951).

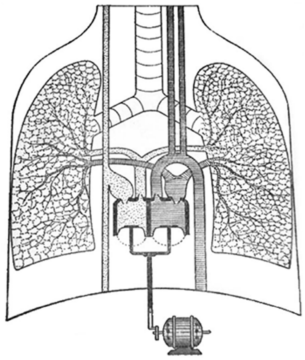

Figure 2.2 First illustration of Demikhov's TAH. *Two pumps were inserted into thoracic cavity, whereas electric motor was extracorporeal* (Glyantsev et al. 2016).

Some years later, Dr. J. H. Gibbon created the first device for extracorporeal circulation with the aim of supporting patients undergoing open heart surgery for pulmonary embolism. The heart-lung machine was first tested in animals (Gibbon 1937) but it was successfully used in humans only from 1954, when the third model was released by IBM in collaboration with the Mayo Clinic (Bartlett 2014).

In 1948, a promising medical student of Yale University, W. H. Sewell, built a TAH for his master's thesis using an Erector® set bought from a toy shop for a total cost of $ 24.90. The pneumatically powered pump was made of glass, polyethylene and silicone, whereas the valves were a toy nose maker (The Eli Whitney Museum and Workshop 2018). The device was used to bypass the right heart of dogs for more than one hour (Sewell and Glenn 1950).

In 1952, collaboration between Dr. F. D. Dodrill from the Harper Hospital in Detroit and the General Motors Research Division produced a mechanical pump (the Michigan Heart) which bypassed the patient's left heart for 50 minutes during surgery for mitral valve repair (Jarvik 1981). This open heart surgery was considered the first success of the use of an artificial device (Stephenson et al. 2002). The artificial pump was made of metal, chromium, rubber and glass (National Museum of American History 2018).

In 1957, Dr. T. Akutsu and Dr. W J. Kolff developed an electromechanically actuated TAH, driven by compressed air and made of polyvinyl chloride. The device maintained a heartless dog alive for 90 minutes (Akutsu and Kolff 1958). Further research performed at the Cleveland Clinic

by Dr. Kolff's group led to new models completely made of polyurethane and electromagnetically activated by oil displacement (Kolff et al. 1959).

In 1958, Dr. D. Liotta started a series of experiments in dogs with a new TAH fabricated of poly(methyl methacrylate) (PMMA, Lucite), polytetrafluoroethylene (PTFE, Teflon), polyurethane, and silk. This series of tests revealed the main functional problems related to the implant of these devices. Implantation and the survival of the animals, even in the short-term, was relatively simple to achieve, but wakening and preservation of circulatory system functionality was not ensured (Liotta et al. 1961).

In 1960, Dr. T. Akutsu started developing a sac-type TAH composed only of a single piece. The initial use of polyurethane was rapidly abandoned, due to frequent embolic events in a dog model (Kolff et al. 1962). In 1964, a modified pump made of Silastic impregnated with Dacron was implanted in calves for a maximum of 5 hours, due to insufficient oxygenation (Akutsu et al. 1963). The following year, the experiments were reproduced in dogs (Akutsu et al. 1964).

The race for the development of a mechanical cardiac substitute rapidly attracted several organizations and agencies. In 1963, the National Aeronautics and Space Administration (NASA) collaborated on the development of a sophisticated control system based on the acquisition of biological signals to regulate pump output. In 1964, the National Institute of Health (NIH) strongly promoted the Artificial Heart Program, aimed at supporting the development of TAHs and mechanical circulatory support devices for long-term clinical use (Institute of Medicine (US) et al. 1991; Jarvik 1981). Starting from 1968, the Atomic Energy Commission (AEC) financed the 10year project of the "atomic heart". The fully implantable pump would have been supplied by the radioactive decay of plutonium-238 isotope for a decade without any need for maintenance or external battery recharging or substitution. Concerns about the possibility of radiation poisoning caused the withdrawal of this project (Jarvik 1981).

In 1969, Dr. D. Cooley implanted the first TAH in human as BTT (Figure 2.3). The device, named "Liotta TAH", was a diaphragm-type pneumatically-activated blood pump made of Dacron-impregnated Silastic and equipped with Wada-Cutter hingeless tilting-disc valves in titanium and polyurethane. The

pump supported the patient for 64 hours and, once explanted, showed the absence of thrombi. However, signs of early hemolysis were reported (Cooley et al. 1969b, 1969a).

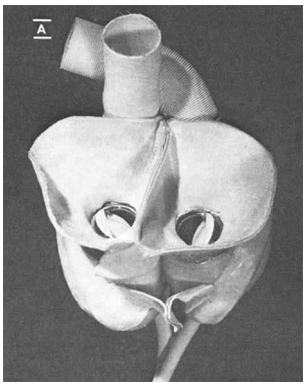

Figure 2.3 Liotta TAH was the first total artificial pump implanted in humans. *Liotta TAH was implanted in 1969* (Cooley et al. 1969b).

In 1967, the relocation of W J. Kolff and C. S. Kwan-Gett to the University of Utah started the development of the device that was to become, today, the only TAH fully approved for clinical use. The device was a diaphragm-type pump pneumatically driven and able to autoregulate cardiac output without any electric control (Kwan-Gett et al. 1969). The Kwan-Gett heart was made of two hemispheric ventricles with an aluminum base, Dacron-reinforced Silastic velour lining the ventricles and the atrial cuffs, the housing and the diaphragm. The valves were different at inflow (polypropylene Hammersmith valves) and outflow tracts (Wada-Cutter valves) (Kwan-Gett et al. 1970). Dacron was added to silicon rubber with the aim preventing detachment of possible clots and promoting the endothelialization of the pump (Jarvik 1981).

In order to improve endothelial coverage, in the 1970's the Department of Artificial Organs of the Cleveland Clinic Foundation introduced the concept of biolized surfaces. The creation of this new family of materials was suggested by the observation that repetitive implants of the same device improved its blood compatibility if the adsorbed protein layer was fixed with cross-linking agents (Imai, Tajima, and Nosé 1971).

In 1977 T. Akutsu and co-workers proposed a new TAH prototype. Moving from the previous sac-type models made of silicon, the novel device was a single-piece pump fabricated to avoid discontinuities in the diaphragm-housing (D-H) junction, and was provided with a wave-shaped base-plate in Avcothane

and Dacron mesh (Cheng et al. 1977). Following several *in vitro* and *in vivo* studies, the device was implanted in humans in 1981 as BTT for 55 hours (Figure 2.4). The one-piece seamless and diaphragm-type pump was made of Avcothane 51 (Avco Everett Corporation, Waltham, MA, USA), a multi-segmented elastomer with good hemocompatibility (Cheng et al. 1977; Nyilas and Ward Jr. 1977). The Akutsu Model III was composed of smooth ventricular chambers and Björk-Shiley prosthetic heart valves, whereas the Dacron used for cuffs and vascular grafts was preclotted with autologous plasma and autoclaved. Explants confirmed the absence of thrombi (Cooley et al. 1981).

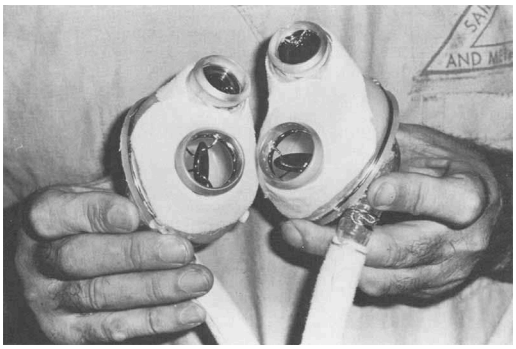

Figure 2.4 Akutsu Model III TAH. *The device was implanted in 1981 (Cooley et al. 1981).*

In the meantime, the Kwan-Gett heart further developed into the Jarvik-3 model. The materials were inherited from the former model with some improvements: the housing and diaphragm were composed of two Silastic layers reinforced with Dacron mesh, the atrial chambers were made of Silastic and Biomer (segmented polyether urethane by Ethicon Inc., Somerville, NJ, USA), and the valves were four Björk-Shiley models (Jarvik et al. 1974). In order to improve the hemocompatibility of the blood-contacting surfaces, textured (Dacron-fibrilized silicone rubber) and smooth (polyurethane) surfaces were tested for the internal lining. However, for most of the animals, the occurrence of thromboembolism caused by turbulence and stagnation regions was reported (Olsen et al. 1975).

The Jarvik-5 model was specifically developed to remove these critical areas, located on the D-H connection. The blood-contacting surfaces were made of polyurethane (Biomer or Avcothane 51), and the diaphragm was made of Dacron mesh embedded in two polyurethane layers. The smooth surface was fabricated by innovative processes by directly pouring the polymers into the ventricles to give a uniform, and single coating without discontinuities (Kessler

et al. 1978). Four Björk-Shiley valves were inserted into a rigid polycarbonate system connecting the Dacron atrial cuffs and vascular grafts (Olsen et al. 1977). The new design reduced the occurrence of thrombosis at the D-H junction (Kessler et al. 1978).

In order to prove the long-term feasibility of Jarvik 7, the pump was tested in animal models between 1976 and 1980. The materials of the atrial cusps, outflow tracts and valves were improved. As regards the diaphragm, the Dacron mesh was removed, and the number of lubricated polyurethane layers was increased from 2 to 4. Unfortunately, all the devices calcified and some cases of endocarditis occurred (Hastings et al. 1981).

Lastly, the final version of Jarvik-7 was successfully implanted in humans in 1982 without any cases of thrombi or infections (Joyce et al. 1983). The selected materials were smooth, segmented polyurethane for the ventricles, Dacron for the cuffs and vascular grafts, and Björk-Shiley valves supported by polycarbonate connectors. The drivelines were in polyurethane and presented velour skin buttons (DeVries et al. 1984).

The device changed several names and companies but maintained its design and most of its original materials. When named CardioWest TAH (Figure 2.5), the rigid parts of the pumps were made of Isoplast (thermoplastic polyurethane, Lubrizol, Orlando, FL, USA), whereas the dome was composed of a solution of polyurethane reinforced by Dacron. The blood-contacting surfaces were created by a single casting and the diaphragm maintained the usual four lubricated layers. As regards valves, Medtronic-Hall pyrolytic carbon monodisc valves were inserted into Isoplast connectors (Slepian et al. 2013). Nowadays it is known as SynCardia TAH, the only TAH which received approval as BTT by the FDA in 2004 and CE mark in 2006, and as DT for humanitarian use by the FDA in 2012 (Torregrossa et al. 2014).

Figure 2.5 CardioWest TAH. *It is the only TAH which received approval as BTT by the FDA in 2004 and CE mark in 2006 (Slepian et al. 2013).*

The end of the 1980's saw to the development of a novel pump specifically designed to reduce the risk of infections associated with percutaneous drivelines (Figure 2.6). AbioMed created a proprietary polyurethane (Angioflex) for ventricles and valves. A solution-casting technique was used to eliminate possible areas of turbulence and stagnation. Although the pump underwent several upgrades over the years, the materials remained unvaried. In the 1990's, the second model of AbioCor started *in vitro* (Yu et al. 1993) and *in vivo* (Kung et al. 1995; Parnis et al. 1994) testing. Long-term experiments on calves gave good results in terms of hemolysis and thromboembolism. The later model was characterized by reduction of pump size (Dowling et al. 2001; Kung et al. 1995). However, further tests evidenced the occurrence of bleeding, respiratory complications, and malposition of power supply which caused the death of several animals (Dowling et al. 2004). In 2001, AbioCor TAH was implanted for the first time in humans in a multicenter trial approved by FDA (Dowling et al. 2003). Unlike the preclinical experience in animals, the early human results reported device failure due to the development of thrombi (Dowling et al. 2000). In 2006, the pumps received FDA approval for humanitarian use as DT (Nosé 2007).

Figure 2.6 AbioCor TAH. *The internal components of AbioCor TAH thoracic unit, controller, batteries, and transcutaneous energy transfer (Dowling et al. 2004).*

The 1993 was crucial year for the development of another TAH, the CARMAT TAH (CARMAT, Velizy, France) (Mohacsi and Leprince 2014). The main innovation of this artificial heart was the internal lining, composed of a hybrid membrane (Figure 2.7). One of the "fathers" of this device was A. Carpentier, a French surgeon and pioneer of bioprosthetic heart valves (Marchand et al. 2001; Poirer et al. 1998). The material involved coupling of glutaraldehyde (GA)-treated bovine pericardium (Neovasc Inc., Richmond, BC, Canada) with a polycarbonate urethane (AdvanSource Biomaterials, Wilmington, MA, USA), following a proprietary process. The non-moving parts of the artificial ventricles were made of expanded polytetrafluoroethylene (ePTFE), the atrial cuffs of bioprosthetic flanges, and Dacron tubes were adopted as arterial grafts (Mohacsi and Leprince 2014). Commercially available Carpentier-Edwards bioprosthetic heart valves (Edwards Lifesciences, Irvine, CA, USA) were placed between ventricles and artificial atria and outflow conduits (Carpentier et al. 2015). The hybrid membrane was tested *in vitro* for blood compatibility (Jansen et al. 2012) and the results were confirmed by *in vivo* studies in calves (Latremouille et al. 2013, 2015). Human implantations took place from 2013. Despite good hemocompatibility allowed avoiding the administration of anticoagulants, the first two patients died because of electronic failure of the device (Carpentier et al. 2015). Two more patients, enrolled in the same feasibility study, survived for 254 and 29 days respectively, and of device-independent causes (Latrémouille et al. 2017). Later, the pivotal study started in 2016, was temporally suspended because of a tragic incident. It was renewed the following year with the aim of extending the implantation to other countries (CARMAT 2018).

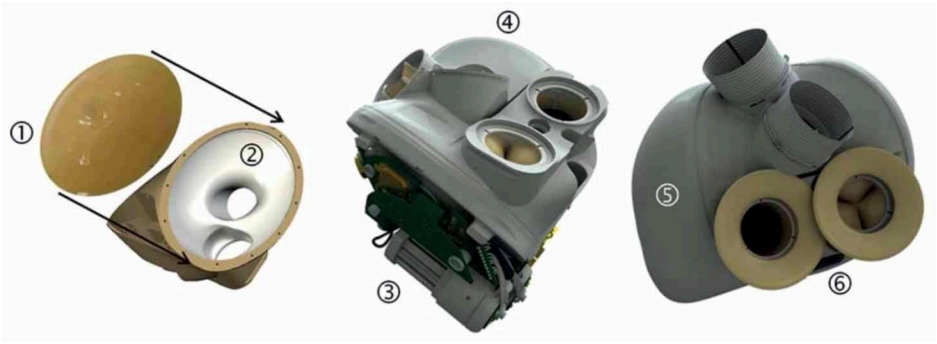

Figure 2.7 CARMAT TAH. *The CARMAT TAH was implanted for the first time in human in 2013 (Jansen et al. 2012).*

2.1.2 Biomaterial-driven issues in TAHs

The fate of any material intended for surgical implantation is not independent of the constituting materials (Dal Sasso et al. *submitted*). At the beginning of the TAH era, the definitions of "biomaterial" and "biocompatibility" has not yet been established. Knowledge of these concepts was very poor and underestimated (Ratner et al. 2004). The materials in question were not specifically developed or biologically investigated for medical applications, but were inherited from the mechanical industry (Akutsu and Kantrowitz 1967; Nosé, Phillips, and Kolff 1968).

Nowadays, the number of implanted TAHs is constantly increasing (INTERMACS 2016) although not without difficulties and obstacles. The nature of blood-material interactions is still not completely explained or predictable. Therefore, the occurrence of hemolysis, thromboembolic events, calcification and infections cannot be completely excluded, despite recent advances in the Medical and Material Sciences.

2.1.2.1 Blood compatibility

The first axiom of hemocompatibility is that the selection of appropriate biomaterials does not automatically imply the compatibility of the whole device (Ratner et al. 2004). This aspect is so wide and complicated that it involves several biomedical variables (from platelet activation to the immune system) and engineering requirements (from design to hemodynamics) (Cumming, Phillips, and Singh 1983; Grasel et al. 1986; Sevastianov et al. 1996).

The only surface known to be fully blood-compatible is the healthy living endothelium lining the lumen of blood and lymphatic vessels. Therefore, early attempts to enhance blood compatibility were performed by trying to reproduce the endothelial layer or promoting the formation of a pseudo-neointima (PNI).

Despite initial hesitation regarding immunological compatibility and the possibility of obtaining a stable coverage in flexible components or in critical flow conditions (Harasaki, Kiraly, and Nosé 1978), several experiments were performed to assess this approach. Endothelial cell seeding on internal pump surfaces proved the suitability of a stable monolayer on artificial materials (Fasol et al. 1987; Szycher et al. 1980). However, clinical implantation was difficult, due to the time necessary to obtain the *in vitro* lining. A fast cell seeding method was introduced to overcome this limitation and turned out to be effective in terms of reduction of platelet adhesion (Jantzen et al. 2011; Noviani et al. 2016).

Most of the strategies adopted in TAH design were based on surface morphology and the use of smooth, textured and biolized surfaces. Smooth surfaces were introduced because of their affinity with the surface properties of the vascular intima. However, practical achievement was very complicated, because these surfaces required advanced manufacturing technologies, because the smallest imperfection might trigger blood activation (Coleman, Lawson, and Kolff 1978). Polyurethanes were selected as preferential materials because of their optimal long-term mechanical properties (durability, elasticity, compliance, and fatigue) and good biological features (biostability, biodurability, biocompatibility, and hemocompatibility) (Zdrahala and Zdrahala 1999). Although these features, polyurethanes did not support cell adhesion or proliferation (Bélanger et al. 2000; Nichols et al. 1981).

Textured surfaces were introduced specifically to promote the formation of a stable PNI. These materials were able to trap absorbed proteins and blood elements in a synthetic mesh and, therefore, to prevent embolic complications and promote autologous endothelialization (Harasaki et al. 1978; Wolf., M., and Boutrand 2012; Zapanta et al. 2006). The irregular surfaces were produced with several strategies, including polyester (Harasaki et al. 1980, 1983; Metman et al. 1987), polyurethane flocked fibrils (Szycher et al. 1980), titanium

microspheres (Dasse et al. 1987; Graham et al. 1990; Whalen et al. 1980; Zapanta et al. 2006), polyurethane casting on a negative flocked molds (Dasse et al. 1987; Graham et al. 1990), and deposition of dissolvable salts on a polyurethane surface. The common *in vivo* outcome was the progressive smoothing of the surfaces due to the deposition of biological molecules and PNI coverage. However, in some cases, flocked fibrils had a negative impact on PNI formation, due to the constant movement caused by the pump (Harasaki et al. 1980). In addition, rupture of the biological layer and the detachment of thrombi were the causes of embolic events (Coleman et al. 1978; Harasaki et al. 1983).

The use of biolized surfaces promoted the introduction of biological components, such as tissues (homologous or heterologous pericardium, *dura mater*, aorta) and coatings (albumin, heparin, skin gelatin) of synthetic materials (polyether-based elastomers) in blood pumps. The surfaces were treated with alcohols and aldehydes to suppress the immune response and create durable layers (Kiraly and Nosé 1974; Nosé, Tajima, et al. 1971). Biolized surfaces developed after 1971 (Nosé, Imai, et al. 1971). In that year, the first biolized pump had ventricles made of formaldehyde-treated bovine pericardium sutured to two aortic valves. The whole heart was dipped into a solution of natural rubber, exploring for the first time the use of hybrid materials in TAHs (Nosé, Tajima, et al. 1971). Endothelialization of these aldehyde-treated surfaces was confirmed in several experiments (Harasaki et al. 1978; Hayashi et al. 1977; Picha et al. 1976). More recently, knowledge of biolized materials was rediscovered in a TAH made of a GA-treated porcine pericardium inserted in a polymer sac (Pebax, Elf Atochem Inc., Paris, France) (Chatel 1996; Chatel et al. 1997) and in CARMAT TAH.

The chemical modifications of the surfaces were introduced as an alternative strategy but, nowadays, they are mainly used in prosthetic vascular grafts and VADs. A heparin coating was applied in the Berlin Heart (Koster et al. 2001), Excor displacement pump (Hetzer et al. 1998) and Incor axial pump (Hetzer et al. 2004) (Berlin Heart, Berlin, Germany). This treatment was called Carmeda BioActive Surface (Carmeda, Upplands Väsby, Sweden) and involved the immobilization of unfractionated heparin on polyurethanes. A diamond-like carbon coating was applied to the titanium alloy of the Sun

Medical centrifugal pump (Yamazaki et al. 1998) (Sun Medical, Nagano, Japan), VentrAssist diagonal pump (Esmore et al. 2007) (VentraCor Inc., Foster City, CA, USA), and Eva Heart radial pump (Snyder et al. 2007) (Sun Medical). This last device was originally coated with polymers (2-methacryloyloxyethyl phosphorylcholine-coated (MCP) (Yamazaki et al. 2002).

2.1.2.2 Calcification

Although calcification is a common problem of cardiovascular devices and affects a wide range of materials, it was never observed nor expected in TAHs before the achievement of long-term animal experiments. The severity of its incidence is closely related to the location of calcific deposits: on non-moving parts it may be a secondary concern, but when present on the valves or pump diaphragm, it could compromise the entire functionality of the device (Harasaki et al. 1979). TAH calcification was in fact responsible for flexural failure, systemic embolization, deformation, abrasion, thinning, and perforation of pump surfaces and linings (Coleman et al. 1981; Turner et al. 1982; Vasku and Urbanek 1995).

Mineralization of blood pumps is mainly defined as dystrophic because it is induced by damaged cells lining the pump (Harasaki et al. 1985; Nosé, Harasaki, and Murray 1981) and/or may be introduced by dead bacterial debris remaining after sterilization (Hughes et al. 1984). It may also be caused by a cell-free mechanism (*i.e.*, surface imperfections, precipitation of calcium phosphate of adsorbed lipids and proteins, direct binding with polymers) and have a primary occurrence.

Most calcific blood pump lesions were located on moving parts or in regions subjected to high cyclic strain, and confirmed that mechanical stress was the main cause (Harasaki et al. 1979; Hughes et al. 1984; Pierce et al. 1980; Turner et al. 1982; Whalen et al. 1980). Pump movements may also cause mechanical disruption of the PNI on textured surfaces and induce calcification due to cell damage (Coleman 1981; Whalen et al. 1980).

Another mechanism of PNI calcification was related to the thickness of the endothelial layer. In the deepest portions, the diffusion of oxygen and nutrients

was limited and cell death released molecules responsible for calcium precipitation and mineralization (Harasaki et al. 1979; Nosé et al. 1981; Turner et al. 1982; Whalen et al. 1980). However, calcification of thinner linings cannot be excluded (Nosé et al. 1981).

On smooth surfaces, wear induced microscopic defects sometimes serving as foci for dystrophic mineralization due to calcified thrombi or injured blood elements (Coleman et al. 1981; Harasaki et al. 1979, 1987; Turner et al. 1982). Nevertheless, the calcification of these surfaces may also have been related to the direct accumulation of calcium-binding proteins or lipids in these discontinuities (Coleman 1981; Coleman et al. 1981; Owen and Zone 1981; Turner et al. 1982). Polyurethane mineralization may also have been caused by their chemical composition and structure. The soft segment can concur by providing binding sites for salt and phosphate deposition (Yang, Zhang, Hahn, King, et al. 1999). In addition, these regions are highly flexible and subject to deformation and loosening, and may adsorb proteins and phospholipids with high affinity for calcium and phosphorus (Imachi et al. 2001).

Biolized surfaces were affected by calcification, like prosthetic valves. Calcification of the deepest layers of the GA-treated bovine pericardium was reported without any cellular reactions (Harasaki et al. 1979). The same study reported calcium deposition on diaphragms, due to the presence of necrotic blood cells.

In order to avoid TAH mineralization, the use of warfarin sodium (Coumadin) was adopted (Hughes et al. 1984; Pierce et al. 1980) because it is an antagonist of vitamin K (Coleman et al. 1981; Mason et al. 1981) and, as an anticoagulant, it prevents the occurrence of thrombi (Nosé et al. 1981). However, it was not effective on textured surfaces (Coleman et al. 1981; Dostal et al. 1990; Mason et al. 1981; Turner et al. 1982; Vasku and Urbanek 1995).

The covalent immobilization of bisphosphonates was proposed for polyurethanes. This strategy was effectively applied to synthetic heart valves (Santos, Cavalcanti, and Bandeira 2012) but not to mechanical pumps.

2.1.2.3 Infections

Infections are one of the most frequent problems in patients on mechanical circulatory support. In particular, the first few days after surgery are the most critical, because patients are more debilitated. Bacteria and, less frequently, fungi can colonize biomaterials with deleterious effects. Biofilm formation provides the possibility of resisting to the host's response and also antibiotics (Costerton, Geesey, and Cheng 1978; Costerton, Montanaro, and Arciola 2005; Khardori and Yassien 1995).

In general, the infections were caused by contaminations of internal chambers and external surfaces, or mediated by percutaneous drivelines (Murray et al. 1983). Biomaterials also played a key role because they were sometimes able to support the adhesion and sequestration of contaminants (Didisheim et al. 1989). Infections affecting internal chambers are the most frequently observed and may lead to occlusions and embolic complications.

In early TAH implants in animals, the incidence of infections was around 52% (Fields et al. 1983) and poor survival was also initially described in humans (McBride et al. 1987). A retrospective study reported the reduction of deaths, with the exception of *Pseudomonas aeruginosa* contamination (Sivaratnam and Duggan 2002). Fungal infections have been acknowledged as severe chronic complications, despite being rare events (Bagdasarian et al. 2009; Firstenberg et al. 2008).

Contamination can be prevented primarily by sterilizing TAHs. Advanced materials were introduced to cover the drivelines and promote skin wound healing in order to avoid driveline contaminations (Hastings et al. 1981). However, when infections affected the internal chambers, blood pumps had to be removed (Didisheim et al. 1989) and pharmacological therapies were administered opportunely (Murray et al. 1983; Sivaratnam and Duggan 2002).

2.2 Aim of the project

Apart from biolized materials, a wide range of biomaterials for tissue engineering applications fall under the definition of "hybrids". Hybrid materials have been studied for urinary applications in terms of electrospun blends of

natural ECM or single purified proteins (*e.g.*, collagen) and synthetic elastomers (Huang et al. 2001; Kwon and Matsuda 2005; Stankus et al. 2008; Stankus, Guan, and Wagner 2004). Several types of polymers and hydrogels have been functionalized with adhesive peptides and growth factors to improve the biocompatibility of the synthetic counterpart (Ren et al. 2015). The ECMs secreted by different cell types seeded on polymeric substrates have been decellularized to yield highly specific and non-immunogenic biological coatings (Bellón et al. 1993; Lee et al. 1993; Schneider et al. 1992).

Synthetic materials have several advantages in terms of controlling and tailoring the physical, chemical and mechanical properties for desired applications. Their good reproducibility and easy workability allow many items with comparable performances to be produced. However, biocompatibility and biostability are not ensured and must be thoroughly investigated. Although progress in Material Science, nowadays it is still impossible to reproduce artificially the sophisticated 3D architecture of natural ECMs. In addition, synthetic materials are often bio-inert. This aspect may be considered as a favorable feature if intended as the inability to elicit an adverse biological response. However, the lack of interactions and recognizability by the biological environment is considered a significant limitation in some applications.

In a different manner, biomaterials like ECM and purified proteins or synthetic peptides have natural biological information, capable of coordinating cell responses by promoting adhesion, differentiation and migration. Moreover, their peculiar structural and functional characteristics may regulate constructive remodeling of tissues. With respect to other solutions, the use of biologically-derived materials is usually associated with enhanced biocompatibility. However, their mechanical properties are often suboptimal and may degrade over time and as a result of tissue remodeling itself.

In this doctoral project, a hybrid strategy was designed in order to overcome the limitations of both approaches and to increase the biocompatibility of TAH internal linings. Theoretically, this strategy allows the creation of unique and completely new materials with customizable mechanical and physicochemical properties, enriched by biological activity and recognizability. The aim of this project is therefore to assess whether the use of decellularized pericardial scaffolds coupled with a medical-grade

polyurethane may be an optimal choice for lining blood-contacting surfaces in mechanical pumps.

The following objectives were investigated:

- Decellularization of bovine pericardium by TriCol protocol;
- Assessment of ECM preservation (histology, immunofluorescence, acquisition of second harmonic generation and two-photon excited fluorescence signals) and quantification of ECM reorganization;
- Assembly of the hybrid membrane;
- Evaluation of the infrared fingerprint and surface microanalysis of the new material;
- *In vitro* assessment of cytotoxicity by MTS reduction, LDH release and Live/Dead staining.

2.3 Materials and methods

The following abbreviations will be used: NBP for native bovine pericardium and DBP for decellularized bovine pericardium.

2.3.1 TriCol decellularization of pericardial tissues

NBP samples were harvested from 8-month-old calves at a local slaughterhouse (Bugin Macellazione Carni, Santa Maria Di Sala, Venezia) and transferred to the laboratory in cold phosphate buffered saline (PBS; 137 mM sodium chloride, 2.7 mM potassium chloride, 10 mM disodium phosphate, 10 mM potassium phosphate, all supplied by Sigma-Aldrich, MO, USA). Within 2 hours of animal death, the pericardia were cleaned by removal of retrosternal fat and surrounding connective tissues and briefly rinsed in cold PBS.

Tissues were treated according to the TriCol procedure, a method proposed for the first time in 2003 to decellularize aortic valves (Spina et al. 2003). The protocol was carried out by constant agitation and cycles of 8-hour-long steps. Briefly, inactivation of cell proteases was followed by alternating hypo- and hypertonic solutions, combined with increasing concentrations of Triton X-100 (0.1-1%, Sigma-Aldrich). Cell components were extracted from the tissue with

10 mM bile salt anionic surfactant sodium cholate (Sigma-Aldrich). Incubation with non-specific endonucleases allowed the complete removal of DNA debris (1500 U/cm^2 Benzonase® Nuclease, Sigma-Aldrich).

2.3.2 Assessment of decellularization

NBP and DBP samples of 1 cm^2 were fixed in 4% (w/v) paraformaldehyde (PFA, PanReac AppliChem, Chicago, IL, USA) for 20 minutes at room temperature and in dark, and then dehydrated overnight in 20% (w/v) sucrose (Sigma-Aldrich) solution in PBS at 4° C.

Tissues were embedded in a 1:1 solution of O.C.T. (Optimal Cutting Temperature Compound, Tissue-Tek, Alphen Aan den Rijn, The Netherlands) and 20% sucrose. Lastly, they were snap-frozen in isopentane (Sigma-Aldrich) and liquid nitrogen before being stored at -80 °C. Cryosections of 5 µm were prepared for subsequent evaluation on a cryostat (Leica Biosystems, Wetzlar, Germany).

2.3.2.1 Histological analysis

The effectiveness of the decellularization protocol was assessed histologically by evaluating the general tissue architecture, collagen pattern, status of the alcianophilic elements, and elastin distribution. To this aim, several staining techniques were used: Hematoxylin and Eosin (H&E), Mallory's trichrome (MT), Alcian Blue (AB), and Weigert-Van Gieson (VG) (all purchased from Bio-Optica, Milan, Italy).

Images were acquired by a light microscope (Olympus BX51, Olympus Corporation, Tokyo, Japan) equipped with a Nikon Eclipse 50i camera and NIS-Elements D 3.2 software (Nikon Corporation Shinagawa, Tokyo, Japan).

2.3.2.2 Two-photon microscopy combined with immunofluorescence assay

In order to evaluate the maintenance of the two main components of the pericardial ECM (collagen I and elastin), cryosections of NBP and DBP tissues were examined under a house-made two-photon microscope (TPM), as reported

previously (Filippi et al. 2018). In detail, a label-free technique was used to detect the second harmonic generation signal (SHG) produced by those tissues in which non-centrosymmetric components were present (mostly collagen I in our case) and two-photon excited fluorescence (TPEF) of elastin.

However, as the main components of the basal lamina cannot be observed directly with this technique, their integrity was evaluated by indirect immunostaining techniques combined with TPM. Laminin, collagen type IV and heparan sulfate were selectively detected and located together with collagen I SHG and elastin TPEF signals. Primary antibodies used were the rabbit polyclonal anti-laminin (1:100, Z0097, Dako, Santa Clara, CA, USA), rabbit polyclonal anti-collagen IV (1:100, ab6586, Abcam), and rat monoclonal anti-heparan sulfate proteoglycan (1:50, MAB1948P, Millipore, Burlington, MA, USA). Rhodamine (rhod)-conjugated anti-rabbit and anti-rat were used as secondary antibodies (1:100 goat anti-rabbit IgG antibody, AP132R, Millipore and 1:100 goat anti-rat IgG antibody, AP136R, Millipore, respectively). Primary and secondary antibodies were diluted in a blocking buffer of 1% (w/v) bovine serum albumin (Sigma-Aldrich) in PBS.

Nuclei were counterstained with Hoechst (Sigma-Aldrich).

Images were acquired at an excitation wavelength of 1,200 nm for the SHG signal and 800 nm for TPEF and the secondary antibody fluorophores. A fixed resolution of 1,024×1,024 pixels and accumulation of 120 frames were adopted.

2.3.2.3 Evaluation of the ECM reorganization

TPM was also used as a preferential tool to perform quantitative evaluation of the integrity and reorganization of collagen and elastin after decellularization.

Analyses were carried out on 0.8 cm circular punches (disposable biopsy punches from Kai Medical, Kai Corporation, Tokyo, Japan) of NBP and DBP samples. The *serosa* and *fibrosa* layers were both analyzed at two depths (z): on the surface (0 µm) and on a deeper plane (about 20 µm). Before the evaluation, samples were immobilized by a thin layer of 4% (w/v) low melting agarose solution prepared in PBS (Sigma-Aldrich) in plastic embedding devices (Bio Optica), as previously described (Filippi et al. 2018). In order to preserve cell viability during transport from the slaughterhouse to the laboratory, NBP

tissues were maintained in warm cell culture medium (Dulbecco's modified Eagle's medium, DMEM, Sigma-Aldrich). Images were acquired no later than the day of harvest.

Quantification of ECM organization was performed according to three parameters previously described (Rezakhaniha et al. 2012) and evaluated on RAW uncompressed files by acquiring nine images for each group (n=3). The first was coherency, a measure of the local dominant orientation in selected ROIs of NBP and DBP samples. In order to obtain this parameter, an ImageJ (Schindelin et al. 2012) plugin, *i.e.*, OrientationJ (Sage 2018), was used. Coherency is defined as the ratio between the difference and the sum of the largest (λ_{max}) and smallest (λ_{min}) eigenvalues of the structure tensor defined for every pixel:

$$C=\frac{\lambda_{max}-\lambda_{min}}{\lambda_{max}+\lambda_{min}} \qquad [Ø]$$

By definition, this value falls between 0 and 1 and indicates the absence (isotropy) or presence (anisotropy) of a dominant orientation, respectively.

The second value considered was straightness parameter (P_s), providing indications about the waviness of fibers at zero-stress state by the ImageJ plugin NeuronJ (Meijering et al. 2004). P_s is defined as the ratio between the distance of two points of a collagen bundle (L_0) and the corresponding length (L_f):

$$P_s=\frac{L_0}{L_f} \qquad [Ø]$$

Values of P_s approaching 1 are indicative of straighter fibers.

The last parameter was the mean thickness (t) of the collagen bundles, calculated as the average of the thicknesses of three bundles for each acquired image.

2.3.3 Assembly of the hybrid membrane

The HM were prepared by a solution casting and solvent evaporation. After decellularization, 6 cm^2 of DBP tissues were washed twice for 30 minutes in deionized water and gently dried with Whatman filter paper (Sigma-Aldrich).

Samples were then placed on the *serosa* and fastened in a customized aluminum frame (Figure 2.8). A thin layer (about 4 ml) of liquid poly(carbonate) urethane was poured (ChronoFlex AR, CF, AdvanSource Biomaterials, Wilmington, MA, US) on the free side of the tissue (*fibrosa*). In more detail, this medical-grade polyurethane was supplied as a 22% (w/v) solution in N,N-dimethylacetamide (DMAc). The hybrid membranes (HM) were dried for 24 hours at 40°C in a vacuum oven under aspiration (Raypa, Barcelona, Spain).

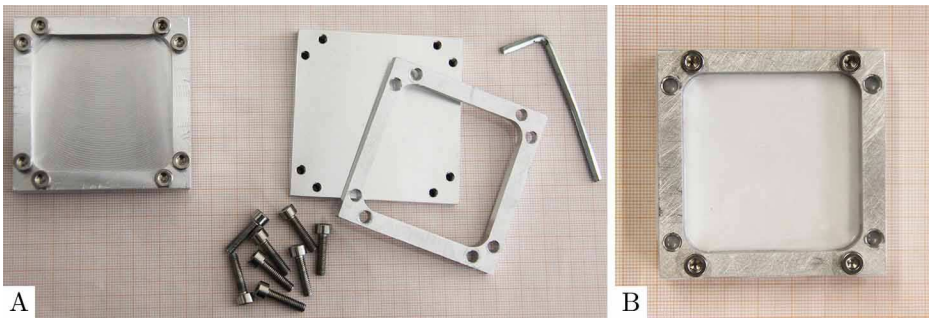

Figure 2.8 Aluminum frame used to assemble HM. *The frame comprises a lower component to support pericardium and an upper element to border liquid polyurethane (A). DBP was fastened to the frame before polymer was poured (B).*

2.3.4 Assessment of the hybrid membrane

2.3.4.1 Fourier transform infrared spectroscopy

Diffusion of the liquid polymer through the biological tissue was evaluated by FTIR-ATR (Fourier Transform Infrared Spectroscopy by Attenuated Total Reflectance).

FTIR spectra were acquired on FTIR spectrometer equipped with ATR accessory and a diamond/ZnSe crystal (Perkin-Elmer, Norwalk, CT, USA). A built-in automatic algorithm was used to correct the CO_2/H_2O vapor spectra from the data. DBP samples were equilibrated for 3-4 hours in heavy water (deuterium oxide) in order to reduce the effect of normal water on the spectral resolution. Water content was not a concern for HM and CF, because the former was dried during fabrication and the latter, being a polyurethane, does not contain water. Spectral analysis was carried out with Omnic^{TM} Spectra Software (Thermo Fisher Scientific, Waltham, MA, USA).

2.3.4.2 Scanning electron microscopy

The morphology of the HM surface was compared with two controls (DBP and CF) in a scanning electron microscope (SEM) (JEOL JSM-6490, Peabody, MA, USA).

DBP tissues were previously fixed in Karnovsky solution (8% (w/v) PFA, 10% (v/v) GA (50%), and 40% (v/v) cacodylate buffer (0.2 M), pH range 7.2-7.4; all reagents were supplied by Sigma-Aldrich) at +4°C in the dark. Before analysis, the tissues were rinsed in PBS and dehydrated through ascending ethanol solutions (70%, 80%, 90%, 100%) for 10 minutes. They were then dried under vacuum in a critical point dryer, in order to substitute ethanol with liquid CO_2 and avoid tissue damage. HM and CF did not undergo fixation, dehydration, or drying because they were already dried (see Section 2.3.4.1). Lastly, DBP, HM and CF samples were sputter-coated with gold and palladium to create a conductive layer on the sample surfaces. Images were acquired in low vacuum mode at 20 kV.

2.3.4.3 Cytocompatibility assessment

In vitro cytotoxicity tests by direct contact were carried out according to International Standard Organization guidelines 10993-5 (International Organization for Standardization 2009). The degree of cytotoxicity induced by the test materials was evaluated with qualitative and quantitative analyses.

2.3.4.3.1 Disinfection protocol

DBP, CF and ML were cut into 0.5 x 1.5 cm size and disinfection was carried out with a cocktail of antibiotics (0.05 mg/ml Vancomycin, 0.24 mg/ml Cefoxitin, 0.08 mg/ml Gentamycin, Sigma-Aldrich) and antimycotic (0.025 ml/ml Amphotericin B, Gibco, Thermo Fisher Scientific, Waltham, MA, US) in PBS, as previously reported (Fidalgo et al. 2017).

After disinfection, samples were secured on the bottom of tissue culture-treated polystyrene 6-well plates (Costar®, Corning Incorporated, Corning, NY, USA) with sterile strips (Steri Strip, 3M, Maplewood, MN, US).

2.3.4.3.2 Selection of cell types and controls

Two types of human cells were used for static seeding in tissue culture-treated 6-well plates (Costar®, Corning Incorporated). Human bone marrow-derived mesenchymal stem cells (hBM-MSCs) and human umbilical vein ECs (HUVECs) were seeded at 150,000 cells/6-well (approximately 15,800 cells/cm^2) and cultivated in standard conditions (37°C, 100% humidity, 5% CO_2). Minimum Essential Medium Eagle (MEMα, Sigma-Aldrich) was supplemented with a 1% penicillin-streptomycin cocktail (Sigma-Aldrich), 1% L-glutamine (Sigma-Aldrich) and 20% of fetal bovine serum (FBS, Sigma-Aldrich) to culture hBM-MSCs; complete endothelial growth medium was used for HUVECs (Lonza, Walkersville, MD, USA).

Polystyrene, the standard plastic support for cell culture, and cyanoacrylate (Super Attak, Loctite, Düsseldorf, Germany), to elicit high cytotoxicity, were used as positive and negative controls, respectively.

2.3.4.3.3 Qualitative classification of cytotoxicity

The effects of cytotoxicity were classified by qualitative grading (from 0 to 5) as reported in ISO 10993-5 (International Organization for Standardization 2009).

Morphology, vacuolization, detachment, and lysis of cells in contact with test materials were evaluated microscopically at 24, 48 and 72 hours. Three days after seeding, cells were fixed in 4% (v/v) PFA and stained with Giemsa's azur eosin methylene blue solution (Merck, Darmstadt, Germany). Images were acquired in the bright field on a fluorescent microscope (Olympus Corporation) equipped with a Nikon Eclipse 50i camera and NIS-Elements D 3.2 software (Nikon Corporation Shinagawa, Japan).

2.3.4.3.4 Quantification of cytotoxicity

Cytotoxicity was quantified by means of two types of colorimetric assays, based on the activity of lactate dehydrogenase enzyme (LDH) and reduction of 3-(4,5-dimethylthiazol-2-yl)-5-(3-carboxymethoxyphenyl)-2-(4-sulfophenyl)-2H-tetrazolium compound (MTS). Viability was also confirmed by staining the cells with fluorescent dyes to distinguish living or dead cells.

- *LDH activity*

LDH is a cytosolic enzyme released when the cell membrane is damaged. Therefore, when it is dissolved in the culture media, it can be quantified and used as a directly proportional measure of cytotoxicity (Figure 2.9).

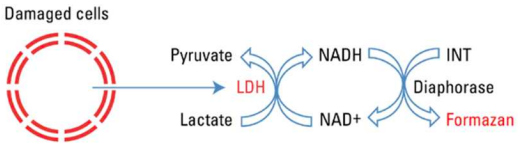

Figure 2.9 LDH activity. *Presence of extracellular LDH indirectly promoted reduction of formazan through coupled enzymatic reactions (Thermo Scientific data sheet).*

Quantification was carried out following Pierce LDH cytotoxicity assay kit (Thermo Scientific). Absorbance at 490 nm was measured on a microplate reader (Bio-Rad, Hercules, CA, USA). The mean value of the non-influence control (NIC, cells seeded onto polystyrene) was considered as the baseline for cytotoxicity, *i.e.*, the reference production of LDH in normal condition, and was subtracted from the values acquired for HM, DBP and CF samples. The resulting values were normalized by high-influence control (HIC, cells seeded on the glue) (Cebotari et al. 2010). It was thus possible to obtain a percentage index ranging from 0 (absence of cell toxicity) up to 100 (highest level of cell toxicity):

$$\%\ \text{of cytotoxicity} = \frac{absorbance_{\text{test material}} - absorbance_{\text{NIC}}}{absorbance_{\text{HIC}} - absorbance_{\text{NIC}}} \cdot 100$$

- *MTS reduction*

This colorimetric assay is based on the reduction of MTS tetrazolium compound into formazan: its amount is directly proportional to the number of living cells (Figure 2.10).

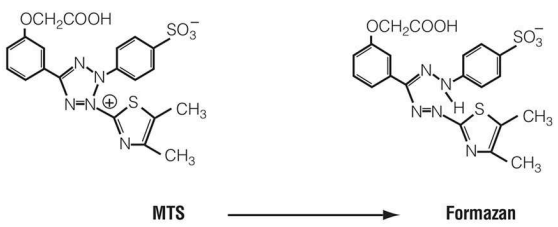

Figure 2.10 Reduction of MTS into formazan. *Reduction of MTS tetrazolium compound into formazan is performed by mitochondrial enzyme of living cells (Promega data sheet).*

The test was carried out with the CellTiter 96 aqueous solution cell proliferation assay (Promega, Madison, WI, USA). After incubation, the solution was loaded in triplicates in a 96-well plate (Sarstedt, Nümbrecht, Germany) and absorbance at 490 nm was measured on a microplate reader (Bio-Rad).

- *Live/Dead staining*

In order to evaluate cell viability, Live/Dead fluorescent-based staining was performed according to the manufacturer's protocol (Live/Dead viability/cytotoxicity kit for mammalian cells, Molecular Probes, Eugene, OR, USA).

Briefly, the two dyes, calcein AM and ethidium homodimer-1, are non-fluorescent before coming into contact with cells. Calcein is enzymatically converted into its fluorescent form by intracellular esterase and is retained by living cells, producing a green signal (excitation 495 nm, emission 515 nm). Instead, ethidium homodimer can penetrate when the plasma membrane is damaged and binds the nucleic acids of dead cells, producing a red signal (excitation 495 nm, emission 635 nm).

DBP, HM and CF samples were seeded in triplicate with hBM-MSCs (15,000 cells/cm^2) and HUVECs (50,000 cells/cm^2) in tissue culture-treated 24-well plates (Costar®, Corning Incorporated). Images were acquired at 24, 72 hours and 7 days by TPM.

2.3.4.4 Complement activation

Activation of the complement system was evaluated with the Complement Convertase Assay Kit (HaemoScan, Groningen, The Netherlands), accordingly to ISO 10993-4 (International Organization for Standardization 2017).

Samples of DBP, HM and CF were cut into 1.0 x 0.5 cm rectangles with an area of 0.5 cm^2. Low-density polyethylene (LDPE, Ref. 1), polydimethyl-siloxane (PDMS, Ref. 2) and medical steel (MS, Ref. 3) were supplied by the manufacturer and used as references for low, medium and high activation, respectively. Test and reference materials were incubated with porcine plasma in order to allow the adsorption of complement factors to the surface. The formation of convertases on biomaterial surfaces promoted conversion of the

complement convertase-specific chromogenic substrate. Quantification of the cleavage of the substrate was measured by acquiring optical density at 405 nm (Labsystem Multiskan Plus Microplate Reader, LabX, Midland, ON, Canada).

2.3.5 Statistical analyses

All data were processed and analyzed with Prism (GraphPad Software, CA, USA). Results are reported as mean ± standard deviation. Groups of data were compared by variance analyses (one- or two-way ANOVA). Significant level was set at 5%. More details about settings are given in the graph captions.

2.4 Results

2.4.1 Assessment of bovine decellularized scaffolds

2.4.1.1 Histology

Histological analyses showed maintenance of general ECM histoarchitecture, in which the two layers composing the parietal pericardium, *i.e.*, *serosa* and *fibrosa*, were fully preserved after TriCol. The major blood vessels supplying the NBP tissues maintained their patency in DBP scaffolds, as the whole panel of Figure 2.11 shows. In the native *fibrosa*, the epipericardial connective tissue, rich in fatty cells and neural components, was mechanically removed by the preliminary cleaning phase and was not present after decellularization (Figure 2.11E-H and M-P).

In H&E staining, the bulging nuclei of the mesothelial cells lining the *serosa*, and those of the other cells populating the tissue, such as fibroblasts, adipocytes and vascular components, were completely removed in DBP tissues, as demonstrated by the absence of basophilic structures (Figure 2.11A, D, I, M).

MT demonstrated the preservation of the distinct wavy pattern of collagen bundles, specifically stained by aniline blue, in DBP samples (Figure 2.11B, F, J, N).

The staining of sulfated and carboxylated mucopolysaccharides and sialomucins (AB stain) exhibited a general slight discoloration, probably due to the loss of alcianophilic components (Figure 2.11C, G, K, O).

The elastic components of the tissue seemed to be unaffected by TriCol, as demonstrated by VG stain. Elastin maintained its parallel distribution to the collagen bundles, whereas blood vessels showed intact *elastic laminae* (Figure 2.11D, H, L, P).

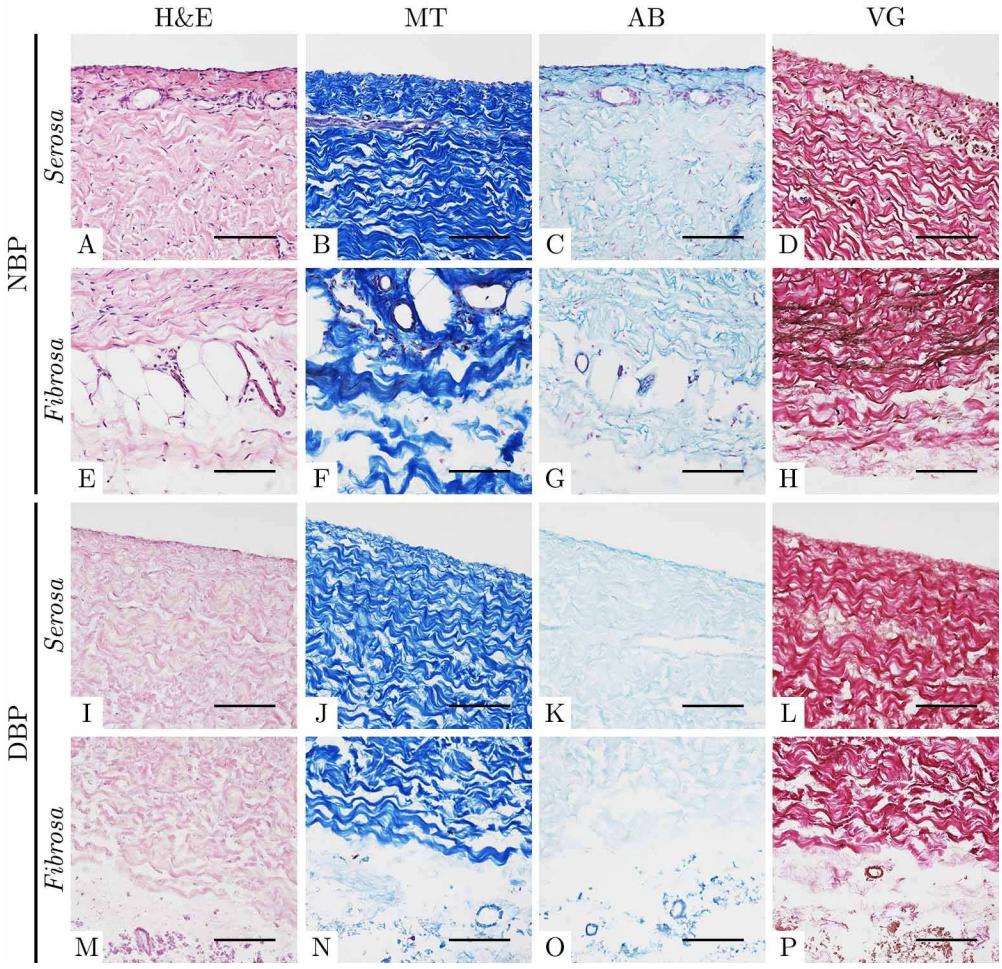

Figure 2.11 Histological comparison of NBP and DBP tissues. *Tissue structure, collagen bundle, and elastic components of NBP (A, B, D, E, F, H) appeared well-maintained in DBP (I, J, L, M, N, P). Decellularization probably caused a slight decrease in alcianophilic components (K, O) with respect to native samples (C, G). Scale bar = 100 μm.*

2.4.1.2 TPM and TPM-combined immunofluorescence analyses

The preservation of main pericardial ECM components, *i.e.*, collagen type I and elastin, was confirmed by the label-free and highly specific acquisition of

SHG and elastin TPEF signals (Figure 2.12). The collagen bundles maintained their waviness and seemed more compact after decellularization (Figure 2.12C, G). The strong elastin TPEF signal appeared unaltered (Figure 2.12D, H).

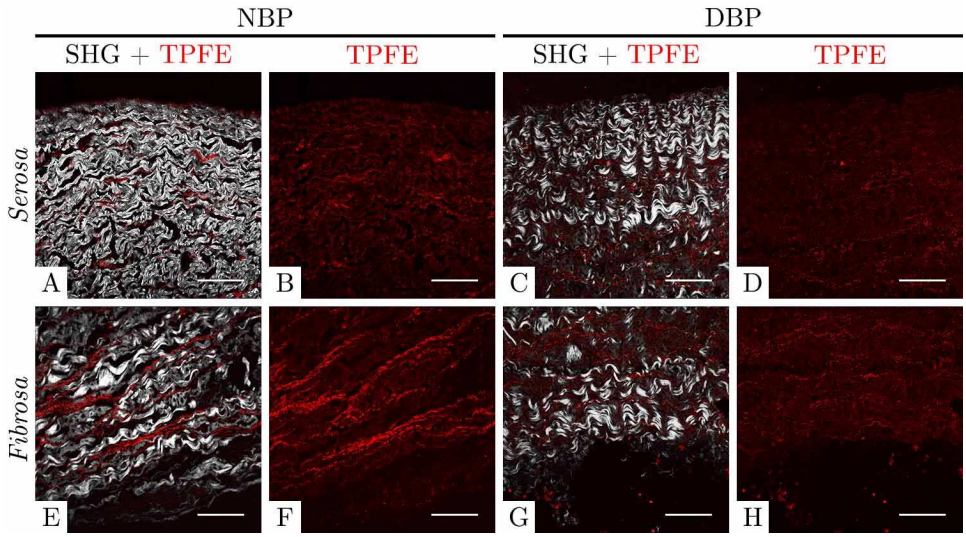

Figure 2.12 Comparison of two ECM main components between NBP and DBP cryosections. *Label-free images of NBP (A, E) and DBP tissues (C, G) showed maintenance of collagen I and elastin. TPEF signal of elastin is shown in (B, F) for NBP and in (D, H) for DBP tissues. Scale bar = 100 μm.*

The selective location of laminin (Figure 2.13C and G), collagen IV (Figure 2.13K and O) and heparan sulfate (Figure 2.13S and W) demonstrated maintenance of the mesothelial and vascular basal laminae.

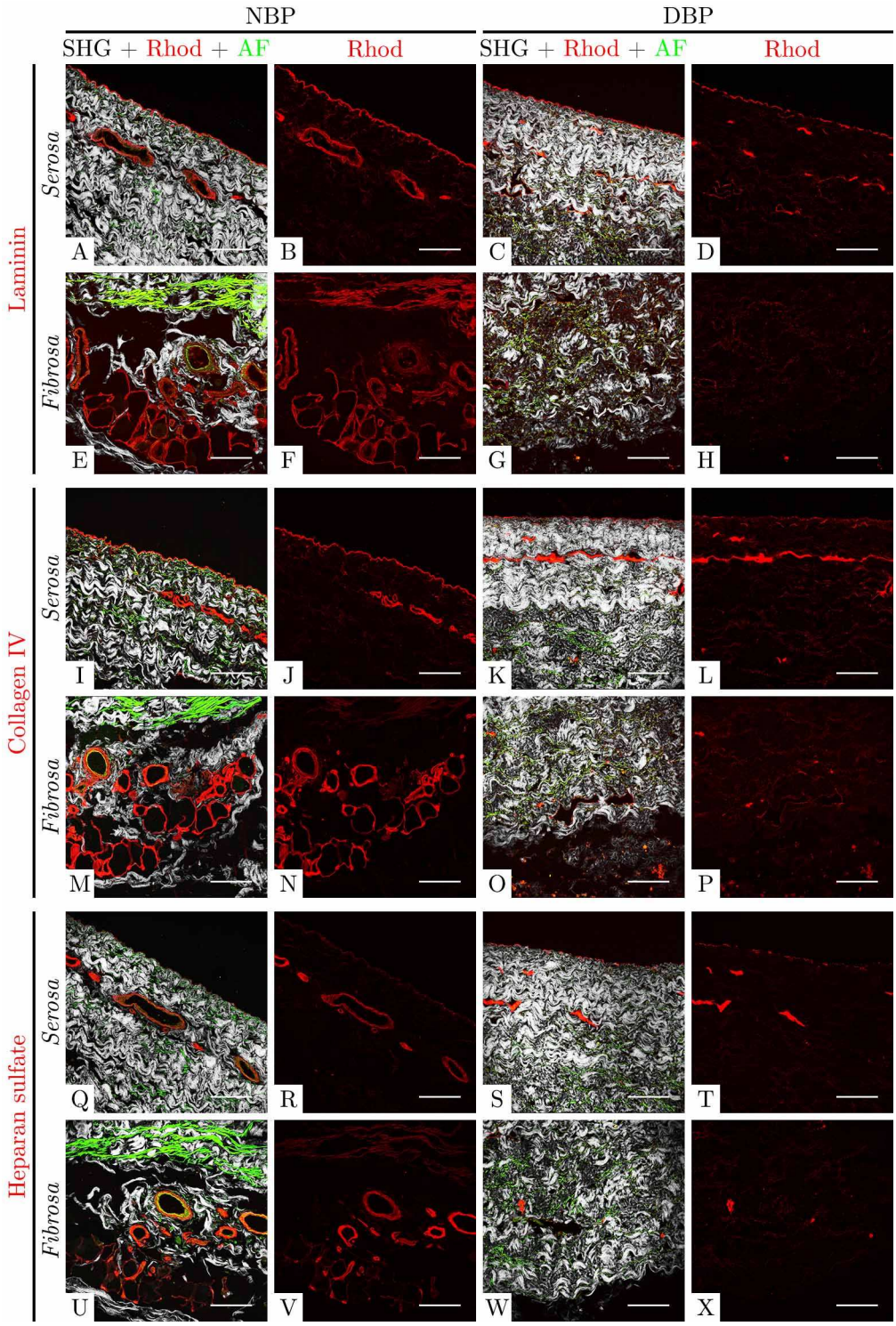

Figure 2.13 Comparison of basal lamina main components between NBP and DBP cryosections. *Laminin (A, B, E, F), collagen type IV (I, J, M, N) and heparan sulfate (Q, R, U, V) appeared well-preserved in submesothelial region of pericardial serosa and subendothelial layer of blood vessels after TriCol (C, D, G, H; K, L, O, P; and S, T, W, X; respectively). Scale bar = 100 μm.*

In addition, Hoechst staining confirmed the complete removal of nucleic acids (Figure 2.14).

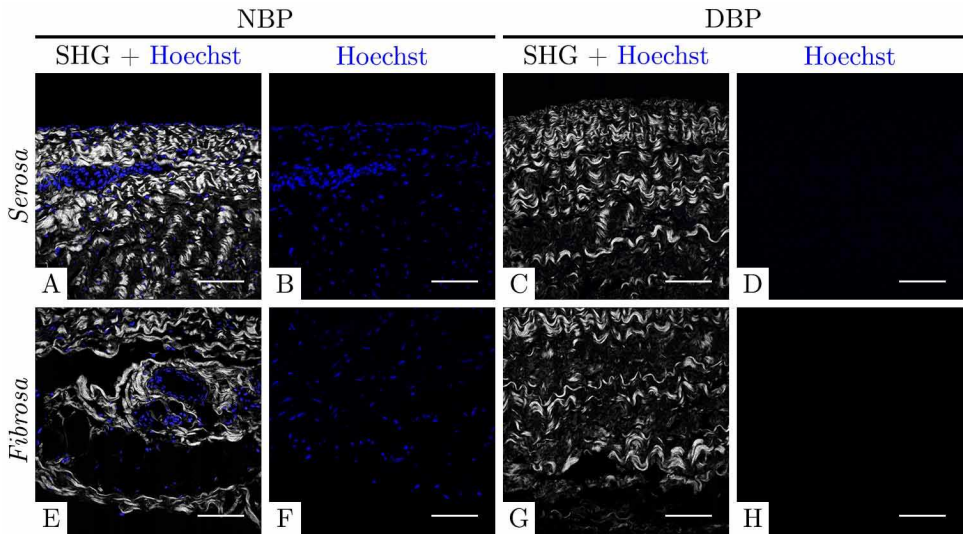

Figure 2.14 Comparison of Hoechst staining between NBP and DBP cryosections. *After TriCol decellularization, there was no Hoechst signal in DBP samples (C, D, G, H) with respect to the NBP tissues (A, B, E, F). Scale bar = 100 µm.*

2.4.1.3 TPM analyses

TPM analyses of NBP and DBP tissues confirmed crimped arrangement of collagen type I. The *serosa* bundles were smaller and more organized (Figure 2.15A, C, E, G) with respect to the *fibrosa*, where larger and looser structures were visible (Figure 2.15I, K, M O). Apparently, the deeper layers (z = -20 µm in Figure 2.15E and G for *serosa* and M and O for *fibrosa*) were more tightly arranged with respect to the surface (z = 0 µm in Figure 2.15A and C, I and K, respectively). The *fibrosa* was in fact also decorated with single dispersed fibers on the outermost part. In general, *serosa* collagen I appeared unaltered, whereas the *fibrosa* showed reorganization and had a more compact aspect.

The elastic fibers of DBP scaffolds were visible, and were parallel with collagen I (Figure 2.15D, H, L, P) and maintained the strong TPEF of native tissues (Figure 2.15B, F; J, N).

In addition, excitation at 800 nm revealed the presence of cellular nuclei on the surface of NBP tissues (Figure 2.15B, J). As expected, this signal was completely absent in DBP samples, where only elastin was visible (Figure 2.15D, L).

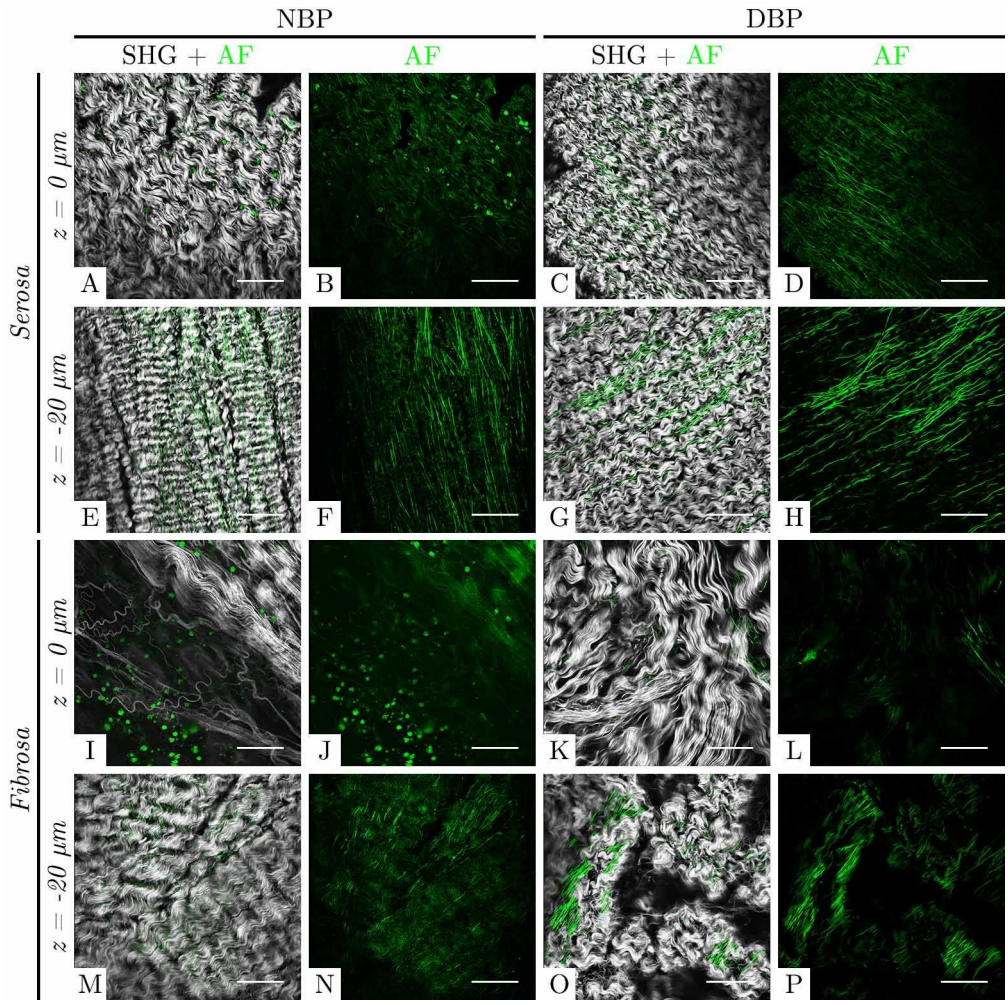

Figure 2.15 TPM images of NBP and DBP samples at different depths. *The highly organized wavy collagen pattern of native serosa (A, E) was maintained in decellularized tissues (C, G); the native fibrosa (I, M) underwent reorganization visible especially on sample surfaces (K, O). The strong elastin signal appeared unaltered (D, H, J, N) with respect to controls (B, F, L, P). Cell nuclei were visible on native samples (B, J) but not on decellularized (D, L). Scale bar = 100 µm.*

Collagen I surface reorganization was significantly increased on *fibrosa* coherency ($p = 0.0060$) but was unaltered in *serosa* (Figure 2.16A). Conversely, the coherency of elastin was not modified by decellularization (Figure 2.16B).

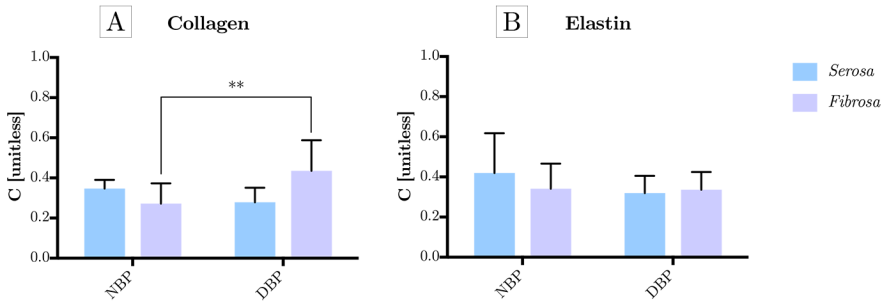

Figure 2.16 Quantification of coherency of collagen type I and elastin in NBP and DBP samples. *After decellularization, coherency of collagen in fibrosa statistically increased, but it was unaltered in serosa (A). Coherency of elastin did not vary (B). Two-way ANOVA, Sidak's multiple comparison test, ** $p < 0.01$.*

In addition, the removal of cellular components caused a statistical increase in the straightness parameter on the *fibrosa* ($p < 0.05$) (Figure 2.17A). Bundle thickness was unaltered on both layers (Figure 2.17B).

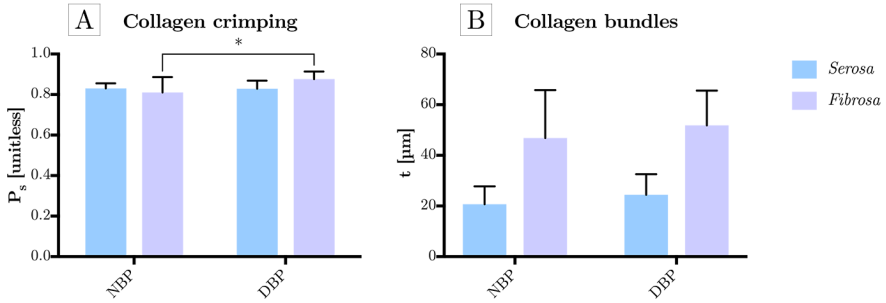

Figure 2.17 Quantification of collagen crimping and bundle thickness in NBP and DBP samples. *TriCol induced stretching of collagen bundles on fibrosa; no alterations were evident on serosa (A). Thickness of collagen bundles was unaltered (B). Two-way ANOVA, Sidak's multiple comparison test, * $p < 0.05$.*

2.4.2 Characterization of hybrid membrane

2.4.2.1 FTIR-ATR

FTIR spectra were acquired on the serosal side of DBP and HM samples, and on CF. Data were compared with the characteristic absorbance peaks of poly(carbonate) urethane (PCU) and the hard segment of CF, reported in the literature (Yang, Zhang, Hahn, Laroche, et al. 1999), as shown in Figure 2.18.

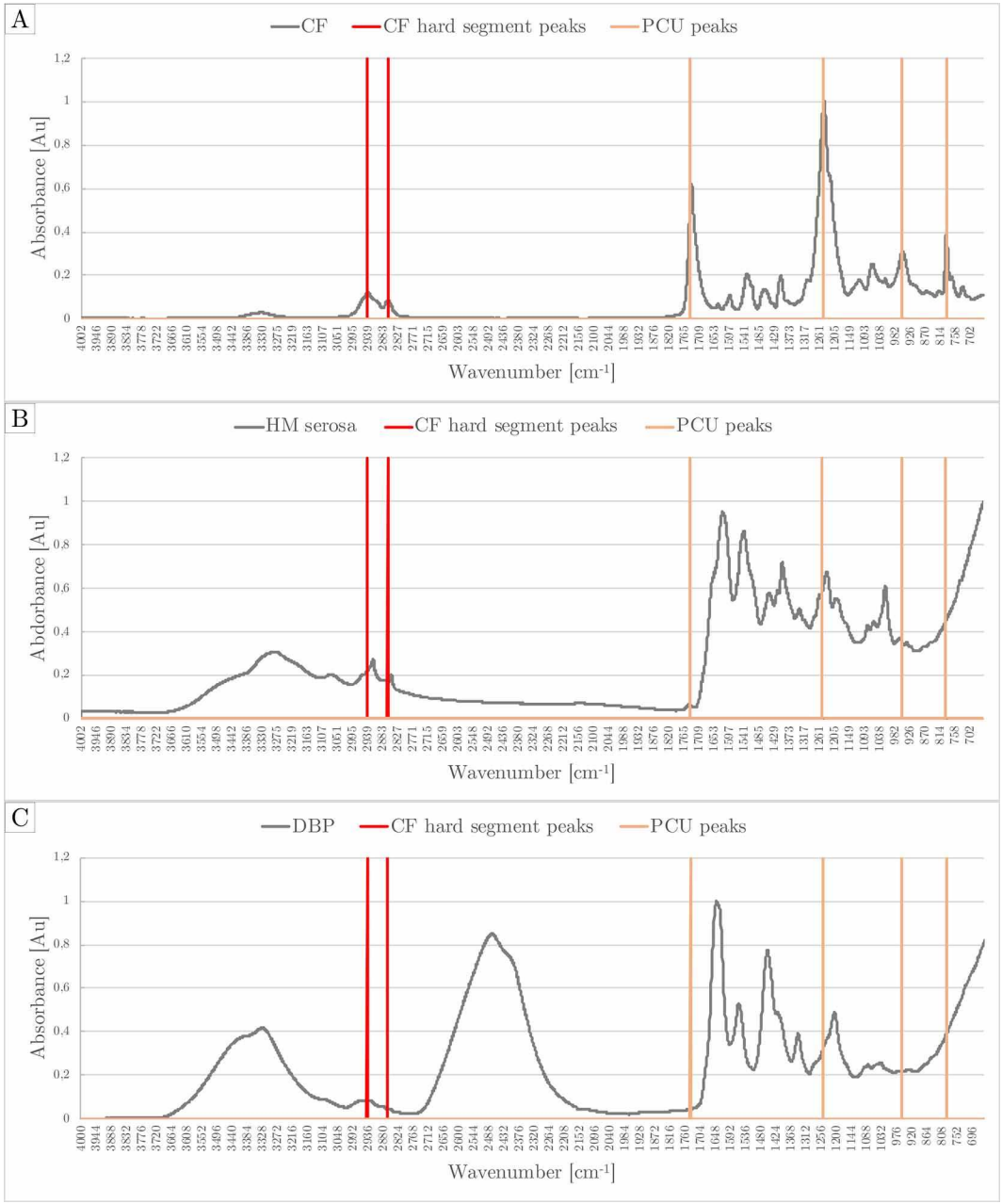

Figure 2.18 FTIR spectra of DBP, HM, and CF compared with characteristic peaks of PCU and CF hard segment. *Four out of six specific absorbance peaks for CF (A) were visible in the spectra of HM (B) but not in those of DBP (C).*

As fingerprints of CF, six specific peaks were considered as indicators for the presence of the polymer (Figure 2.18A). In general, poly(carbonate) urethanes absorb around 1737, 1251, 956, and 971 cm^{-1}, due to the presence of the carbonate group. In the case of CF, the first two peaks are slightly shifted (1740 are 1249 cm^{-1}), whereas the remaining ones are unaltered (Yang, Zhang, Hahn, Laroche, et al. 1999). In addition, the presence of aromatic methylene

diphenyl diisocyanate (MDI) composing the hard segment of CF (Bélanger et al. 2000) may be responsible for stretching the C-H bond of the methylene group (absorption at 2939 and 2863 cm^{-1}).

The FTIR spectra of DBP[1] presented the classical major bands of the protein infrared spectrum: amide band I (1600-1700 cm^{-1}) and amide band II (1510-1580 cm^{-1}) associated with C=O stretching of the carboxyl group and N-H bending of the amino group of peptides, respectively (Gallagher 1997). The selected characteristic peaks of CF were completely absent in DBP samples (Figure 2.18C).

The HM spectra showed intermediate characteristics between DBP and CF. Amide bands I and II of DBP scaffolds were visible. Absorptions at 2939, 2863, 1737 (very small) and 1251 cm^{-1} (reduced with respect to CF) were present, as shown in Figure 2.18B.

2.4.2.2 SEM

As regards the ultrastructure, the collagen of DBP *serosa* showed its usual wavy appearance (Figure 2.19A, D, G). In the HM samples, the bundles were not fully visible but appeared to be soaked of polyurethane and in groups of fibers emerging from the surface (Figure 2.19B, E, H). CF samples showed smooth surfaces, apparently free of defects (Figure 2.19C, F, I).

[1] The spectra of DBP scaffolds were kindly provided by Sabra Zouhair.

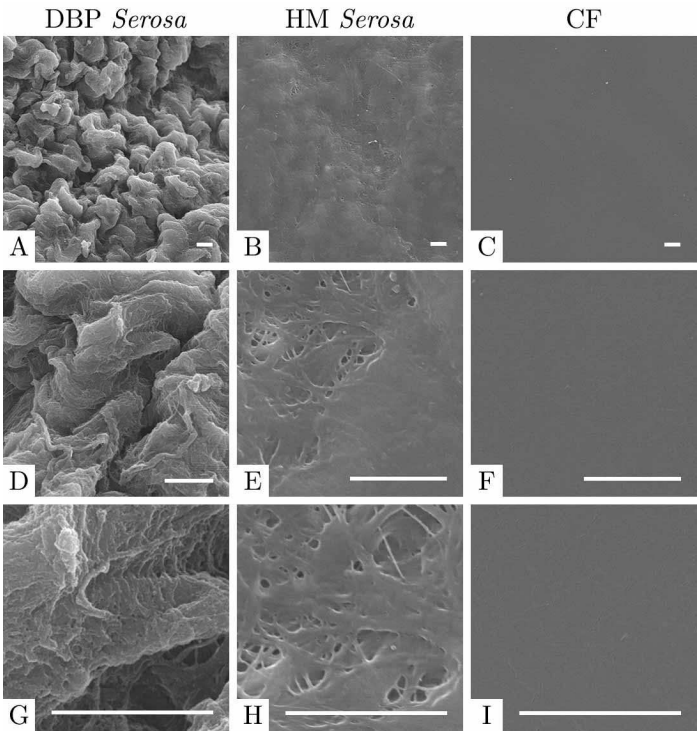

Figure 2.19 SEM images of DBP serosa, HM serosa and CF surfaces. *Bundles of DBP collagen (A, D, G) appeared to be soaked in polyurethane on HM serosal surface (B, E, H). CF was smooth and apparently free of defects. Scale bar = 5 μm.*

2.4.2.3 Cytotoxicity

Figure 2.20 and Figure 2.21 shows the qualitative cytotoxicity induced by direct contact between test materials and hBM-MSCs or HUVECs. The presence of DBP, ML and CF samples did not alter the typical morphology of both types of cells, which was comparable to the corresponding controls: hBM-MSCs presented their spindle-shape fibroblast-like aspect (Figure 2.20A-D, F-I, K-N, P-S) and HUVECs the "cobblestone" features (Figure 2.21A-D, F-I, K-N, P-S). No signs of lysis were observed.

Unaltered proliferation was noted, due to the considerable number of cells in the mitotic phase in all the tested materials and at all the time-points, together with progressive increase in cell density. Starting from 48 hours, both cell types presented visible polarization towards ML, DBP and CF samples (Figure 2.20A-C, F-H, K-M, P-R for hBM-MSCs; Figure 2.21A-C, F-H, K-M, P-R for HUVECs). This aspect was not noted in the positive control, in which a predominant orientation was rare if not absent (Figure 2.20D, I, N, S for hBM-MSCs; Figure 2.21D, I, N, S for HUVECs). These considerations

indicated the effect of DBP, HM and CF as equivalent to the cytotoxicity grading of "0" reported in ISO standard 10993-5.

Conversely, cyanoacrylate induced almost total detachment of the cell layer. Most of the cells were found dead in the suspension and only a few were rounded and weakly attached (Figure 2.20E, J, O, T for hBM-MSCs; Figure 2.21 E, J, O, T for HUVECs). As expected, the cytotoxicity induced by the glue corresponded to "grade 5", the highest.

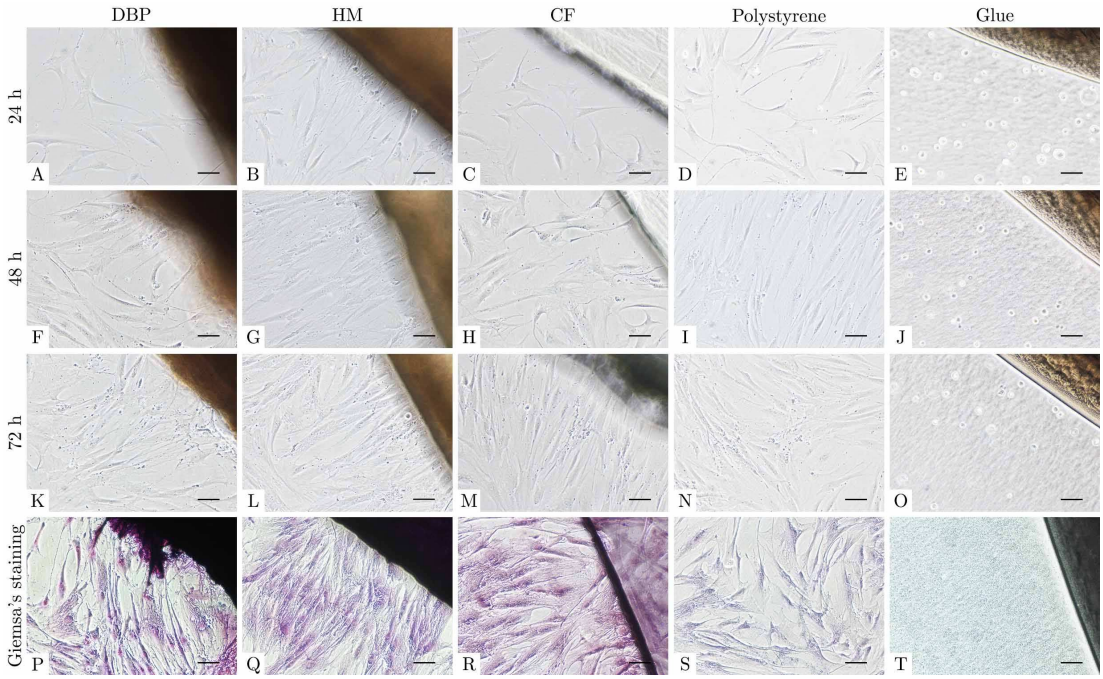

Figure 2.20 Qualitative evaluation of cytotoxicity induced by DBP, HM and CF samples on hBM-MSCs. *For all tested materials and at all time points, hBM-MSCs showed morphology and proliferation comparable with those shown by positive control (polystyrene). Starting from 48 hours, progressive polarization of cells towards tested materials was visible. Glue cytotoxicity induced cell death (negative control). Scale bar = 100 μm.*

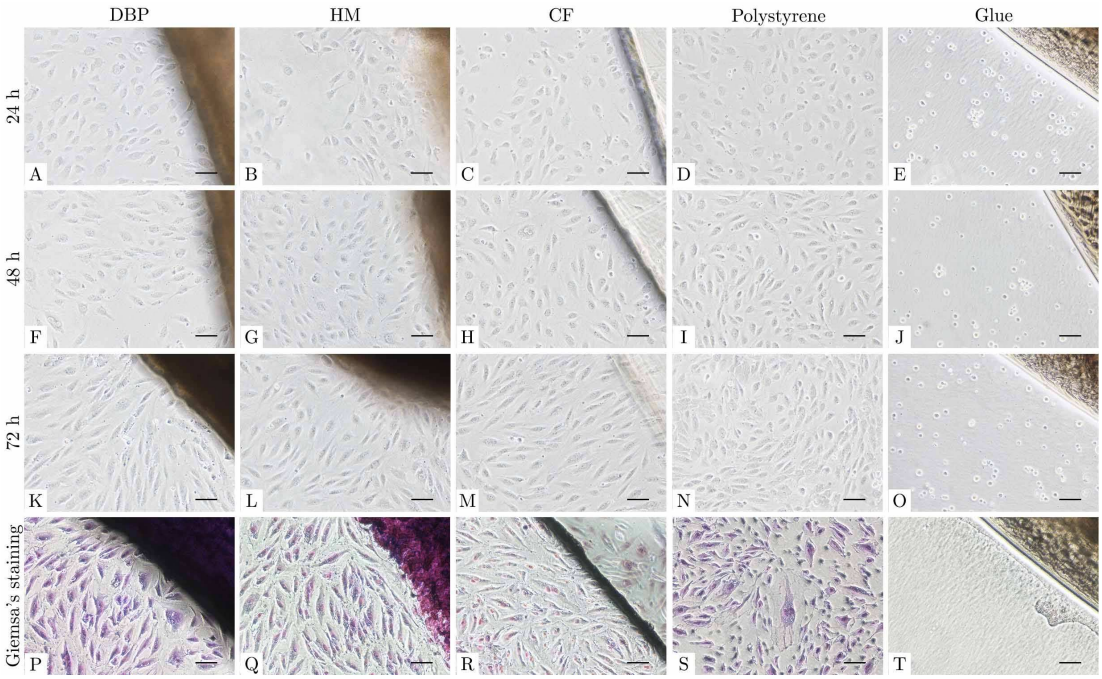

Figure 2.21 Qualitative evaluation of cytotoxicity induced by DBP, HM and CF samples of HUVECs. *For all tested materials and at all time-points, HUVECs showed morphology and proliferation activity comparable with those exhibited in positive control (polystyrene). Starting from 48 hours, progressive polarization of cells towards tested materials was visible. Glue cytotoxicity induced cell death (negative control). Scale bar = 100 μm.*

Proliferation activity, visible in the contact assay, was confirmed by the quantification of MTS reduction at 72 hours (Figure 2.22). The values measured for DBP, ML, CF and the cells on polystyrene were statistically different with respect to the glue ($p < 0.0001$). In more detail, the proliferation of hBM-MSCs was statistically higher in the presence of the tested materials than in the positive control ($p < 0.0001$). However, reduction of MTS was statistically lower in HUVECs in contact with CF with respect to polystyrene ($p < 0.01$).

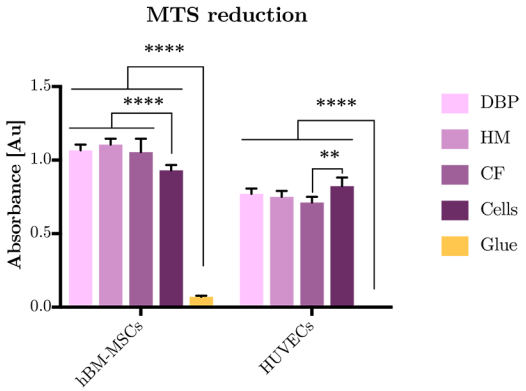

Figure 2.22 Quantification of proliferation activity of hBM-MSCs and HUVECs after 72 hours of contact assay. *Proliferation of hBM-MSCs and HUVECs in contact with DBP, HM and CF samples and positive control were significantly higher with respect to glue. Two-way ANOVA, Tukey's multiple comparison test, ** $p < 0.01$ and **** $p < 0.0001$.*

Quantification of LDH release is shown in Figure 2.23. The percentage of cytotoxicity in hBM-MSCs-seeded samples was negative or close to zero at all time-points. In the case of HUVECs, the highest value was observed after 24 hours for HM. However, cytotoxicity decreased very rapidly at subsequent time-points. The values for DBP scaffolds and CF showed a temporary slight increase near zero at 48 hours, but values were negatively stable. Glue induced 100% of cytotoxicity in both cell lines.

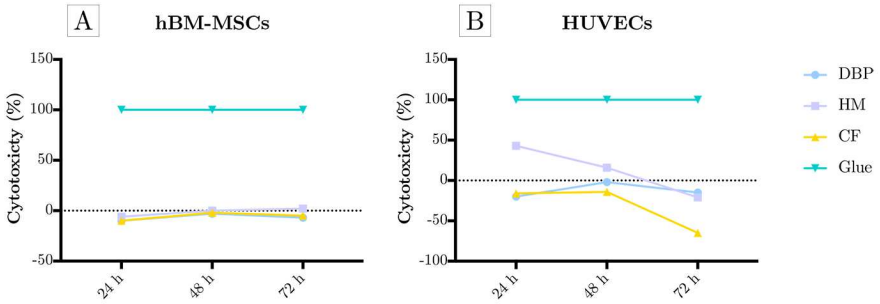

Figure 2.23 Quantification of released LDH. *In general, cytotoxicity values were negative or near zero for both cell types at all time-points. Glue achieved the highest value of cytotoxicity.*

Preliminary data on cell viability provided satisfactory results in all conditions for both HUVECs and hBM-MSCs. Dead cells were very rare in all tested samples, at all time-points (Figure 2.24).

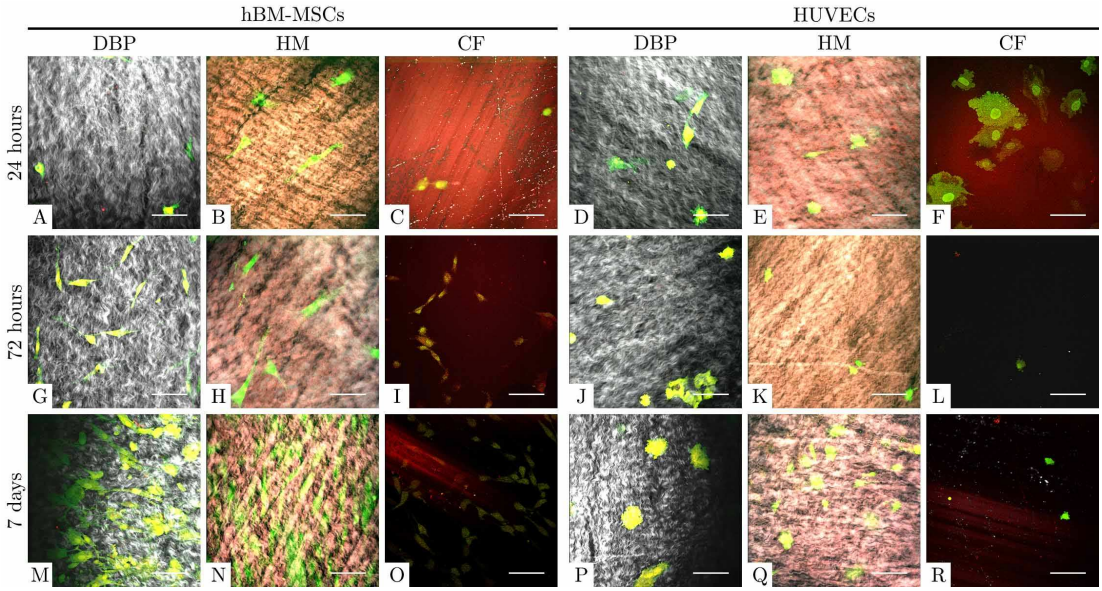

Figure 2.24 Live/dead staining of DBP, HM and CF seeded with hBM-MSCs and HUVECs. *Viable HUVECs and hBM-MSCs were visible for all tested samples and at all time-points. Only few dead cells were found on test materials. Scale bar =100 µm.*

2.4.2.4 Complement activation

DBP samples showed a clear-cut ability to activate the complement system, whereas HM and CF settled in the region of total inactivation. The values for HM and CF were not statistically different from each other, but were lower than those of DBP tissues ($p < 0.0001$), as shown in Figure 2.25.

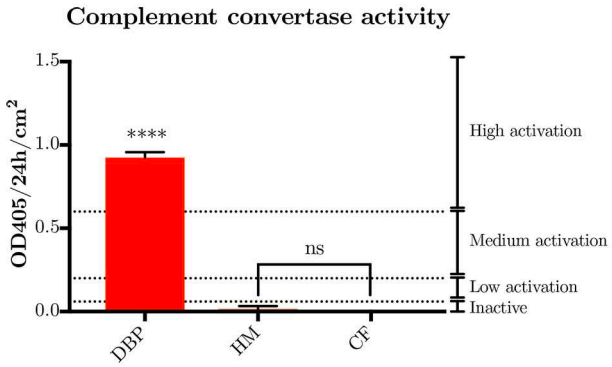

Figure 2.25 Complement system activation by DBP, HM and CF samples. *HM and CF did not induce activation of complement system; conversely DBP complement activation was very high. One-way ANOVA, Tukey's multiple comparison test, **** $p < 0.0001$.*

2.5 Discussion

When the first TAH prototypes were implanted in animals, only marginal attention was given to the appropriate selection of materials. At that time, biocompatibility was not a major concern and most efforts were addressed to demonstrating the feasibility of substituting a natural organ with a mechanical pump by achieving the animal's survival (Liotta et al. 1961).

At present, 81 years after the first reported TAH implantation in an animal (Demikhov 1951) and 49 years after the first implant in human (Cooley et al. 1969b), the search for affordable and effective mechanical substitutes for a failing heart has still not been reached. The task is so onerous that a significant breakthrough has not been witnessed since the early 1990's, *i.e.*, the beginning of CARMAT TAH development.

It was precisely CARMAT SA which enlivened the promising but not fully successful tradition of biolized materials for TAH blood-contacting surfaces. Despite the increased hemocompatibility demonstrated in animal studies (Harasaki et al. 1980; Nosé, Tajima, et al. 1971), these materials had never been implanted in humans until the development of Carpentier's TAH. Since the very early experiments, biolized surfaces have demonstrated their propensity to undergo dystrophic calcification (Harasaki et al. 1979). The lack of endothelialization is a common problem in chemically shielded xenogeneic tissues (see Section 3.1.2.2), but the presence of initial endothelial linings was reported in several studies in terms of PNI formation (Harasaki et al. 1978). The brilliant insight of mechanical blood pump hybridization by the use of biologically derived materials to improve biocompatibility is, *de facto,* compromised by aldehyde fixation. The use of GA carries more concerns than benefits: inflammatory processes, immunogenicity, occurrence of calcification, toxic release of unreacted aldehydes, and the lack of regeneration and tissue integration are far from being limited or extraordinary circumstances (Iop et al. 2018). Considering the latest alternative approaches aimed at eliminating the immunological risk of xenogeneic materials (decellularization (Gilbert, Sellaro, and Badylak 2006)) and at stabilizing and reinforcing tissues (natural cross-linking (Pinheiro et al. 2016)), GA treatment should no longer be considered as an option for the development of novel devices.

Therefore, in this part of the thesis, the quest for a biocompatible ventricular lining for TAH application was translated and investigated by creating a hybrid membrane made of DBP tissue coupled with a medical-grade polycarbonate urethane.

NBP tissues were decellularized with TriCol, a method developed in our laboratory. This protocol, applied initially to aortic roots and pulmonary valves, was systematically investigated preclinically. The potential of TriCol scaffolds to provide an intact ECM free from endogenous cell components (Spina et al. 2003) and immunogenic stimuli, like the disaccharide Galα1,3Gal epitope (Iop et al. 2009; Naso et al. 2011), prone to *in vitro* repopulation (Bertipaglia et al. 2003; Cigliano et al. 2012; Iop et al. 2009; Spina et al. 2003) and *in vivo* self-regeneration (Iop et al. 2014) was extensively confirmed. The low calcification potential was proven in a subdermal rat model (Spina et al. 2003) and on long-term implants in Vietnamese pigs (Iop et al. 2014). In addition, the quantification of sodium deoxycholate and Triton X-100 retained by decellularized scaffolds have been shown to be negligible and did not induce any cytotoxic effect *in vitro* (Iop, Paolin, et al. 2017). These results allowed clinical translation after approval of the decellularization protocol by the Italian Institute of Health and National Transplantation Center. Nowadays, the Treviso Tissue Bank Foundation provides TriCol-decellularized valve homografts for use as substitutes in cardiac surgery.

With regard to TriCol DBP tissues, the scaffolds presented intact histoarchitecture after complete cell removal, including nuclear components. Histological analyses reported the retention of collagen and elastin, whereas, alcianophilic elements shown uniform discoloration. These results were confirmed by quantitative biochemical analyses of hydroxyproline, denaturated collagen, elastin, and sulfated GAG contents, performed by our group but not reported in this doctoral thesis (Zouhair, Dal Sasso, Tuladhar et al., *in preparation*). In particular, the loss of GAGs had already been reported in our previous publications (Cigliano et al. 2012; Naso et al. 2010; Spina et al. 2003). This aspect has also been described in other studies as a consequence of several decellularization protocols (Mendoza-Novelo et al. 2011; Wong et al. 2013). GAGs are in fact more soluble than other ECM molecules. The reduction of GAG content in decellularized scaffolds may have a negative influence on tissue

dynamic biomechanical properties (Mavrilas et al. 2005) and propensity to dystrophic calcification (Cigliano et al. 2012). Conversely, some studies reported the ability of the low-molecular size of hyaluronan residues to activate the immune response (Naso and Gandaglia 2017). Therefore, the reduction of this non-sulfated GAG, described for TriCol porcine pericardial scaffolds (Cigliano et al. 2012), may represent a favorable outcome, to avoid potential acute rejection *in vivo*.

TPM was widely used in this work to evaluate decellularized ECM. It is a powerful, non-destructive tool, which can be used for both *in vivo* and *in vitro* assessments and overcomes the limitations of tissue processing and the use of exogenous fluorescent markers. The SHG generation is a coherent, non-linear process sensitive to non-centrosymmetric tissue components. Therefore, this optical technique is highly specific for fibrillar collagens, such as collagen I (Bueno, Ávila, and Artal 2016; Strupler et al. 2007). For example, TPM does not allow the detection of collagen IV (Pena et al. 2005): in order to locate this protein, in our case, the combination of TPM and immunolabeling was introduced. As a consequence, the selective detection of collagen I can be performed in a label-free modality, and is widely used for quantitative analyses of tissues to evaluate healthy and pathological conditions (Campagnola 2011; Ko et al. 2012; Richards-Kortum and Sevick-Muraca 1996). The acquisition of the SHG signal is often combined with the TPEF produced by endogenous cell and/or tissue components, such as elastin (Filippi et al. 2018). Evaluations performed using TPM on both cryosections and surfaces of decellularized scaffolds reported retention of the main original components of pericardial tissues. The TPEF signal, produced by endogenous cells on *ex vivo* NBP samples surfaces, was described in the literature as an intrinsic property due to NAD(P)H and FAD mitochondrial activity and, to a lesser extent, lysosomes (Monici 2005; Zoumi, Yeh, and Tromberg 2002). As expected, this feature was completely absent in decellularized DBP scaffolds. Moreover, retention of the main pericardial ECM components, such as collagen I and elastin, was confirmed by visual inspection. Quantification of the coherency of these two molecules reported unaltered orientation, with the exception of collagen bundles of *fibrosa*. For this layer, decellularization induced a rearrangement of the looser bundles, resulting in a less crimped configuration but intact bundle thicknesses. The 3D organization of collagen I is influenced by proteoglycans

and GAGs embedded in the main tissue constituents (Braga-Vilela et al. 2008; Simionescu, Iozzo, and Kefalides 1989). Therefore, it may be expected that reduction of GAGs will affect the waveform configuration. This was not confirmed by biomechanical evaluation, which showed unaltered elastic and collagen moduli, although slight increases in tissue extensibility and compliance were observed (Zouhair, Dal Sasso, Tuladhar et al., *in preparation*).

Immunofluorescence studies of the composition of mesothelial and vascular basal lamina have confirmed the retention of laminin in the *lamina lucida*, and collagen IV and heparan sulfate in the *lamina densa*. These molecules are commonly involved in interactions between parenchymal cells and surrounding connective tissues by modulating cell adhesion, differentiation and migration (Yurchenco 2011). Therefore, their preservation is essential in tissue engineering applications.

Counterstaining with Hoechst confirmed the complete absence of the DNA signal in decellularized tissues. In particular, DNA residues were quantified in our laboratory and the resulting amount was reported lower than threshold of 50 ng/mg of tissue dry weight (Zouhair, Dal Sasso, Tuladhar et al., *in preparation*). These two requirements have been defined in the literature as minimal criteria to prevent host adverse response and to achieve constructive ECM remodeling *in vivo* (Crapo, Gilbert, and Badylak 2011).

Selection of the synthetic material focused on medical-grade polyurethanes already used or investigated in blood-contacting implants and mechanical pumps. Polyurethane is a polymer containing urethane links which connect several alternate blocks, called hard and soft segments, which are responsible for the physical, chemical and biological properties of these compounds. They are therefore called "segmented". In the large family of these polymers, polyether-based polyurethanes were avoided *a priori* because they may undergo environmental stress cracking (ESC) (Gallagher et al. 2017; Richard Christ et al. 1992; Stokes 1988) and oxidative degradation (Stachelek et al. 2006). ESC is induced by interactions with the biological system and *in vivo* chemical degeneration is often associated with mechanical stress (Cauich-Rodríguez et al. 2013). Oxidation may be caused by the reactive oxygen and nitrogen species produced by inflammatory cells (Stokes, Urbanski, and Upton 1989). Moreover, permeability to water vapor did not meet the necessary requirements for blood

pump applications (Yang, et al. 1999). Instead, polyester urethanes are more prone to hydrolysis because of the presence of the ester group in the soft segment (Pretsch, Jakob, and Müller 2009; Tanzi et al. 1991). In addition, potential *in vivo* degradation and poor chemical stability may induce toxicity, due to the release of harmful products (Marois and Guidoin 2013).

A polycarbonate urethane was consequently selected for our application. CF was specifically introduced into the biomedical market to substitute Biomer, the traditional ether-based polyurethane used to produce heart pumps and catheters (Reed, Potter, and Szycher 1994). CF is US Pharmacopeia class VI polymer which combines notable biological properties (biodurability, biocompatibility, and thrombogenicity) with good mechanical features (elasticity, strength, long-term durability, resistence to ESC) and easy workability (moldable, castable, usable by means of electrospun, dip coatable) (AdvanSource 2010).

As described above, the degradation of a polyurethane is mainly caused by calcification, hydrolysis, oxidation, and ESC, and depends on chemical composition (Reed et al. 1994). The CF soft segment is a carbonate polyol, whereas the hard segment is composed of MDI and has two types of chain extenders, ethylene diamine and 1,3 diaminocyclohexane (Reed et al. 1994). The presence of the carbonate segment makes the polymer less prone to oxidation, ESC and hydrolysis *in vivo* and *in vitro* (Faré et al. 1999; Khan et al. 2005; Mathur et al. 1997; Tanzi et al. 1997). On the other hand, the risk of mineralization exists for all types of polyurethanes. However, an *in vitro* study reported that polycarbonate urethanes performed slightly better than ether-based materials (Yang, Zhang, Hahn, King, et al. 1999).

Hence, the characteristics of DBP and CF are appealing for the assembly of a more biocompatible TAH hybrid membrane. Nevertheless, the coupled material may have different properties with respect to the starting components. Deeply investigations are therefore required.

The FTIR fingerprint of CF is determined by the composition of the soft and hard segment compositions. Among these characteristic peaks, those also shared by DBP spectra were not considered, in order to identify the presence of CF on HM *serosa* selectively. It was thus possible to confirm the penetration of CF through the pericardial scaffolds. The *serosa* spectra of HMs were in

effect hybrid: the peaks of the soft and hard segment functional groups were visible and also amide bands I and II of amine bonds between amino acids composing DBP tissues. The permeation of DBP tissues with CF was visible by SEM and confirmed the hybrid aspect of the HM *serosa* surface. In addition, TPM analyses showed a diffuse autofluorescent signal, probably due to the TPEF of the aromatic groups within the CF hard chain (Van Duuren 1960).

In terms of cytotoxicity, CF penetration does not present a problem, when the prepolymer components are fully reacted and no residues of any used organic solvent are present. This aspect has in fact been evaluated in acute settings, intracutaneous models, and long-term animal implants, with positive results (Van Duuren 1960). However, most polyurethanes, independently of their chemical composition, are characterized by poor cell adhesion, due to their smooth surfaces. Morphology is not the only parameter which must be considered: physical properties, such as wettability and surface charge should also be studied (Marois and Guidoin 2013), together with the sterility protocol applied. Several types of polyurethanes, including CF, were sterilized by ethylene oxide and gamma irradiation and seeded with fibroblasts and ECs. The poor adhesion and viability were explained by the possible retention of sterilization agents and chemical alteration of treated materials (Bélanger et al. 2000). Strategies of surface functionalization were also applied to CF by covalent immobilization of endothelial-adhesive peptides, such as REDV (Butruk-Raszeja et al. 2016; B. Butruk et al. 2013). Therefore, in our case, concerns about CF penetration through DBP scaffolds were studied by assessing the possible modifications of cytocompatibility and bioactivity. Contact assays with hBM-MSCs and HUVECs were evaluated according to the guidelines of ISO 10993-4. These two cell types were selected because they are among patients' cytotypes which may come into contact with TAH internal surfaces, through blood flow (hBM-MSCs) or migration from anastomotic sites (ECs). HUVECs also constitute a widely adopted model for cytotoxicity, due to their sensitivity to cytotoxic compounds. Interactions with HM, DBP and CF samples confirmed the absence of morphological alterations and lysis, as well as abnormalities of proliferation. The release of LDH was comparable to that of polystyrene control and viability was preserved. In addition, a process of migration and polarization towards the tested materials was clearly visible in both cell types. Focusing on HM, the preliminary results obtained by

Live/Dead staining showed an encouraging improvement in cell adhesion, with respect to CF alone. Although the partial masking and diffusion of the polymer through the biological layer, the bioactivity of the DBP scaffold coupled with HCF was probably intact or only partially affected. However, limited permissiveness for cell attachment was confirmed for CF, as previously demonstrated in (Bélanger et al. 2000).

When an implant comes into contact with blood, the first events are the adsorption and absorption of water and low-molecular-weight solutes and ion bonding to the surface (Andrade and Hlady 1986). Thereafter, the rapid adsorption of plasma proteins and macromolecules give rise to a new blood interface which may trigger several phenomena, such as coagulation and complement activation (Ekdahl et al. 2011). In the case of biomaterials, the complement system is activated prevalently by the alternative pathway through the covalent binding of C3b, and occurs in the absence of antibodies (Kazatchkine and Carreno 2006). It represents an inflammatory response towards non-self materials, leading to severe clinical complications, such as infections, coagulopathies, stent stenosis, and thrombosis (Nilsson et al. 2007). It is also frequently observed in the cases of cardiopulmonary by-pass and dialysis filters (Hakim 1993). The role of the complement system has also been investigated in the cases of mechanical circulatory support devices. In the past, there was a tendency to consider the influence of the underlying pathology and the severity of the activation, instead of the type of pump implanted (Loebe et al. 1998). Nonetheless, this aspect should not be underestimated in TAHs. In our study, activation of the complement system was tested as part of the analyses required by ISO 10993-4 to confirm the *in vitro* blood response to the materials tested (International Organization for Standardization 2017). In the evaluation, DBP scaffolds had the highest values. The significant activation may have been caused by specific binding sites for complement proteins on the constituents of pericardial scaffolds. The study of Shields *et al.* did report the presence of C3 and C4 colocalized on collagen and elastin of murine aortic *adventitia*, indicating the critical role played by the complement system in the pathogenesis of atherosclerosis (Shields et al. 2011). *In vivo*, activation may occur when the basal lamina is damaged. Proteoglycans and GAGs can modulate the complement by determining its activation or inactivation through the alternative pathway. The loss of heparan sulfate has been reported to

impair this mechanism (Clark, Bishop, and Day 2013). On DBP scaffolds, immunolabelling of heparan sulfate confirmed the presence of this molecule on both mesothelial and vascular basal lamina, indicating that this aspect may have caused unlikely activation of the complement. Another element which should be taken into consideration is the following: hyperacute rejection of xenogeneic tissues involves, among other processes, complement activation driven by xenoreactive antibodies (*e.g.*, anti-α-Gal) (Schuurman, Cheng, and Lam 2003) through the classical pathway. The TriCol protocol, applied to valvular tissues, was proven to be effective in α-Gal removal (Iop et al. 2009; Naso et al. 2011). Its efficacy on pericardial scaffolds was only evaluated for a modified version of the protocol, in which sodium cholate was replaced by taurodeoxycholate. In that case, the decellularized tissues resulted in medium complement activation, even when GA-treated (Aguiari et al. 2017). In addition, ordinary GA-treated bioprostheses should not expose xenoantigens due to chemical shielding, but exhibited various levels of activation (from medium to high) (Aguiari et al. 2017; Naso et al. 2017). Similar results were confirmed when bioprostheses underwent a process aimed at directly inactivating α-Gal (Naso et al. 2017). This antigen is not the only cause of concern: sialic acid may also modulate the complement system (Langford-Smith et al. 2015), but its quantification in our DBP scaffolds has not yet been assessed and will be subject of future investigations.

Activation of complement system by polymers has been investigated especially due to the associated risk of infections on vascular catheters of extracorporeal circulation and dialyzer membranes (Craddock et al. 1977; Kuroki et al. 1995). Generally, complement activation is less marked in polyurethanes than in silicon, polyamide, polyethylene or PTFE (Kuroki et al. 1995; Marosok et al. 1996). The area and chemistry of the blood-exposed surface were the main modulators and determined the type of interaction with this system (Chenoweth 1988). The presence of amino and hydroxyl groups on the material promote binding with C3 and activation of the system (Chenoweth 1988; Law, Lichtenberg, and Levine 1979; Pangburn et al. 1980; Pangburn and Müller-Eberhard 1980). In the case of CF, Bélanger *et al.* reported that the release of C3a, after the contact with human blood was higher than that for LPDE and PDMS, respectively the reference materials for low and medium activation respectively (Bélanger et al. 2000). Instead, quantification of the

coagulation product sC5b-9 showed no significant activation for CF modified with branched polyethyleneimine and human antithrombin III and untreated (Lukas et al. 2017). Our results confirmed the absence of activation for CF. The contribution of CF, which crossed the DBP layer, was probably responsible for the non-activation of the complement by the HM. The masking of collagen and elastin sites for C3 and C5 binding of *fibrosa* and the partial coverage of the heparan sulfate-rich *serosa* layer, may have positively affected *in vitro* activation. This feature is particularly desirable for this novel material because it may reduce the future *in vivo* occurrence of inflammation related to the activation of the complement system (Zaferes 2002). In addition, it may avoid the cleavage of adsorbed complement proteins by serine protease from the coagulation system (Amara et al. 2008).

In conclusion, this first generation of a hybrid membrane for TAHs, based on DBP and polycarbonate urethane, appeared to be promising for *in vitro* cell viability. In fact, the presence of the polymer did not alter the biological activity of DBP in terms of cell migration and proliferation; nor did it induce cytotoxicity. The absence of complement activation was also demonstrated. Further analyses will be performed to complete the *in vitro* blood compatibility tests required by the ISO10993-4: the activation of the coagulation system, occurrence of thrombosis, hemolysis, and platelet activation must also be investigated.

3 Endothelial cell-selective REDV functionalization of pericardial scaffolds as strategy to improve blood compatibility of TAHs

3.1 Introduction

The endothelium is the highly selective natural barrier between circulatory compartment and body tissues. ECs mediate thrombotic, fibrinolytic and inflammatory pathways by regulating the expression of specific bioactive molecules. For these reasons, the endothelium is described by definition as Nature's blood compatible container (Gimbrone Jr. 1987).

From this perspective, the promotion or restoration of a living endothelium on biomaterials for cardiovascular applications has been recognized as a possible solution to the occurrence of thrombotic events. Therefore, the quest for *in vitro* or *in vivo* endothelialization of synthetic and biological surfaces paved the way to a wide research area where biological competences blend with Chemistry and Biomaterial Science.

3.1.1 The healthy endothelium

The endothelium is a simple squamous epithelium, like mesothelium and endocardium. It is composed of a single-cell-thick layer of ECs lining the inner surface of blood and lymphatic vessels (Ross and Pawlina 2010). Endothelial

phenotype is quite variable among species and organs (Moncada and Higgs 2006).

3.1.1.1 General characteristics of epithelia

In general, epithelial cells show a specific polarity based on which it is possible to distinguish an apical (facing the lumen of the cavity or external surface), lateral (in contact with adjacent cells) and basal (anchoring underlying basal lamina) domains characterized by distinct functions.

The apical domain is responsible for transporting substances through the cells, due to the presence of enzymes, ion channels and carrier proteins. It is also characterized by external projections of cytoplasm with sensory and transport functions (*i.e.*, microvilli).

The molecular composition of cytoplasmic membrane varies significantly in lateral domain, which is decorated with cell adhesion molecules (CAMs), such as integrins (cell-ECM junctions), cadherins (cell-cell junctions), selectins, and immunoglobulins. The type of connection between adjacent cells is distinguished into occluding (diffusion is hindered), anchoring (cytoskeletons are connected) and communicating junctions (free diffusion of small molecules).

The basal domain is in continuity with basement membrane and have cell-ECM junctions. The basement membrane is subdivided into basal lamina or lamina *densa*, in contact with the underlying connective tissue and composed of laminin, collagen IV, proteoglycans, and glycoproteins, and lamina *lucida*, in contact with cells and containing the extracellular part of fibronectin and laminins receptors (Ross and Pawlina 2010).

3.1.1.2 Histological properties of endothelial cells

ECs are 1-2 µm thick and have a diameter of 10-20 µm. These cells have flattened cytoplasm, with few organelles (mitochondria, the rough endoplasmic reticulum, Golgi apparatus) located perinuclearly. The nucleus is central, bulging into the lumen and covered by numerous microvilli (Figure 3.1). Cell vesicles are close to the membranes as a result of transcytosis of molecules and liquids (Krstic 1985).

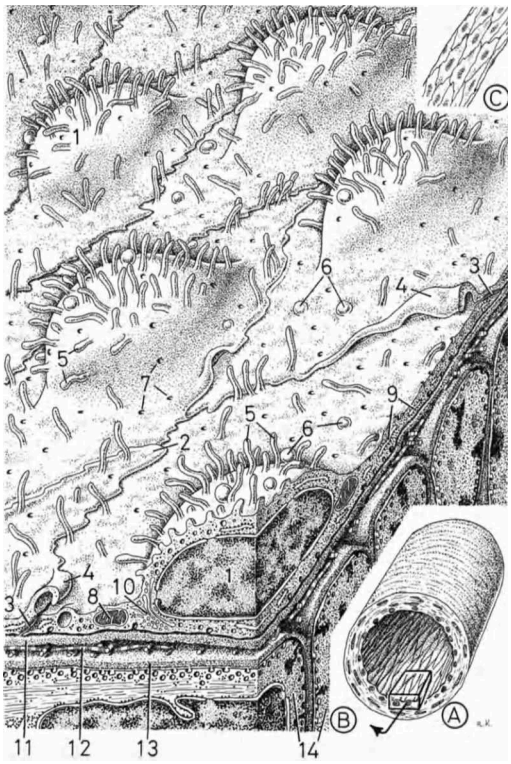

Figure 3.1 Vascular endothelium. *ECs have flattened cytoplasm, whereas nucleus bulges into vascular lumen. Numerous microvilli are present in nuclear region* (Krstic 1985).

Endothelial surface is decorated with the extracellular domain of large membrane-bound molecules, such as proteins, glycolipids, glycoproteins and proteoglycans, forming the glycocalyx (Figure 3.2). These molecules have charged functional groups and are involved in cell adhesion, immune reactions, inflammatory processes, coagulation, and fibrinolysis. In addition, a thick surface layer of adsorbed soluble plasma proteins covers the endothelium, inhibiting the flow of plasma and the contact with red blood cells and other molecules (Pries, Secomb, and Gaehtgens 2000).

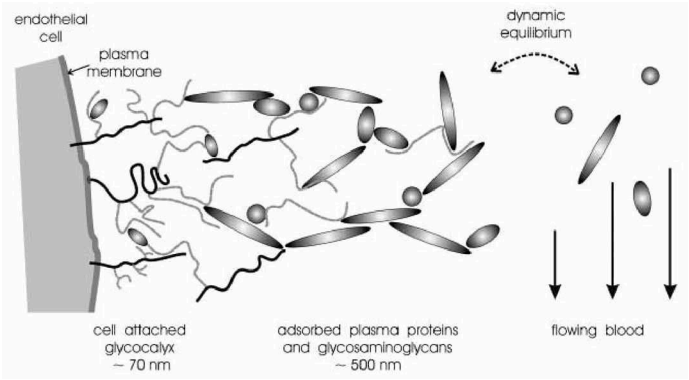

Figure 3.2 Blood/endothelium interface. *Endothelial surface is decorated with glycocalyx rich in glycoproteins and proteoglycans. A layer of soluble plasma molecules is adsorbed on glycocalyx and is in dynamic equilibrium with flowing plasma* (Pries et al. 2000).

3.1.1.3 Functions of the endothelium

Although early studies described the endothelium as a mere passive lining, it is actively involved in several key functions of cardiovascular system occurring at the interface between tissue and blood. Endothelium regulates the vascular tone, tissues perfusion, exchange of fluids and solutes, hemostasis, coagulation, inflammatory response, vasculogenesis, and angiogenesis (Pries et al. 2000).

- *Hemostasis and coagulation*

In 1856 R. Virchow recognized for the first time the importance of intact vascular endothelium in maintaining blood fluidity, and described the endothelial injury as one of three factors responsible for the occurrence of thrombotic events (Virchow 1856). As a matter of fact, endothelium plays two opposite roles in hemostasis and coagulation.

In healthy conditions, the antithrombotic nature of endothelium is due to the failure in coagulation system activation and platelets aggregation. ECs produce bioactive substances, such as prostacyclin and nitric oxide, which inhibit the activation of platelets and monocytes. In addition, ECs regulate the following mechanisms (Figure 3.3):

1. *heparin-antithrombin mechanism*: heparin sulfate present on endothelial surface is one of the two proteoglycans which can activate plasma antithrombin III, boosting the protease inhibitor activity and, in turn, neutralizing the enzymes of intrinsic coagulation cascade, such as thrombin and factors IXa, Xa, XIa, and XIIa. Heparan sulfate

proteoglycan, directly synthesized by ECs, also accelerate the function of antithrombin III by involving heparin-like mechanisms (Rosenberg 1989);

2. *protein C-thrombomodulin mechanism*: thrombomodulin is expressed on ECs surface and binds thrombin by activating protein C, inactivates factors Va and VIIIa on phospholipid surface, and inhibits the formation of new thrombin (Esmon 1992; Ikezoe 2015);
3. *tissue plasminogen activator mechanism*: formation of a thrombus and the presence of thrombin and factor Xa activate the release of tissue plasminogen activator from the endothelium, which catalyzes the conversion of plasminogen into plasmin, causing proteolytic lysis of fibrin (Oliver, Webb, and Newby 2005).

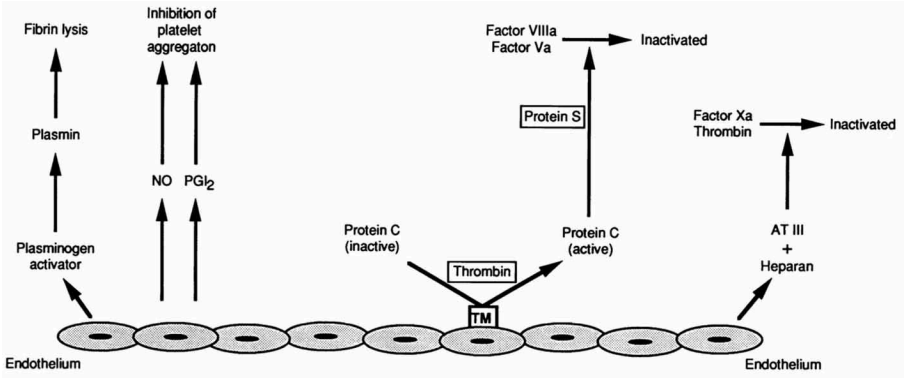

Figure 3.3 Antithrombotic effects of healthy endothelium. *ECs produce nitric oxide and prostacyclin, and regulate heparin antithrombin, protein C-thrombomodulin and tissue plasminogen activator mechanisms* (Benedict, Pakala, and Willerson 1994).

Conversely, any mechanical or chemical damage triggers the adhesion of platelets and fibrin, with subsequent activation of fibrinolysis system. In these conditions, the endothelium synthesizes adhesive cofactors (von Willebrand factor, vWF, fibronectin, thrombospondin) and procoagulant molecules (factor V, factor VIII). In addition, it offers a suitable surface for their activation (Gimbrone Jr. 1987; Lijnen and Collen 1997; Wu, M.D and Thiagarajan, M.D 1996). This behavior is often enhanced by inflammation, which can reduce the presence of proteoglycans on cell surface and the synthesis of antithrombin, protein C and thrombomodulin, whereas it upregulates expression of procoagulant tissue factors (Benedict et al. 1994; Verhamme and Hoylaerts 2006).

- *Inflammatory response*

In normal conditions, endothelium inhibits the activation of leucocytes by downregulating the expression of adhesion molecules and leucocytes-interactive proteins (Alexander, Granger, and Harris 2017).

The activation of endothelium causes the expression of adhesion molecules and the production of cytokines and chemotactic factors (Alexander et al. 2017; Swerlick and Lawley 1993). As a consequence, circulating leucocytes slow down and start to roll on the ECs with subsequent strong adhesion and transendothelial migration (diapedesis), in order to reach lymphatic vessels, inflammation site or injured tissue.

This activation is time-dependent and can be slow, independent from gene expression and mediated by histamine (type I activation), or fast, involving new gene expression and mediated by inflammatory cytokines (type II activation) (Alexander et al. 2017).

- *Vasculogenesis and angiogenesis*

The formation of new blood vessels is regulated by two different phenomena: the proliferation and migration of ECs from adjacent vessels, defined as angiogenesis, and the differentiation of circulating endothelial progenitor cells, named vasculogenesis (Tang and Conti 2004).

Proteoglycans and glycosaminoglycans of ECs' glycocalyx contribute to these processes by binding circulating growth factors (vascular endothelial growth factor, VEGF) and cytokines involved in the development of new blood vessels (Pries et al. 2000).

- *Regeneration potential of endothelium*

Endothelial ability to reconstruct the luminal lining is closely dependent on species and severity of the damage (Walluscheck, Steinhoff, and Haverich 1996). In the case of extensive injuries, migration and proliferation of ECs from the intact borders are not sufficient to restore the continuity of the monolayer and wide areas of the vessel can remain denuded (Walluscheck et al. 1996).

Two hypotheses have been proposed to explain the poor regeneration potential of the endothelium. The first one suggested that ECs can probably

undergo a finite number of divisions and, thus, there is an innate limit. The second hypothesis considered the interactions with particular smooth muscle cells, which shift their phenotype towards an endothelial-like one and line the surface of wounded endothelium (Simionescu and Simionescu 1988).

3.1.2 Endothelialization of biomaterials: issues and plans of action

The challenge of biomaterial endothelialization affects every year the outcome of thousands of synthetic and biological materials implanted in the cardiovascular system. The presence of an endothelial lining has been proven to be a strong inhibitor of macrophage adhesion (Gillis, Bengtsson, and Haegerstrand 1995), smooth muscle cells migration from anastomotic sites, attachment of platelets, adsorption of fibrin, and calcification (Liao ' et al. 1993). Conversely, it has been reported that the biomaterial surface is often covered by fibrin, platelet aggregates, and thrombi in the case of absence of a stable endothelial lining.

3.1.2.1 Vascular grafts and stents

Polyethylene terephthalate (PET, Dacron), expanded polytetrafluoroethylene (ePTFE), and polyurethanes are artificial polymers widely investigated and used in the fabrication of vascular grafts. These materials are considered hemocompatible but share the identical disadvantages in term of *in vivo* endothelialization ability.

The limited healing capacity of novel endothelial linings on artificial materials became evident first in small-diameter grafts, in which the recurrence of obstructive thrombi was the main responsible for prosthesis failure. Encouraging results achieved in animal studies were unfortunately not confirmed in humans. Several explants reported the presence of endothelialization in perianastomotic areas, whereas the central regions of the grafts presented diffuse deposits of fibrin, resulting in an almost acellular fibrotic neointima (De Bakey et al. 1964; Berger et al. 1972; Warren and McCombs 1965; Wesolowski et al. 1964). In addition, the overstimulation of ECs caused smooth muscle cell uncontrolled proliferation in healing regions,

with subsequent neointima thickening and luminal stenosis (Clowes, Kirkman, and Clowes 1986)

The seeding of autologous ECs prior to the implantation was one of the first *in vitro* strategies adopted to improve the endothelialization of artificial vascular grafts (Boyd et al. 1987; Herring et al. 1984, 1987; Herring, Gardner, and Glover 1978). Autologous ECs can be mechanically or enzymatically harvested from non-essential vessels (saphenous vein) and subcutaneous adipose tissue of patients (Pawlowski et al. 2004). The seeding can be performed with several methodologies. For example, by taking advantage of the gravitational force, *i.e.*, rotating periodically the graft, homogeneous cell coverages have been obtained (Anderson et al. 1987; Foxall et al. 1986; Herring et al. 1978; Mazzucotelli et al. 2008). Hydrostatical forces, through the application of vacuum, promoted cells attachment to the graft surfaces (van Wachem et al. 1990). The natural negative charge of ECs has been used to improve the adhesion by temporally modifying the synthetic material charge (negative as well in normal condition) (Bowlin et al. 1998; Bowlin and Rittgers 1997; Fields et al. 2002). ECs have been also enriched with iron oxide microspheres, in order to be magnetically attracted towards the material (Pislaru et al. 2006).

However, *in vitro* cell seeding of synthetic polymers was not sufficient to overcome the poor adhesion capacity of these materials, resulting in long-term unstable or incomplete lining. Therefore, precoating strategies were introduced to support *in vivo* adhesion.

The ECM is the natural product of resident cells and constitutes the optimal substrate for cell adhesion, growth, differentiation and migration. For this reason, surface coatings with one or more ECM-derived molecules or full matrices appeared to be a promising approach, due to their ability to mimic the natural subendothelial layer of normal vessels. Precoating with collagen demonstrated better results with respect to denaturated collagen (gelatin), laminin, fibronectin, and fibrin (Anderson et al. 1987; He et al. 2005), whereas low molecular weight hyaluronic acid was more effective than PEG and heparin (Chuang and Masters 2009). Collagen I and III contributed to surface smoothening, but the adhesive properties were strongly increased by fibronectin coating (Kaehler et al. 1989). This glycoprotein is present in the

extracellular matrix and was used as a strong mediator of endothelial adhesion via cellular integrin interaction (Ramalanjaona et al. 1986; Seeger and Klingman 1988; van Wachem et al. 1987). In order to fully exploit the natural potential of ECM, graft surfaces have been preseeded with specific cell types to take advantage of the synthesis of a 3D matrix. In particular, the matrix produced by fibroblasts was rich in collagen I and III, heparan sulfate and chondroitin sulfate and was obtained by decellularizing the confluent layer with surfactants (Triton X-100), antibiotic (mitomycin), and gamma-ray irradiation (Lee et al. 1993) or ethanol, extremely effective in removing polar phospholipidic cell membrane and as fixative (Bellón et al. 1993). In the same way, corneal ECs have been used to synthesize highly polarized ECM rich in collagen (mostly III and IV), proteoglycans (HS and dermatan sulfate), laminins, fibronectin, elastin, and growth factors (basic, fibroblast growth factor, bFGF). Cells were removed with Triton X-100 and ammonium hydroxide (Schneider et al. 1992).

Angiogenic growth factors are currently studied as crucial molecules to promote angiogenesis in bioengineering applications (Golub et al. 2010; Zhang et al. 2013). Vascular endothelial growth factor (VEGF) has been used to coat vascular stents, in order to enhance endothelial regeneration following implant-related injuries (Swanson et al. 2003). Gene-eluting stents enriched by DNA encoding for VEGF demonstrated that gene-based strategies may be effective to accelerate endothelialization(Walter et al. 2004).

A completely different strategy is based on antibodies. Anti-human CD34 can be used to target $CD34^{+}$ cells, such as EPCs circulating in peripheral blood. This approach has been applied to vascular stents (Aoki et al. 2005; Choi et al. 2015; Ong et al. 2005; Sethi and Lee 2012) and grafts (Griese et al. 2003; Markway et al. 2008). Despite the promising results, some concerns have been raised regarding the adoption of only one marker to select EPCs and the effective ability of these cells to differentiate into ECs *in vivo* (Leopold 2013).

3.1.2.2 Bioprosthetic heart valves

The use of GA is one of the major limitations of bioprosthetic substitutes. This aldehyde was first introduced as a tissue fixative but was rapidly applied as a stabilizer of biological heart valves, patches and biolized materials. Under well-

defined chemical conditions, GA creates intramolecular and intermolecular cross-links by reacting mainly with the amino groups of several molecules but mainly proteins (Migneault et al. 2004).

GA-treated tissues entered in the clinical practice because of their supposed hemocompatibility, low thrombogenicity, high durability and immunocompatibility. However, several *in vitro* and *in vivo* studies immediately reported cases of chronic inflammation and early mechanical failure. Immunogenicity resulted not fully guaranteed due to the probable presence of unmasked antigens responsible for leukocyte migration (Dahm et al. 1989; Salgaller and Bajpai 1985; Umashankar et al. 2012). Most of the cases of early implant degeneration have been caused by the calcification of GA-treated biomaterials. The severity and extent of mineralization have been found directly proportional to the amount of incorporated GA and degree of cross-linking (Golomb et al. 1987). The causes of this pathological mechanism have been correlated to calcium accumulation in damaged cells or entrapped by membrane phospholipids, rich in high-affinity phosphorous. In addition, ECM components, such as collagen and elastin, also mineralized (Schoen and Levy 2005).

The endothelialization of bioprosthetic heart valves may have a significant role in preventing calcification. However, the progressive release of free unbounded aldehydes, entangled in treated tissues, causes poor endothelial lining and severe cytotoxicity (Gendler, Gendler, and Nimni 1984; Hoffman et al. 1992; Huang-Lee, Cheung, and Nimni 1990; Speer et al. 1980; Umashankar et al. 2012; Wiebe et al. 1988). The adhesion is often very poor, limited to short-term and associated with unstable and not viable linings. This inability to support the endothelial attachment lead to the adsorption of fibrin and the formation of thrombi (Ishihara et al. 1981).

Strategies of *in vitro* autologous preseeding have been applied to bioprosthetic GA-treated heart valves to improve *in vivo* proliferation of ECs, but the results were often conflicting. Generally, no endothelial lining have been found on the long-term, even in the case of GA-neutralization with aminoacidic solutions (Bengtsson, Radegran, and Haegerstrand 1993; Fischlein et al. 1994) or precoating with ECM-derived molecules (fibronectin (Eberl et al. 1992); fibronectin, heparin, acidic fibroblast growth factors (Fischlein and

Fasol 1996)). Other studies reported the effectiveness of preseeding in promoting endothelial adhesion (Fu et al. 1997; Gulbins et al. 2003; Jansson et al. 2001; Lehner et al. 1997).

Eventually, the conjugation of specific antibodies for epitopes expressed by circulating EPCs have been tested also on decellularized heart valves with some improvements. In this case, anti-CD133 antibody have been used to selectively attract endothelial progenitors from the blood flow on engineered tissues, in order to induce the formation of a stable layer of differentiated ECs. The conjugation achieved good results in terms of *in situ* recruitment in both *in vitro* and *in vivo* experiments. So-treated heart valve tissues developed a full endothelial lining, whereas thrombi and calcific deposits were completely absent after 3 months of implantation (Jordan et al. 2012; Vossler et al. 2015; Williams et al. 2015).

3.1.2.3 Peptide functionalization

Membrane receptors and cell adhesion proteins are the most important players in regulating the fine mechanism of cell adhesion. Synthetic biomaterials are usually deficient of bioactive sequences able to coordinate these complex interactions. Therefore, the immobilization of naturally inspired short synthetic peptides, mimicking the function of natural proteins, was investigated in tissue engineering and regenerative medicine applications, such as bio-inert cardiovascular implants in which the improvement of *in situ* endothelialization is crucial.

The use of peptides is preferred to the whole protein because of low immunoreactive potential and reduced possibility of pathogen transmission. The sequences can be produced with relatively modest costs and it is possible to fully control the binding process by a careful biomaterial design (Bellis 2011). The functionalization may be performed by surface modification (aimed to create functional groups suitable for covalent bond), peptide grafting to the bulks or incorporation in the backbones of polymers, and insertion of the bioactive molecule in cross-linked hydrogels, as shown in Figure 3.4 (Hollander and Hatton 2003).

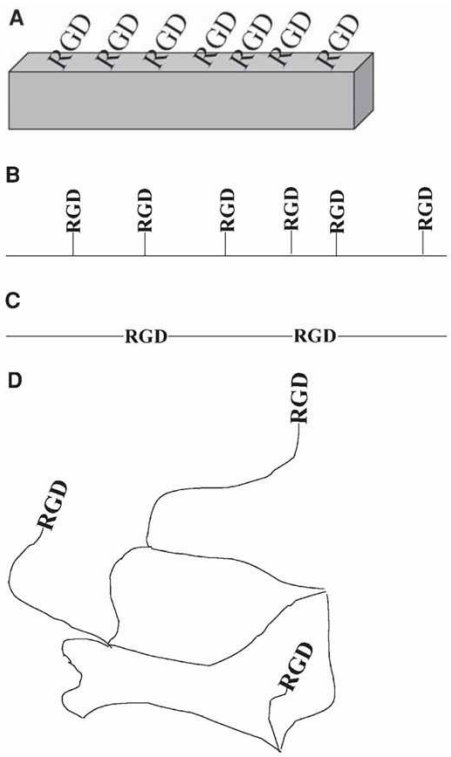

Figure 3.4 Methods for peptide functionalization of bio-inert materials. *Peptide functionalization can be performed by surface modification (A), polymer grafting (B), incorporation into polymer backbone (C), and hydrogel cross-linking (D) (Hollander and Hatton 2003).*

The bioactivity is conditioned by several variables, such as pattern distribution, density and orientation. Therefore, the uncontrolled *in vivo* adsorption of plasma proteins, containing integrin-binding molecules, or specific growth factors may reduce peptide functionality. These adsorbed proteins can have higher affinity with respect to the isolated peptide, due to the presence of additional domains (Bellis 2011). In the case of adhesive sequences, the competitive attachment and growth of other cell types can hamper the adhesion of targeted cells. For this reason, chosen bioactive motifs should be highly specific.

The ECs express several cell surface glycoprotein and receptors involved in ECM adhesion, some of which are still not known. The Arginine-Glycine-Aspartic acid (RGD) is one of the most diffuse amino acid sequences among the ECM proteins (Ruoslahti and Pierschbacher 1987). It is present in fibronectin (Pierschbacher and Ruoslahti 1984), laminin (Tashiro et al. 1991), vWF (Denis et al. 1993), collagen I (Ruoslahti and Pierschbacher 1987), fibrinogen (Gartner and Bennett 1985), vitronectin (Smith and Cheresh 1988),

and many others (Ruoslahti 1996). Since it is well-recognized by endothelial integrin receptors as an adhesive sequence, RGD was extensively used in the functionalization of polymeric materials (Hersel, Dahmen, and Kessler 2003; Lin et al. 1992). Decellularized porcine aortic valves were also cross-linked with cyclic RGD and PEG. Increase of tensile strength, decrease of scaffold degradation rate and improvement of HUVECs adhesion and proliferation were reported with respect to decellularized control (Zhou et al. 2015). The further incorporation of VEGF was tested with EPCs by confirming these results (Zhou et al. 2016). Unfortunately, this tripeptide is also involved, by means of the integrin glycoprotein IIb/IIIa of platelets, in the interaction with fibrinogen, the plasma protein responsible for clot aggregation and anchoring of activated endothelium. It may therefore trigger occurrence of thrombi (Phillips et al. 1988; Pytela et al. 1986).

The isoleucine-lysine-valine-alanine-valine (IKVAV), derived from the α-chain of laminin, has been reported as involved in the process of angiogenesis. Upon *in vivo* evaluation, IKVAV-based treatment was associated with ECs mobilization, branching, and capillary formation by mimicking the natural reaction to basal lamina disruption or fragmentation (Ali et al. 2013; Grant et al. 1992). This sequence was combined with elastin-derived domains (promoting the formation of endothelial tubular structures), RGD sequence (for cell adhesion) and motif with affinity for collagen, in order to create a customized artificial ECM able to promote angiogenesis (Nakamura et al. 2008). These fascinating results suggested IKVAV also as an angiogenic factor for revascularization of ischemic tissues (Grant and Zukowska 2000).

Tyrosine-isoleucine-glycine-serine-arginine (YIGSR) is a non-integrin receptor of laminin and induces ECs to form tubular networks when cultured on Matrigel (Corning Incorporated) (Grant et al. 1989). This motif has efficiently been used for endothelialization of synthetic surfaces, such as glycophase glass, PET and PTFE (Hubbell et al. 1991). Its incorporation into polyurethaneurea backbone demonstrated an improved endothelial adhesion, proliferation, migration, and ECM deposition, whereas did not support platelet attachment (Jun and West 2004). In further experiments, YIGSR has been used as chain extender and PEG was inserted in the soft segment to prevent platelets adhesion (Jun and West 2005b, 2005a).

The tetrapeptide arginine-glutamic acid-aspartic acid-valine (REDV) was identified for the first time in 1986 (Humphries et al. 1986). This short active sequence is located in the alternative spliced type III connecting segment (IIICS) of human plasma fibronectin, in a highly hydrophilic region (Mould et al. 1991), as shown in Figure 3.5.

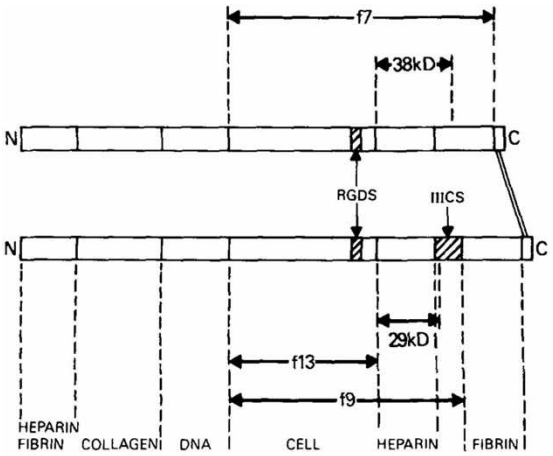

Figure 3.5 Human plasma fibronectin. *Fibronectin binds ECM components and cells in specific domains. REDV tetrapeptide is located in IIICS (Humphries et al. 1986).*

REDV is highly-specific for ECs through the α4β1 subunits of endothelial integrins (Massia and Hubbell 1992). Instead, it was demonstrated that fibroblasts, smooth muscle cells, and platelets did not recognize the sequence (Butruk-Raszeja et al. 2016; Hubbell et al. 1991; Ji et al. 2012; Wei et al. 2011; Yang et al. 2015; Yu et al. 2016) and the adsorption of fibrinogen was also reduced (Butruk-Raszeja et al. 2016). The efficacy of REDV was prevalently verified on grafted synthetic materials such as glycophase glass (Hubbell et al. 1991; Massia and Hubbell 1992), PEG-modified PET (Hubbell et al. 1991), PEG (Wei et al. 2011), polyurethanes (Butruk-Raszeja et al. 2016; Butruk et al. 2013; Yang et al. 2015), and poly(ε-caprolactone) coated with hyaluronic acid (Yu et al. 2016). The use of zwitterionic-based materials was tested to improve the selectivity. The antifouling properties of these compounds could further reduce non-specific interactions with smooth muscle cells and platelets (Ji et al. 2012). Eventually, REDV was also incorporated into artificial ECMs based on elastin-like domains and containing the entire CS5 adhesion domain of fibronectin. (Heilshorn et al. 2003). Recombinant elastin was enriched with REDV tetrapeptide and covalently bounded to cobalt chromium stents (Castellanos et al. 2015). In another stent application, REDV was combined

with a methacryloyloxyethyl phosphorylcholine, inhibiting protein adsorption and cell adhesion (Wei et al. 2013). REDV functionalized nanoparticles has been used to specifically target ECs in order to transfect them with genes aimed to promote the proliferation and migration (Shi et al. 2015; Wang et al. 2015).

3.2 Aim of the project

The aim of this project is to assess whether the covalent immobilization of EC-selective REDV tetrapeptide on pericardial scaffolds might accelerate *in vitro* endothelialization. This approach is tested in order to verify its future applicability as strategy to improve blood compatibility of TAHs.

In order to obtain these goals, the project focused on:

- Synthesis and characterization of REDV and rhodamine-conjugated REDV;
- Decellularization of pericardial scaffolds by means of TriCol protocol;
- Functionalization of the scaffolds with three concentration (10^{-5}, 10^{-6}, and 10^{-7} M) of rhodamine-conjugated REDV and quantification of the final amount linked;
- Functionalization of the scaffolds with 10^{-5} and 10^{-6} M of REDV and evaluation of endothelial adhesion and cytotoxicity.

3.3 Materials and methods

3.3.1 Decellularization of TriCol pericardial scaffolds

NBP tissues obtained at local abattoir were decellularized using the TriCol protocol, as previously described in Section 2.3.1.

3.3.2 Synthesis and characterization of REDV

REDV was produced in laboratory by solid-phase peptide synthesis (SPPS) in an automatic synthesizer (Syro I, MultiSynTech GmbH, Witten, Germany).

Two spacers (7-aminoeptanoic acid, Novabiochem, Merck Millipore) were added to the biologically active peptide sequence (REDV) facilitating the pericardial functionalization and enhancing the flexibility of the whole chain.

3.3.2.1 Solid phase peptide synthesis

The SPPS method was introduced by the Nobel Prized biochemist Robert Merrifield in 1963 (Merrifield 1963) and is based on consecutive addition of single amino acids to a growing peptide chain anchored to an insoluble porous support in a reactor.

The synthesis was performed on spherical resin beads made of amino PEG-PS copolymer and preloaded with an amino acid (phenylalanine, phe, in this case) to assure the presence of an aldehyde group in REDV C-terminus (H-Phe-H NovaSyn® TG resin, 856144, Merck Millipore, Figure 3.6) The resin's loading was 0.18 mmol/g. Before the start of the process, the resin was washed with synthesis solvent (N,N-dimethylformamide, DMF, Sigma-Aldrich) to maximize the swelling of functional groups.

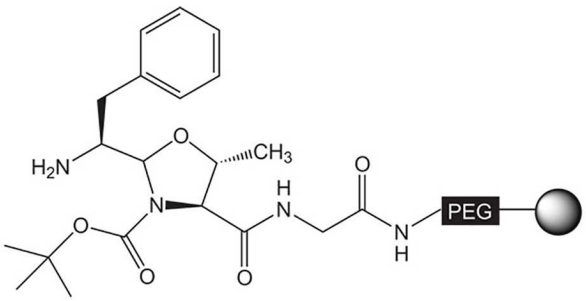

Figure 3.6 Resin for solid phase synthesis of REDV. *Resin was a PEG-PS copolymer preloaded with a Phe, protected in N-terminal and side chains.*

In order to avoid undesired reactions, the N-terminals of the amino acids to be coupled were protected by base-labile 9-fluorenylmethyloxycarbonyl (Fmoc chemistry), whereas acid-labile protecting groups were used for side chains: pentamethyl-2,3-dihydrobenzofuran-5- sulfonyl (Pbf) for Arg and tert-Butyl (OBut) for Asp and Glu.

The synthesis was achieved by single coupling and automatically iterating the steps of N-terminal deprotection, carboxyl group (COOH) activation, and formation of peptide bond by means of condensation reaction. At the end of the process, when the desired peptide was formed, the side chains groups were

deprotected and the peptide was cleaved from the solid support, as shown in Figure 3.7 (Stawikowski and Fields 2002). In our case, on the base of the selected resin and linker, the cleavage resulted in an aldehyde group in the peptide C-terminal.

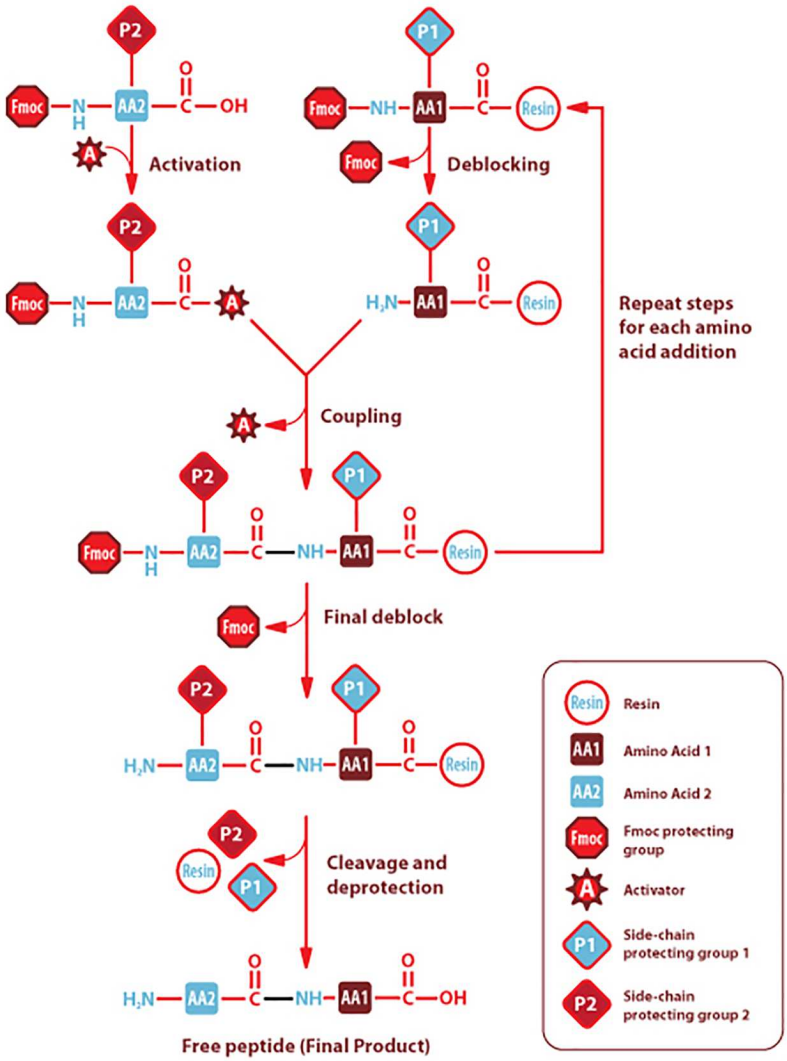

Figure 3.7 Scheme of solid phase synthesis. *Automatic synthesizer iterates steps of N-terminal deprotection, COOH activation, and formation of peptide bond to produce desired motif. Side chains protecting groups are deprotected and resin is cleaved manually. (Image from Sigma Aldrich 2017).*

The α-amino temporary protecting group was deprotected with solutions of 40% and 20% piperidine (Biosolve Chimie, Dieuze, France) in DMF for 3 and 12 minutes, respectively, and followed by washes in DMF (Fmoc deprotection).

COOH groups were activated with a 0.45 M solution N,N,N′,N′-tetramethyl-O-(1H-benzotriazol-1-yl)uronium hexafluorophosphate (HBTU,

Advanced Biotech, Totowa, NJ, USA) and 1-hydroxybenzotriazole hydrate (HOBt, Advanced Biotech) in DMF and a solution of 2 M N,N-diisopropylethylamine (DIPEA, Biosolve Chimie) in N-methyl-2-pyrrolidinone (NMP, Biosolve Chimie). To these activators was added a solution 0.45 M of the amino acid or spacer to be coupled (all the amino acids and the spacer were supplied by Novabiochem). The reaction time was 45 minutes and was followed by washes in DMF.

Once completed the synthesis, the peptide linked to resin was washed 3 times in dichloromethane (DCM, Biosolve Chimie) and dried for 2 hours under vacuum. The material was divided into two parts: the first was coupled with 5(6)-carboxytetramethyl-rhodamine (Novabiochem), a fluorescent dye inserted to locate and quantify Rhod-conjugated REDV tetrapeptide (RhodREDV) in the tissue after the functionalization, whereas the second remained unconjugated and was used for the evaluation of HUVECs adhesion and cytotoxicity assays.

The final step was the Fmoc deprotection of last coupled amino acid (Arg, *i.e.*, the first of the sequence), as described above.

3.3.2.2 Ninhydrin or Kaiser test

Ninhydrin test is a quantitative colorimetric test used to monitor the effectiveness of coupling reactions by detecting free primary amines (Sarin et al. 1981).

The test was performed with a dedicated kit supplied by Applied Biosystems (Foster City, CA, USA) and composed of three monitors: a solution of 76% (w/w) phenol/ethanol, a solution of 0.2 mM of potassium cyanide/pyridine, and a solution of 0.28 M of ninhydrin/ethanol. The absorbance at 570 nm was read in a Perkin-Elmer spectrophotometer.

The amount of free amino groups was calculated with the following formula:

$$\frac{\mu\text{mol}}{\text{g}} = \frac{\left[\left(\text{Abs}_{\text{sample}}\text{-Abs}_{\text{blank}}\right)\ \text{dilution}\right]\ 10^6}{(\text{molar extinction coefficient})\ (\text{sample weight})}$$

where:

- Dilution = 5 ml,
- Molar extinction coefficient = 15000 M^{-1} $cm^{-1,}$
- Samples weight = 2.35 mg.

The percentage of coupling is calculated as follow:

$$\%=\left(1-\frac{\frac{\mu mol}{g}\text{ of amino groups}}{10^3\left(\frac{mmol}{g}\text{of new resin substitution}\right)}\right)100$$

where:

$$\frac{mmol}{g}\text{ of new resin substitution}=\frac{1000}{\text{PM of growing peptide}}.$$

3.3.2.3 Side chain groups deprotection and resin cleavage

The acid-labile side chains protecting groups were deblocked with trifluoroacetic acid (TFA, Biosolve Chimie) for 1 hour under stirring.

After three washes in DCM and 30 minutes of vacuum drying, the resin was cleaved with solution of 11% (v/v) acetic acid (Sigma-Aldrich), 23% (v/v) methanol (Sigma-Aldrich), and 70% (v/v) DCM in deionized water for 1 hour under stirring.

Lastly, the reactor was washed three times in DCM and the obtained solution was reduced to small volumes by means of solvent evaporation in a rotary evaporator (Heidolph Instruments GmbH & CO KG, Schwabach, Germany) and lyophilized (Labconco Corporation, Kansas City, MO, USA).

3.3.2.4 Crude peptide purification

Crude peptides were characterized and purified by reversed-phase high-performance liquid chromatography (RP-HPLC). This technique allows to identify and isolate one or more compounds from a liquid solution. For this purpose, the aqueous solution to be characterized (mobile phase) flows through a nonpolar stationary phase made of a porous silica layer functionalized with hydrocarbon linear chains. The different affinity of compounds for mobile and stationary phases determines the time spent inside the column (retention time).

The analytic RP-HPLC was performed with Water 600 HLPC system (Waters Corporation, Milford, MA, USA), supplied with autosampler (model 717) and UV/Vis detector (model 2487), and the Vydac Everest C_{18} column (5 µm particle size, 300 Å pore size, 4.6 x 250 mm length, Hichrom, Theale, UK). Empower software (Waters) was used to set up the analysis and acquire the data. Waters 600 HPLC pump and Delta Pack C_{18} column (15 µm particle size, 100 Å pore size, 7.8 x 300 mm length, Waters) were used for semipreparative chromatographic analyses. Data were acquired by a Kipp & Zonen recorder (Delft, The Netherlands).

RP-HPLC analyses were carried out by gradient method. The amount of organic solvent of mobile phase was dynamically increased during the evaluation, in order to enhance the competitiveness in terms of affinity with the stationary phase and its elution potential. For these reasons, a solution of 0.05 % TFA in MilliQ water (A eluent) and a solution of 0.05% TFA in acetonitrile (B eluent) were used. The gradient was set at 15% to 30% of B eluent in 30 minutes for REDV, and at 20% to 40% in 30 minutes for RhodREDV. The absorbance was read at 214 nm (absorption peak of the peptide bond).

Crude REDV peptide was dissolved in MilliQ water, whereas RhodREDV was prepared in a solution of 20% (v/v) acetonitrile (Sigma-Aldrich) to improve the solubility. Prior to the analyses, the solutions were filtered with a 0.22 µm PVDF filter.

After semipreparative RP-HPLC, the fractions of interest were lyophilized and maintained at 4°C in the dark.

3.3.2.5 Mass spectrometry

Mass spectrometric analyses (matrix-assisted laser desorption/ionization time of flight mass spectrometry, MALDI-TOF) were carried out to quantify the mass of purified REDV and RhodREDV. The instrument used was a 4800 MALDI-TOF/TOF TM analyzer provided with 4000 Series Explorer TM software (Applied Biosystem/ MDS Sciex, Foster City, CA, USA).

Briefly, samples were mixed with a matrix and loaded on a metal plate. A laser irradiated the matrix/sample compound and the developed energy caused

the rapid heating and vaporization of the material surface (desorption). The process generated ions (ionization), which were protonated or deprotonated by matrix components and analyzed by a detector on the base of their mass and charge (m/z ratio).

3.3.3 Functionalization of pericardial scaffolds

In order to functionalize the pericardial scaffolds, peptides were dissolved in PBS at starting concentration of 10^{-5} M (stock solution). The aldehyde groups of REDV and RhodREDV reacted with the primary amines of the biological molecules and, through a condensation reaction, formed Schiff bases. Hence, the imines were stabilized by a reducing agent, the sodium cyanoborohydride (Merck Millipore), added to the stock solution (2.13 mg of $NaBH_3CN$ for 1 mg of peptide). Stock solution was then serially diluted to produce lower concentrations (10^{-6} and 10^{-7} M).

Circular punches of 0.8 cm diameter (Kai Medical) were placed into a 96-well plate (Sarstedt) and functionalized with 100 µl of peptide solution for 24 hours at room temperature.

After functionalization, the punches were deeply washed in PBS: two washes of 30 minutes were performed at room temperature and one wash overnight at 4°C, all under agitation. Samples were preserved in 3% (v/v) penicillin-streptomycin (Sigma-Aldrich) and 0.25% (v/v) Amphotericin B (Gibco) in PBS at 4°C until use.

3.3.4 Quantification of functionalization

The quantification of RhodREDV peptide concentrations in functionalized DBP scaffolds was performed in a TPM as reported in (Gaigalas et al. 2005; Schwartz et al. 2002). The original method was proposed to quantify the fluorescence of fluorescein isothiocyanate (FITC) immobilized on microspheres in suspension in a fluorometer. Therefore, it was adapted to our case (labelled peptides anchored on solid supports) on the base of some assumptions. The measured intensity (I) was defined as follow:

$$I = I_0 \ \Omega \ \varepsilon(\lambda_{ex}) \ N \ \Phi$$

where:

- I_0 was the incidence intensity,
- Ω was a geometrical factor depending on the instrument,
- $\varepsilon(\lambda_{ex})$ was the molar extinction coefficient or molar absorptivity, a sample property depending on the excitation wavelength,
- N was the number of fluorophores per unit of volume and depends on the sample,
- Φ was the quantum yield, *i.e.*, the ratio between emitted and absorbed photons.

Parameters Ω, $\varepsilon(\lambda_{ex})$, N, and Φ were unknown. As regards to the measured intensity of the RhodREDV in solution (sol) with a known concentration or the anchored RhodREDV (anch) on DBP scaffolds, it was possible to write:

$$I_0\ \Omega\ \varepsilon_{sol}(\lambda_{ex})\ N_{sol}\ \Phi_{sol} = I_0\ \Omega\ \varepsilon_{anch}(\lambda_{ex})\ N_{anch}\ \Phi_{anch}$$

in which I_0 and Ω were the same on both sides of equation because did not depend on samples. Accordingly, the equation became:

$$\varepsilon_{sol}(\lambda_{ex})\ N_{sol}\ \Phi_{sol} = \varepsilon_{anch}(\lambda_{ex})\ N_{anch}\ \Phi_{anch}$$

In our case, the molar extinction coefficient was the same for anchored or non-anchored RhodREDV. The 5(6)-carboxytetramethyl-rhodamine is already coupled to Arg. The functionalization of DBP with RhodREDV did not therefore alter this bond and the molar extinction coefficient was not modified.

Based on these considerations, the equivalent concentration (C_{eq}) could be quantified by a calibration curve and the following formula:

$$C_{eq} = 10^{-q}\ (I\ P_{adj})^{m}$$

where:

- q is the y-intercept of the calibration curve,
- m is the slope of the calibration curve.

The calibration curve was prepared with serial dilutions of free RhodREDV in PBS (from 10^{-5} M to 10^{-10} M). Intensity was measured with Fiji (Schindelin et al. 2012), considering six ROIs for each concentration. The fluorescence of PBS was subtracted as blank for calibration curve. The natural fluorescence of pericardial ECM components (Croce and Bottiroli 2014; Monici 2005) was considered as blank for tissue samples. This background signal is due to the

presence of aromatic amino acids, such as tryptophan, phenylalanine and tyrosine, in elastin and collagen (Shoulders and Raines 2009; Starcher and Galione 1976). Peptide surface densities were calculated by multiplying the estimated concentrations by the depth of collected focal volume (1.5 µm).

Images were acquired at excitation wavelength of 1,200 nm for SHG signal and 800 nm for rhodamine. A fixed resolution of 1,024×1,024 pixels and accumulation of 120 frames were used.

3.3.5 Assessment of ECM functionalized scaffolds

Thicknesses and area of 10^{-5} M, 10^{-6} M REDV-functionalized and control DBP scaffolds were measured in order to evaluate whether the functionalization affected the geometrical properties of treated tissues. Thicknesses were measured with a digital caliper (Mitutoyo, Kawasaki, Japan). Areas were calculated on sample images elaborated in Fiji (Schindelin et al. 2012).

The assessment of the integrity of main components of functionalized DBP tissues, *i.e.*, collagen type I and elastin, was carried out as described in Section 2.3.2.2. Briefly, samples of 10^{-5} M, 10^{-6} M REDV functionalized and control DBP samples were fixed in 2% PFA and snap-frozen. Then, 5 µm-thick cryosections were acquired with TPM.

3.3.6 Assessment of REDV-functionalization bioactivity and toxicity

Endothelial cell adhesion was evaluated by staining cells with a viability assay. *In vitro* cytotoxicity tests were carried out according to ISO requirements (International Organization for Standardization 2009).

3.3.6.1 Disinfection protocol

Functionalized and control samples were cut into circular punches (0.8 cm of diameter, Kai Medical). The disinfection was achieved as described in Section 2.3.4.3.1 and reported in (Fidalgo et al. 2017).

3.3.6.2 Seeding conditions

The static cell seeding was accomplished with HUVECs. The cells were seeded at 100,000 cells/cm^2 and cultivated in standard conditions. Complete endothelial growth medium, supplemented with 1% (v/v) penicillin-streptomycin, was used (PromoCell GmbH, Heidelberg, Germany).

Polystyrene of tissue culture-treated 24-well plates (Costar®, Corning Incorporated) and cyanoacrylate Super Attack (Loctite) were used as positive and negative controls of cytotoxicity, respectively.

3.3.6.3 Cell adhesion and viability

Cell viability and adhesion were evaluated using fluorescent Live/Dead staining, according to manufacturer's protocol (Molecular Probes), at 1, 3, 7, and 14 days.

Samples were analyzed in the TPM by acquiring three ROIs for each sample. Due to tissue irregularities or in presence of incline, images were acquired as z-stacks and elaborated as projections with Fiji built-in plugins.

The percentage of viable cells was calculated with the following equation:

$$\%\ \text{viable cells} = \frac{\text{live cells}}{\text{live cells} + \text{dead cells}} \cdot 100$$

The presence of cell lining was confirmed histologically. Samples were fixed in a solution of 2% PFA in PBS for 10 minutes at room temperature. After two washes in PBS, tissues were dehydrated in a solution of 20% sucrose in PBS overnight at 4°C, embedded in 20% sucrose-O.C.T. (1:1), snap-frozen in isopentane and liquid nitrogen, and stored at -80°C. Cryosections of 5 µm thickness were obtained in a cryostat (Leica) and stained with H&E (BioOptica).

In order to evaluate the expression of platelet-endothelial cell adhesion molecule (CD31), vWF and connexin-43 (conx43), TPM-combined indirect immunofluorescent analyses were performed. Rabbit polyclonal anti-CD31 (1:50, 250590, Abbiotec, San Diego, CA, USA), rabbit polyclonal anti-vWF (1:50, A0082, Dako) and rabbit polyclonal anti-conx43 (1:100, ab11370, Abcam) were used as primary antibody. Rhod-conjugated anti-rabbit

(Millipore) was used as secondary antibodies (1:100). Primary and secondary antibodies were diluted in a solution of 1% (w/v) bovine serum albumin in PBS. Nuclei were counterstained with Hoechst (Sigma-Aldrich).

Images were acquired at excitation wavelength of 1,200 nm for the SHG signal and 800 nm for elastin and the secondary antibody fluorophores. A fixed resolution of 1,024×1,024 pixels and accumulation of 120 frames were adopted.

3.3.6.4 Quantification of cytotoxicity

Cytotoxicity was evaluated by quantifying LDH activity and MTS production, as described in Section 2.3.4.3.4.

Cell media were collected from tested tissues and controls at 24, 48, and 72 hours and maintained at -80°C until the analyses were performed. Released LDH was quantified with Pierce LDH cytotoxicity assay kit (Thermo Scientific) and the percentage of cytotoxicity was calculated as reported in (Cebotari et al. 2010).

All tested samples and controls were incubated with MTS reagent for 3 hours and 20 minutes (Promega) at 1, 3, 7, and 14 days. The absorbance was acquired at 490 nm in a plate reader (Bio-Rad).

3.3.7 Statistical analyses

All data were processed and analyzed with Prism (GraphPad Software). Results are reported as mean ± standard deviation. Groups of data were compared by variance analyses (one- or two-way ANOVA). Significant level was set at 5%. More details about settings are given in the graph captions.

3.4 Results

3.4.1 REDV and RhodREDV characterization

The coupling percentage resulting from the Kaiser test made on RhodREDV was of 95.16%.

The results of analytic HPLC analyses performed on REDV and RhodREDV are shown in Figure 3.8. Chromatograms showed that REDV retention times was at 26.4 minutes (Figure 3.8A), whereas RhodREDV was eluted at 22.0 minutes (Figure 3.8B). The carboxytetramethyl-rhodamine used for the functionalization was a mixture and, therefore, the two peaks of Figure 3.8B refer to the two isomers.

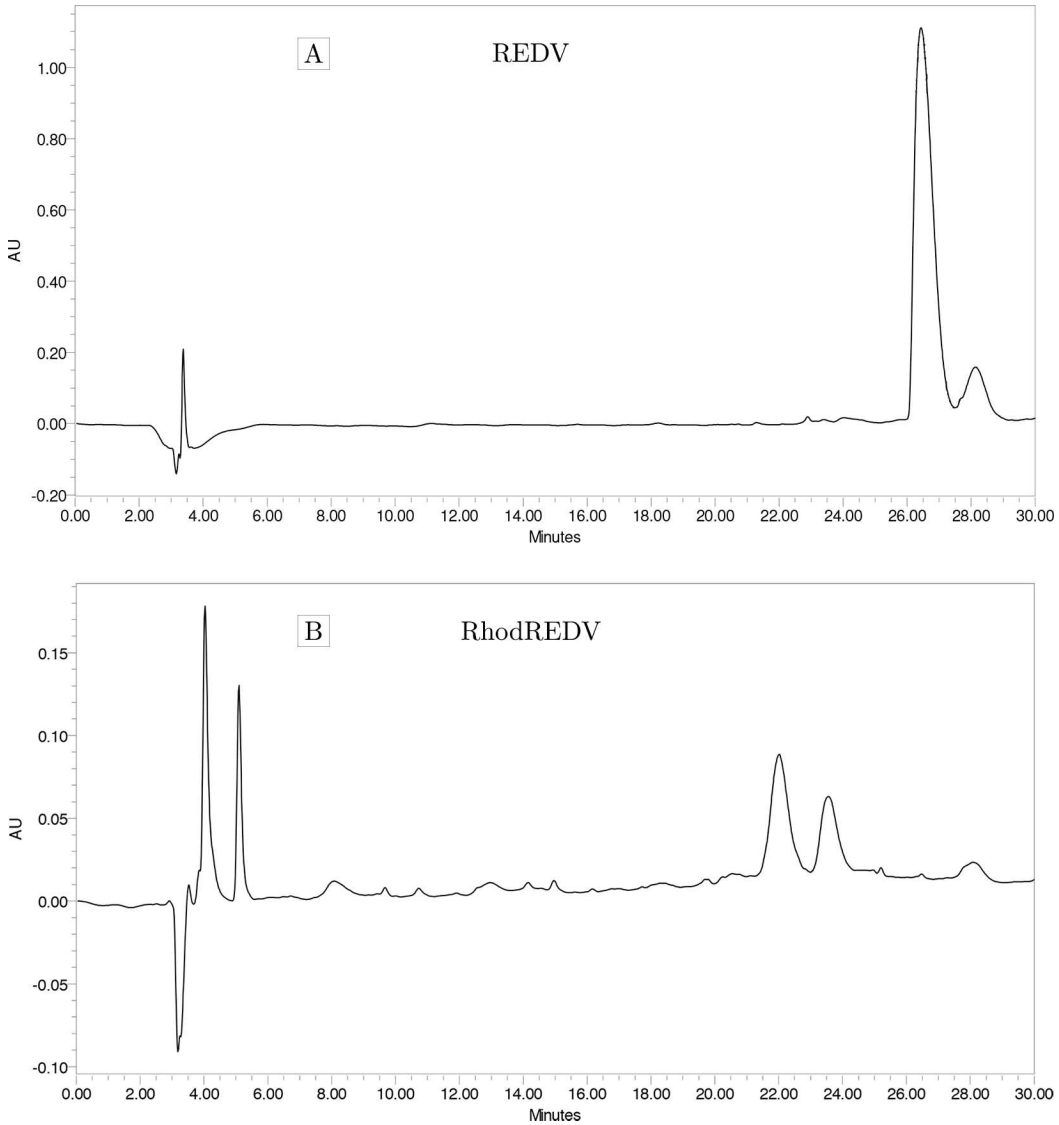

Figure 3.8 Analytical RP-HPLC graphs of crude REDV and RhodREDV peptides. *Analysis conditions for REDV (A) were: Vydac Everest C_{18} Column, flow of 1 ml/min, A eluent 0.05% TFA in deionized water, B eluent 0.05% TFA in acetonitrile, injection of 100 µl di REDV dissolved in deionized water (1 mg / 1 ml), gradient from 15% to 30% of B eluent in 30 minutes, absorbance acquired at 214 nm. The analysis conditions for RhodREDV (B) were: Vydac Everest C_{18} Column, flow of 1 ml/min, A eluent composed of 0.05% TFA in deionized water, B eluent composed of 0.05% TFA in acetonitrile, injection of 100 µl di REDV dissolved in 20% acetonitrile and deionized water (1 mg / 1 ml), gradient from 20% to 40% of B eluent in 30 minutes, absorbance acquired at 214 nm.*

The semipreparative analyses allowed to subdivide the solutions of crude REDV and RhodREDV in 13 fractions each, as shown in Figure 3.9.

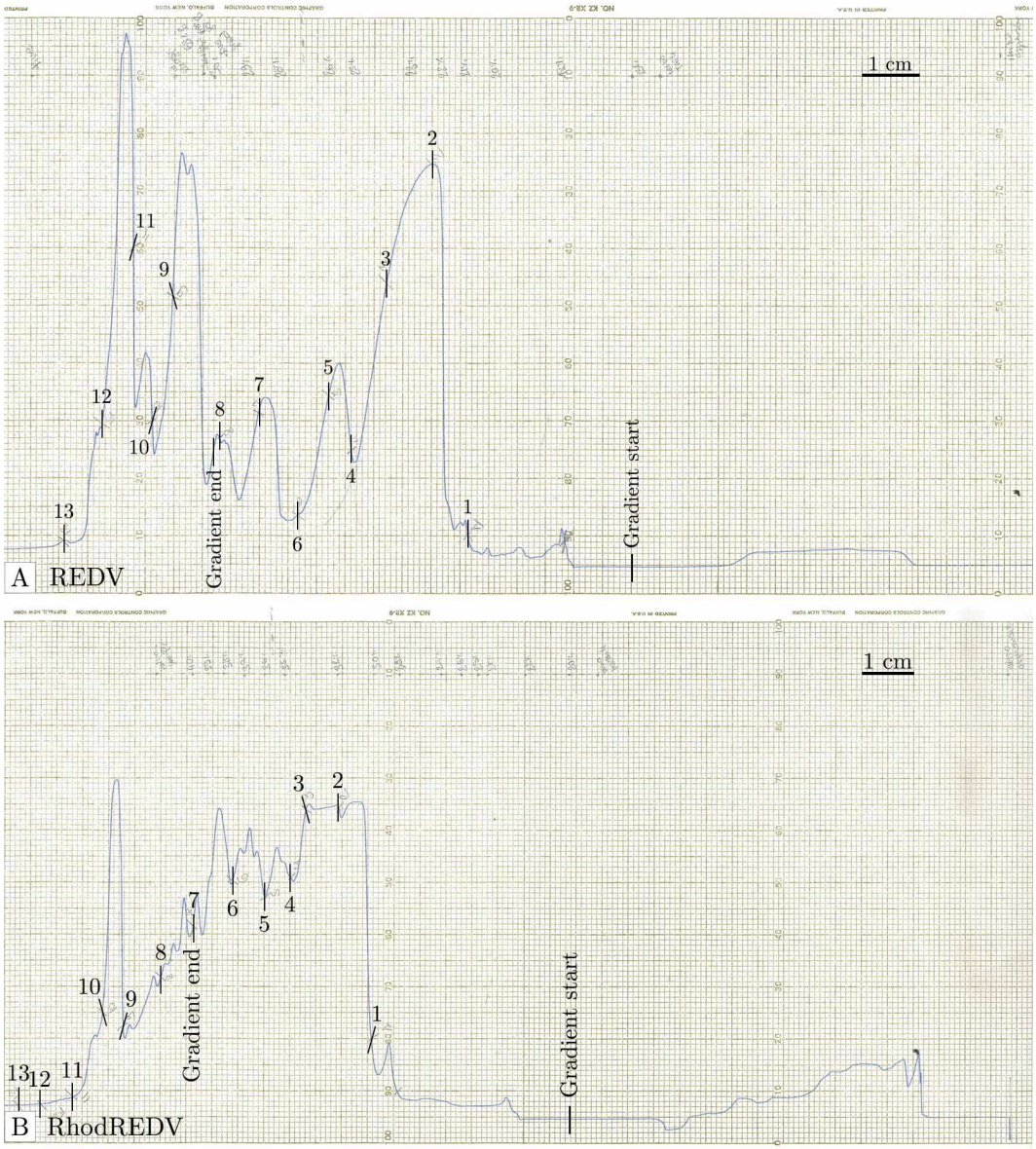

Figure 3.9 Semipreparative RP-HPLC graphs of crude REDV and RhodREDV peptides. *HPLC conditions for REDV (A) were: Delta Pack C_{18} Column, flow of 1 ml/min, A eluent 0.05% composed of TFA in MilliQ water, B eluent composed of 0.05% TFA in acetonitrile, injection of 100 µl di REDV dissolved in MilliQ water (1 mg / 1 ml), gradient from 15% to 30% of B eluent in 30 minutes, 4 ml/min flow, full-scale value of 4.0 Abs, paper speed of 0.5 cm/min, absorbance acquired at 214 nm. HPLC conditions for RhodREDV (B) were: Delta Pack C_{18} Column, flow of 1 ml/min, A eluent 0.05% TFA in deionized water, B eluent 0.05% TFA in acetonitrile, injection of 100 µl di REDV dissolved in 20% acetonitrile and deionized water (1 mg/1 ml), gradient from 20% to 40% of B eluent in 30 minutes, 4 ml/min flow, full-scale value of 4.0 Abs, paper speed of 0.5 cm/min, absorbance acquired at 214 nm.*

The fractions 2, 3, 4, 5, 6, and 12 of purified REDV were examined by analytical RP-HPLC, as reported in Figure 3.10. It was possible to appreciate

the gradual and progressive reduction of REDV peak (around 15 minutes) as the fraction number increased. The peak was totally absent in fraction 12 (Figure 3.10F). The homogeneity of component at 14.95 min, obtained by integrating the analytic chromatographic pattern, was 99.70% for fraction 3.

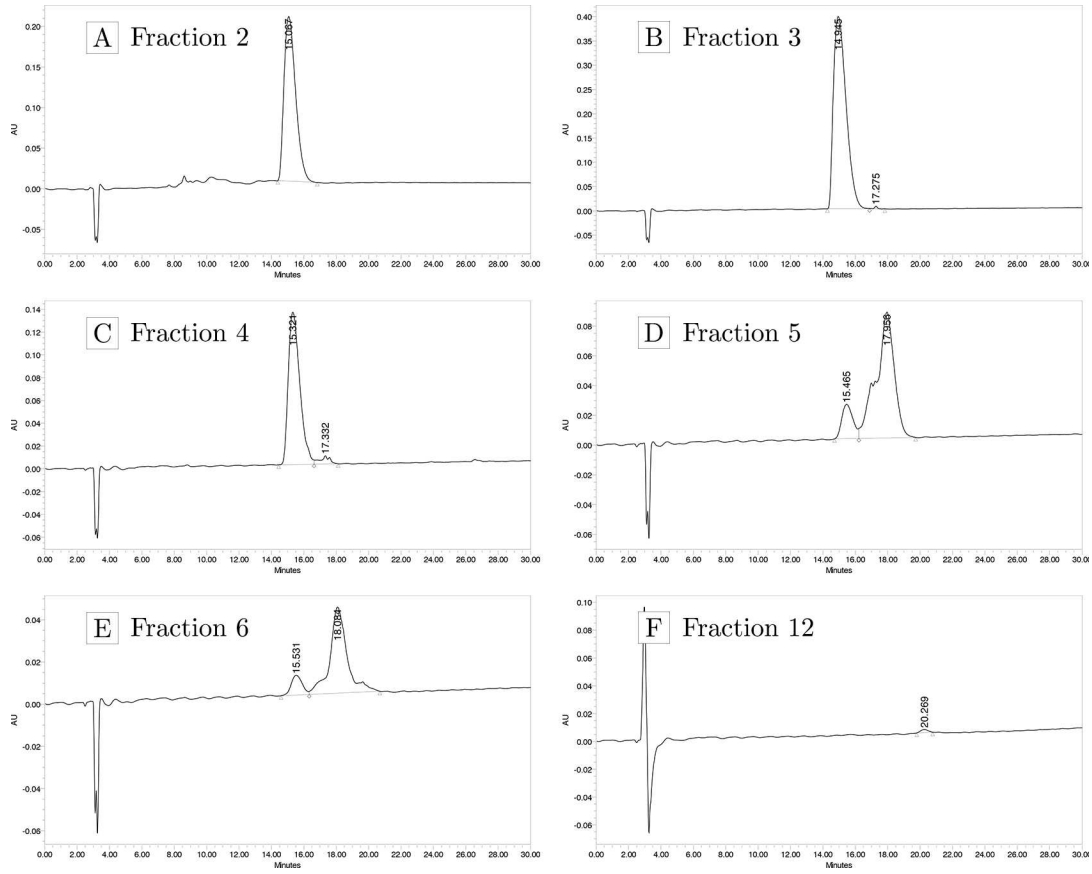

Figure 3.10 Analytical RP-HPLC graphs of fractions 2, 3, 4, 5, 6, and 12 of purified REDV peptide. *Analysis conditions were: Vydac Everest C_{18} Column, flow of 1 ml/min, A eluent composed of 0.05% TFA in deionized water, B eluent composed of 0.05% TFA in acetonitrile, injection of 100 µl di REDV dissolved in deionized water (1 mg / 1 ml), gradient from 15% to 30% of B eluent in 30 minutes, absorbance acquired at 214 nm.*

Analogously, the fraction 2, 3, 4, 5, and 10 of RhodREDV were analyzed (Figure 3.11). The homogeneity of the major peak at retention time of 16.62 min of fraction 3 was 89.09%.

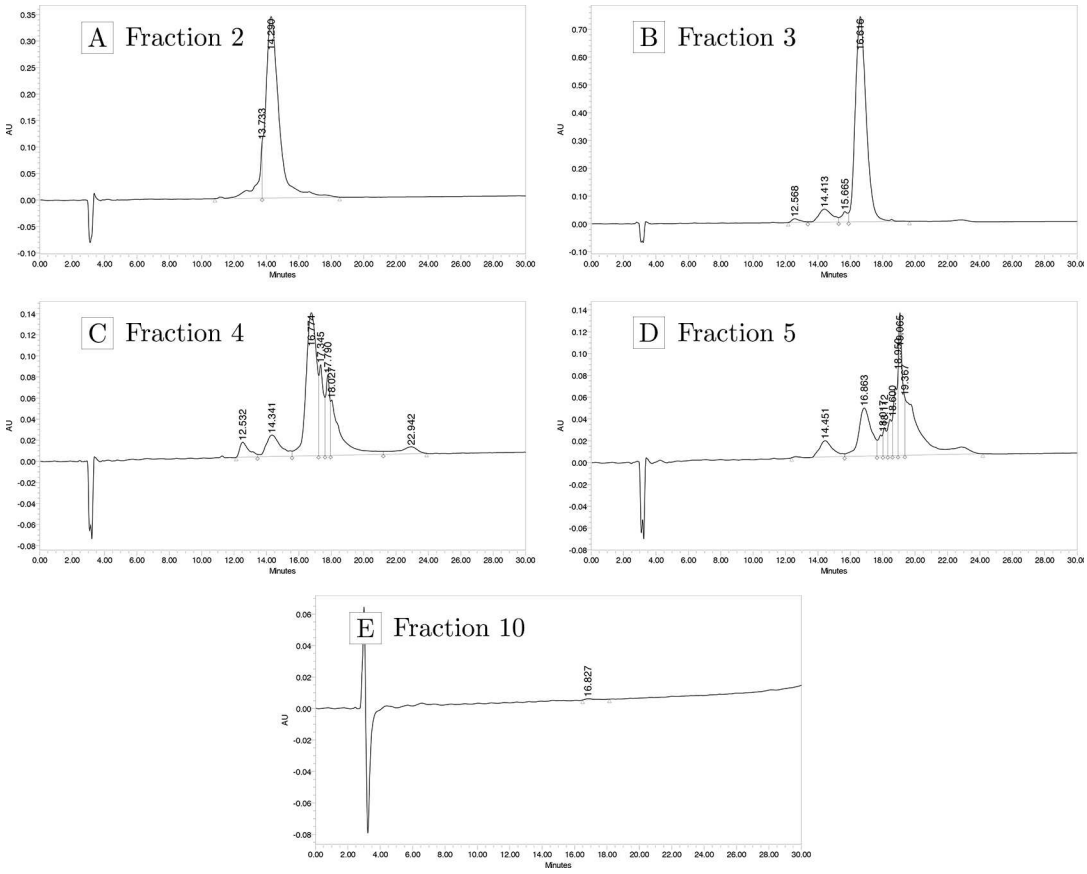

Figure 3.11 Analytical RP-HPLC graphs of fractions 2, 3, 4, 5, and 10 of purified RhodREDV peptide. *Analysis conditions were: Vydac Everest C_{18} Column, flow of 1 ml/min, A eluent composed of 0.05% TFA in deionized water, B eluent composed of 0.05% TFA in acetonitrile, injection of 100 µl di REDV dissolved in deionized water (1 mg / 1 ml), gradient from 20% to 40% of B eluent in 30 minutes, absorbance acquired at 214 nm.*

The fractions 2, 3, 4, 5, and 6 of purified REDV and 2, 3, 4, and 5 of RhodREDV underwent MALDI-TOF analyses in order to confirm the presence and the molecular weight (MW) of the peptide of interest. The theoretical MW of REDV was 903.09 Da and of RhodREDV 1332.54 Da. The experimental masses were 903.73 Da and 1316.14 Da, respectively. In Figure 3.12 are reported the MALDI-TOF results evaluated in fractions 3 of REDV and RhodREDV, the selected ones for DBP functionalization.

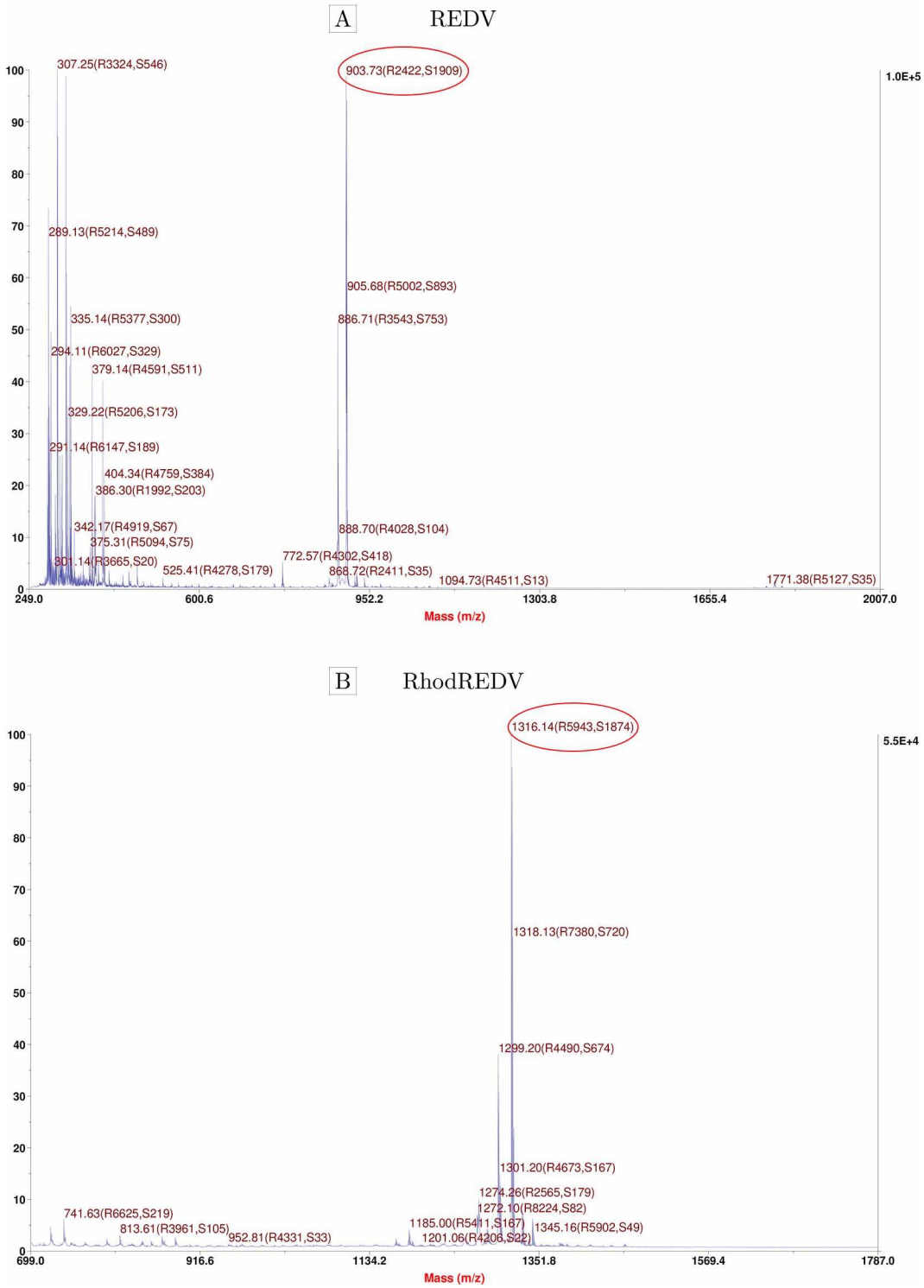

Figure 3.12 Mass analyses of REDV and RhodREDV. *MALDI-TOF evaluation performed on fraction 3 of REDV (A) and RhodREDV (B) confirmed the identity of the purified peptides (red circles). REDV: experimental mass = 903.73 Da, theoretical mass = 903.09 Da. RhodREDV: experimental mass = 1316.14 Da, theoretical mass = 1332.54 Da.*

3.4.2 Quantification of RhodREDV functionalization

The calibration curve of RhodREDV in PBS is reported in Figure 3.13. The results demonstrated a linear relation between the concentration of RhodREDV in solution and the intensity of the fluorescent signal. The estimated coefficient of determination (R^2) was 0.98 and confirmed the goodness of the linear fit.

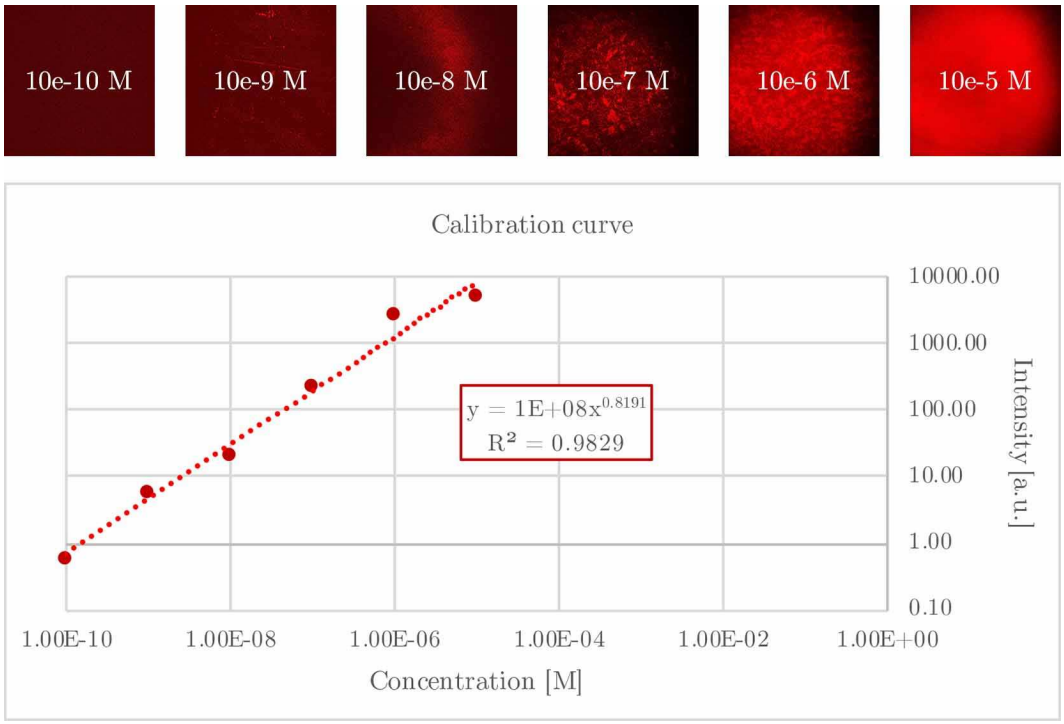

Figure 3.13 Calibration curve of RhodREDV in solution. *Calibration curve was obtained by acquiring images of serial dilutions of RhodREDV in PBS (from 10^{-5} M to 10^{-10} M).*

Surface images of control and RhodREDV DBP scaffolds showed that it was possible to modulate the functionalization by varying the peptide concentration (Figure 3.14). With respect to the control (Figure 3.14A, E, I, M), the highest intensity was acquired for 10^{-5} M REDV-functionalized DBP samples (Figure 3.14B, F, J, N), whereas 10^{-6} and 10^{-7} M concentrations generated a very low signal in treated scaffolds (Figure 3.14C, D, G, H, K, L, O, P). Generally, for a given concentration and on *serosa* layer, the peptide appeared uniformly distributed (Figure 3.14B-D, F-H). On *fibrosa*, due to the presence of loser collagen bundles and isolated fibers, it was possible to appreciate a higher affinity of the peptide towards these structures (Figure 3.14J-L, N-P).

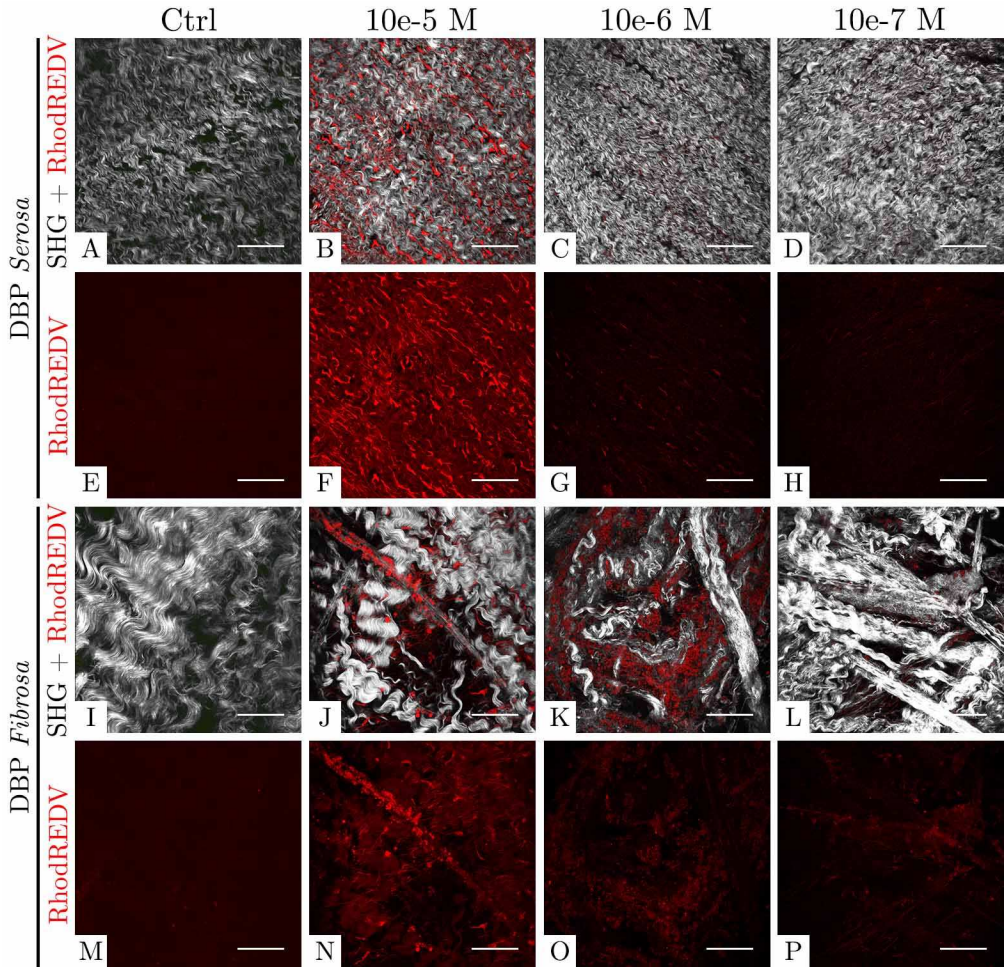

Figure 3.14 RhodREDV-functionalized DBP scaffolds. *Images of functionalized DBP scaffolds qualitatively confirmed correlation between concentration of peptide and fluorescent intensity (B-D, F-H, J-L, N-P). The serosa (B-D, F-H) and fibrosa (J-L, N-P) layers behaved differently. Results were compared with control unfunctionalized DBP scaffolds (A, E, I, M). Scale bar = 100 μm.*

Results of bonded peptide concentration and surface density, based on fluorescent intensity quantifications, are reported in Table 3.1 and Figure 3.15. RhodREDV was distributed uniformly on DBP *serosa*, whereas on *fibrosa* a few aggregates of peptide were located along the collagen bundles. The relation between peptide dose and fluorescent intensity was clearly directly proportional: increase of concentration determined increase of intensity. The 10^{-5} M RhodREDV functionalization generated highest values of fluorescence intensity and, therefore, amount of bonded peptide to the scaffolds. These quantities were statistically different with respect to the control and other two considered concentrations ($p < 0.0001$), on both *serosa* and *fibrosa*. The intensities of 10^{-6} and 10^{-7} M functionalized DBP tissues were not statistically

different from control autofluorescence. Consequently, the comparison between respective concentrations was not significant as well.

	Serosa			*Fibrosa*		
	Intensity [a.u.]	Concentration [M]	Surface density [mol/cm^2]	Intensity [a.u.]	Concentration [M]	Surface density [mol/cm^2]
Ctrl	241.94 ± 11.45	-	-	249.86 ± 8.30	-	-
10^{-5} M	1,575.37 ± 349.67	7.83 ± 2.44 * 10^{-7}	1.17 ± 0.37 * 10^{-13}	1,422.86 ± 467.04	6.76 ± 3.31 * 10^{-7}	1.01 ± 0.50 * 10^{-13}
10^{-6} M	264.74 ± 4.13	5.43 ± 1.18 * 10^{-9}	8.14 ± 1.77 * 10^{-16}	276.37 ± 13.52	6.69 ± 4.14 * 10^{-9}	1.00 ± 0.62 * 10^{-15}
10^{-7} M	254.12 ± 1.54	2.52 ± 0.39 * 10^{-9}	3.78 ± 0.58 * 10^{-16}	261.44 ± 4.66	2.41 ± 1.18 * 10^{-9}	3.61 ± 1.77 * 10^{-16}

Table 3.1 Values of intensity, concentration and surface density quantified on RhodREDV-functionalized DBP scaffolds.

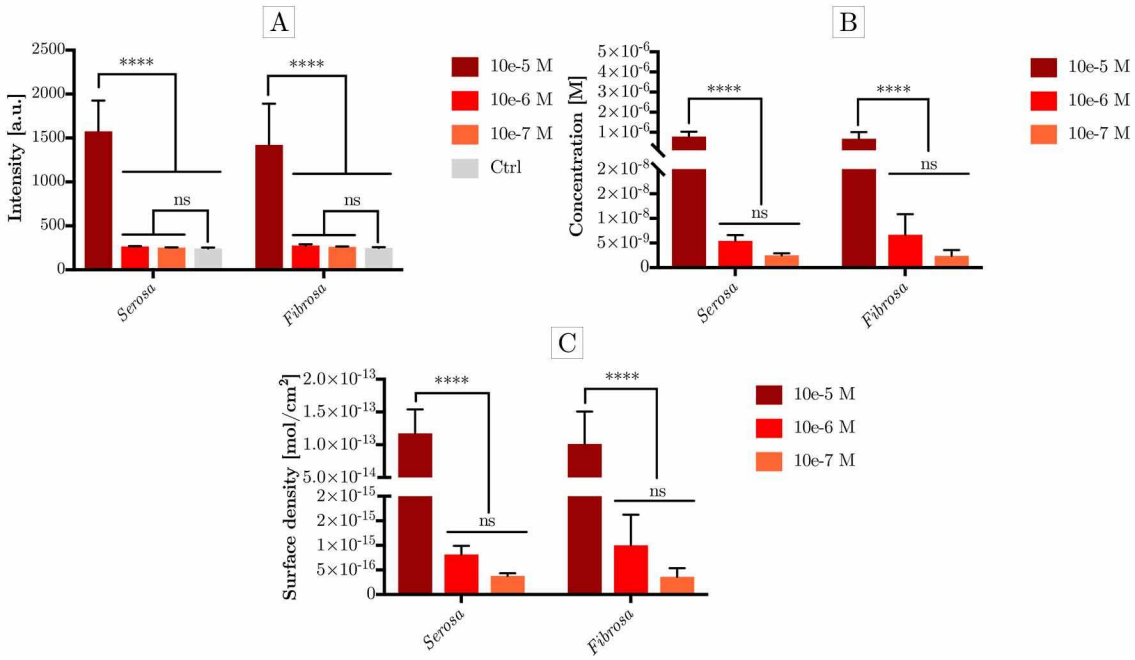

Figure 3.15 Quantification of intensity, concentration and surface density of RhodREDV functionalized DBP scaffolds. *Intensity (A), concentration (B) and surface density (C) of 10^{-5} M functionalized scaffolds were statistically higher with respect to the other two considered concentrations. Intensities, concentrations and surface densities of 10^{-6} and 10^{-7} M functionalized DBP scaffolds were not statistically different from that observed for the control or between each other's. Two-way ANOVA, Sidak's (A) and Tukey's (B, C) multiple comparison tests, **** $p < 0.0001$.*

3.4.3 Evaluation of functionalized ECM

After functionalization, the geometrical properties of the samples (thickness and area) were maintained with respect to control scaffolds for 10^{-5} and 10^{-6} M concentrations (Figure 3.16).

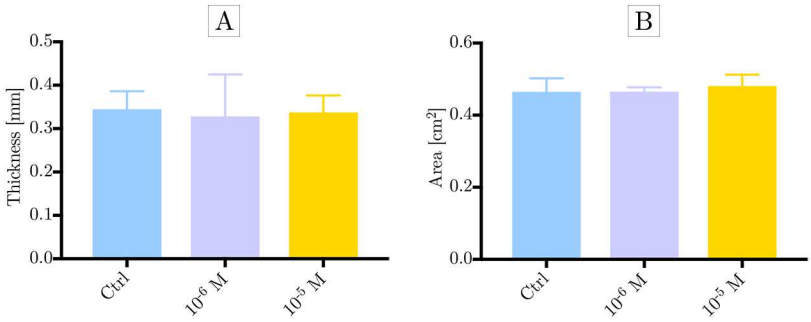

Figure 3.16 Evaluation of thickness and area of functionalized DBP scaffolds. *After functionalization, there was no statistical difference in terms of thickness (A) and area (B) with respect to control DBP for both concentrations. One-way ANOVA, Tukey's multiple comparison test.*

Main ECM components were also fully preserved. Collagen I showed unaltered SHG signal and elastin maintained strong TPEF (Figure 3.17).

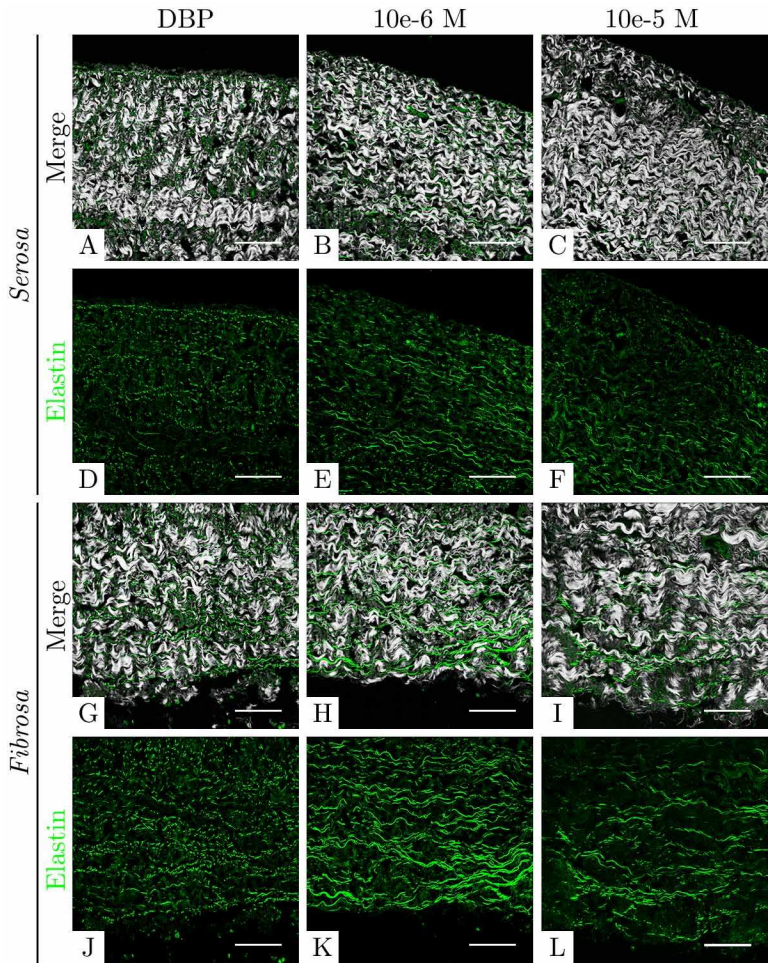

Figure 3.17 TPM images of ECM main components of functionalized DBP scaffolds. *Functionalization did not affect the optical properties of collagen (B, C, H, I) and elastin (E, F, K, L) with respect to the control (A, D, G, J). Scale bar = 100 μm.*

3.4.4 Evaluation of cell adhesion, viability and toxicity

Data of cell density at 1, 3, 7, and 14 days are reported in Figure 3.18 and Table 3.2. Density progressively increased statistically within each group until day 7. Between days 7 and 14, growth slightly slowed down and the number of HUVECs did not increase significantly.

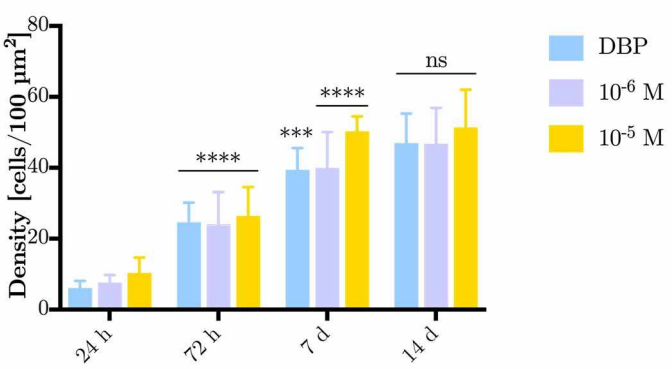

Figure 3.18 Progression of HUVECs density at 1, 3 7, and 14 days. *Cell density constantly increased during observation period. Statistical analyses for each day are shown with respect to the previous time-point within the groups. Two-way ANOVA, Tukey's multiple comparison test, *** $p < 0.001$, **** $p < 0.0001$, ns = not significant.*

	Ctrl	*10^{-6} M*	*10^{-5} M*
24 hours	6.1 ± 2.0	7.6 ± 2.1	10.4 ± 4.3
72 hours	24.7 ± 5.5	24.0 ± 9.2	29.2 ± 11.4
7 days	39.5 ± 6.1	39.9 ± 10.2	50.3 ±4.2
14 days	47.0 ± 8.3	46.8 ± 10.1	51.4 ± 10.7

Table 3.2 Cell density at 1,3, 7, and 14days of HUVECs seeded on control and functionalized samples. Data are shown as number of cells in 100 µm^2.

The DBP scaffolds functionalized with 10^{-5} M REDV (Figure 3.19C, K) showed a significantly higher amount of living HUVECs at 24 hours and 7 days (Figure 3.19D and L) with respect to control DBP (Figure 3.19A and I) and the lower concentrations of functionalization (Figure 3.19B, J). The percentage increase of 10^{-5} M REDV-functionalized DBP scaffolds was 83% at 24 hours and 27% at 7 days with respect to DBP control, whereas in the case of 10^{-6} M REDV-functionalized DBP scaffolds was respectively 33% and 1%. At 72 hours and 14 days, the number of living cells was not statistically different among the groups (E-G, M-O). For each time-point, number of dead cells was also not statistically different among the groups (Figure 3.19D, H, L, P).

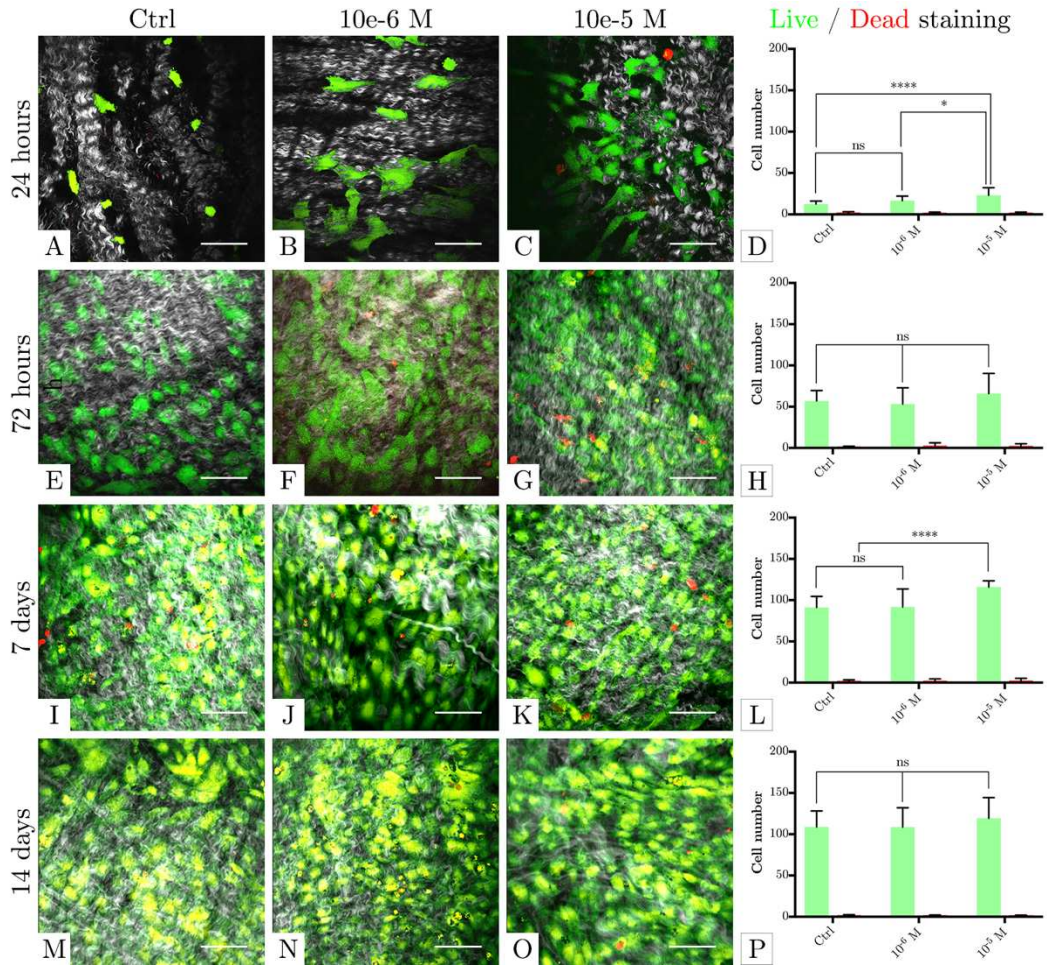

Figure 3.19 Live/Dead staining of control and functionalized DBP scaffolds. *Number of viable cells (D, L) was statistically higher in 10^{-5} M REDV-functionalized DBP scaffolds (C, K) with respect to control (A, I) and lower concentration (B, J). At 72 hours and 14 days, the amount was not different in the three groups (E-G, M-O). Scale bar = 100 μm. Two-way ANOVA, Tukey's multiple comparison test, * $p < 0.05$, **** $p < 0.0001$, ns = not significant.*

At 24 hours the cell viability was higher in the case of 10^{-5} M REDV-functionalized scaffolds. In the following days, it rapidly increased in all groups, and the highest values were achieved by functionalized samples at 14 days (Table 3.3).

	Ctrl	*10^{-6} M*	*10^{-5} M*
24 hours	88.3%	93.2%	94.5%
72 hours	98.7%	94.9%	96.6%

7 days	98.7%	98.1%	98.3%
14 days	99.0%	99.1%	99.3%

Table 3.3 Cell viability at 1, 3, 7, and 14 days of HUVECs seeded on control and functionalized samples.

The progressive scaffold endothelialization determined a near-continuous lining in all groups from day 7 (Figure 3.20I-K, M-O). This aspect was confirmed by H&E and Hoechst staining (Figure 3.20). A few rounded cells were present on surface samples at 24 hours (Figure 3.20A, D, G, J, M, P). From day 7, HUVECs were homogenously diffused and showed a flatter aspect (Figure 3.20B, C, E, F, H, I, K, L, N, O, Q, R).

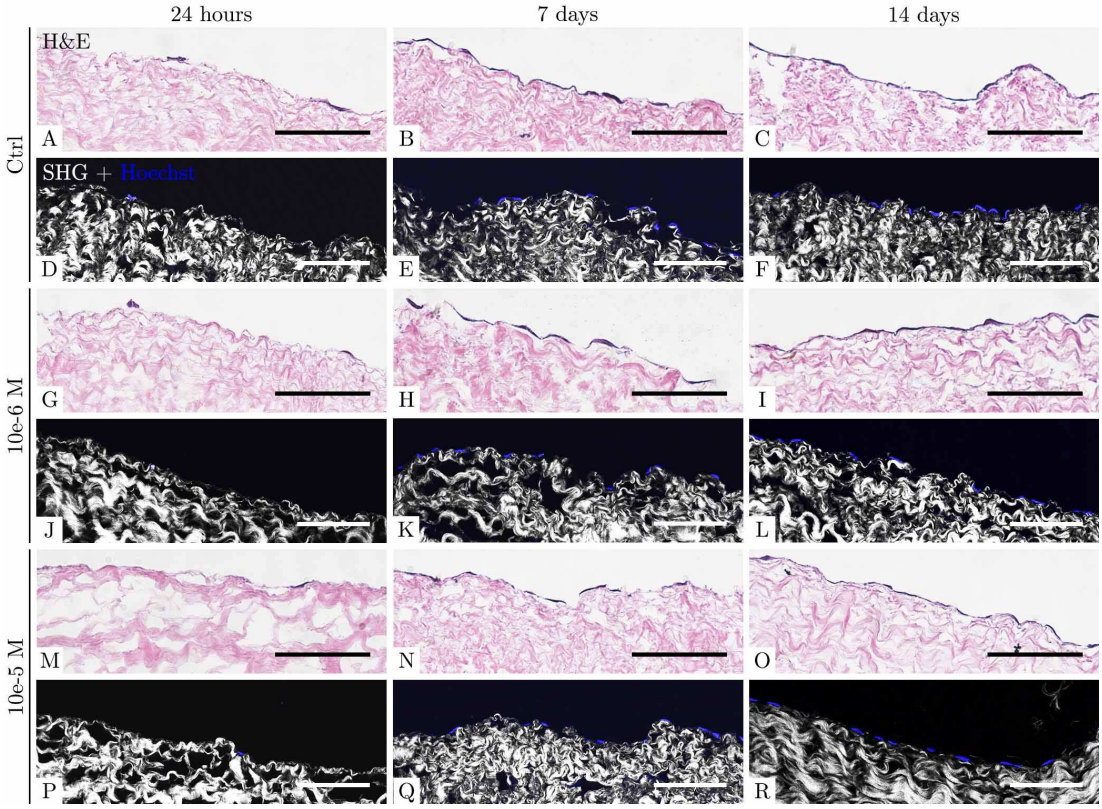

Figure 3.20 Histological and immunofluorescence evaluation of cell lining at 1, 7, 14 days. *Progressive proliferation induced spreading of seeded HUVECs (A, D, G, J, M, P) and it was possible to appreciate development of a near-continuous lining at day 7 (B, E, H, K, N, Q) and 14 (C, F, I, L, O, R). Scale bar = 100 μm.*

The quantification of MTS reduction confirmed increased cell proliferation (Figure 3.21). At 24 hours the 10^{-5} M REDV-functionalized scaffolds achieved the highest values and were statistically different ($p < 0.0001$) from the positive control (HUVECs on polystyrene), whereas 10^{-6} M REDV-functionalized and

control DBP scaffolds were not. At the following time-point, all tested DBP scaffolds were not different from positive control. The 10^{-5} M working concentration presented the highest proliferation values again at 7 days ($p < 0.0001$) when also 10^{-6} M REDV-functionalized DBP tissues were significant ($p < 0.5$) with respect to positive control. At 14 days, cell proliferation in all DBP groups was statistically higher than HUVECs on polystyrene ($p< 0.0001$). At all time-points, tested materials presented higher cell proliferation than HUVECs seeded on negative control ($p < 0.0001$). Cytotoxicity of glue induced complete cell death on day 14.

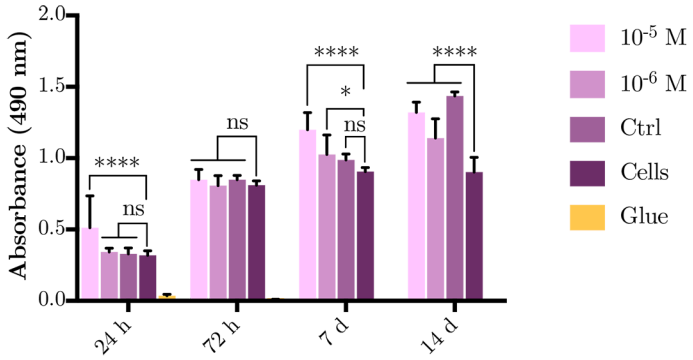

Figure 3.21 Evaluation of MTS reduction by HUVECs seeded on functionalized DBP scaffolds and controls. *Proliferation of 10^{-5} M REDV functionalized DBP scaffolds was significantly higher at 24 hours and 7 days with respect to cells on polystyrene. At 72 hours, all groups were not different from positive control, whereas at 14 days they all were. Two-way ANOVA, Tukey's multiple comparison test, * $p < 0.05$, **** $p < 0.0001$, ns not significant.*

Quantification of LDH released in the culture media confirmed negligible cytotoxicity induced by tested materials (Figure 3.22). Functionalized DBP scaffolds presented a trend comparable to control DBP: the percentages were negative or positive but close to zero (10^{-6} M REDV-functionalized DBP at 24 hours and 10^{-5} M DBP at 48 hours). The highest values were reached on the first two days, whereas on the third a substantial fall was evident. The glue achieved 100% of cytotoxicity at all time-points.

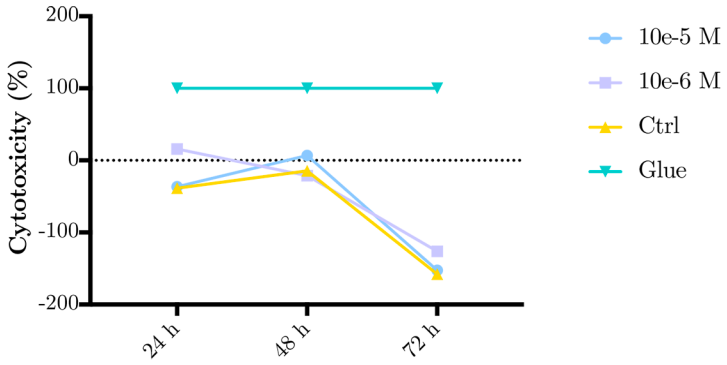

Figure 3.22 Quantification of released LDH by HUVECs seeded on functionalized DBP scaffolds and controls. *Tested material presented values of cytotoxicity negative or near zero, whereas glue achieved 100% cytotoxicity.*

Expression of CD31 and vWF was temporarily reduced at 24 hours (Figure 3.20A, D, G and I, J, M, respectively). On the following days, these molecules were highly present with typical granular aspect on HUVEC cellular membrane (Figure 3.20B, C, E, F, H, I and K, L, N, O, Q, R, respectively).

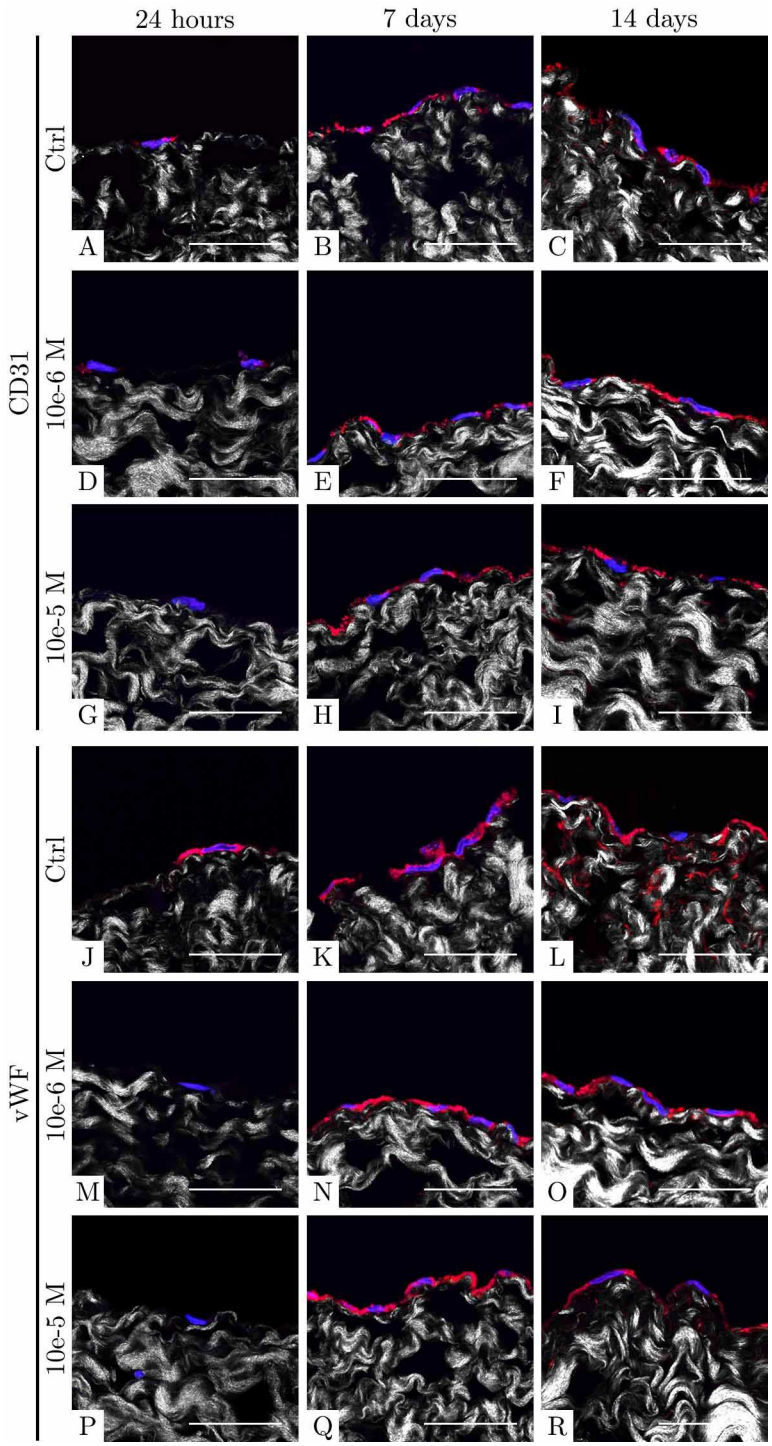

Figure 3.23 Expression of CD31 and vWF on HUVECs seeded on functionalized and control DBP scaffolds. *Twenty-four hours after cell seeding, expression of CD31 (A, D, G) and vWF (J, M, P) was slightly reduced, whereas at 7 and 14 days HUVECs showed characteristic pattern for these molecules (B, C, E, F, H, I and K, L, N, O, Q, R, respectively). Scale bar = 100 μm.*

Gap junction protein connexin 43 (conx43) confirmed the continuous-like distribution of HUVECs lining at 7 and 14 days in all groups (Figure 3.24B, E, H and C, F, I, respectively).

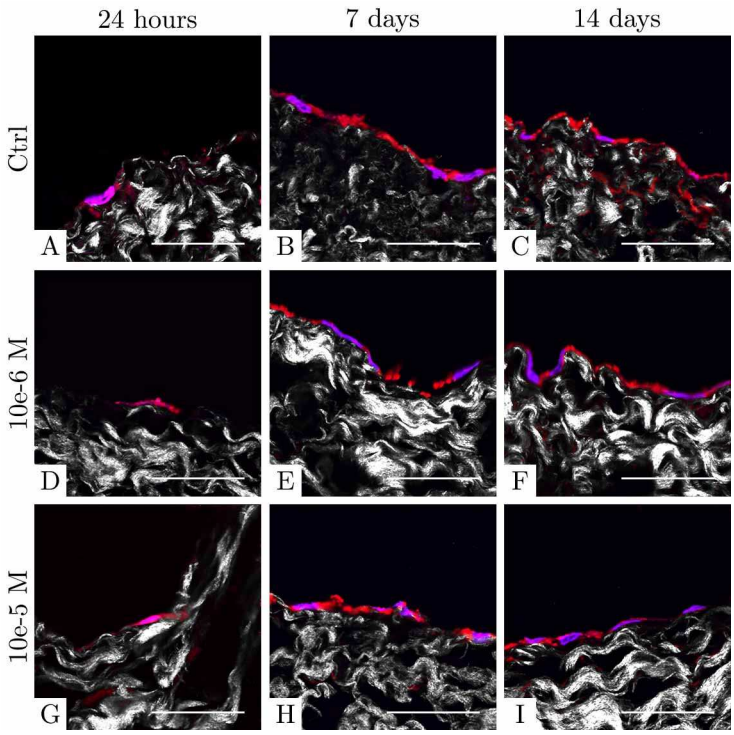

Figure 3.24 Expression of conx43 on HUVECs seeded on functionalized and control DBP scaffolds. *At days 7 (B, E, H) and 14 (C, F, I), near-continuous lining of HUVECs was confirmed. Scale bar = 100 μm.*

3.5 Discussion

Hemocompatibility is one of the main requirements for biocompatibility of medical devices intended for blood-contacting applications. This topic has been widely investigated in the fields of Medicine, Engineering and Material Sciences, but no conclusions have yet been reached (Ratner 1993, 2000, 2007).

There are many ways of trying to solve the quest for blood compatibility, such as acting on the coagulation cascade, complement system, or platelets, but none of these strategies turned out to be fully effective.

The ideal biomaterial should:

1) inhibit or prevent adsorption of proteins that may activate coagulation, complement systems and platelet adhesion;
2) promote the selective adsorption of specific plasma proteins;
3) support and facilitate endothelialization.

The first task may be achieved by hydrophobization or hydrophilization strategies (Sevastianov 2002). Surface hydrophobization strongly supports *in vitro* or *in vivo* adsorption of proteins. For example, albumin immobilization on polyurethane surfaces allows the reduced adsorption of fibrinogen, platelet adhesion and thrombogenicity with respect to non-treated controls (Ryu et al. 1992). Similar results have been demonstrated for Dacron vascular grafts (Kottke-Marchant et al. 1989). Material passivation is a desirable result because the surface becomes inert to its biological environment. However, the efficacy of this approach depends on coating duration and effectiveness in competitively preventing the adsorption of other undesired molecules. Instead, hydrophilization minimizes adsorption by means of non-fouling materials (Sevastianov 2002). This is, *de facto*, another form of passivation occurring during biomaterial fabrication and may be achieved with polyethylene oxide (PEO), PEG and dextran-based hydrogels (de Mel, Cousins, and Seifalian 2012).

The second approach uses ECs as the key point of blood compatibility, due to their natural ability in modulating the coagulation cascade as a result of the release of pro- and anticoagulant factors. Several strategies are under study to promote the *in vivo* and *in vitro* endothelialization of biomaterials and enhance the hemocompatibility of vascular grafts, heart valve substitutes, and other medical devices with blood-contacting surfaces, such as TAHs. In the field of mechanical circulatory support devices, the problem of blood compatibility has mainly been addressed by pharmacological approaches (life-long anticoagulant and antiaggregant therapies) and pump design; other strategies based on material surface modifications remain marginal.

In vivo preseeding with ECs or *in vitro* promotion of endothelialization may be enhanced with short adhesive peptides, proposed to support *in situ* cell engraftment. The rationale of this method therefore relies on exploitation of the specificity of these peptide sequences towards a given cell type. Several peptides have been tested to boost endothelial adhesion. Among these sequences, the integrin receptor REDV supported the selective adhesion of ECs against smooth muscle cells, fibroblasts and platelets. Since its identification in 1991 (Hubbell et al. 1991), this tetrapeptide has been used to functionalize several types of synthetic non-adhesive substrates.

In this thesis, the possibility of promoting and accelerating the early endothelialization by covalent and selective immobilization of endothelial cell-selective REDV tetrapeptide has been studied in decellularized scaffolds of bovine pericardium by HUVEC static cell seeding.

So far, functionalization with adhesive peptides has mainly been explored with synthetic polymers, because of their poor bioactive properties. In these cases, functionalization necessarily required chemical modifications of the material surface or inclusion of the peptide into polymer backbones. Instead, only a few examples are reported for biological matrices. The incorporation of PEG into N-(3-dimethylaminopropyl)-N'-ethylcarbodiimide and N-hydroxysuccinimide (EDC/NHS) cross-linked collagen sponges was studied as a platform to enrich the protein further by means of bioactive sequences (Ward et al. 2010). In a similar approach, decellularized porcine aortic valves were chemically modified to introduce a sulfhydryl group, which was used to functionalize the matrix with cyclic RGD reacted with branched PEG (Zhou et al. 2015). Decellularized valves were functionalized with RGD with sulfosuccinimidyl-6-(3'-(2-pyridyldithio)-propionamido)-hexanoate as coupling agent (Shi, Dong, and Sun 2009). DBP scaffolds have also been treated with acetic acid to enhance tissue porosity, and enriched by the RGD motif after activation of carboxyl groups of aspartic acid and glutamic acid with a solution of EDC/NHS (Dong et al. 2009). All these methods accomplished the covalent grafting between the bioactive peptide and ECM components using non-selective methods, *i.e.*, involving side-chains fundamental for cell receptor building. In a milder approach, decellularized ovine pulmonary cusps and pericardium were functionalized by physical adsorption of RGD, REDV and YIGSR dissolved in PBS. The efficacy and durability of the binding were demonstrated in *in vivo* implantation of decellularized aortic grafts in rats up to 10 days (Aubin et al. 2016).

Our experience is in clear contrast with the literature. The abundance of functional groups in biological scaffolds offers an extraordinary opportunity for functionalization. In our case, the synthesized REDV and RhodREDV were immobilized on DBP by exploiting the aldehyde groups at the peptide C-terminal, and the primary amine (ε-amino groups) of lysine and hydroxylysine present in the scaffolds, mainly available in collagen (Yamauchi and

Sricholpech 2012). The chemistry was similar to that used for covalent cross-linking the biological tissues with GA (Paul and Bailey 2003). Besides the use of a reducing agent to make the link irreversible, functionalization did not require any chemical or structural modification of the DBP. This choice aimed at preserving the promising biological characteristics and structural integrity of TriCol DBP scaffolds. TPM analyses performed to evaluate the integrity of collagen I and elastin confirmed the maintenance of the main ECM constituents. In addition, sample thickness and area were not affected by functionalization, indicating that no major modifications had been made to the structure of the scaffold.

Quantification of the actual linked peptide was performed with an innovative method based on TPM and the acquisition of TPEF of rhod-conjugated REDV. With respect to synthetic materials or PEG-based approaches, it was necessary to develop a new technique to distinguish the contribution of the peptide from the endogenous matrix clearly. Evaluation of FTIR spectra, often adopted in other studies (Jun and West 2005b; Lin et al. 1992; Wang et al. 2015; Zhou et al. 2015), was not feasible because of the similarity between the target molecule and the biological context in which it was inserted. In the same way, immunolabelling of REDV was not a practicable approach. Although the peptide was first identified in human plasma fibronectin, it may also be found in bovine fibronectin of ECM, hindering attempts to distinguish the synthetic motif from the natural one. The fluorescence of conjugated peptides has been evaluated in several works (B Butruk et al. 2013; Castellanos et al. 2015; Dong et al. 2009; Zhou et al. 2016). However, a quantitative evaluation has only been performed once (Ji et al. 2012), whereas a semiqualitative analysis is reported in (Aubin et al. 2016). Our results were confirmed by (Ji et al. 2012): independently of the concentration used (10^{-5}, 10^{-6}, 10^{-7} M in our case), the final amount of peptide retained in the matrix was less than the initial dose. Based on a dose-dependent trend, the highest functionalization of both sides of the pericardium was achieved with 10^{-5} M functionalization with respect to lower ones (10^{-6} and 10^{-7} M, not statistically different from each other).

Bioactivity was evaluated by static HUVEC seeding. Enhanced adhesion, viability and proliferation were observed at 24 hours and 7 days for the

scaffolds functionalized at the 10^{-5} M concentration. At all time-points, the number of dead cells was very limited and non-statistically different among groups. At day 14, the differences between functionalized and non-functionalized samples became less pronounced, indicating that REDV treatment is probably essential in the early stages of endothelialization. Conversely, in the study of Aubin the only adsorption of REDV by decellularized matrices was not sufficient to elicit a significant increase of HUVEC adhesion with respect to the control at 1 and 4 hours (Aubin et al. 2016).

Cytotoxicity was negligible for the functionalized group, as confirmed by the efficacious removal of sodium cyanoborohydride - the main drawback of functionalization for cell viability, but essential to guarantee irreversibility of the covalent bond of REDV and RhodREDV (Figure 3.25). In the near future, the use of a different and less toxic reductive reagent will be experimented.

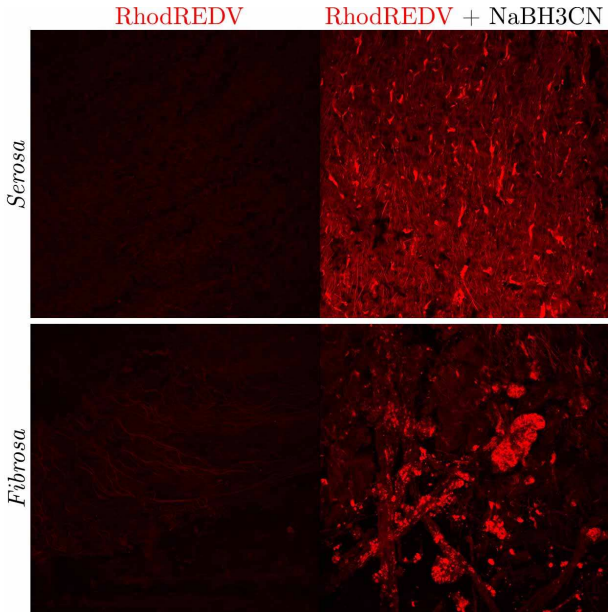

Figure 3.25 Comparison of 10^{-5} M RhodREDV functionalization of DBP scaffolds with and without sodium cyanoborohydride. *Reducing agent was necessary to stabilize covalent bond of RhodREDV, otherwise easily removed by washes.*

As a further indication of cell functionality, the classical endothelial markers CD31 and vWF were rarely expressed at 24 hours, probably due to the use of trypsin to detach cells from culture flasks before tissue seeding, but were fully present in all groups from day 7.

Histological analyses and location of conx43 revealed the ongoing development of a continuous-like cell lining, which progressively covered the DBP *serosa*. Longer evaluation of seeded scaffolds will be useful to establish whether a complete, stable lining can be achieved thanks to REDV functionalization.

As demonstrated in this project, the endothelial cell-selective REDV functionalization of DBP scaffolds allowed *in vitro* promotion of early endothelial adhesion and proliferation by minimal tissue manipulation to preserve and improve the natural biological activity of DBP matrices without structural modification. The final goal of this tissue engineering is the generation of functionalized DBP scaffolds to manufacture improved HM for TAH lining. This approach may promote the overall blood compatibility of the pump and drastically reduce, if not eliminate, the need for anticoagulant and antiaggregant therapies, causing increased risk of neurological complications (Hart and Sherman 1987). In turn, the promoted early immobilization of ECs may control the initial interactions between biomaterial and blood in marked contrast to the adhesion of other cytotypes and platelets.

With this aim in mind, further *in vitro* analyses will be performed to investigate the effects exerted by REDV functionalization on the regulatory activity of ECs - for example by quantifying the secretion of fibrinolytic regulators, thrombin activation, and platelet adhesion. The possibility of REDV influencing endothelial migration will be evaluated by mimicking the formation of anastomotic sites *in vitro*. Functionalized DBP will be tested in dynamic conditions to assess the stability of the lining in simulated conditions of shear stress. Lastly, *in vivo* experiments will be performed to confirm the *in situ* recruitment and adhesion of ECs and to assess the compatibility of the new material.

4 The Total Bioengineered Heart

4.1 Introduction

The irreversible structural and functional degeneration caused by HF is hardly hindered by pharmacological therapies and the ideal surgical treatment. *i.e.*, cardiac transplantation is dramatically limited by organ shortage. The search for alternative way of treatments or cardiac substitutes is therefore mandatory. In this panorama, tissue engineering (TE) and regenerative medicine strategies tried to give innovative answers which, in the future, may hopefully represent the final cure for end-stage HF.

4.1.1.1 The regeneration of myocardium

Myocardial regeneration in response to an injury is strongly limited due to poor differentiation ability of adult cardiomyocytes (Pasumarthi and Field 2002). The lack of endogenous restoration can be overcome by applying strategies based on cells injection/infusion, cell reprogramming, gene therapy, boost of self-regeneration, and TE (Etzion, Kedes, et al. 2001). The main common goals of these approaches are the reduction of fibrosis in infarcted myocardial tissue and the prevention of healthy myocardium impairment by repopulating scars with new contractile cells.

- *Cell therapy*

The successful implantation of fetal cardiomyocytes was demonstrated in myocardial tissues affected by cryodamage, ischemic injuries, and cardiomyopathies. Although graft was occasionally surrounded by scar tissue (Etzion, Battler, et al. 2001; Reinecke et al. 1999), a general improvement of

cardiac functionality was acknowledged (Leor et al. 1996; Li, et al. 1996; Li, Mickle, et al. 1996; Li et al. 1997; Matsushita et al. 1999; Ruvinov et al. 2008; Scorsin et al. 1996, 1997; Yoo et al. 2000). This approach was affected by limited proliferation and dramatic cell lost occurring in the early days after grafting, probably due to immune reaction or inflammatory processes (Müller-Ehmsen et al. 2002; Varda-Bloom et al. 2000; Zhang et al. 2001).

The low proliferative activity and potential immunogenicity of fetal cardiomyocytes may be overcome by autologous skeletal myoblasts. These cytotypes can be isolated from muscle biopsied and can transdifferentiate into cardiomyocyte-like cells (Dorfman et al. 1998; Menasché et al. 2001; Murry et al. 1996; Pouzet et al. 2000; Souza et al. 2002; Taylor et al. 1998). The efficacy of this approach is not fully accepted and some doubts were raised about the actual possibility of creating a regenerate myocardium. Although most of the studies confirmed the differentiation of myoblast into skeletal myotubes, promising results in terms of improved cardiac functionality have been disclosed (Dowell et al. 2003). As a matter of fact, it was reported the absence connnexin-43 expression, suggesting that the electromechanical coupling between engrafted cells and autologous myocardium was probably precluded *in vivo* (Reinecke et al. 2000; Scorsin et al. 2000). Cases of early arrhythmias were described after cell transplantation (Hagège et al. 2006; Menasché et al. 2008). In spite of these results, several human trials are currently ongoing for the purpose of demonstrating the technique feasibility and long-term engraftment of myoblasts in patient with left ventricular failure. The trials are based on surgical approaches (Hagège et al. 2006; Menasché 2008; Menasché et al. 2001) and catheter delivery (Ince et al. 2004; Siminiak et al. 2005).

Bone marrow is a highly heterogeneous tissue populated by several cytotypes. Bone marrow-derived stem cells were widely investigated at the beginning, when it was demonstrated the possibility of deriving cardiac muscle cells by their differentiation (Orlic et al. 2001). However, this ability is still under discussion since hematopoietic cells appeared to be more prone to produce only mature blood elements once implanted (Balsam et al. 2004; Murry et al. 2004). Conversely, multipotent BM-MSCs were efficiently differentiated if properly stimulated *in vitro* (Makino et al. 1999; Tomita et al. 1999; Wakitani, Saito, and Caplan 1995) or implanted *in vivo* and "tissue-

conditioned" (Toma et al. 2002). Decellularized scaffolds also demonstrated *in vitro* ability to induce differentiation of BM-MSCs into ECs, fibroblasts, myoblasts, and smooth muscle cells (Iop et al. 2009). The results were confirmed by means of *in vivo* animal implants (Iop et al. 2014). The possibility to give rise to vascular cells was also demonstrated (Dai 2005; Jiang et al. 2006; Kocher et al. 2001; Oswald et al. 2004; Silva et al. 2005). Myocardial regeneration of MSCs appeared to be more influenced by the release of cytokines and growth factors with paracrine antiinflammatory, antiapoptotic, and proangiogenic actions rather than effective cell differentiation into viable cardiomyocytes (Gnecchi 2006; Gnecchi et al. 2008; Hashemi et al. 2008; Kinnaird et al. 2004; Mirotsou et al. 2007; Noiseux et al. 2006; Yao et al. 2005). The presence of proangiogenic molecules stimulated also the differentiation of circulating EPCs (Ii et al. 2005), into vascular citotypes (Johansson et al. 2008). Therefore, other strategies to improve neovascularization were performed by direct injection of EPCs (Kawamoto et al. 2001) or bone marrow mononuclear cells, which can generate functional EPCs (Shintani et al. 2001). Upon the observation of bone marrow-derived cardyomyocytes in cardiac biopsies of patients which undergone gender-mismatch heart or bone marrow transplantations (Deb et al. 2003; Müller et al. 2002), the strategy of intracoronary administration of bone marrow-derived cells was evaluated in acute and chronic myocardial infaction (Britten et al. 2003; Strauer et al. 2002). Although one study reported the accumulation of infused cells in liver and spleen (Qian et al. 2007), other groups disclosed the slight increase of ejection fraction (Assmus et al. 2002), improvement of cardiac motility (Chen et al. 2004) and reduction of infarcted scar dimension (Perin et al. 2003). The most successful outcomes in left ventricular improvment were achieved with the use of BM-MSCs exposed to cardiogenic cocktail in the C-CURE randomized clinical trial (Bartunek et al. 2013). The paracrine effects induced by transplanted cells on host myocardium was considered also involved in the increase of cardiac performances after introduction of fibroblasts (Hutcheson et al. 2000) and smooth muscle cells (Fujii et al. 2003).

The existence of cardicac adult stem cells was disputed at length until they were identified raising considerable enthusiasm. Once isolated from myocardial biopsies, these cells showed ability to form spheric aggregates and differentiate into cardiomyocytes and vascular cells (Messina et al. 2004). Their use in

regeneration strategies has been tested in several studies with opposite results about regeneration ability and ability to differentiate into appropriate cell types (Bearzi et al. 2007; Beltrami et al. 2003; Tallini et al. 2009; Tang et al. 2010; Zaruba et al. 2010). This ambiguity may probably be explained by the selection of sorting techniques, based on receptor tirosin kinase c-Kit expression. It was reported that the majority of biopsy cells, expressing c-Kit, co-expressed also markers for mast cells, from 90 to 100%, but not for cardiac progenitor cells (Pouly et al. 2008; Vicinanza et al. 2017). Nevertheless, cardiospheres of cardiac progentor cells are currently under investigation in clinical trials for the regeneration of post-infacrt myocardium (Chimenti et al. 2010).

Adult stem cells can differentiate into a limited number of cell types, whereas embryonic stem cell (ESCs), derived from human blastocysts (Thomson 1998) are characterized by unlimited proliferation potential and pluripotency. In addition, they can be differentiated into cardiomyocytes (Kehat et al. 2001; Sartiani et al. 2007; Xu et al. 2002) maintaining their proliferation abilities (Doetschman et al. 1985; Kehat et al. 2001; Laflamme et al. 2007; Leor et al. 2007; Mummery 2003; Xu et al. 2002). The development of teratomas and arrhythmogenic complications was associated to the lack of proper differentiation and integration into host tissue or low cell purification. Allogeneic ESCs may cause immune rejection of transplanted graft (Zhu et al. 2009). Although these challenges and the maintenance of the undifferentiated state, sorting techniques, concern for teratoma formation (Nussbaum et al. 2007), and ethical issues, ESCs represent a promising strategy also as biological pacemaker (Kehat et al. 2004; Xue et al. 2005). Induced pluripotent stem cells (iPSCs), generated by reprograming of adult somatic cells (Takahashi et al. 2007), were efficinetly differentiated into cardiomyocites (Yoshida and Yamanaka 2011; Zhang et al. 2009; Zwi et al. 2009), as well. The use of these type of cells has advantages in terms of immunocompaitibility, since they can be patient-derived, and ethical isssues, because they are not obtained from the destruction of embryos. However, gene transudction is mediated by viral vectors and may induce mutagenesis, whereas reprogrammining factors are known to be oncogenic (Pappas and Yang 2008)

Cardiac macrophages represent a dynamic and varied population, whose phenotype, regenerative potential and ability to enhance vascularization are inversely proportional to the subject age (Aurora et al. 2014; Lavine et al. 2014; Molawi et al. 2014). In this scenario, macrophages may be specifically targeted for myocardial repair to reduce inflammatory responses, which influence the severity of the ischemia/reperfusion injury (Gao et al. 2011) and ventricular remodeling (Kaikita et al. 2004). The injection of a machropge suspension in ischemic tissue showed to positively affect the neovascularizaition and remodeling by improving the cardiac functionality (Leor et al. 2006).

- *Cell reprogramming*

Fibroblasts responsible for post-infarct scar formation may be selectively targeted with reprogramming strategies to induce transdifferentiation into working myocardium (Doppler et al. 2015; Muraoka and Ieda 2014). This approach may overcome the limitations of cell-based approaches, such as transplanted cell survival and risk of developing tumors. Conversely, there are concerns relating the use of viral vectors and the poor specificity towards fibroblasts involved in reprogramming (Efe et al. 2011; Ieda et al. 2010; Qian et al. 2012).

- *Gene therapy and the stimulation of self-regeneration potential*

Gene therapies in curing myocardial infarction have been used to target specific clinical features of HF, such as β-adrenergic receptors and mechanisms involved in calcium handling, or increase vessel density (Scimia, Gumpert, and Koch 2014).

Cardiac regeneration may be also stimulated endogenously. Recruitment, mobilization, and proliferation of local and peripheral stem cells can be promoted by several proteins and growth factors, *i.e.*, chemotactic and angiogenic molecules, cardioprotective compounds and enhancer of cell engraftment and proliferation (Askari et al. 2003; Dong et al. 2012; Iwasaki et al. 2011; Schenk et al. 2007; Smart et al. 2007; Zangi et al. 2013; Zohlnhöfer et al. 2008).

- *Tissue engineering*

The field of TE offers alternative approaches to cellular cardiomyoplasty. The principal aim is to develop implants able to restore, maintain, or improve the function of damaged tissues or organs by inducing desirable host response and constructive *in vivo* remodeling (O'Brien 2011). These goals may be achieved through the use of cardiac patches and implantable/injectable biomaterials. In particular, the restoration of impaired myocardium is normally performed by acting on destructive ventricular remodeling, stabilizing cardiac geometry, and preventing the thinning or dilation of ventricular walls (Christman and Lee 2006).

Degradable (Fujimoto et al. 2007) and non-degradable (Enomoto et al. 2005; Kelley et al. 1999; Konertz et al. 2001a) meshes, anchored to the heart surface, have been to restrain ventricles and demonstrated to be effective in the augmentation of cardiac performances in infarcted patients (Franco-Cereceda et al. 2004; Konertz et al. 2001b; Olsson, Bredin, and Franco-Cereceda 2005). The major drawback of cardiac restrains was the implantation, which necessarily required surgical procedures.

In addition, the ventricular wall stabilization has been achieved through the injection of fibrin glue (Christman, Fok, et al. 2004), Matrigel, a protein-rich matrix of mouse sarcoma, (Huang et al. 2005), collagen (Dai et al. 2005), alginate (Landa et al. 2008; Leor et al. 2009) also functionalized with RGD peptide (Yu et al. 2009), self-assembling peptides (Davis et al. 2005a), and hydrogels (So et al. 2009). These materials usually remained in the body up to 8 weeks and promoted myocardial regeneration by enhancing angiogenesis.

The use of TE scaffolds and constructs allowed to overcome some limitations of above-mentioned cell-based approaches. The aggressive and hostile environment of injured myocardium is undoubtedly a complicate bench test for transplanted cells, which have to engraft and proliferate into a necrotic tissue often infiltrated by inflammatory activation. A TE scaffold should support cell homing and tissue development by acting as a pattern. The TE applications consist of a preliminary *in vitro* step or can be directly applied *in situ*. The main difference between these two approaches is the bioreactor used to grow cells: in the first case, a device stimulates seeded scaffolds with mechanical, electric and chemicals adequate stimuli and scaffold is named TE

"construct", whereas in the second case this role is played by human body (O'Brien 2011). The peculiar combination of scaffolds, cells, and biophysical stimuli may facilitate tissue regeneration by replacing the wound and regulating whole healing process.

The ideal scaffolds should be biocompatible, biodegradable, mechanically stable, and present a suitable 3D architecture (O'Brien 2011). Consequently, a cardiovascular TE construct should present similar properties to natural working myocardium, such as ability to contract, appropriate electrophysiological characteristics, mechanical competence, high vascularization, and immunocompatibility (Zimmermann, Melnychenko, and Eschenhagen 2004). *In vitro* TE constructs were created using scaffolds made of porous alginate (Dar et al. 2002), polymers (Bursac et al. 2003) and collagen (Akhyari et al. 2002; Kofidis et al. 2002). Matrigel was also used in the preparation of so-called engineered heart tissue. In these preparations, mechanical and electrical stimuli were fundamental in obtaining physioelectrically-competent constructs. However, cell survival was not easy to maintain, especially after implantation (Zimmermann et al. 2000). *In situ* strategies may be based on biodegradable liquid scaffolds and patches. With this aim fibrin glue (Christman, Fok, et al. 2004; Christman, Vardanian, et al. 2004), liquid Matrigel (Kofidis et al. 2004), and liquid alginate (Landa et al. 2008) demonstrated to improve the functionality of infarcted hearts and induced tissue vascularization.

Cell-sheet-based approaches were developed to fabricate tridimensional tissues starting from 2D structures stacked on each other. Specific temperature-responsive polymers were used to seed cells and easily allow the detachment and manipulation of developed cell layers (Kwon et al. 2000). This technology supported the vascularization of 3D novel tissue by ECs coculture and contact with a vascular beds in bioreactors (Masuda and Shimizu 2016; Sekine et al. 2013).

A great interest was raised by the use of self-assembling peptides because of their peculiar ability in forming definite structures in function of boundary conditions, such as pH and temperature, when injected or implanted. Self-assembling peptides allowed angiogenesis and vascular cell recruitment (Davis et al. 2005b; Narmoneva et al. 2005).

Among all these approaches, only a few products have currently been translated in the clinic (Iop et al. 2018). There are some ongoing promising trials based on bone marrow cells seeded on collagen scaffold (Chachques et al. 2008, 2010) and muscle cell-sheets (Miyagawa et al. 2017; Sawa et al. 2015). In addition, cell-free strategies based on alginate hydrogels are under evaluation (Lee et al. 2015; Mann et al. 2016).

4.1.1.2 The bioengineerization of the whole heart

Cell cardiomyoplasty can only partially ameliorate cardiac functionality. Improvements are often moderate and not sufficient in restoring whole heart functionality, due to poor graft viability and low cell retention. Strategies based on TE constructs have been developed to guarantee a favorable support for cell implantation and tissue restoration. However, applications are limited by vascular supply and oxygen delivery, which if insufficient may cause construct core necrosis.

In whole heart bioengineering, the natural cardiac ECM is isolated by means of decellularization processes. Therefore, endogenous cell material is completely eliminated to avoid immune-mediated rejection and inflammatory responses, which are driven by allogeneic and xenogeneic epitopes. The so-obtained scaffold is composed of largely molecule preserved among species. The most important advantage is the presence of native vasculature, fundamental for cell viability during repopulation and the functionality of future regenerated organ.

- *Ode to ECM*

ECM is the highly specialized custom-designed product of resident cells of every tissue and organ. This extraordinary relationship is often described as "dynamic reciprocity", to underline the tight bidirectional communication existing (Bissell and Aggeler 1987). This unique interaction involves several matrix molecular sites, cell receptors and intracellular signaling pathways related to cell growth, differentiation and polarity (Albelda and Buck 1990; Kleinman, Philp, and Hoffman 2003). ECM has a dominant role in developmental processes, such as organ and vascular morphogenesis (Kleinman et al. 2003;

Rhodes and Simons 2007) and also disease pathogenesis (Farhadian et al. 1996).

This wealth of biological signals and molecules is currently commercialized as decellularized scaffolds for several clinical applications. The high conservation of ECM components among species constitutes the main advantage of these materials (Bernard, Chu, et al. 1983; Bernard, Myers, et al. 1983). The absence of cells, the main responsible for activation of host response, may induce the ECM to positively influence immune system by modulating a constructive regeneration and remodeling (Badylak 2004, 2005; Badylak, Freytes, and Gilbert 2015).

- *General principles of bioengineered organs*

The *in vitro* synthesis of natural ECM is an almost impossible goal to achieve although the advancements of current bioprinting technologies (Jung, Bhuiyan, and Ogle 2016). The extremely heterogeneous structure, richness of bioactive molecules and stimuli, and vascularization are currently not completely reproducible *in vitro* (Mironov et al. 2009; Visconti et al. 2010)

The decellularization is used to take advantage of 3D histoarchitecture and biological functionality of natural solid organ ECM. These methods have the difficult task of preserving natural ECM while completely removing endogenous cellular components, in order to avoid inflammatory events, immune rejection and scaffold calcification. The unavoidable structural and functional impairment induced by cell extraction has to be necessarily minimized as much as possible by the careful design of decellularization protocols.

Whole organ decellularization procedures are based on optimized combinations of physical, chemical and enzymatic approaches. In the case of heart, the coronary system is directly used to administrate decellularization solutions. Organ perfusion maximizes solution penetration and, therefore, the efficiency of cell removal (Crapo et al. 2011; Gilbert et al. 2006).

- *Decellularization cornerstones*

The first protocol applied to whole heart decellularization was proposed in 2008 and was based on the use of ionic and non-ionic detergents, such as sodium dodecyl sulfate (SDS) and Triton X-100. This successful attempt demonstrated

the possibility in obtaining a fully decellularized whole heart, which supported an initial pump action after 8 days of dynamic seeding in conditions of simulated flow and electric activity (Ott et al. 2008). Later, rat heart decellularization was further improved by testing several protocols and submerging the organ in the solutions (Akhyari et al. 2011).

The pioneering experience of Ott was scaled up to porcine organs in 2010 by introducing a more articulate protocol composed of osmotic shock, enzymes and surfactants (Wainwright et al. 2010). In order to achieve the optimal ECM, several combinations of detergents and enzymes have been further tested with conflicting results: SDS (Weymann, Loganathan, Takahashi, Schies, Claus, Hirschberg, Soós, et al. 2011; Weymann, Patil, Sabashnikov, Jungebluth, Korkmaz, Li, Veres, Soos, Ishtok, Chaimow, Pätzold, et al. 2014), Triton X-100 and trypsin (Merna et al. 2013), sodium deoxycholate and Triton X-100 (Methe et al. 2014), SDS and Triton X-100 (Kitahara et al. 2016; Momtahan et al. 2015). The progressive increase of flow through the coronary tree has been also evaluated to reduce the damage of vasculature (Remlinger, Wearden, and Gilbert 2012).

Translation to human organs took place in 2015 with the collaboration between the Texas Heart Institute and several Spanish groups. The protocol was based on SDS and it was applied to hearts not suitable for transplantation (Sanchez et al. 2016; Sánchez et al. 2015). Another successful cooperation, involving Harvard Medical School and New England Organ Bank, led to the decellularization of whole human hearts by means of a similar SDS-based protocol (Guyette et al. 2016).

A comprehensive summery of decellularization protocols applied so far to rat, porcine, and human heart is reported in Table 4.1.

Author	Year	Species	Decellularization protocol															
Ott	2008	Rat	10 μM adenosine in heparanized PBS, 15 min, 77.4 mm Hg				1% SDS in deionized water, 12 h, 77.4 mm Hg				Deionized water, 15 min, 77.4 mm Hg			1% Triton X-100 in deionized water, 30 min, 77.4 mm Hg			100 IU/ml penicillin-G/streptomycin and 100 IU/ml amphotericin B in PBS 124 h	
Wainwright	2010	Pig	Freezing, 16 h, -80°C	Thawing in distilled water, RT	Distilled water, 15 min, 1 l/min, RT	2x PBS, 15 min, 1 l/min, RT	0.02% trypsin, 0.05% EDTA, and 0.05% NaN_3, 2 h, 1 l/min, 37°C	Distilled water, 5 min, RT	2x PBS, 15 min, 1 l/min, RT	3% Triton X-100, 0.05% EDTA, and 0.05% NaN_3 in distilled water, 2 h, 1.3 l/min, RT	Distilled water, 5 min, RT	2x PBS, 15 min, 1 l/min, RT	4% DCA in distilled water, 2 h, 1.3 l/min, RT	Distilled water, 5 min, RT	2x PBS, 15 min, 1 l/min, RT	0.1% peracetic acid and 4% ethanol, 1h, 1.7 l/min	PBS, 15 + 15 min, 1.7 l/min	Distilled water, 15 + 15 + 15 min, 1.7 l/min
Weymann	2011 / 2014	Pig	4% SDS in PBS, 3 h, 2 l/min, 100 mm Hg, 37°C		PBS, 15 min, 37°C	4% SDS in PBS, 3 h, 2 l/min, 100 mm Hg, 37°C		PBS, 15 min, 37°C	4% SDS in PBS, 3 h, 2 l/min, 100 mm Hg, 37°C		PBS, 15 min, 37°C	4% SDS in PBS, 3 h, 2 l/min, 100 mm Hg, 37°C			PBS, 24 h, 1.5 l/min / 100 μg/ml penicillin/streptomycin in PBS, 24 h, 1.5 l/min			
Akhyari	2011	Rat	I	10 mM adenosine in heparanized PBS, 15 min, 77.5 mm Hg			1% SDS in deionized water, 12 h, 77.5 mm Hg			Deionized water, 15 min, 77.5 mm Hg			1% Triton X-100 in deionized water, 30 min, 77.5 mm Hg			100 IU/ml penicillin-G/streptomycin and amphotericin B, 124 h		
			II	0.025% trypsin and 0.05% EDTA in PBS, 1 h, 77.5 mm Hg, 37°C	Deionized water, 15 min		3% Triton X-100 in deionized water, 1 h, 77.5 mmHG			Deionized water, 15 min		4% DCA in deionized water, 1 h, 77.5 mm Hg, RT			Deionized water, 15 min, RT	0.1% acetic acid in deionized water, 1 h	
			III	20% glycerol, 0.05% NaN_3, and 25 mM EDTA in 0.9% NaCl, 3 d, 77.5 mm Hg		4.2% DCA and 0.05% NaN_3 in deionized water, 3 d, 77.5 mm Hg			20% glycerol, 0.05% NaN_3, and 25 mM EDTA in 0.9% NaCl, 2 d, 77.5 mm Hg			1% SDS and 0.05% NaN_3 in deionized water, 2 d, 77.5 mm Hg			3% Triton X-100 and 0.05% NaN3 in deionized water, 2 d, 77.5 mm Hg		100 IU/ml penicillin-G/streptomycin, 12 h
			IV	10 mM adenosine in heparanized PBS, 15 min, 77.5 mm Hg	1% SDS, 1% DCA, and 0.05% NaN_3 in deionized water, 12 h, 77.5 mm Hg	Deionized water, 15 min, 77.5 mm Hg	20% glycerol, 0.05% NaN_3 and 25 mM EDTA in 0.9% NaCl, 12 h, 77.5 mm Hg	Deionized water, 15 min, 77.5 mm Hg	1% Saponin and 0.05% NaN_3 in deionzed water, 12 h, 77.5 mm Hg	Deionized water, 15 min, 77.5 mm Hg	20% glycerol, 0.05% NaN_3 and 25 mM EDTA in 0.9% NaCl, 12 h, 77.5 mm Hg	Deionized water, 15 min, 77.5 mm Hg	200 IU/ml Dnase I and 50 ml/mol MgCl in PBS				
Aubin	2013	Rat	10 mM adenosine in heparanized PBS, 15 min, 77.5 mm Hg	1% SDS, 1% DCA, and 0.05% NaN_3 in deionized water, 12 h, 77.5 mm Hg	Deionized water, 15 min, 77.5 mm Hg	20% glycerol, 0.05% NaN_3, and 25 mM EDTA in 0.9% NaCl, 12 h, 77.5 mm Hg	Deionized water, 15 min, 77.5 mm Hg	1% Saponin and 0.05% NaN_3 in deionzed water, 12 h, 77.5 mm Hg	Deionized water, 15 min, 77.5 mm Hg	20% glycerol, 0.05% NaN_3, and 25 mM EDTA in 0.9% NaCl, 12 h, 77.5 mm Hg	Deionized water, 15 min, 77.5 mm Hg	200 IU/ml Dnase I and 50 mM MgCl in PBS	100 IU/ml penicillin/streptomycin in PBS, 12 h, 4°C				
Remlinger	2012	Pig	Freezing, 24 h, -80°C	Thawing in deionized water, ON, 4°C	Deionized water, 15-25 min, 400 ml/min	2X PBS, 15 min, 700 ml/min	Deionized water, 10 min, 750 ml/min	0.2% trypsin, 0.05% EDTA, and 0.05% NaN_3, 3 h, 1200-1800 ml/min, 37°C	Deionized water, 10 min, 1900 ml/min, RT	2X PBS, 10 min, 1950 ml/min, RT	3% Triton X-100, 0.05% EDTA, and 0.05% NaN_3, 2.5 h, 2000-2100 ml/min, RT	Deionized water, 10 min, 2150 ml/min, RT	2X PBS, 10 min, 2180 ml/min, RT	4% SDC, 3 h, 2200 ml/min, RT	Deionized water, 15 min, 2200 ml/min, RT	2X PBS, 15 min, 2200 ml/min, RT	Deionized water, 5 min, 750 ml/min, RT	1X PBS, 5 min, 1500 ml/min, RT
Merna	2013	Pig	I	Freezing, 24 h, -80°C	Thawing, RT	0.02% Trypsin, 0.05% EDTA, and 0.05% NaN_3, 3 d								3% Triton X-100, 0.05% EDTA, 0.05% NaN_3, 4 d				
			II	Freezing, 24 h, -80°C	Thawing, RT	0.02% Trypsin, 0.05% EDTA, and 0.05% NaN_3, 1 d	3% Triton X-100, 0.05% EDTA, and 0.05% NaN_3, 6 d											
			II I	Freezing, 24 h, -80°C	Thawing, RT	0.02% Trypsin, 0.05% EDTA, and 0.05% NaN_3, 7 d												
			I V	Freezing, 24 h, -80°C	Thawing, RT	3% Triton X-100, 0.05% EDTA, and 0.05% NaN_3, 7 d												
Methe	2014	Pig	Wash in 1% penicillin/streptomycin and 1% amphotericin B,	Freezing in PBS, 24 h, -80°C	Thawing, RT	Wash in distilled water,	Short perfusion of 4% SDC *	Immersion and agitation in 4% SDC, 6 h, 37°C *		Perusion with 1% SDC, 6 h, RT *		Perfusion with distilled water, 6 h, RT *		Perfusion with 1% Triton X-100, 12 h *		Immersion and agitatio in 1% Triton X-100, 12 h *		Perfusion with 0.1% peracetic acid in PBS, 3 h
Momtahan	2015	Pig	Wash in heparin (10 IU/m), 100 IU/ml penicillin, 100 μg/ml streptomycin, 25 μg/ml amphotericin B	Freezing in heparanized water, -20°C	Thawing, ON, 4°C	1X PBS, 1 h, 0-4 psi, 23°C	Distilled water, 1 h, 5 psi, 23°C	0.5% SDS in distilled water, 2 h, 5 psi, 23°C **		Distilled water, 2 h, 5 psi, 23°C **		Distilled water, ON, 3 psi, 23°C		1% Triton X-100, 2 h, 3-5 psi, 23°C		Distilled water, 5 h, 5 psi, 23°C		
Guyette	2016	Human	Heparanized PBS (1 IU/ml), 1 h, 60 mm Hg, RT				1% SDS in deionized water, 168 h, 60 mm Hg, RT			Deionized water, 24 h, 60 mm Hg, RT			1% Triton X-100 in deionized water, 24 h, 60 mm Hg, RT			PBS, 168 h, 60 mm Hg, RT		
Kitahara	2016	Pig	Freezing, 24 h, -80°C		Thawing, 4°C		Deionized water, 15 min, 100 ml/min	1% SDS in deionized water, 3 h, 100 mm Hg, 200-1000 ml/min, 37°C ***			Deionized water, 15 min, 1000 ml/min ***		1% Triton X-100 in deionized water, 3 h, 1000 ml/min			Deionized water, 1 h, 1000 ml/min		
Sanchez	2016	Human	1% SDS in deionized water, 60 l in 4 d, 80-100 mm Hg					Wash in water, 20 l, 80-100 mm Hg					Penicillin/streptomycin in PBS, 10 l, 80-100 mm Hg					

Legend
* This group of washes has been repeated 8 times
** This group of washes has been repeated 3 times
*** This group of washes has been repeated 3 times

Table 4.1 State of art of whole heart decellularization protocols. *Table is reported in (Iop, et al. 2017)*

- *Organ selection*

The crucial choice of decellularization protocol must be organ-dependent. The use of young or adult organs of animal or human origin definitely affects the outcome of entire decellularization process.

Most of the studies focused the attention on adult hearts and the protocols were therefore tailored on mature ECMs, which are mainly composed of collagen (Borg and Caulfield 1981; Caulfield and Borg 1979). It has been reported that collagen increases the cross-linking (Mccormick and Thomas 1998) and bundle thickness with age (Gazoti Debessa, Mesiano Maifrino, and Rodrigues de Souza 2001). Conversely, fetal and neonatal ECMs contain fibronectin, as the most abundant protein, and other soluble proteins. Hence, in order to decellularize young tissues and organs by preserving their delicate structure, it is necessary to reduce the harshness of protocols (Williams et al. 2014).

Moreover, the decellularization of adult human organs was reported to be ineffective in removing the lipofuscin, which was retained in obtained scaffolds (Guyette et al. 2016; Oberwallner et al. 2014). This age-related pigment may induce cell-toxicity and immunogenic reactions.

Donors older than 50 years may also carry severe cardiovascular pathologies, such as hypertension or atherosclerosis. These diseases inevitably activate compensatory mechanisms responsible for permanent structural alterations and which cannot be reversed by decellularization.

Considering the increasing age of donors and lack of suitable organs, the option of porcine hearts is very attractive for an effective reply to clinical demands. The two species share similar organ size and anatomy. The affinity between the compositions of porcine and human ECM was also confirmed (Oberwallner et al. 2014). However, the use of xenogeneic organs is more hazardous in terms of immunocompatibility when xenoantigens, such as α-gal sugar residue or sialic acids, are not effectively removed (Iop, Dal Sasso, et al. 2017).

- *Strategies for whole heart repopulation*

Differently from other cardiovascular scaffolds, such as heart valves, vascular grafts and pericardial patches, the heart necessarily needs to be repopulated prior to its implantation (Iop, Dal Sasso, et al. 2017).

The choices of cell types, origin, and number are critical for the successful and complete repopulation of cardiac scaffolds. The heart is composed of several types of tissues, and therefore, the chosen cytotype should give rise to parenchyma, vascular components and connective tissues. Cells may be autologous or allogeneic, but both alternatives present some pros and cons in terms of availability and potential immunogenicity. Seeding strategy is also important: coronaries can be used as principal carrier, but the repopulation of parenchyma usually requires cell injections. Bioreactors and biophysical stimuli are also used to condition the cells (Badylak, Taylor, and Uygun 2010).

The first rat decellularized heart was seeded in a bioreactor with rat neonatal cardiomyocytes, through intramural injection, and rat aortic ECs by means of coronary perfusion. After 7 days, coronary tree and ventricular chambers appeared to be endothelialized, whereas after 8 days the construct could pump under simulated physiologic load and electric stimuli (Ott et al. 2008).

Analogously, murine neonatal cardiomyocytes and HUVECs were used to repopulate porcine scaffolds. The experiments resulted in partial endothelial coverage of large and small arterial *intima* and parenchymal repopulation around injection areas. Endogenous electrical activity was recorded after 10 days (Weymann, et al. 2014)

Human iPSCs were differentiated into cardiomyocytes and injected into the left ventricles of human decellularized scaffolds. The seeding was conditioned in a bioreactor with mechanical stimulation of the left ventricle. A recellularization of 50% was visible at 14 days in the seeded regions. Although the myocardium could contract under electric stimulation, the cells presented heterogeneous grades of maturity (Guyette et al. 2016).

4.2 Aim of the project

The integrity of ECM obtained by means of decellularization strategies plays a key role in TE applications. The aim of this project was therefore the development of a more preservative and cytocompatible protocol for whole decellularization of rat hearts, in view of its future translation to larger organs.

In order to achieve this goal, the following objectives were evaluated:

- Decellularization of rat hearts, reducing the perfusion time and concentration of the detergents, and introducing protease inhibitors and myorelaxant;
- Evaluation of cardiac ECM maintenance and decellularization effectiveness by means of histology, immunofluorescence, quantification of residual DNA, and proteomics.
- *In vitro* assessment of cytocompatibility and quantification of MTS reduction and released LDH.

4.3 Materials and methods

4.3.1 Heart isolation

Pharmacological and surgical procedures adopted for cardiac isolation were executed according to the Italian Ministry of Health guidelines (Decreto Legislativo 116, art. 12 of 21/01/1992) and European Directive 2010/69/EU valid since the 1st January 2013.

After systemic heparinization (0.9 µl/unit per body weight) and general anesthesia using Xilor (0.4 mg / 100 g xylazine, Bio 98 srl, Milan, Italy) and Zoletil (9 mg / 100 g 50% tiletamine and 50% zolazepan, Virbac, Carros, France), 6-weeks-old male Wistar rats were sacrificed by cervical dislocation. Medial sternotomy allowed to expose the heart enveloped into the pericardial sac. After the dissection of ascending aorta, venae cavae, and pulmonary vessels, the isolated organs were immediately stored in cold heparinized PBS (5 UI/ml).

A customized cannula was gently inserted into the ascending aorta of each heart in a stereomicroscope (Zeiss Stemi 2000, Carl-Zeiss, Oberkochen, Germany). Cannulated hearts were inserted in a modified[2] Langendorff apparatus (Langendorff 1985) and perfused with heparinized PBS (5 UI/ml) in a peristaltic pump (Minipuls 3, Gilson Inc., Middleton, WI, USA). The excess of surrounding tissues (thymus gland, lungs, pericardium, and retrosternal fat) was carefully removed (Figure 4.1).

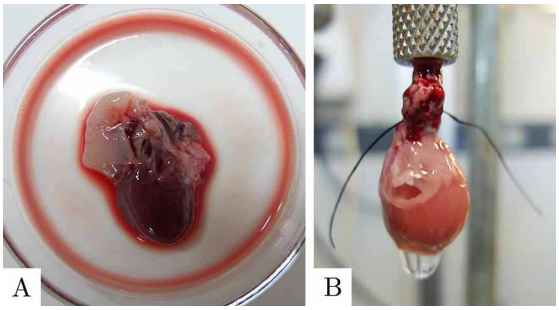

Figure 4.1 Native rat heart. *Isolated heart is surrounded by remains of lungs, pericardium, thymus gland, and retrosternal fat (A). Cleaning from these tissues was performed once organ was cannulated and inserted in modified Langendorff apparatus.*

4.3.2 Whole heart decellularization

Total heart decellularization was carried out by means of retrograde coronary perfusion and submersion in decellularization solutions (Figure 4.2).

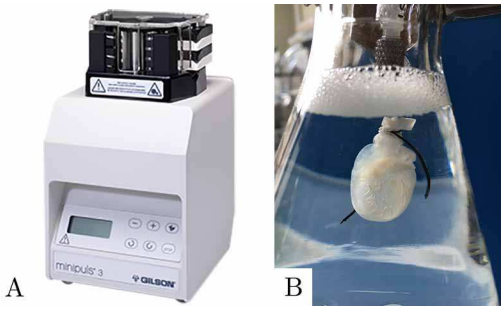

Figure 4.2 Setup of decellularization apparatus*. Decellularization procedure was carried out in modified Langendorff apparatus using a peristaltic pump to perfuse the solutions (A), meanwhile hearts were maintained submerged (B).*

[2] The original Langendorff apparatus was composed of peristaltic pump, heat exchanger, air trap, reservoir for administered solutions and organ bath. In our case, only pump, reservoir, and organ bath were used.

In more detail, the decellularization inherited the first two steps from TriCol protocol (Section 3.3.1). Serine protease inhibitors (Sigma-Aldrich), dissolved in DMSO (Sigma-Aldrich) were administered in order to avoid ECM degradation. This step was followed by hypotonic solution. Cell removal was carried out with 0.5% sodium dodecyl sulfate (SDS, Sigma-Aldrich) perfused for 5 hours. A myorelaxant (2,3-butanedione monoxime, Sigma-Aldrich) was used to promote muscle cell relaxation. Residues of SDS were removed by a non-ionic surfactant (1% Triton X-100, Sigma-Aldrich) and extensive washes in PBS. Lastly, non-specific endonucleases (Benzonase® Nucleases) were used to extract nucleic acids.

The decellularization samples were sterilized by a double-step procedure developed in our laboratory (Fidalgo et al. 2017). Briefly, a cocktail of antibiotics-antimycotic (described in the Section 2.3.4.3.1) was followed by an incubation in 0.05% (v/v) peracetic acid (Sigma-Aldrich) for 3 hours at 27°C. Afterwards, samples were deeply washed in PBS.

4.3.3 Histology and immunofluorescence

Native hearts were washed in PBS, excess of water was removed using filters paper and were frozen in nitrogen fumes. Decellularized hearts were perfused at 10 ml/min for 1 hour in 2% paraformaldehyde (PanReac AppliChem) solution, washed three times in saline for 10 minutes and in 20% sucrose solution overnight. Then the hearts were perfused at 2.5 ml/min and embedded in a 1:1 solution of O.C.T. (Tissue-Tek) and 20% sucrose (Sigma-Aldrich) and snap-frozen in isopentane (Sigma-Aldrich) and nitrogen fumes. All samples were stored at -80 °C until further processing. Cryosections of 8 µm were obtained for both native and decellularized samples using cryostat (Leica).

The effectiveness of newly applied decellularization protocol and preservation of the ECM were evaluated by several histological techniques: Hematoxylin and Eosin (H&E) for investigating general tissue architecture, Masson's trichrome (MT) for collagen, Alcian Blue (AB) for alcianophilic components, and Weigert-Van Gieson (VG) for elastin (all purchased from Bio-Optica). Images were acquired in a light microscope (Olympus Corporation), equipped with a Nikon Eclipse 50i camera and NIS-Elements D 3.2 software.

In order to evaluate the maintenance collagen I and elastin, cryosections of native and decellularized samples were assessed in a house-made TPM (Filippi et al. 2018). The SHG and TPEF signals were collected at excitation wavelength of 1,200 nm and 800 nm, respectively. A fixed resolution of 1,024×1,024 pixels and frame accumulation of 120 frames were adopted.

The integrity of basal lamina was evaluated by means of indirect immunostaining techniques combined with TPM. The following primary antibodies were used: rabbit polyclonal anti-collagen IV (1:100, ab6586, Abcam) and rabbit polyclonal anti-laminin (1:100, Z0097, Dako). Rhodamine (rhod)-conjugated anti-rabbit (Millipore) was used as secondary antibodies (1:100 Millipore goat anti-rabbit IgG antibody AP132R). Primary and secondary antibodies were diluted in a solution of 1% (w/v) bovine serum albumin (Sigma-Aldrich) in PBS. Nuclei were counterstained with Hoechst (Sigma-Aldrich).

4.3.4 DNA quantification

Wet native and decellularized ventricles were cut into samples of 10 to 20 mg, digested overnight with a solution of 10% proteinase K and purified with DNeasy ® blood and tissue assay kit (Qiagen, Germany). Extracted DNA was quantified with NanoDrop (Thermo Scientific).

4.3.5 Proteomics

The extraction of cardiac ECM components was carried out according to a method proposed in (Barallobre-Barreiro et al. 2012) and (Barallobre-Barreiro et al. 2013) and specifically developed for decellularized cardiac tissues.

After decellularization, hearts were blot with filter paper, minced and weights were recorded. Tissues were frozen in nitrogen fumes and stored at -80°C till they were homogenized in PBS. ECM proteins were extracted with a buffer of 4 M guanidine hydrochloride (Sigma-Aldrich), 50 mM sodium acetate and 25 mM EDTA. The solution was supplemented with a cocktail of protease inhibitors: 104 mM 4-(2-Aminoethyl)benzenesulfonyl fluoride hydrochloride (AEBSF), 80 µM aprotinin, 4 mM bestatin, 1.4 mM E-64, 2 mM leupeptin, 1.5

M pepstatin A (Sigma-Aldrich) at pH 5.8. Supernatant was collected and the amount of proteins was quantified measuring the UV absorbance at 280 nm (Bio-Rad). The material was then stored at -20 °C.

Once thawed, samples were filtered with the method of filter-aided sample preparation (FASP) and Vivacon filters of 10,000 Da (Sartorius, Göttingen, Germany). This step allowed the removal of contaminants, whereas extracted proteins were retained by the filter.

A deglycosylation buffer was used to solubilize large proteoglycans. The solution was prepared with 0.05 U chondroitinase ABC from Proteus Vulgaris, 0.05 U keratanase (endo β-galactosidase) from *Bacteroides fragilis*, and 0.05 U haparinase II, 150 mM sodium chloride, 50 mM sodium phosphate dibasic supplemented with the protease inhibitors cocktail (supplied by Sigma-Aldrich). Samples were incubated with deglycosylation buffer for 16 hours at 37 °C.

Samples were denatured in Laemmli sample buffer (60 mM tris-HCl at pH 6.8, 2% SDS, 10% glycerol, 5% β-mercaptoethanol, and 0.01% bromophenol blue, all supplied by Sigma-Aldrich) for 10 minutes at 96 °C.

Lastly, one-dimension electrophoresis and proteomic analyses on extracts were performed by the Proteomics Laboratory of Prof. Arrigoni at University of Padua.

4.3.6 Evaluation of cardiac scaffold cytotoxicity

Cytotoxic effects induced by decellularized cardiac scaffolds on hBM-MSCs were evaluated by according to ISO 10993-5 requirements (International Organization for Standardization 2009).

4.3.6.1 Seeding conditions

Cells were statically seeded on endocardium of isolated decellularized ventricles (DVs). A concentration of 150,000 cells/6-well was used in contact assay, whereas 15,000 cell/cm^2 were used in evaluation of cell adhesion. In both experiments, hBM-MSCs were cultivated in standard conditions (37 °C, 100% humidity, 5% CO_2). As regard to culture medium, MEMα (Sigma-Aldrich) was

used and supplemented with 1% penicillin-streptomycin cocktail (Sigma-Aldrich), 1% L-glutamine (Sigma-Aldrich) and 20% fetal bovine serum (Sigma-Aldrich).

In the case of contact assay, tissue stripes of 0.5×1 cm were secured on the bottom of tissue culture-treated 6-well plates with sterile strips (3M). Samples for cell adhesion evaluation were cut into 0.5 cm circular punches, inserted in tissue culture-treated 96-well plates (Costar®, Corning Incorporated) and conditioned in FBS (Sigma-Aldrich) overnight in incubator at 37 °C. Then, ventricles were coated with 0.02 µg/µl fibronectin (Sigma-Aldrich) for 8 hours in incubator at 37 °C.

Polystyrene of tissue culture 6- and 96-well plates (Costar®, Corning Incorporated) and cyanoacrylate Super Attack (Loctite) were respectively adopted as positive and negative controls for cytotoxicity tests.

4.3.6.2 Qualitative evaluation of cytotoxicity

Qualitative evaluation of cytotoxicity was performed as described in Section 2.3.4.3.3.

4.3.6.3 Quantification of cytotoxicity

LDH activity and MTS production were quantified as described in Section 2.3.4.3.4.

Cell media were collected from tested materials and controls at 1, 2, 3, 7, 10, and 14 days and maintained at -80 °C until the analyses were carried out. LDH was quantified with Pierce LDH cytotoxicity assay kit (Thermo scientific) and percentage of cytotoxicity was calculated as reported in (Cebotari et al. 2010).

All tested samples and controls were incubated with MTS reagent of CellTiter 96 aqueous solution cell proliferation assay (Promega) at 1, 7 and 14 days. Absorbance at 490 nm was acquired after 2 hours.

4.3.6.4 Cell adhesion and penetration

Cell adhesion and penetration were evaluated histologically. Seeded samples were fixed in 2% PFA in PBS for 10 minutes at room temperature. After two washes in PBS, they were dehydrated in 20% sucrose in PBS overnight at 4 °C. The following day, DVs were embedded in a solution of 20% sucrose-O.C.T. (1:1) and snap-frozen in isopentane and nitrogen fumes. Cryosections of 5 µm-thickness were obtained in a cryostat and stained with H&E. Images were acquired in a light microscope (Olympus Corporation).

4.3.7 Statistical analyses

All data were processed and analyzed with Prism (GraphPad Software, CA, USA). Results are reported as mean ± standard deviation. Groups were compared by mean (Student's t-test) and variance analyses (two-way ANOVA). Significant level was set at 5%. More details about settings are given in the graph captions.

4.4 Results

4.4.1 Assessment of decellularized scaffolds

At macroscopic observation, decellularization caused gradual discoloration of treated hearts. The reddish-brown color of native organs was replaced by a whitish and translucent aspect (Figure 4.3). The original turgid consistency was lost, and cardiac walls appeared collapsed. It was possible to appreciate the coronary tree and interventricular septum, previously concealed, through ventricular surfaces.

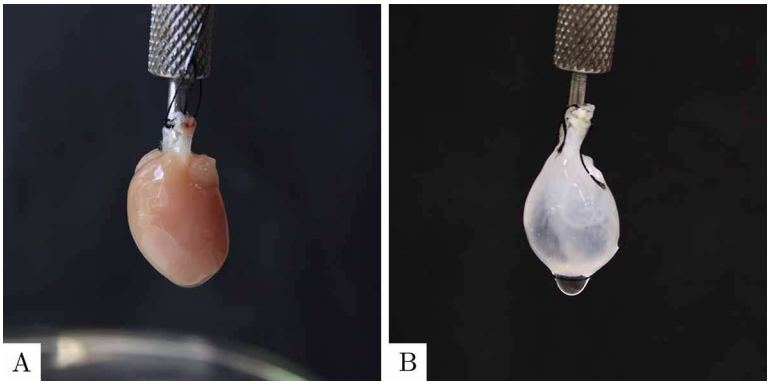

Figure 4.3 Macroscopic comparison of native and decellularized heart. *Reddish-brown color of native organ (A) was replaced by whitish and translucent aspect after decellularization (B). Coronary tree and interventricular septum became visible through ventricular surfaces.*

At microscopic level, the most evident aspect of histological analyses was the thinning of cardiac walls (ventricles and interventricular septum), due to the cell removal (Figure 4.4). This feature was visible in all analyzed sections.

In the H&E-stained decellularized sections, the removal of native cells (Figure 4.4A, C, E) revealed the refined mesh composing the cardiac ECM (Figure 4.4B, D, F). The vessels, which have been the major carriers of decellularization solutions, appeared intact and patent (Figure 4.4B, F).

The MT staining evidenced the maintenance of matrix collagens in decellularized tissues (Figure 4.4H, J, L), clearly visible in native tissues only in vascular *adventitia* (Figure 4.4G, I, K).

The sulfated and carboxylated mucopolysaccharides and sialomucins appeared preserved, as revealed by AB staining (Figure 4.4M-R).

The elastic component, rare into cardiac myocardium, was present in *elastic laminae* of vascular *media* (Figure 4.4S-X).

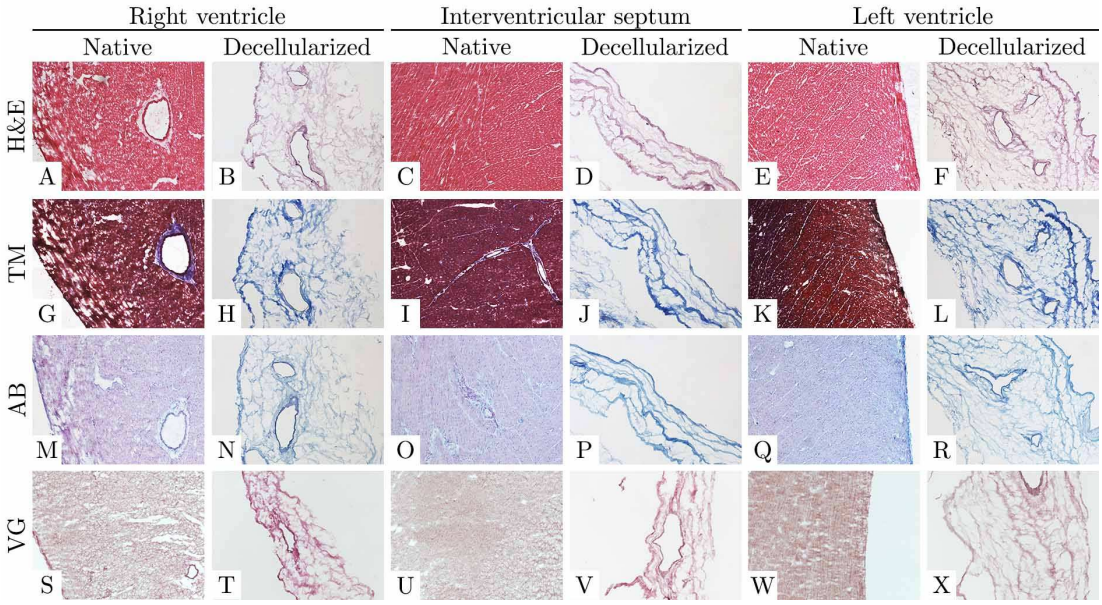

Figure 4.4 Histological comparison of native and decellularized ventricles and interventricular septum. *General histoarchitecture, collagen, alcianophilic components, and elastic elements of native heart (A, C, E, G, I, K, M, O, Q, S, U, W) were maintained in decellularized samples (B, D, F, H, J, L, N, P, R, T, V, X) although dramatic reduction of cardiac wall thickness. Scale bar = 100 μm.*

The decellularization seemed to not negatively affect aortic valve competence. The general architecture appeared maintained (Figure 4.5A, B) and also collagen, elastin and alcianophilic components (Figure 4.5C-D, E-F, G-H, respectively).

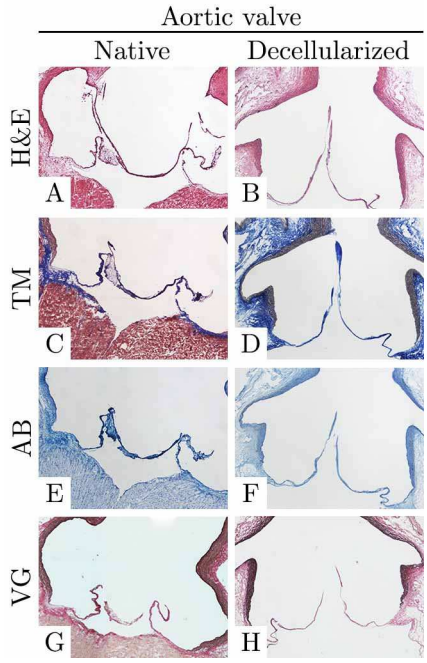

Figure 4.5 Comparison of native and decellularized aortic valve. *Aortic valve maintained original competence. General histoarchitecture (A, B), collagen (C, D), alcianophilic components (E, F), and elastin (G, H) were preserved. Scale bar = 100 µm.*

The strong autofluorescence of cardiac sarcomeres, present in all native sections (Figure 4.6A-F, M-R), was totally absent in decellularized tissues. In the latter, only the green signal of elastin TPEF was visible (Figure 4.6G-L and S-X). The basal lamina elements, such as collagen IV (Figure 4.6A-F) and laminin (Figure 4.6M-R), appeared well-preserved in decellularized cardiac wall and vessels, as shown by selective immunodetection of these molecules (Figure 4.6G-L, S-X, respectively).

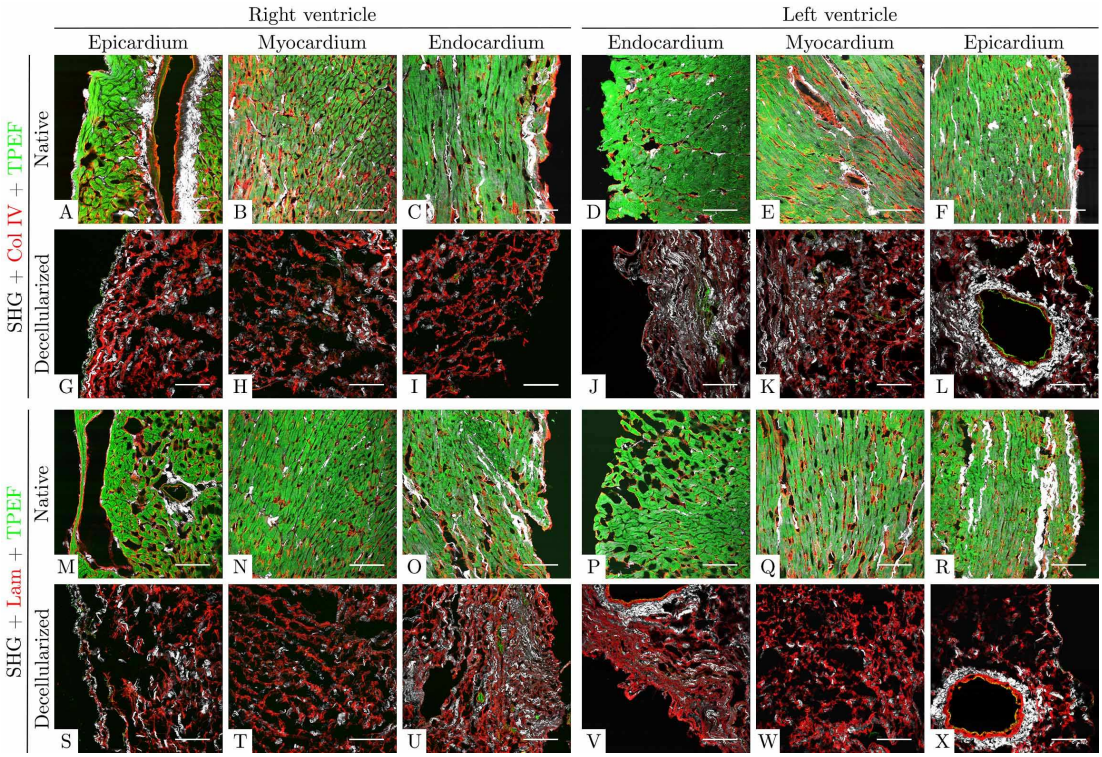

Figure 4.6 Basal membrane of native and decellularized cardiac walls. *After decellularization, basal lamina main components, collagen IV (A-F) and laminin (M-R), were maintained in cardiac ECM and vessels (G-L and S-X, respectively). Scale bar = 100 μm.*

The decellularization caused the reduction of 98.9% of native DNA. The amount in decellularized scaffolds was also below the conventional threshold fixed in the literature (Crapo et al. 2011): 13.1 ± 5.8 ng/mg against 1,145.8 ± 98.2 ng/mg of native tissues (Figure 4.7).

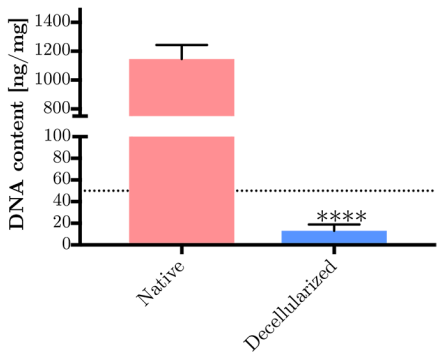

Figure 4.7 DNA quantification of native and decellularized hearts. *Reduction of DNA was statistically significant with respect to native tissues. Two-tailed t-test, **** $p < 0.0001$.*

Proteomic analyses demonstrated retention of key ECM components. It was confirmed the preservation of the main proteins, such as collagen I, and

constituents of basal lamina (Collagen IV, XV, XVIII). Molecules responsible for cell-ECM interactions and ECM assembly (Fibronectin, Dermatopontin, Fibulin, collagen V) and with cytoprotective functions (collagen VI) were present.

4.4.2 Cytotoxicity

Cytotoxic effects induced by direct contact of hBM-MSCs with DVs are reported in Figure 4.8. At all time-points, cells presented normal morphology, with the exception of negative control (glue). Limited presence of intracytoplasmic granules, no signs of suffering, unaltered proliferation, and polarization towards the DVs were observed. These considerations confirmed the equivalent cytotoxicity grading of "0", whereas cyanoacrylate effect corresponded to a "grade 5" with reference to ISO classification.

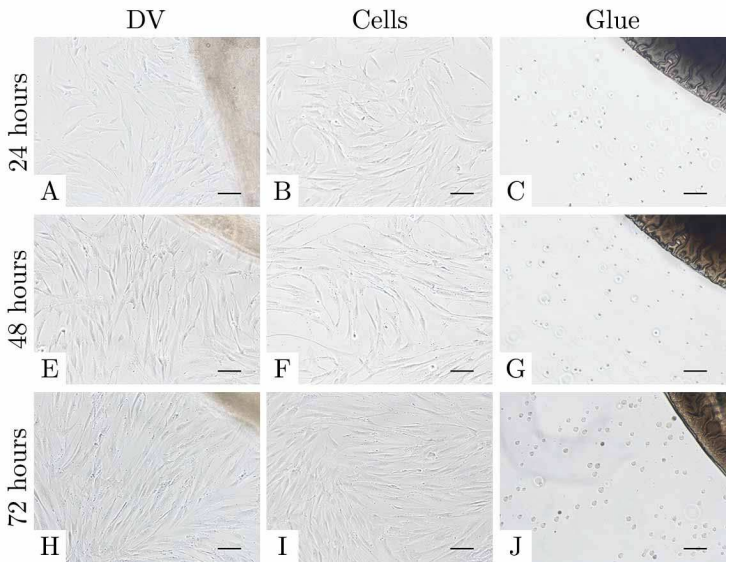

Figure 4.8 Contact assay of decellularized ventricles. *Tested material did not affect cell morphology, which appeared similar to positive control. Negative control caused cell death and detachment. Scale bar = 100 μm.*

Proliferation activities of hBM-MSCs seeded on DV scaffolds and polystyrene remained unaltered over the three time-points and were not statistically different between each other, whereas they were statistically higher with respect to the glue ($p < 0.0001$). Negative control caused also progressive decrease of reduced MTS (Figure 4.9).

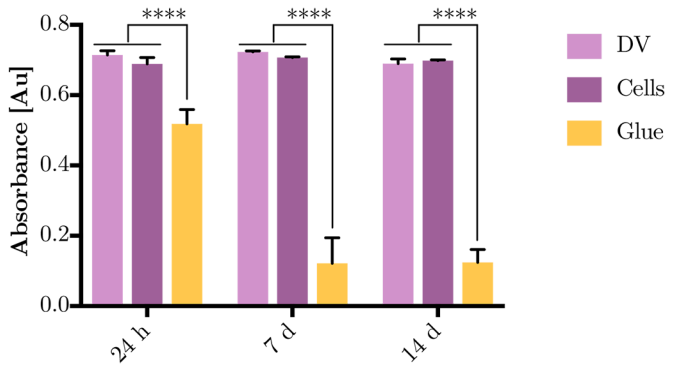

Figure 4.9 MTS reduction of hBM-MSCs seeded on decellularized ventricles and controls. *Proliferation activity was higher in DV tissues and cells on polystyrene. Glue reached the lowest values. Statistic differences are shown with respect to negative control. Two-way ANOVA, Tukey's multiple comparison test, **** $p < 0.0001$.*

Percentage of cytotoxicity induced by DV scaffolds increased from 24 hours and reached the maximum at 10 days when it started to decrease. However, it remained negative or near to zero at all considered time-points, whereas the glue caused 100% of toxicity (Figure 4.10).

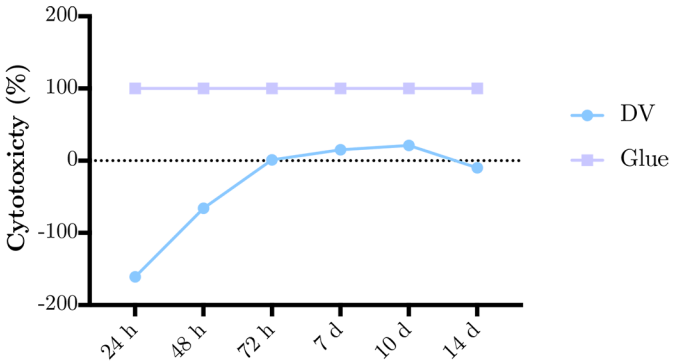

Figure 4.10 Quantification of LDH released by hBM-MSCs seeded on decellularized ventricles and controls. *At all time points, percentage of cytotoxicity induced by DV scaffolds was negative or near zero, whereas glue reached 100%.*

The static seeding produced a continuous monolayer of hBM-MSCs lining endocardial surface after 24 hours (Figure 4.11A-D). At 7 and 14 days, the cell penetration through cardiac ECM was visible in several areas of the scaffolds, with initial invasion of perivascular space of coronary arteries (Figure 4.11E-H, I-L, respectively).

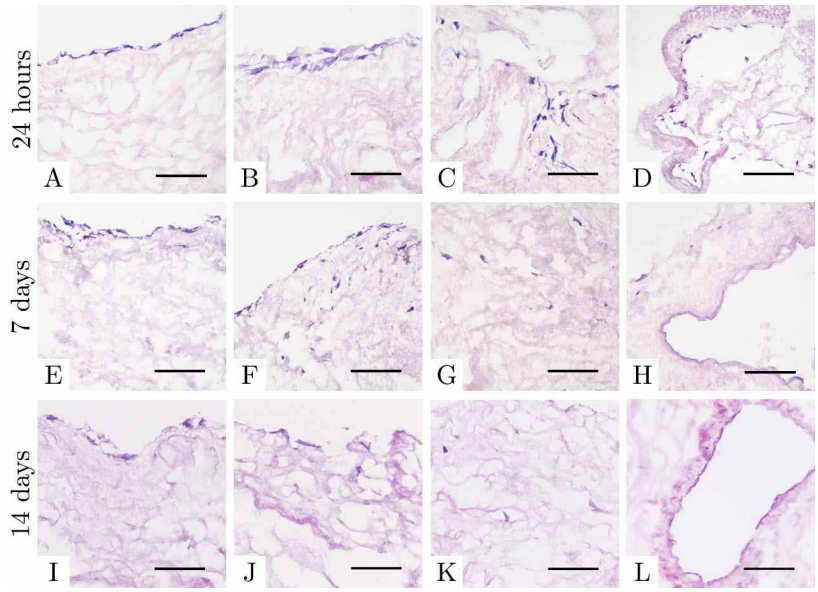

Figure 4.11 Evaluation of hBM-MSCs lining and penetration on decellularized ventricles. *Cell lining was visible immediately after 24 hours (A-D). At 7 and 14 days, it was possible to appreciate cell penetration and perivascular invasion (E-H, I-L, respectively). Scale bar = 100 μm.*

4.5 Discussion

The development of a whole bioengineered heart is one of the most challenging responses to cardiac organ shortage. The initial step of this demanding process is represented by total heart decellularization. The complete elimination of endogenous cell components (cell membranes and intracellular elements comprising the nucleus) and full maintenance of the cardiac ECM represent the necessary prerequisite to prevent immune response and to promote functional tissue reconstruction and remodeling.

In the fields of regenerative medicine and tissue engineering, the unique structure and molecular composition of the natural 3D ECM is considered the key element, due to its biological activity, signaling, and mechanical functions. Several decellularization protocols have therefore been proposed with the goal of optimal ECM preservation.

The aim of this final project was to develop a highly preservative technique for decellularizing the whole heart prior to its repopulation. In particular, we evaluated whether organ submersion, reduction of perfusion time, concentration of decellularization detergents, and use of protease inhibitors and BDM might enhance ECM preservation and cytocompatibility in rat hearts.

The tested protocol shares aortic perfusion and the use of SDS and Triton X-100 surfactants with the first whole cardiac decellularization method (Ott et al. 2008). SDS is present in the majority of protocols of myocardium and whole heart decellularization (Guyette et al. 2016; Kitahara et al. 2016; Momtahan et al. 2015; Sanchez et al. 2016; Weymann, et al. 2014), also in combination with deoxycholic acid (Akhyari et al. 2011; Aubin et al. 2013). Our new protocol was enriched by introducing the immersion of organs and greatly reducing SDS perfusion time (from 12 to 5 hours) and concentration (from 1% to 0.5%). The disadvantages associated with the use of this ionic detergent are due to destructive effects on collagen bundles, elastin precipitation, GAG reduction, and extraction of growth factors. Instead, GAG reduction has been reported as the most effective detergent for removing nuclear and cytoplasmic components (Crapo et al. 2011; Gilbert et al. 2006). In the conception of the above novel decellularization treatment, protease inhibitors were introduced to protect the ECM from cellular proteases released after osmotic shock, the myorelaxant action of adenosine was substituted with BDM, and treatment with non-specific endonucleases was added at the end of process to achieve maximal removal of nucleic acids.

The first and most evident macroscopic consequence of decellularization is the progressive discoloration of the native organ due to cell extraction, as already reported by Ott et al. (Ott et al. 2008). The new translucent aspect of the decellularized heart could be appreciated, by the naked eye, together with the internal organization of cardiac chambers and valve apparatus. Coronary vasculature also became fully visible through the ventricular walls.

The preservation of ECM was confirmed by histology, immunofluorescence and proteomic analysis. The native myocardium is one of the tissues with highest cell density. Therefore, after decellularization, both right and left ventricles appeared to be greatly thinned, whereas the lacunae of cardiomyocytes were clearly visible. The outcomes obtained with MT, TPEF detection of native sarcomeres and proteomic evaluations indicated the absence of any muscle cell components (*i.e.*, contractile elements). The same analyses confirmed the presence of collagen I, the main constituent of cardiac ECM, also retained by other SDS-based protocols applied to porcine and human organs (Guyette et al. 2016; Momtahan et al. 2015). The alcianophilic components

and elastin appeared to be preserved. As regards these two molecules, the results in the literature are often conflicting: reduction of GAGs and elastin in human organs has been reported (Guyette et al. 2016), whereas no variations has been found in rats (Ott et al. 2008), indicating that selection of species probably plays a role in the final outcome.

Major problems were related to the maintenance of vascular integrity and valve competence. Vasculature was used as a carrier of the decellularization solution but, with the aim of repopulation, it will also be employed to diffuse the cells through decellularized tissues. Its preservation is therefore mandatory. On a similar fashion, the aortic valve plays a fundamental role in decellularization. Rat heart was cannulated through the ascending aorta and, in order to allow correct perfusion of the coronary tree, the valve had to remain closed for most of the process. In addition, the delicate structure of the cusps may undergo structural deterioration. After the new decellularization method had been applied, the cusp structure appeared to be well-preserved, together with the sinuses of Valsalva and coronary origins, as shown in the histological staining.

The dominant elements of the vascular and muscular basal lamina, collagen IV and laminin, were probably well-preserved, as shown by their distribution in immunofluorescence analysis. These results were confirmed in the literature: basal laminae were also retained at higher concentrations of SDS: 1% (Ott et al. 2008) and 4% (Weymann, Patil, Sabashnikov, Jungebluth, Korkmaz, Li, Veres, Soos, Ishtok, Chaimow, Patzold, et al. 2014). These constituents are essential for cell adhesion and migration during tissue and organ repopulation.

In addition, two other constituents, collagen XV and XVIII, were revealed by proteomic analysis. Like the heparan sulfate proteoglycan of the basal membrane, collagen XV enhances the mechanical stability of muscle cells within the ECM and contributes to microvessel patency (Eklund et al. 2001), whereas collagen XVIII regulates angiogenesis and EC proliferation and migration, by means of endostatin (Ferreras et al. 2000; Heljasvaara et al. 2017; O'Reilly et al. 1997), and ECM organization (Mouw, Ou, and Weaver 2014). Other proteins responsible for interactions between cardiac cells and matrix and involved in ECM development were also detected, *i.e.*, fibronectin, dermatopontin, fibulin and collagen V. Fibronectin plays a crucial role in

regulating cell adhesion, migration and proliferation, and also as a mediator of cell-matrix relationships (Pankov 2002). In addition, it is fundamental for preserving cardiac stem cells in the niches of the native heart (Konstandin et al. 2013; Singh and Schwarzbauer 2012). Dermatopontin regulates collagen fibrillogenesis and may be involved in healing infarcted tissues and in cell proliferation (Okamoto and Fujiwara 2006). Fibulin contributes to assembling the fibers of the vascular elastic lamina and regulates healing of injured vessels and angiogenesis (Chapman et al. 2010; Yanagisawa, Schluterman, and Brekken 2009). Collagen V is responsible for ECM structure and regulation of collagen fiber diameter (Wenstrup et al. 2004). These molecules may contribute to constructive remodeling of repopulated cardiac ECM and support cell engraftment and proliferation.

Lastly, the nuclei were not visible in H&E staining and the quantity of endogenous DNA retained after decellularization was below the threshold proposed in the literature to prevent immune rejection and adverse host response *in vivo* (Crapo et al. 2011).

Apart from the preservation of ECM molecules and removal of cell elements, maintenance of original cytocompatibility is a key aspect for the effective repopulation of decellularized organs and tissues *in vitro* and *in vivo*. In general, the literature of whole organ decellularization is focused more on repopulation strategies. The assessment of cytotoxicity is a fundamental step because the presence of toxic compounds, such as remains of detergents, may compromise recellularization. In our case, evaluation of cell morphology, quantification of MTS reduction, and percentage of cytotoxicity were indicative of low levels of toxicity induced by the DV scaffolds on seeded hBM-MSCs. These results were also confirmed by histological findings, which demonstrated the ability of hBM-MSCs to form stable linings on DVs after 24 hours and penetrate the scaffolds 7 days after static seeding as confirmed in (Sánchez et al. 2015).

In conclusion, this novel protocol could achieve whole heart decellularization by fully preserving natural cardiac ECM. Retained proteins and molecules are involved in structural organization, tissue morphogenesis and cell interaction, and may also promote repopulation and favorable tissue remodeling and regeneration. In addition, the scaffolds demonstrated low

cytotoxicity and propensity to support cell adhesion, proliferation and penetration. The next step will be to scale up to larger organs. Optimization of the decellularization protocol to porcine hearts is currently under evaluation with promising results (Figure 4.12). Lastly, repopulation will be performed with patients' cells, in order to produce a completely natural bioequivalent for the failing heart.

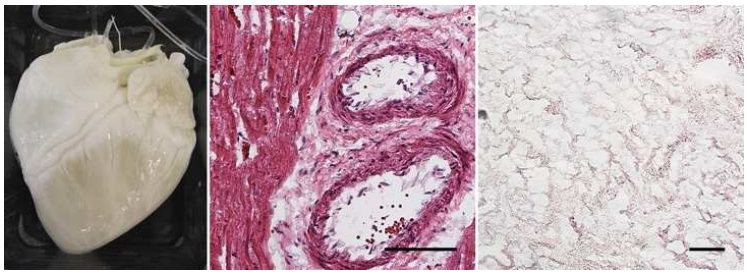

Figure 4.12 Preliminary results of porcine whole heart decellularization. *After decellularization, organ discoloration was visible macroscopically; microscopically, histological analysis reported complete cell removal.*

Conclusions

The Total Bioengineered Organ shortage is still the driving force of one of the most fascinating, but yet demanding, challenges of modern Medicine: the development of novel heart substitutes. The search for alternatives to solid organ transplantation is still a question without a conclusive answer.

This doctoral thesis concerned two pivotal and apparently antithetical approaches for end-stage HF treatment: the production of a more biocompatible lining for TAHs and the development of the optimal ECM for whole heart bioengineering.

On the last years, the biomedical healthcare industry progressively developed a superior level of consciousness about biocompatibility and, as a consequence, an increasing number of ECM-based products have been approved by the regulatory agencies to overcome the limitations of current synthetic materials. In addition, hybrid solutions based on ECM blends, purified proteins and synthesized peptides coupled with several types of polymers are becoming a well-established approach.

Our concept of TAH has more to do with native organs than conventional mechanical pumps. The first developed generation of HM, based on DBP and polycarbonate urethane, showed promising features in terms of cytotoxicity and complement activation. Our final aim is to create a biological substrate, rich in crucial biological, chemical and mechanical stimuli, where ECs can migrate, firmly adhere and perform their biological function for long-term. This goal may be further improved using the endothelial cell-selective functionalization of DBP with REDV tetrapeptide. The healthy and stable endothelial lining may be the solution to enhance pump blood compatibility.

However, the development of the hybrid membrane is just a small *tessera* in the wider mosaic of a totally innovative TAH development. The clinical application of these devices is regulated by several requirements, ranging from geometrical features (dimensions, fitting, weight of the prosthesis), functional aspects (power supply, drivelines, noise), fulfillment of physiologic parameters (cardiac output, stroke volume, adaptation of venous return) and the biocompatibility ambition (avoidance of thromboembolic events, hemorrhages, calcification, infections). Therefore, the novel device will be characterized by a high miniaturization and a modern energy supply system, which will enlarge the number of possible recipients, guaranteeing survival and supporting patients for the rest of their lifetime with a decent quality of life.

The development of more biocompatible TAH was investigated as a more immediate solution to organ shortage. Conversely, whole organ regeneration may represent the fully biocompatible and definitive strategy. The step from using a decellularized matrix as part of a heart (the HM into the TAH) to relying on a scaffold as framework to develop a cardiac organ equivalent is not a short or straightforward process. Decellularization has the difficult task of eliminating the endogenous cell component, which may trigger immune responses, rejection and calcification, while preserving the structure, 3D architecture, vasculature, bioactivity, and biocompatibility of the ECM. After the treatment, the cardiac scaffold has to be necessarily repopulated but so far there are some unsolved matters related to the source of tissue, type and quantity of cells, and culture methods. Great hopes arise from the approach of whole heart bioengineering: in the future of personalized medicine, highly biocompatible organs replacements will be patient-specific and available without any limitation.

List of figures

List of tables

References

Adams, K. F. et al. 1999. "Gender Differences in Survival in Advanced Heart Failure. Insights from the FIRST Study." *Circulation* 99(14):1816–21.

AdvanSource. 2010. "ChronoFlex AR." Retrieved (http://www.advbiomaterials.com/products/polycarbonate/chronoflex_ar.html).

Aguiari, P. et al. 2017. "In Vitro Comparative Assessment of Decellularized Bovine Pericardial Patches and Commercial Bioprosthetic Heart Valves." *Biomedical Materials* 12(1):015021.

Akhyari, P. et al. 2002. "Mechanical Stretch Regimen Enhances the Formation of Bioengineered Autologous Cardiac Muscle Grafts." *Circulation*.

Akhyari, P. et al. 2011. "The Quest for an Optimized Protocol for Whole-Heart Decellularization: A Comparison of Three Popular and a Novel Decellularization Technique and Their Diverse Effects on Crucial Extracellular Matrix Qualities." *Tissue Eng Part C Methods* 17(9):915–26.

Akutsu, T. and A. Kantrowitz. 1967. "Problems of Materials in Mechanical Heart Systems." *J Biomed Mater Res* 1(1):33–54.

Akutsu, T. and W. J. Kolff. 1958. "Permanent Substitutes for Valves and Hearts." *Trans Am Soc Artif Intern Organs* 4(1):230–34.

Akutsu, T., V. Mirkovitch, S. R. Topaz, and W. J. Kolff. 1963. "Silastic Sac Type Artificial Heart Ans Its Use in Calves." *ASAIO J* 9(1):281–85.

Akutsu, T., V. Mirkovitch, S. R. Topaz, and W. J. Kolff. 1964. "A Sac Type of Artificial Heart inside the Chest of Dogs." *J Thorac Cardiovasc Surg* 47:512–27.

Albelda, S. M. and C. A. Buck. 1990. "Integrins and Other Cell Adhesion

Molecules." *FASEB Journal : Official Publication of the Federation of American Societies for Experimental Biology* 4(11):2868–80.

Alexander, J. Steven, D. Neil Granger, and Norman R. Harris. 2017. "Inflammation: The Role of Endothelial Cells." Pp. 457–76 in *Inflammation - From Molecular and Cellular Mechanisms to the Clinic*. Weinheim, Germany: Wiley-VCH Verlag GmbH & Co. KGaA.

Ali, S., J. E. Saik, D. J. Gould, M. E. Dickinson, and J. L. West. 2013. "Immobilization of Cell-Adhesive Laminin Peptides in Degradable PEGDA Hydrogels Influences Endothelial Cell Tubulogenesis." *BioResearch Open Access* 2(4):241–49.

Amara, U. et al. 2008. "Interaction Between the Coagulation and Complement System." *Advances in Experimental Medicine and Biology* 632:68–76.

Ambrosy, Andrew P. et al. 2014. "The Global Health and Economic Burden of Hospitalizations for Heart Failure: Lessons Learned from Hospitalized Heart Failure Registries." *Journal of the American College of Cardiology* 63(12):1123–33.

Anastasi, Giuseppe et al. 2006. *Anatomia Umana - Trattato*. 4th ed. Edi-Ermes.

Anderson, J. S., T. M. Price, S. R. Hanson, and L. A. Harker. 1987. "In Vitro Endothelialization of Small-Caliber Vascular Grafts." *Surgery* 101(5):577–86.

Andrade, J. D. and V. Hlady. 1986. "Protein Adsorption and Materials Biocompatibility: A Tutorial Review and Suggested Hypotheses." Pp. 1–63 in. Springer, Berlin, Heidelberg.

Aoki, Jiro et al. 2005. "Endothelial Progenitor Cell Capture by Stents Coated with Antibody against CD34: The HEALING-FIM (Healthy Endothelial Accelerated Lining Inhibits Neointimal Growth-First in Man) Registry." *Journal of the American College of Cardiology* 45(10):1574–79.

Armato, Ubaldo et al. 2012. *Embriologia Umana*. Città di Castello (PG): Idelson-Gnocchi.

Askari, A. T. et al. 2003. "Effect of Stromal-Cell-Derived Factor 1 on Stem-Cell Homing and Tissue Regeneration in Ischaemic Cardiomyopathy." *Lancet* 362(9385):697–703.

Assmus, B. et al. 2002. “Transplantation of Progenitor Cells and Regeneration Enhancement in Acute Myocardial Infarction (TOPCARE-AMI).” *Circulation*.

Aubin, H. et al. 2016. “Customized Interface Biofunctionalization of Decellularized Extracellular Matrix: Toward Enhanced Endothelialization.” *Tissue Engineering Part C: Methods*.

Aubin, H., A. Kranz, J. Hulsmann, A. Lichtenberg, and P. Akhyari. 2013. “Decellularized Whole Heart for Bioartificial Heart.” *Methods Mol Biol* 1036:163–78.

Aurora, A. B. et al. 2014. “Macrophages Are Required for Neonatal Heart Regeneration.” *Journal of Clinical Investigation* 124(3):1382–92.

Badylak, S. F., D. Taylor, and K. Uygun. 2010. “Whole Organ Tissue Engineering: Decellularization and Recellularization of Three-Dimensional Matrix Scaffolds.” *Annual Review of Biomedical Engineering* 13(1):110301095218061.

Badylak, Stephen F. 2004. “Xenogeneic Extracellular Matrix as a Scaffold for Tissue Reconstruction.” *Transplant Immunology* 12(3–4):367–77.

Badylak, Stephen F. 2005. “Regenerative Medicine and Developmental Biology: The Role of the Extracellular Matrix.” *Anatomical Record - Part B New Anatomist* 287(1):36–41.

Badylak, Stephen F., Donald O. Freytes, and Thomas W. Gilbert. 2015. “Extracellular Matrix as a Biological Scaffold Material: Structure and Function.” *Acta Biomaterialia* 23(1):1–13.

Bagdasarian, N. G., A. N. Malani, F. D. Pagani, and P. N. Malani. 2009. “Fungemia Associated with Left Ventricular Assist Device Support.” *J Card Surg* 24(6):763–65.

De Bakey, Michael E., George L. Jordan, Jack P. Abbott, Bela Halpert, and Robert M. O’neal. 1964. “The Fate of Dacron Vascular Grafts.” *Archives of Surgery* 89(5):755–82.

Balsam, L. B. et al. 2004. “Haematopoietic Stem Cells Adopt Mature Haematopoietic Fates in Ischaemic Myocardium.” *Nature* 428(6983):668–73.

Barallobre-Barreiro, J. et al. 2012. "Proteomics Analysis of Cardiac Extracellular Matrix Remodeling in a Porcine Model of Ischemia/Reperfusion Injury." *Circulation* 125(6):789–802.

Barallobre-Barreiro, J., A. Didangelos, X. Yin, N. Doménech, and M. Mayr. 2013. "A Sequential Extraction Methodology for Cardiac Extracellular Matrix Prior to Proteomics Analysis." *Methods in Molecular Biology (Clifton, N.J.)* 1005:215–23.

Bartlett, Robert H. 2014. "Extracorporeal Life Support: Gibbon Fulfilled." *Journal of the American College of Surgeons* 218(3):317–27.

Bartunek, J. et al. 2013. "Cardiopoietic Stem Cell Therapy in Heart Failure: The C-CURE (Cardiopoietic Stem Cell Therapy in Heart FailURE) Multicenter Randomized Trial with Lineage-Specified Biologics." *Journal of the American College of Cardiology* 61(23):2329–38.

Bearzi, C. et al. 2007. "Human Cardiac Stem Cells." *Proceedings of the National Academy of Sciences* 104(35):14068–73.

Bélanger, M. C. et al. 2000. "Selection of a Polyurethane Membrane for the Manufacture of Ventricles for a Totally Implantable Artificial Heart: Blood Compatibility and Biocompatibility Studies." *Artif Organs* 24(11):879–88.

Bellis, S. L. 2011. "Advantages of RGD Peptides for Directing Cell Association with Biomaterials." *Biomaterials* 32(18):4205–10.

Bellón, J. M., J. Buján, N. G. Honduvilla, A. Hernando, and J. Navlet. 1993. "Endothelial Cell Seeding of Polytetrafluoroethylene Vascular Prostheses Coated With a Fibroblastic Matrix." *Annals of Vascular Surgery* 7(6):549–55.

Beltrami, A. P. et al. 2003. "Adult Cardiac Stem Cells Are Multipotent and Support Myocardial Regeneration." *Cell* 114(6):763–76.

Benedict, Claude R., R. Pakala, and J. T. Willerson. 1994. "Endothelial-Dependent Procoagulant and Anticoagulant Mechanisms. Recent Advances in Understanding." *Texas Heart Institute Journal* 21(1):86–90.

Bengtsson, L., K. Radegran, and I. A. Haegerstrand. 1993. "In Vitro Endothelialization of Commercially Available Heart Valve Bioprostheses with Cultured Adult Human Cells." *European Journal of Cardio-Thoracic*

Surgery 7(8):393–98.

Benjamin, Emelia J. et al. 2018. "Heart Disease and Stroke Statistics—2018 Update: A Report From the American Heart Association." *Circulation* CIR.0000000000000558.

Berger, K., L. R. Sauvage, A. M. Rao, and S. J. Wood. 1972. "Healing of Arterial Prostheses in Man: Its Incompleteness." *Annals of Surgery* 175(1):118–27.

Bernard, M. P., M. L. Chu, et al. 1983. "Nucleotide Sequences of Complementary Deoxyribonucleic Acids for the Proal Chain of Human Type I Procollagen. Statistical Evaluation of Structures That Are Conserved during Evolution." *Biochemistry* 22(22):5213–23.

Bernard, M. P., J. C. Myers, et al. 1983. "Structure of a CDNA for the pro.Alpha.2 Chain of Human Type I Procollagen. Comparison with Chick CDNA for pro.Alpha.2(I) Identifies Structurally Conserved Features of the Protein and the Gene." *Biochemistry* 22(5):1139–45.

Bertipaglia, B. et al. 2003. "Cell Characterization of Porcine Aortic Valve and Decellularized Leaflets Repopulated with Aortic Valve Interstitial Cells: The VESALIO Project (Vitalitate Exornatum Succedaneum Aorticum Labore Ingenioso Obtenibitur)." *Ann Thorac Surg* 75(4):1274–82.

Bissell, M. J. and J. Aggeler. 1987. "Dynamic Reciprocity: How Do Extracellular Matrix and Hormones Direct Gene Expression?" *Prog Clin Biol Res* 249:251–62.

Borg, T. K. and J. B. Caulfield. 1981. "The Collagen Matrix of the Heart." *Fed Proc* 40(7):2037–41.

Borlaug, Barry A. 2014. "The Pathophysiology of Heart Failure with Preserved Ejection Fraction." *Nature Reviews Cardiology* 11(9):507–15.

Bowlin, Gary L. and Stanley E. Rittgers. 1997. "Electrostatic Endothelial Cell Seeding Technique for Small-Diameter (<6 Mm) Vascular Prostheses: Feasibility Testing." *Cell Transplantation* 6(6):623–29.

Bowlin, Gary L., Stanley E. Rittgers, Amy Milsted, and Steven P. Schmidt. 1998. "In Vitro Evaluation of Electrostatic Endothelial Cell Transplantation onto 4 Mm Interior Diameter Expanded Polytetrafluroethylene Grafts." *Journal of Vascular Surgery* 27(3):504–11.

Boyd, K. L., S. P. Schmidt, T. R. Pippert, and W. V Sharp. 1987. "Endothelial Cell Seeding of ULTI Carbon-Coated Small-Diameter PTFE Vascular Grafts." *ASAIO Trans* 33(3):631–35.

Braga-Vilela, A. S., E. R. Pimentel, S. Marangoni, M. H. Toyama, and B. De Campos Vidal. 2008. "Extracellular Matrix of Porcine Pericardium: Biochemistry and Collagen Architecture." *Journal of Membrane Biology* 221(1):15–25.

Braunwald, Eugene, John Ross, and Edmund H. Sonnenblick. 1967. "Mechanisms of Contraction of the Normal and Failing Heart." *New England Journal of Medicine* 277(19):1012–22.

Britten, M. B. et al. 2003. "Infarct Remodeling After Intracoronary Progenitor Cell Treatment in Patients With Acute Myocardial Infarction (TOPCARE-AMI): Mechanistic Insights From Serial Contrast-Enhanced Magnetic Resonance Imaging." *Circulation* 108(18):2212–18.

Bueno, J. M., F. J. Ávila, and P. Artal. 2016. "Second Harmonic Generation Microscopy: A Tool for Quantitative Analysis of Tissues." in *Microscopy and Analysis*. InTech.

Bursac, N. et al. 2003. "Cultivation in Rotating Bioreactors Promotes Maintenance of Cardiac Myocyte Electrophysiology and Molecular Properties." *Tissue Engineering*.

Butruk-Raszeja, B. A., M. S. Dresler, A. Kuźmińska, and T. Ciach. 2016. "Endothelialization of Polyurethanes: Surface Silanization and Immobilization of REDV Peptide." *Colloids and Surfaces B: Biointerfaces* 144:335–43.

Butruk, B., P. Bąbik, B. Marczak, and T. Ciach. 2013. "Surface Endothelialization of Polyurethanes." *Procedia Engineering* 59:126–32.

Butruk, B., P. Bąbik, B. Marczak, and T. Ciach. 2013. "Surface Endothelialization of Polyurethanes." Pp. 126–32 in *Procedia Engineering*, vol. 59. Elsevier.

Campagnola, P. 2011. "Second Harmonic Generation Imaging Microscopy: Applications to Diseases Diagnostics." *Anal Chem* 83(9):3224–31.

CARMAT. 2018. *Press Release (Avalilable Online: Https://Www.Carmatsa.Com/En/Media-Gb/Press-Releases)*. Avalilable

online: https://www.carmatsa.com/en/media-gb/press-releases.

Carpentier, A. et al. 2015. "First Clinical Use of a Bioprosthetic Total Artificial Heart: Report of Two Cases." *Lancet* 386(10003):1556–63.

Carrel, A. and C. Lindbergh. 1938. *The Culture of Organs*. American Medical Association.

Castellanos, M. I. et al. 2015. "Biofunctionalization of REDV Elastin-like Recombinamers Improves Endothelialization on CoCr Alloy Surfaces for Cardiovascular Applications." *Colloids and Surfaces B: Biointerfaces* 127:22–32.

Cattaneo, Luigi. 2005. *Compendio Di Anatomia Umana*. Monduzzi.

Cauich-Rodríguez, J. V, L. H. Chan-Chan, F. Hernandez-Sánchez, and J. M. Cervantes-Uc. 2013. "Degradation of Polyurethanes for Cardiovascular Applications." in *Advances in Biomaterials Science and Biomedical Applications*. IntechOpen.

Caulfield, J. B. and T. K. Borg. 1979. "The Collagen Network of the Heart." *Laboratory Investigation; a Journal of Technical Methods and Pathology* 40(3):364–72.

Cebotari, S. et al. 2010. "Detergent Decellularization of Heart Valves for Tissue Engineering: Toxicological Effects of Residual Detergents on Human Endothelial Cells." *Artif Organs* 34(3):206–10.

Celermajer, David S., Clara K. Chow, Eloi Marijon, Nicholas M. Anstey, and Kam S. Woo. 2012. "Cardiovascular Disease in the Developing World: Prevalences, Patterns, and the Potential of Early Disease Detection." *Journal of the American College of Cardiology* 60(14):1207–16.

Chachques, J. C. et al. 2008. "Myocardial Assistance by Grafting a New Bioartificial Upgraded Myocardium (MAGNUM Trial): Clinical Feasibility Study." *The Annals of Thoracic Surgery* 85(3):901–8.

Chachques, J. C. et al. 2010. "Myocardial Assistance by Grafting a New Upgraded Bioartificial Myocardium (MAGNUM Trial): Clinical Results at 2 Years." *European Heart Journal* 13(9):S48.

Chapman, S. L. et al. 2010. "Fibulin-2 and Fibulin-5 Cooperatively Function to Form the Internal Elastic Lamina and Protect from Vascular Injury."

Arteriosclerosis, Thrombosis, and Vascular Biology 30(1):68–74.

Chatel, D. 1996. "Concept of Totally Biological Internal Coating for Newly Shaped Artificial Ventricles." *Artif Organs* 20(7):814–17.

Chatel, D., L. Delamare, P. Dang, D. Lebouvier, and F. Trocherie. 1997. "A Biomechanical Double Sac (Pericardium-Pebax) for Specially Shaped Artificial Ventricles: A Computerized Study to Evaluate Its Mechanical and Volumetric Properties." *Artif Organs* 21(10):1098–1104.

Chen, S. L. et al. 2004. "Effect on Left Ventricular Function of Intracoronary Transplantation of Autologous Bone Marrow Mesenchymal Stem Cell in Patients with Acute Myocardial Infarction." *American Journal of Cardiology* 94(1):92–95.

Cheng, K., J. W. Meador, M. A. Serrato, and T. Akutsu. 1977. "The Design and Fabrication of a New Total Artificial Heart." *Cardiovasc Dis* 4(1):7–17.

Chenoweth, D. E. 1988. "Complement Activation Produced by Biomaterials." *Artificial Organs* 12(6):508–10.

Chimenti, I. et al. 2010. "Relative Roles of Direct Regeneration versus Paracrine Effects of Human Cardiosphere-Derived Cells Transplanted into Infarcted Mice." *Circulation Research* 106(5):971–80.

Choi, Woong Gil, Soo Hyun Kim, Hyung Seok Yoon, Eun Joo Lee, and Dong Woon Kim. 2015. "Impact of an Endothelial Progenitor Cell Capturing Stent on Coronary Microvascular Function: Comparison with Drug-Eluting Stents." *The Korean Journal of Internal Medicine* 30(1):42.

Christman, K. L., A. J. Vardanian, et al. 2004. "Injectable Fibrin Scaffold Improves Cell Transplant Survival, Reduces Infarct Expansion, and Induces Neovasculature Formation in Ischemic Myocardium." *Journal of the American College of Cardiology*.

Christman, K. L., H. H. Fok, R. E. Sievers, Q. Fang, and R. J. Lee. 2004. "Fibrin Glue Alone and Skeletal Myoblasts in a Fibrin Scaffold Preserve Cardiac Function after Myocardial Infarction." *Tissue Engineering*.

Christman, K. L. and R. J. Lee. 2006. "Biomaterials for the Treatment of Myocardial Infarction." *Journal of the American College of Cardiology*, September 5, 907–13.

Chuang, Tzu Wen and Kristyn S. Masters. 2009. "Regulation of Polyurethane Hemocompatibility and Endothelialization by Tethered Hyaluronic Acid Oligosaccharides." *Biomaterials* 30(29):5341–51.

Cigliano, A. et al. 2012. "Fine Structure of Glycosaminoglycans from Fresh and Decellularized Porcine Cardiac Valves and Pericardium." *Biochem Res Int* 2012:979351.

Clark, S. J., P. N. Bishop, and A. J. Day. 2013. "The Proteoglycan Glycomatrix: A Sugar Microenvironment Essential for Complement Regulation." *Frontiers in Immunology* 4(NOV):412.

Clowes, Alexander W., Thomas R. Kirkman, and Monika M. Clowes. 1986. "Mechanisms of Arterial Graft Failure. II. Chronic Endothelial and Smooth Muscle Cell Proliferation in Healing Polytetrafluoroethylene Prostheses." *Journal of Vascular Surgery* 3(6):877–84.

Coleman, D. L. 1981. "Mineralization of Blood Pump Bladders." *Trans Am Soc Artif Intern Organs* 27:708–13.

Coleman, D. L., D. Lim, T. Kessler, and J. D. Andrade. 1981. "Calcification of Nontextured Implantable Blood Pumps." *ASAIO Journal* 27(1):97–104.

Coleman, D., J. Lawson, and W. J. Kolff. 1978. "Scanning Electron Microscopic Evaluation of the Surfaces of Artificial Hearts." *Artif Organs* 2(2):166–72.

Cooley, D. A. et al. 1969a. "First Human Implantation of Cardiac Prosthesis for Staged Total Replacement of the Heart." *Trans Am Soc Artif Intern Organs* 15(1):252–66.

Cooley, D. A. et al. 1969b. "Orthotopic Cardiac Prosthesis for Two-Staged Cardiac Replacement." *Am J Cardiol* 24(5):723–30.

Cooley, D. A., T. Akutsu, J. C. Norman, M. A. Serrato, and O. H. Frazier. 1981. "Total Artificial Heart in Two-Staged Cardiac Transplantation." *Cardiovasc Dis* 8(3):305–19.

Costello, John P., Thalachallour Mohanakumar, and Dilip S. Nath. 2013. "Mechanisms of Chronic Cardiac Allograft Rejection." *Texas Heart Institute Journal / from the Texas Heart Institute of St. Luke's Episcopal Hospital, Texas Children's Hospital* 40(4):395–99.

Costerton, J. W., G. G. Geesey, and K. J. Cheng. 1978. "How Bacteria Stick."

Sci Am 238(1):86–95.

Costerton, J. W., L. Montanaro, and C. R. Arciola. 2005. "Biofilm in Implant Infections: Its Production and Regulation." *Int J Artif Organs* 28(11):1062–68.

Craddock, P. R., J. Fehr, A. P. Dalmasso, K. L. Brighan, and H. S. Jacob. 1977. "Hemodialysis Leukopenia. Pulmonary Vascular Leukostasis Resulting from Complement Activation by Dialyzer Cellophane Membranes." *Journal of Clinical Investigation* 59(5):879–88.

Crapo, P. M., T. W. Gilbert, and S. F. Badylak. 2011. "An Overview of Tissue and Whole Organ Decellularization Processes." *Biomaterials* 32(12):3233–43.

Croce, A. C. and G. Bottiroli. 2014. "Autofluorescence Spectroscopy and Imaging: A Tool for Biomedical Research and Diagnosis." *European Journal of Histochemistry* 58(4):2461.

Cumming, R. D., P. A. Phillips, and P. I. Singh. 1983. "Surface Chemistry and Blood Material Interactions." *Trans Am Soc Artif Intern Organs* 29(1):163–68.

Dahm, M., W. D. Lyman, S. M. Factor, A. B. Schwell, and R. W. M. Frater. 1989. "Immunogenicity of Glutaraldehyde-Tanned Bovine Pericardium." Pp. 360–66 in *Cardiac Reconstructions*. Berlin, Heidelberg: Springer Berlin Heidelberg.

Dai, W. 2005. "Allogeneic Mesenchymal Stem Cell Transplantation in Postinfarcted Rat Myocardium: Short- and Long-Term Effects." *Circulation* 112(2):214–23.

Dai, W., L. E. Wold, J. S. Dow, and R. A. Kloner. 2005. "Thickening of the Infarcted Wall by Collagen Injection Improves Left Ventricular Function in Rats: A Novel Approach to Preserve Cardiac Function after Myocardial Infarction." *Journal of the American College of Cardiology*.

Dale, H. H. and E. H. J. Schuster. 1928. "A Double Perfusion-pump." *The Journal of Physiology* 64(4):356–64.

Dalla Volta, S., L. Daliento, and R. Razzolini. 1996. *Malattie Del Cuore e Dei Vasi*. Mc Graw-Hill.

Damiani, E. 2014. *Argomenti Di Fisiopatologia Generale per Gli Studenti Di Medicina e Chirurgia*. 1st ed. Padova: Cleup.

Dar, A., M. Shachar, J. Leor, and S. Cohen. 2002. "Optimization of Cardiac Cell Seeding and Distribution in 3D Porous Alginate Scaffolds." *Biotechnology and Bioengineering*.

Dasse, K. A., S. D. Chipman, C. N. Sherman, A. H. Levine, and O. H. Frazier. 1987. "Clinical Experience with Textured Blood Contacting Surfaces in Ventricular Assist Devices." *ASAIO Trans* 33(3):418–25.

Davis, M. E. et al. 2005a. "Injectable Self-Assembling Peptide Nanofibers Create Intramyocardial Microenvironments for Endothelial Cells." *Circulation*.

Davis, M. E. et al. 2005b. "Injectable Self-Assembling Peptide Nanofibers Create Intramyocardial Microenvironments for Endothelial Cells." *Circulation* 111(4):442–50.

Deb, A. et al. 2003. "Bone Marrow-Derived Cardiomyocytes Are Present in Adult Human Heart: A Study of Gender-Mismatched Bone Marrow Transplantation Patients." *Circulation* 107(9):1247–49.

Demikhov, V. P. 1951. "Experimental Basis for Replacement of the Heart with a Mechanical Device in Acute Experiments." *Bulletin of Experimental Biology and Medicine* 32:22–24.

Denis, C., J. A. Williams, X. Lu, D. Meyer, and D. Baruch. 1993. "Solid-Phase von Willebrand Factor Contains a Conformationally Active RGD Motif That Mediates Endothelial Cell Adhesion through the Alpha v Beta 3 Receptor." *Blood* 82(12):3622–30.

DeVries, W. C. et al. 1984. "Clinical Use of the Total Artificial Heart." *N Engl J Med* 310(5):273–78.

Didisheim, P. et al. 1989. "Infections and Thromboembolism with Implantable Cardiovascular Devices." *ASAIO Trans* 35(1):54–70.

Doetschman, T. C., H. Eistetter, M. Katz, W. Schmidt, and R. Kemler. 1985. "The in Vitro Development of Blastocyst-Derived Embryonic Stem Cell Lines: Formation of Visceral Yolk Sac, Blood Islands and Myocardium." *Journal of Embryology and Experimental Morphology* 87:27–45.

Dong, F. et al. 2012. "Myocardial CXCR4 Expression Is Required for Mesenchymal Stem Cell Mediated Repair Following Acute Myocardial Infarction." *Circulation* 126(3):314–24.

Dong, X. et al. 2009. "RGD-Modified Acellular Bovine Pericardium as a Bioprosthetic Scaffold for Tissue Engineering." *Journal of Materials Science: Materials in Medicine* 20(11):2327–36.

Doppler, S. A., M. A. Deutsch, R. Lange, and M. Krane. 2015. "Direct Reprogramming—The Future of Cardiac Regeneration?" *International Journal of Molecular Sciences*.

Dorfman, J. et al. 1998. "Myocardial Tissue Engineering with Autologous Myoblast Implantation." *Journal of Thoracic and Cardiovascular Surgery* 116(5):744–51.

Dostal, M. et al. 1990. "Mineralization of Polyurethane Membranes in the Total Artificial Heart (TAH): A Retrospective Study from Long-Term Animal Experiments." *Int J Artif Organs* 13(8):498–502.

Dowell, J. D., M. Rubart, K. B. S. Pasumarthi, M. H. Soonpaa, and L. J. Field. 2003. "Myocyte and Myogenic Stem Cell Transplantation in the Heart." *Cardiovascular Research* 58(2):336–50.

Dowling, R. D. et al. 2000. "Initial Experience with the AbioCor Implantable Replacement Heart at the University of Louisville." *ASAIO J* (46):579–81.

Dowling, R. D. et al. 2001. "Current Status of the AbioCor Implantable Replacement Heart." *Ann Thorac Surg* 71(3 Suppl):S147-9; discussion S183-4.

Dowling, R. D. et al. 2003. "The AbioCor Implantable Replacement Heart." *Ann Thorac Surg* 75(6 Suppl):S93-9.

Dowling, R. D. et al. 2004. "Initial Experience with the AbioCor Implantable Replacement Heart System." *J Thorac Cardiovasc Surg* 127(1):131–41.

Van Duuren, B. L. 1960. "The Fluorescence Spectra of Aromatic Hydrocarbons and Heterocyclic Aromatic Compounds." *Analytical Chemistry* 32(11):1436–42.

Eberl, Thomas et al. 1992. "Experimental in Vitro Endothelialization of Cardiac Valve Leaflets." *The Annals of Thoracic Surgery* 53(3):487–92.

Efe, J. A. et al. 2011. "Conversion of Mouse Fibroblasts into Cardiomyocytes Using a Direct Reprogramming Strategy." *Nature Cell Biology* 13(3):215–22.

Ehrlich, Joseph C. 1985. "The Artificial Heart Charles Lindbergh Helped Develop in 1935." *The New York Times*.

Ekdahl, K. N. et al. 2011. "Innate Immunity Activation on Biomaterial Surfaces: A Mechanistic Model and Coping Strategies." *Advanced Drug Delivery Reviews* 63(12):1042–50.

Eklund, L. et al. 2001. "Lack of Type XV Collagen Causes a Skeletal Myopathy and Cardiovascular Defects in Mice." *Proceedings of the National Academy of Sciences*.

Enomoto, Y. et al. 2005. "Early Ventricular Restraint after Myocardial Infarction: Extent of the Wrap Determines the Outcome of Remodeling." *Annals of Thoracic Surgery* 79(3):881–87.

Esmon, C. T. 1992. "The Protein C Anticoagulant Pathway." *Arteriosclerosis and Thrombosis : A Journal of Vascular Biology* 12(2):135–45.

Esmore, D. et al. 2007. "VentrAssist Left Ventricular Assist Device: Clinical Trial Results and Clinical Development Plan Update." *Eur J Cardiothorac Surg* 32(5):735–44.

Etzion, S., A. Battler, et al. 2001. "Influence of Embryonic Cardiomyocyte Transplantation on the Progression of Heart Failure in a Rat Model of Extensive Myocardial Infarction." *Journal of Molecular and Cellular Cardiology* 33(7):1321–30.

Etzion, S., L. H. Kedes, R. A. Kloner, and J. Leor. 2001. "Myocardial Regeneration: Present and Future Trends." *American Journal of Cardiovascular Drugs : Drugs, Devices, and Other Interventions* 1(4):233–44.

Faré, S., P. Petrini, A. Motta, A. Cigada, and M. C. Tanzi. 1999. "Synergistic Effects of Oxidative Environments and Mechanical Stress on in Vitro Stability of Polyetherurethanes and Polycarbonateurethanes." *Journal of Biomedical Materials Research* 45(1):62–74.

Farhadian, F., F. Contard, A. Sabri, J. L. Samuel, and L. Rappaport. 1996. "Fibronectin and Basement Membrane in Cardiovascular Organogenesis

and Disease Pathogenesis." *Cardiovascular Research* 32(3):433–42.

Fasol, R. et al. 1987. "Endothelialization of Artificial Surfaces: Does Surface Tension Determine in Vitro Growth of Human Saphenous Vein Endothelial Cells?" *Tex Heart Inst J* 14(2):119–26.

Ferreras, M., U. Felbor, T. Lenhard, B. R. Olsen, and J. M. Delaissé. 2000. "Generation and Degradation of Human Endostatin Proteins by Various Proteinases." *FEBS Letters*.

Fidalgo, Cátia et al. 2017. "A Sterilization Method for Decellularized Xenogeneic Cardiovascular Scaffolds." *Acta Biomaterialia*.

Fields, A., H. Harasaki, D. Sands, and Y. Nosé. 1983. "Infection in Artificial Blood Pump Implantation." *Trans Am Soc Artif Intern Organs* 29:532–38.

Fields, Charles et al. 2002. "Evaluation of Electrostatically Endothelial Cell Seeded Expanded Polytetrafluoroethylene Grafts in a Canine Femoral Artery Model." *Journal of Biomaterials Applications* 17(2):135–52.

Filippi, A. et al. 2018. "Multimodal Label-Free Ex Vivo Imaging Using a Dual-Wavelength Microscope with Axial Chromatic Aberration Compensation." *Journal of Biomedical Optics* 23(09):1.

Firstenberg, M. S. et al. 2008. "Fungemia in Patients with Long-Term Left Ventricular Assist Devices: A Chronic Problem, but Not the Kiss of Death." *J Heart Lung Transplant* 27(2S):S157–S157.

Fischlein, T. et al. 1994. "Endothelialization of Cardiac Valve Bioprostheses." *International Journal of Artificial Organs* 17(6):345–52.

Fischlein, T. and R. Fasol. 1996. "In Vitro Endothelialization of Bioprosthetic Heart Valves." *The Journal of Heart Valve Disease* 5(1):58–65.

Foxall, Thomas L., Kurt R. Auger, Allan D. Callow, and Peter Libby. 1986. "Adult Human Endothelial Cell Coverage of Small-Caliber Dacron and Polytetrafluoroethylene Vascular Prostheses in Vitro." *Journal of Surgical Research* 41(2):158–72.

Franco-Cereceda, A. et al. 2004. "Early Results with Cardiac Support Device Implant in Patients with Ischemic and Non-Ischemic Cardiomyopathy." *Scand Cardiovasc J* 38(3):159–63.

Fu, P., H. Lan, D. Wang, and H. Guan. 1997. "Experimental Study on Modified Treatment and Endothelialization of Bovine Pericardial Valves." *Journal of Tongji Medical University = Tong Ji Yi Ke Da Xue Xue Bao* 17(3):136–39.

Fujii, T. et al. 2003. "Cell Transplantation to Prevent Heart Failure: A Comparison of Cell Types." *Ann Thorac Surg* 76(6):2062–70; discussion 2070.

Fujimoto, K. L. et al. 2007. "An Elastic, Biodegradable Cardiac Patch Induces Contractile Smooth Muscle and Improves Cardiac Remodeling and Function in Subacute Myocardial Infarction." *Journal of the American College of Cardiology* 49(23):2292–2300.

Gaigalas, A. K., L. L. Wang, A. Schwartz, G. E. Marti, and R. F. Vogt. 2005. "Quantitating Fluorescence Intensity from Fluorophore: Assignment of MESF Values." *Journal of Research of the National Institute of Standards and Technology* 110(2):101.

Gallagher, Genevieve et al. 2017. "Environmental Stress Cracking Performance of Polyether and PDMS-Based Polyurethanes in an in Vitro Oxidation Model." *Journal of Biomedical Materials Research - Part B Applied Biomaterials* 105(6):1544–58.

Gallagher, Warren. 1997. "FTIR Analysis of Protein Structure." *Biochemistry* (1958):662–66.

Le Gallois, J. J. C. 1813. "Experiments on the Principle of Life, and Particularly on the Principle of the Motions of the Heart, and on the Seat of This Principle." Pp. 130–31 in. Philadelphia: Thomas, M.

Gao, X. M. et al. 2011. "Deletion of Macrophage Migration Inhibitory Factor Protects the Heart from Severe Ischemia-Reperfusion Injury: A Predominant Role of Anti-Inflammation." *Journal of Molecular and Cellular Cardiology* 50(6):991–99.

Gartner, T. K. and J. S. Bennett. 1985. "The Tetrapeptide Analogue of the Cell Attachment Site of Fibronectin Inhibits Platelet Aggregation and Fibrinogen Binding to Activated Platelets." *Journal of Biological Chemistry* 260(22):11891–94.

Gazoti Debessa, C. R., L. B. Mesiano Maifrino, and R. Rodrigues de Souza. 2001. "Age Related Changes of the Collagen Network of the Human Heart."

Mechanisms of Ageing and Development 122(10):1049–58.

Gendler, E., S. Gendler, and M. E. Nimni. 1984. "Toxic Reactions Evoked by Glutaraldehyde-Fixed Pericardium and Cardiac Valve Tissue Bioprosthesis." *Journal of Biomedical Materials Research* 18(7):727–36.

Gibbon, J. H. 1937. "Artificial Maintenance of Circulation during Experimental Occlusion of Pulmonary Artery." *Archives of Surgery* 34(6):1105.

Gibbs, O. S. 1930. "An Artificial Heart." *Journal of Pharmacology and Experimental Therapeutics* 38(2).

Gilbert, T. W., T. L. Sellaro, and S. F. Badylak. 2006. "Decellularization of Tissues and Organs." *Biomaterials* 27(19):3675–83.

Gillis, C., L. Bengtsson, and A. Haegerstrand. 1995. "Reduction of Monocyte Adhesion to Xenogenic Tissue by Endothelialization: An Adhesion Molecule and Time-Dependent Mechanism." *J Thorac Cardiovasc Surg* 110(6):1583–89.

Gimbrone Jr., M. A. 1987. "Vascular Endothelium: Nature's Blood-Compatible Container." *Ann N Y Acad Sci* 516:5–11.

Glyantsev, Sergey P., Vakhtang Tchantchaleishvili, and Leo A. Bockeria. 2016. "Demikhov's 'Mechanical Heart': The Circumstances Surrounding Creation of the World's First Implantable Total Artificial Heart in 1937." *ASAIO Journal* 62(1):106–9.

Gnecchi, M. 2006. "Evidence Supporting Paracrine Hypothesis for Akt-Modified Mesenchymal Stem Cell-Mediated Cardiac Protection and Functional Improvement." *The FASEB Journal* 20(6):661–69.

Gnecchi, M., Z. Zhang, A. Ni, and V. J. Dzau. 2008. "Paracrine Mechanisms in Adult Stem Cell Signaling and Therapy." *Circulation Research* 103(11):1204–19.

Golomb, Gershon et al. 1987. "The Role of Glutaraldehyde-Induced Cross-Links in Calcification of Bovine Pericardium Used in Cardiac Valve Bioprostheses." *The American Journal of Pathology* 127(1):122–30.

Golub, Justin S. et al. 2010. "Sustained VEGF Delivery via PLGA Nanoparticles Promotes Vascular Growth." *American Journal of Physiology-Heart and Circulatory Physiology* 298(6):H1959–65.

Graham, T. R. et al. 1990. "Neo-Intimal Development on Textured Biomaterial Surfaces during Clinical Use of an Implantable Ventricular Assist Device." *Eur J Cardiothorac Surg* (4):182–90.

Grant, D. S. et al. 1989. "Two Different Laminin Domains Mediate the Differentiation of Human Endothelial Cells into Capillary-like Structures in Vitro." *Cell* 58(5):933–43.

Grant, D. S. et al. 1992. "Interaction of Endothelial Cells with a Laminin A Chain Peptide (SIKVAV) in Vitro and Induction of Angiogenic Behavior in Vivo." *Journal of Cellular Physiology* 153(3):614–25.

Grant, D. S. and Z. Zukowska. 2000. "Revascularization of Ischemic Tissues with SIKVAV and Neuropeptide Y (NPY)." *Advances in Experimental Medicine and Biology* 476:139–54.

Grasel, T. G., R. S. Wilson, M. D. Lelah, H. W. Bielich, and S. L. Cooper. 1986. "Blood Flow and Surface-Induced Thrombosis." *ASAIO Trans* 32(1):515–20.

Gray, Henry. 2008. *Gray's Anatomy: The Anatomical Basis of Clinical Practice*. 40th ed. edited by S. Standring. Churchill Livingstone/Elsevier.

Griese, D. P. et al. 2003. "Isolation and Transplantation of Autologous Circulating Endothelial Cells into Denuded Vessels and Prosthetic Grafts: Implications for Cell-Based Vascular Therapy." *Circulation* 108(21):2710–15.

Gulbins, Helmut et al. 2003. "Preseeding with Autologous Fibroblasts Improves Endothelialization of Glutaraldehyde-Fixed Porcine Aortic Valves." *Journal of Thoracic and Cardiovascular Surgery* 125(3):592–601.

Guyette, J. P. et al. 2016. "Bioengineering Human Myocardium on Native Extracellular Matrix." *Circ Res* 118(1):56–72.

Guyton, Arthur C. et al. 2012. *Guyton e Hall: Fisiologia Medica*. XII. Elsevier.

Hagège, A. A. et al. 2006. "Skeletal Myoblast Transplantation in Ischemic Heart Failure: Long-Term Follow-up of the First Phase I Cohort of Patients." *Circulation* 114(SUPPL. 1):I-108-I-113.

Hakim, Raymond M. 1993. "Complement Activation by Biomaterials." *Cardiovascular Pathology* 2(3 SUPPL.):187–97.

Hall, C. W., W. W. Akers, W. O'Bannon, D. Liotta, and M. E. DeBakey. 1961. "Intraventricular Artificial Heart." *Trans Am Soc Artif Intern Organs* 11(1):263–64.

Halushka, Marc K., Richard N. Mitchell, and Robert F. Padera. 2016. "Heart Failure Therapies: New Strategies for Old Treatments and New Treatments for Old Strategies." *Cardiovascular Pathology* 25(6):503–11.

Harasaki, H. et al. 1980. "Comparative Study of Flocked vs Biolized Surface for Long-Term Assist Pumps." *Trans Am Soc Artif Intern Organs* 26:470–74.

Harasaki, H. et al. 1983. "Polyester Fibril Flocked Surface for Blood Pumps." *Trans Am Soc Artif Intern Organs* 29:563–68.

Harasaki, H. et al. 1985. "Calcification in Cardiovascular Implants: Degraded Cell Related Phenomena." *Trans Am Soc Artif Intern Organs* 31:489–94.

Harasaki, H. et al. 1987. "Initiation and Growth of Calcification in a Polyurethane-Coated Blood Pump." *ASAIO Trans* 33(3):643–49.

Harasaki, H., R. Gerrity, R. Kiraly, G. Jacobs, and Y. Nosé. 1979. "Calcification in Blood Pumps." *Trans Am Soc Artif Intern Organs* 25:305–10.

Harasaki, H., R. Kiraly, and Y. Nosé. 1978. "Endothelialization in Blood Pumps." *Trans Am Soc Artif Intern Organs* 24:415–25.

Hart, R. G. and D. G. Sherman. 1987. "Stroke and the Total Artificial Heart: Neurologic Considerations." *Texas Heart Institute Journal / from the Texas Heart Institute of St. Luke's Episcopal Hospital, Texas Children's Hospital* 14(1):63–71.

Hashemi, S. M. et al. 2008. "A Placebo Controlled, Dose-Ranging, Safety Study of Allogenic Mesenchymal Stem Cells Injected by Endomyocardial Delivery after an Acute Myocardial Infarction." *European Heart Journal* 29(2):251–59.

Hastings, W. L. et al. 1981. "A Retrospective Study of Nine Calves Surviving Five Months on the Pneumatic Total Artificial Heart." *Trans Am Soc Artif Intern Organs* 27:71–76.

Hayashi, K. et al. 1977. "Biolized Intrathoracic Left Ventricular Assist Device

(LVAD)." *Med Instrum* 11(4):202–7.

He, J. Q. 2003. "Human Embryonic Stem Cells Develop Into Multiple Types of Cardiac Myocytes: Action Potential Characterization." *Circulation Research* 93(1):32–39.

He, Wei, ZuWei Ma, Thomas Yong, Wee Eong Teo, and Seeram Ramakrishna. 2005. "Fabrication of Collagen-Coated Biodegradable Polymer Nanofiber Mesh and Its Potential for Endothelial Cells Growth." *Biomaterials* 26(36):7606–15.

Heilshorn, S. C., K. A. DiZio, E. R. Welsh, and D. A. Tirrell. 2003. "Endothelial Cell Adhesion to the Fibronectin CS5 Domain in Artificial Extracellular Matrix Proteins." *Biomaterials* 24(23):4245–52.

Heljasvaara, R., M. Aikio, H. Ruotsalainen, and T. Pihlajaniemi. 2017. "Collagen XVIII in Tissue Homeostasis and Dysregulation — Lessons Learned from Model Organisms and Human Patients." *Matrix Biology* 57–58:55–75.

Herring, M. et al. 1984. "Endothelial Seeding of Dacron and Polytetrafluoroethylene Grafts: The Cellular Events of Healing." *Surgery* 96(4):745–55.

Herring, M., A. Gardner, and J. Glover. 1978. "A Single-Staged Technique for Seeding Vascular Grafts with Autgenous Endothelium." *Surgery* 84(4):498–504.

Herring, Malcolm B. et al. 1987. "Endothelial Seeding of Polytetrafluoroethylene Popliteal Bypasses: A Preliminary Report." *Journal of Vascular Surgery* 6(2):114–18.

Hersel, U., C. Dahmen, and H. Kessler. 2003. "RGD Modified Polymers: Biomaterials for Stimulated Cell Adhesion and Beyond." *Biomaterials* 24(24):4385–4415.

Hetzer, R. et al. 1998. "Circulatory Support with Pneumatic Paracorporeal Ventricular Assist Device in Infants and Children." *Ann Thorac Surg* 66(5):1498–1506.

Hetzer, R. et al. 2004. "First Experiences with a Novel Magnetically Suspended Axial Flow Left Ventricular Assist Device." *Eur J Cardiothorac Surg* 25(6):964–70.

Ho, Kalon K. L., Joan L. Pinsky, William B. Kannel, and Daniel Levy. 1993. "The Epidemiology of Heart Failure: The Framingham Study." *Journal of the American College of Cardiology* 22(4 Suppl A):6A–13A.

Hoffman, D. et al. 1992. "Spontaneous Host Endothelial Growth on Bioprostheses - Influence of Fixation." *Circulation* 86(5):75–79.

Hogness, J. R. and M. Van Antwerp. 1991. *The Artificial Heart: Prototypes, Policies, and Patients*. National Academies Press (US).

Hollander, A. P. and P. V Hatton. 2003. *Biopolymer Methods in Tissue Engineering*. Humana Press.

Huang-Lee, Lynn L. H., David T. Cheung, and Marcel E. Nimni. 1990. "Biochemical Changes and Cytotoxicity Associated with the Degradation of Polymeric Glutaraldehyde Derived Crosslinks." *Journal of Biomedical Materials Research* 24(9):1185–1201.

Huang, L., K. Nagapudi, P. R. Apkarian, and E. L. Chaikof. 2001. "Engineered Collagen - PEO Nanofibers and Fabrics." *Journal of Biomaterials Science, Polymer Edition* 12(9):979–93.

Huang, N. F., J. Yu, R. Sievers, S. Li, and R. J. Lee. 2005. "Injectable Biopolymers Enhance Angiogenesis after Myocardial Infarction." *Tissue Engineering*.

Hubbell, J. A., S. P. Massia, N. P. Desai, and P. D. Drumheller. 1991. "Endothelial Cell-Selective Materials for Tissue Engineering in the Vascular Graft Via a New Receptor." *Nature Biotechnology* 9(6):568–72.

Hughes, S. D. et al. 1984. "Effects of Coumadin on Thrombus and Mineralization in Total Artificial Hearts." *Trans Am Soc Artif Intern Organs* 30:75–80.

Humphries, M. J., S. K. Akiyama, A. Komoriya, K. Olden, and K. M. Yamada. 1986. "Identification of an Alternatively Spliced Site in Human Plasma Fibronectin That Mediates Cell Type-Specific Adhesion." *The Journal of Cell Biology* 103(6 Pt 2):2637–47.

Hutcheson, K. A. et al. 2000. "Comparison of Benefits on Myocardial Performance of Cellular Cardiomyoplasty with Skeletal Myoblasts and Fibroblasts." *Cell Transplantation* 9(3):359–68.

Ieda, M. et al. 2010. "Direct Reprogramming of Fibroblasts into Functional Cardiomyocytes by Defined Factors." *Cell* 142(3):375–86.

Ii, M. et al. 2005. "Endothelial Progenitor Cells Are Rapidly Recruited to Myocardium and Mediate Protective Effect of Ischemic Preconditioning via 'Imported' Nitric Oxide Synthase Activity." *Circulation* 111(9):1114–20.

Ikezoe, Takayuki. 2015. "Thrombomodulin/Activated Protein C System in Septic Disseminated Intravascular Coagulation." *Journal of Intensive Care* 3(1):1.

Imachi, K. et al. 2001. "A New Hypothesis on the Mechanism of Calcification Formed on a Blood-Contacted Polymer Surface." *Journal of Artificial Organs* 4(1):74–82.

Imai, Y., K. Tajima, and Y. Nosé. 1971. "Biolized Materials for Cardiovascular Prosthesis." *Trans Am Soc Artif Intern Organs* 17:6–9.

Ince, H., M. Petzsch, T. C. Rehders, T. Chatterjee, and C. A. Nienaber. 2004. "Transcatheter Transplantation of Autologous Skeletal Myoblasts in Postinfarction Patients With Severe Left Ventricular Dysfunction." *Journal of Endovascular Therapy* 11(6):695–704.

Institute of Medicine (US), Committee to Evaluate the Artificial Heart Program of the National Heart Lung and blood, Division of Health Care Services, John R. Hogness, and Malin VanAntwerp. 1991. *The Artificial Heart Program: Current Status and History*. National Academies Press (US).

INTERMACS. 2016. "Interagency Registry for Mechanically Assisted Circulatory Support. Quarterly Statistical Report 2016 Q1."

International Organization for Standardization. 2009. "ISO 10993-5 Biological Evaluation of Medical Devices - Part 5: Tests for in Vitro Cytotoxicity." 34.

International Organization for Standardization. 2017. "ISO 10993-4 Biological Evaluation of Medical Devices - Part 4: Selection of Tests for Interactions with Blood." 69.

Iop, L. et al. 2009. "The Influence of Heart Valve Leaflet Matrix Characteristics on the Interaction between Human Mesenchymal Stem Cells and

Decellularized Scaffolds." *Biomaterials* 30(25):4104–16.

Iop, L. et al. 2014. "Decellularized Allogeneic Heart Valves Demonstrate Self-Regeneration Potential after a Long-Term Preclinical Evaluation." *PLoS One* 9(6):e99593.

Iop, L., A. Paolin, et al. 2017. "Decellularized Cryopreserved Allografts as Off-the-Shelf Allogeneic Alternative for Heart Valve Replacement: In Vitro Assessment Before Clinical Translation." *Journal of Cardiovascular Translational Research* 10(2):93–103.

Iop, L., E. Dal Sasso, R. Menabò, F. Di Lisa, and G. Gerosa. 2017. "The Rapidly Evolving Concept of Whole Heart Engineering." *Stem Cells International* 8920940:1–18.

Iop, L., T. Palmosi, E. Dal Sasso, and G. Gerosa. 2018. "Bioengineered Tissue Solutions for Repair, Correction and Reconstruction in Cardiovascular Surgery." *Journal of Thoracic Disease* 8(7):E503–10.

Ishihara, Tokuhiro, Victor J. Ferrans, Michael Jones, Steven W. Boyce, and William C. Roberts. 1981. "Occurrence and Significance of Endothelial Cells in Implanted Porcine Bioprosthetic Valves." *The American Journal of Cardiology* 48(3):443–54.

Iwasaki, H. et al. 2011. "PLGF Repairs Myocardial Ischemia through Mechanisms of Angiogenesis, Cardioprotection and Recruitment of Myo-Angiogenic Competent Marrow Progenitors" edited by M. J. Goumans. *PLoS ONE* 6(9):e24872.

Jansen, P., W. van Oeveren, A. Capel, and A. Carpentier. 2012. "In Vitro Haemocompatibility of a Novel Bioprosthetic Total Artificial Heart." *Eur J Cardiothorac Surg* 41(6):e166-72.

Jansson, K., L. Bengtsson, J. Swedenborg, and A. Haegerstrand. 2001. "In Vitro Endothelialization of Bioprosthetic Heart Valves Provides a Cell Monolayer with Proliferative Capacities and Resistance to Pulsatile Flow." *Journal of Thoracic and Cardiovascular Surgery* 121(1):108–15.

Jantzen, A. E. et al. 2011. "Use of Autologous Blood-Derived Endothelial Progenitor Cells at Point-of-Care to Protect against Implant Thrombosis in a Large Animal Model." *Biomaterials* 32(33):8356–63.

Jarvik, R. K. 1981. "The Total Artificial Heart." *Scientific American* 244(1):74–

81.

Jarvik, R., J. Volder, D. Olsen, S. Moulopoulos, and W. J. Kolff. 1974. "Venous Return of an Artificial Heart Designed to Prevent Right Heart Syndrome." *Ann Biomed Eng* 2(4):335–42.

Jessup, Mariell and Susan Brozena. 2003. "Heart Failure." *New England Journal of Medicine* 348(20):2007–18.

Ji, Y. et al. 2012. "Zwitterionic Polycarboxybetaine Coating Functionalized with REDV Peptide to Improve Selectivity for Endothelial Cells." *Journal of Biomedical Materials Research - Part A* 100 A(6):1387–97.

Jiang, Wenhui et al. 2006. "Homing and Differentiation of Mesenchymal Stem Cells Delivered Intravenously to Ischemic Myocardium in Vivo: A Time-Series Study." *Pflugers Archiv European Journal of Physiology* 453(1):43–52.

Johansson, U. et al. 2008. "Formation of Composite Endothelial Cell-Mesenchymal Stem Cell Islets: A Novel Approach to Promote Islet Revascularization." *Diabetes* 57(9):2393–2401.

Jordan, James E. et al. 2012. "Bioengineered Self-Seeding Heart Valves." *Journal of Thoracic and Cardiovascular Surgery* 143(1):201–8.

Joyce, L. D. et al. 1983. "Response of the Human Body to the First Permanent Implant of the Jarvik-7 Total Artificial Heart." *Trans Am Soc Artif Intern Organs* 29:81–87.

Jun, H. W. and J. West. 2004. "Development of a YIGSR-Peptide-Modified Polyurethaneurea to Enhance Endothelialization." *Journal of Biomaterials Science, Polymer Edition* 15(1):73–94.

Jun, H. W. and J. L. West. 2005a. "Endothelialization of Microporous YIGSR/PEG-Modified Polyurethaneurea." *Tissue Engineering* 11(7):1133–40.

Jun, H. W. and J. L. West. 2005b. "Modification of Polyurethaneurea with PEG and YIGSR Peptide to Enhance Endothelialization without Platelet Adhesion." *Journal of Biomedical Materials Research - Part B Applied Biomaterials* 72(1):131–39.

Jung, J. P., D. B. Bhuiyan, and B. M. Ogle. 2016. "Solid Organ Fabrication:

Comparison of Decellularization to 3D Bioprinting." *Biomater Res* 20(1):27.

Kaehler, Jan, Peter Zilla, Roland Fasol, Manfred Deutsch, and Margit Kadletz. 1989. "Precoating Substrate and Surface Configuration Determine Adherence and Spreading of Seeded Endothelial Cells on Polytetrafluoroethylene Grafts." *Journal of Vascular Surgery* 9(4):535–41.

Kaikita, K. et al. 2004. "Targeted Deletion of CC Chemokine Receptor 2 Attenuates Left Ventricular Remodeling after Experimental Myocardial Infarction." *American Journal of Pathology* 165(2):439–47.

Kawamoto, A. et al. 2001. "Therapeutic Potential of Ex Vivo Expanded Endothelial Progenitor Cells for Myocardial Ischemia." *Circulation* 103(5):634–37.

Kazatchkine, M. D. and M. P. Carreno. 2006. "Activation of the Complement System at the Interface between Blood and Artificial Surfaces." Pp. 45–50 in *The Biomaterials: Silver Jubilee Compendium*, vol. 9. Elsevier.

Kehat, I. et al. 2001. "Human Embryonic Stem Cells Can Differentiate into Myocytes with Structural and Functional Properties of Cardiomyocytes." *The Journal of Clinical Investigation* 108(3):407–14.

Kehat, I. et al. 2004. "Electromechanical Integration of Cardiomyocytes Derived from Human Embryonic Stem Cells." *Nature Biotechnology* 22(10):1282–89.

Kelley, S. T. et al. 1999. "Restraining Infarct Expansion Preserves Left Ventricular Geometry and Function after Acute Anteroapical Infarction." *Circulation* 99(1):135–42.

Kemp, Clinton D. and John V. Conte. 2012. "The Pathophysiology of Heart Failure." *Cardiovascular Pathology* 21(5):365–71.

Kessler, T. R. et al. 1978. "Elimination of Predilection Sites for Thrombus Formation in the Total Artificial Heart--before and After." *Trans Am Soc Artif Intern Organs* 24:532–36.

Khan, Imran, Nigel Smith, Eric Jones, Dudley S. Finch, and Ruth Elizabeth Cameron. 2005. "Analysis and Evaluation of a Biomedical Polycarbonate Urethane Tested in an in Vitro Study and an Ovine Arthroplasty Model. Part I: Materials Selection and Evaluation." *Biomaterials*.

Khardori, N. and M. Yassien. 1995. "Biofilms in Device-Related Infections." *J Ind Microbiol* 15(3):141–47.

Kinnaird, T. et al. 2004. "Marrow-Derived Stromal Cells Express Genes Encoding a Broad Spectrum of Arteriogenic Cytokines and Promote In Vitro and In Vivo Arteriogenesis Through Paracrine Mechanisms." *Circulation Research* 94(5):678–85.

Kiraly, R. J. and Y. Nosé. 1974. "Natural Tissue as a Biomaterial." *Biomat Med Devices Artif Organs* 2(3):207–24.

Kitahara, H. et al. 2016. "Heterotopic Transplantation of a Decellularized and Recellularized Whole Porcine Heart." *Interact Cardiovasc Thorac Surg* 22(5):571–79.

Klabunde, Richard E. 2012. *Cardiovascular Physiology Concepts*. Lippincott Williams & Wilkins.

Kleinman, H. K., D. Philp, and M. P. Hoffman. 2003. "Role of the Extracellular Matrix in Morphogenesis." *Curr Opin Biotechnol* 14(5):526–32.

Kloesel, Benjamin, James A. Dinardo, and Simon C. Body. 2016. "Cardiac Embryology and Molecular Mechanisms of Congenital Heart Disease: A Primer for Anesthesiologists." *Anesthesia and Analgesia* 123(3):551–69.

Ko, A. C. T. et al. 2012. "Nonlinear Optical Microscopy in Decoding Arterial Diseases." *Biophysical Reviews* 4(4):323–34.

Kocher, A. A. et al. 2001. "Neovascularization of Ischemic Myocardium by Human Bone-Marrow-Derived Angioblasts Prevents Cardiomyocyte Apoptosis, Reduces Remodeling and Improves Cardiac Function." *Nature Medicine* 7(4):430–36.

Kofidis, T. et al. 2002. "In Vitro Engineering of Heart Muscle: Artificial Myocardial Tissue." *Journal of Thoracic and Cardiovascular Surgery*.

Kofidis, T. et al. 2004. "Injectable Bioartificial Myocardial Tissue for Large-Scale Intramural Cell Transfer and Functional Recovery of Injured Heart Muscle." *Journal of Thoracic and Cardiovascular Surgery*.

Kolff, W. J. et al. 1962. "Results Obtained with Artificial Hearts Driven by the N.A.S.A., Servomechanism and Pathologic Physiology of Artifcial Hearts." *Trans Am Soc Artif Intern Organs* 8(1):135–39.

Kolff, W. J., T. Akutsu, B. Dreyer, and H. Norton. 1959. "Artificial Heart in the Chest and Use of Polyurethane for Making Hearts, Valves and Aortas." *ASAIO J* 5(1):298–303.

Konertz, W. F. et al. 2001a. "Passive Containment and Reverse Remodeling by a Novel Textile Cardiac Support Device." *Circulation* 104(12 Suppl 1):I270-5.

Konertz, W. F. et al. 2001b. "Passive Containment and Reverse Remodeling by a Novel Textile Cardiac Support Device." *Circulation*.

Konstandin, M. H. et al. 2013. "Fibronectin Is Essential for Reparative Cardiac Progenitor Cell Response after Myocardial Infarction." *Circulation Research* 113(2):115–25.

Koster, A. et al. 2001. "Heparin Antibodies and Thromboembolism in Heparin-Coated and Noncoated Ventricular Assist Devices." *J Thorac Cardiovasc Surg* 121(2):331–35.

Kottke-Marchant, K., J. M. Anderson, Y. Umemura, and R. E. Marchant. 1989. "Effect of Albumin Coating on the in Vitro Blood Compatibility of Dacron® Arterial Prostheses." *Biomaterials* 10(3):147–55.

Krstic, R. V. 1985. "General Histology of the Mammal : An Atlas for Students of Medicine and Biology."

Krstic, Radivoj V. 1992. *Human Microscopic Anatomy: An Atlas for Students of Medicine and Biology*. Springer-Verlag.

Kung, R. T. et al. 1995. "Progress in the Development of the ABIOMED Total Artificial Heart." *ASAIO J* 41(3):M245-8.

Kuroki, K. et al. 1995. "Complement Activation by Angiographic Catheters in Vitro." *Journal of Vascular and Interventional Radiology : JVIR* 6(5):819–26.

Kwan-Gett, C. et al. 1970. "A Prosthetic Heart with Hemispherical Ventricles Designed for Low Hemolytic Action." *Trans Am Soc Artif Intern Organs* 16:409–15.

Kwan-Gett, C. S., Y. Wu, R. Collan, S. Jacobsen, and W. J. Kolff. 1969. "Total Replacement Artificial Heart and Driving System with Inherent Regulation of Cardiac Output." *Transactions - American Society for*

Artificial Internal Organs 15:245–66.

Kwon, I. K. and T. Matsuda. 2005. "Co-Electrospun Nanofiber Fabrics of Poly(L-Lactide-Co-ε-Caprolactone) with Type I Collagen or Heparin." *Biomacromolecules* 6(4):2096–2105.

Kwon, O. H., A. Kikuchi, M. Yamato, Y. Sakurai, and T. Okano. 2000. "Rapid Cell Sheet Detachment from Poly(N-Isopropylacrylamide)-Grafted Porous Cell Culture Membranes." *Journal of Biomedical Materials Research* 50(1):82–89.

Laflamme, M. A. et al. 2007. "Cardiomyocytes Derived from Human Embryonic Stem Cells in Pro-Survival Factors Enhance Function of Infarcted Rat Hearts." *Nature Biotechnology* 25(9):1015–24.

Landa, N. et al. 2008. "Effect of Injectable Alginate Implant on Cardiac Remodeling and Function after Recent and Old Infarcts in Rat." *Circulation*.

Langendorff, O. 1985. "Untersuchungen Am Überlebenden Säugetierherzen." P. 61:291-332 in *Pflügers Archiv für die gesamte Physiologie des Menschen und der Tiere*.

Langford-Smith, A., A. J. Day, P. N. Bishop, and S. J. Clark. 2015. "Complementing the Sugar Code: Role of GAGs and Sialic Acid in Complement Regulation." *Frontiers in Immunology* 6(FEB):25.

Latremouille, C. et al. 2013. "Sub-Acute Animal Implantation of a Novel Bioprosthethic Artificial Heart." *J Heart Lung Transplant* 32(4S).

Latremouille, C. et al. 2015. "Animal Studies with the Carmat Bioprosthetic Total Artificial Heart." *Eur J Cardiothorac Surg* 47(5):e172-8; discussion e178-9.

Latrémouille, Christian et al. 2017. "A Bioprosthetic Total Artificial Heart for End-Stage Heart Failure: Results from a Pilot Study." *The Journal of Heart and Lung Transplantation* 37(1):33–37.

Lavine, K. J. et al. 2014. "Distinct Macrophage Lineages Contribute to Disparate Patterns of Cardiac Recovery and Remodeling in the Neonatal and Adult Heart." *Proceedings of the National Academy of Sciences* 111(45):16029–34.

Law, S. K., N. A. Lichtenberg, and R. P. Levine. 1979. "Evidence for an Ester Linkage between the Labile Binding Site of C3b and Receptive Surfaces." *Journal of Immunology* 123(3):1388–94.

Lee, R. J. et al. 2015. "The Feasibility and Safety of Algisyl-LVR^{TM} as a Method of Left Ventricular Augmentation in Patients with Dilated Cardiomyopathy: Initial First in Man Clinical Results." *International Journal of Cardiology* 199:18–24.

Lee, Y. S. et al. 1993. "Endothelial Cell Seeding onto the Extracellular Matrix of Fibroblasts for the Development of a Small Diameter Polyurethane Vessel." *ASAIO Journal* 39(3):M740-5.

Lehner, G., T. Fischlein, G. Baretton, J. G. Murphy, and B. Reichart. 1997. "Endothelialized Biological Heart Valve Prostheses in the Non-Human Primate Model." *European Journal of Cardio-Thoracic Surgery* 11(3):498–504.

Leopold, Jane A. 2013. "Prohealing Endothelial Progenitor Cell Capture Stents: Do the Cells Captured Explain the Clinical Outcomes?" *Circulation. Cardiovascular Interventions* 6(5):494–95.

Leor, J. et al. 2006. "Ex Vivo Activated Human Macrophages Improve Healing, Remodeling, and Function of the Infarcted Heart." *Circulation* 114(SUPPL. 1):I-94-I-100.

Leor, J. et al. 2009. "Intracoronary Injection of In Situ Forming Alginate Hydrogel Reverses Left Ventricular Remodeling After Myocardial Infarction in Swine." *Journal of the American College of Cardiology.*

Leor, J., M. Patterson, M. J. Quinones, L. H. Kedes, and R. A. Kloner. 1996. "Transplantation of Fetal Myocardial Tissue into the Infarcted Myocardium of Rat. A Potential Method for Repair of Infarcted Myocardium?" *Circulation* 94(9 Suppl):II332-II336.

Leor, Jonathan et al. 2007. "Human Embryonic Stem Cell Transplantation to Repair the Infarcted Myocardium." *Heart* 93(10):1278–84.

Levy, Daniel et al. 2002. "Long-Term Trends in the Incidence of and Survival with Heart Failure." *New England Journal of Medicine* 347(18):1397–1402.

Li, R. K., Z. Q. Jia, et al. 1996. "Cardiomyocyte Transplantation Improves Heart Function." *Annals of Thoracic Surgery* 62(3):654–61.

Li, R. K. et al. 1997. "Natural History of Fetal Rat Cardiomyocytes Transplanted into Adult Rat Myocardial Scar Tissue." *Circulation* 96(9 Suppl):II-179-86; discussion 186-7.

Li, R. K., D. A. G. Mickle, R. D. Weisel, J. Zhang, and K. Mohabeer. 1996. "In Vivo Survival and Function of Transplanted Rat Cardiomyocytes." *Circulation Research* 78(2):283–88.

Liao ', K. et al. 1993. "Spontaneous Host Endothelial Growth on Bioprosthetic Valves and Its Relation to Calcification." *European Journal of Cardio-Thoracic Surgery* 7(11):591–96.

Lijnen, Henri R. and Désiré Collen. 1997. "Endothelium in Hemostasis and Thrombosis." *Progress in Cardiovascular Diseases* 39(4):343–50.

Lin, H. B. et al. 1992. "Endothelial Cell Adhesion on Polyurethanes Containing Covalently Attached RGD-Peptides." *Biomaterials* 13(13):905–14.

Lindbergh, C. A. 1935. "An Apparatus for the Culture of Whole Organs." *Journal of Experimental Medicine* 62(3):409–31.

Lindbergh, C. A., V. P. Perry, T. I. Malinin, and G. H. Mouer. 1966. "An Apparatus for the Pulsating Perfusion of Whole Organs." *Cryobiology* 3(3):252–60.

Liotta, D. et al. 1961. "Artificial Heart in the Chest: Preliminary Report." *Trans Am Soc Artif Intern Organs* 7:318–22.

Loebe, M. et al. 1998. "Complement Activation in Patients Undergoing Mechanical Circulatory Support." *ASAIO J* 44(5):M340-6.

Lopez, A. D. 1993. "Assessing the Burden of Mortality from Cardiovascular Diseases." *World Health Stat Q* 46(2):91–96.

Lopez, A. D., C. D. Mathers, M. Ezzati, D. T. Jamison, and C. J. L. Murray. 2006. *Global Burden of Disease and Risk Factors*. The International Bank for Reconstruction and Development / The World Bank.

Lukas, K. et al. 2017. "Effect of Immobilized Antithrombin III on the Thromboresistance of Polycarbonate Urethane." *Materials* 10(4).

Lund, Lars H. et al. 2017. "The Registry of the International Society for Heart and Lung Transplantation: Thirty-Fourth Adult Heart Transplantation

Report—2017; Focus Theme: Allograft Ischemic Time." *Journal of Heart and Lung Transplantation* 36(10):1037–46.

Makino, S. et al. 1999. "Cardiomyocytes Can Be Generated from Marrow Stromal Cells in Vitro." *Journal of Clinical Investigation* 103(5):697–705.

Malinin, T. I. 1996. "Remembering Alexis Carrel and Charles A. Lindbergh." *Texas Heart Institute Journal / from the Texas Heart Institute of St. Luke's Episcopal Hospital, Texas Children's Hospital* 23(1):28–35.

Mann, D. L. et al. 2016. "One-Year Follow-up Results from AUGMENT-HF: A Multicentre Randomized Controlled Clinical Trial of the Efficacy of Left Ventricular Augmentation with Algisyl in the Treatment of Heart Failure." *European Journal of Heart Failure* 18(3):314–25.

Marchand, M. A. et al. 2001. "Fifteen-Year Experience with the Mitral Carpentier-Edwards PERIMOUNT Pericardial Bioprosthesis." *Ann Thorac Surg* 71(5 Suppl):S236-9.

Markway, Brandon D. et al. 2008. "Capture of Flowing Endothelial Cells Using Surface-Immobilized Anti-Kinase Insert Domain Receptor Antibody." *Tissue Engineering Part C: Methods* 14(2):97–105.

Marois, Yves and Robert Guidoin. 2013. "Biocompatibility of Polyurethanes." Pp. 1–16 in *Madame Curie Bioscience Database*. Austin, TX: Landes Bioscience.

Marosok, R., R. Washbum, A. Indorf, D. Solomon, and R. Shetertz. 1996. "Contribution of Vascular Catheter Material to the Pathogenesis of Infection: Depletion of Complement by Silicone Elastomer in Vitro." *Journal of Biomedical Materials Research* 30(2):245–50.

Martini, Frederic H., Michael J. Timmons, and Robert B. Tallitsch. 2012. *Human Anatomy*. 8th ed. Pearson Education.

Mason, R. G., J. B. Lian, R. J. Levy, W. Bernhard, and M. Szycher. 1981. "LVAD Mineralization and Gamma-Carboxyglutamic Acid Containing Proteins in Normal and Pathologically Mineralized Tissues." *Trans Am Soc Artif Intern Organs* 27:683–89.

Massia, S. P. and J. A. Hubbell. 1992. "Vascular Endothelial Cell Adhesion and Spreading Promoted by the Peptide REDV of the IIICS Region of Plasma Fibronectin Is Mediated by Integrin Alpha4beta1." *Journal of*

Biological Chemistry 267(20):14019–26.

Masuda, S. and T. Shimizu. 2016. "Three-Dimensional Cardiac Tissue Fabrication Based on Cell Sheet Technology." *Advanced Drug Delivery Reviews* 96:103–9.

Mathur, A. B. et al. 1997. "In Vivo Biocompatibility and Biostability of Modified Polyurethanes." *Journal of Biomedical Materials Research* 36(2):246–57.

Matsushita, T. et al. 1999. "Formation of Cell Junctions between Grafted and Host Cardiomyocytes at the Border Zone of Rat Myocardial Infarction." *Circulation*.

Mavrilas, D., E. A. Sinouris, D. H. Vynios, and N. Papageorgakopoulou. 2005. "Dynamic Mechanical Characteristics of Intact and Structurally Modified Bovine Pericardial Tissues." *Journal of Biomechanics* 38(4):761–68.

Mazzucotelli, Jean Philippe et al. 2008. "A New Device for Endothelial Cell Seeding of a Small-Caliber Vascular Prosthesis." *Artificial Organs* 17(9):787–90.

McBride, L. R. et al. 1987. "Infectious Complications Associated with Ventricular Assist Device Support." *ASAIO Trans* 33(3):201–2.

Mccormick, R. J. and D. P. Thomas. 1998. "Collagen Crosslinking in the Heart: Relationship to Development and Function." *Basic And Applied Myology* 143–50.

McMurray, J. J. V. et al. 2012. "ESC Guidelines for the Diagnosis and Treatment of Acute and Chronic Heart Failure 2012: The Task Force for the Diagnosis and Treatment of Acute and Chronic Heart Failure 2012 of the European Society of Cardiology. Developed in Collaboration with the Heart." *European Heart Journal* 33(14):1787–1847.

Meijering, E. et al. 2004. "Design and Validation of a Tool for Neurite Tracing and Analysis in Fluorescence Microscopy Images." *Cytometry A* 58(2):167–76.

de Mel, A., B. G. Cousins, and A. M. Seifalian. 2012. "Surface Modification of Biomaterials: A Quest for Blood Compatibility." *International Journal of Biomaterials* 2012:707863.

Menasché, P. et al. 2001. "Myoblast Transplantation for Heart Failure." *Lancet* 357(9252):279–80.

Menasché, P. 2008. "Skeletal Myoblasts and Cardiac Repair." *Journal of Molecular and Cellular Cardiology*, October, 545–53.

Menasché, P. et al. 2008. "The Myoblast Autologous Grafting in Ischemic Cardiomyopathy (MAGIC) Trial: First Randomized Placebo-Controlled Study of Myoblast Transplantation." *Circulation* 117(9):1189–1200.

Mendez, Gustavo F. et al. 2001. "The Epidemiological Features of Heart Failure in Developing Countries: A Review of the Literature." *International Journal of Cardiology* 80(2–3):213–19.

Mendoza-Novelo, Birzabith et al. 2011. "Decellularization of Pericardial Tissue and Its Impact on Tensile Viscoelasticity and Glycosaminoglycan Content." *Acta Biomaterialia* 7(3):1241–48.

Merna, N., C. Robertson, A. La, and S. C. George. 2013. "Optical Imaging Predicts Mechanical Properties during Decellularization of Cardiac Tissue." *Tissue Eng Part C Methods* 19(10):802–9.

Merrifield, R. B. 1963. "Solid Phase Peptide Synthesis. I. The Synthesis of a Tetrapeptide." *Journal of the American Chemical Society* 85(14):2149–54.

Messina, E. et al. 2004. "Isolation and Expansion of Adult Cardiac Stem Cells from Human and Murine Heart." *Circulation Research* 95(9):911–21.

Methe, K. et al. 2014. "An Alternative Approach to Decellularize Whole Porcine Heart." *Biores Open Access* 3(6):327–38.

Metman, L. V, R. De Paulis, S. F. Mohammad, and W. J. Kolff. 1987. "Evaluation of Thrombogenesis on Smooth and Rough Intima in Artificial Ventricles." *ASAIO Trans* 33(3):732–37.

Migneault, Isabelle, Catherine Dartiguenave, Michel J. Bertrand, and Karen C. Waldron. 2004. "Glutaraldehyde: Behavior in Aqueous Solution, Reaction with Proteins, and Application to Enzyme Crosslinking." *BioTechniques* 37(5):790–802.

Mironov, V. et al. 2009. "Biofabrication: A 21st Century Manufacturing Paradigm." *Biofabrication* 1(2):022001.

Mirotsou, M. et al. 2007. "Secreted Frizzled Related Protein 2 (Sfrp2) Is the Key Akt-Mesenchymal Stem Cell-Released Paracrine Factor Mediating Myocardial Survival and Repair." *Proceedings of the National Academy of Sciences* 104(5):1643–48.

Miyagawa, S. et al. 2017. "Phase I Clinical Trial of Autologous Stem Cell-Sheet Transplantation Therapy for Treating Cardiomyopathy." *Journal of the American Heart Association* 6(4).

Mohacsi, P. and P. Leprince. 2014. "The CARMAT Total Artificial Heart." *Eur J Cardiothorac Surg* 46(6):933–34.

Molawi, K. et al. 2014. "Progressive Replacement of Embryo-Derived Cardiac Macrophages with Age." *The Journal of Experimental Medicine* 211(11):2151–58.

Momtahan, N. et al. 2015. "Automation of Pressure Control Improves Whole Porcine Heart Decellularization." *Tissue Eng Part C Methods* 21(11):1148–61.

Moncada, Salvador and Annie Higgs. 2006. *Handbook of Experimental Pharmacology: The Vascular Endothelium Part 1.* edited by S. Moncada and A. Higgs. Springer-Verlag Berlin Heidelberg.

Monici, M. 2005. "Cell and Tissue Autofluorescence Research and Diagnostic Applications." *Biotechnology Annual Review* 11(SUPPL.):227–56.

Morris, D. T. and C. M. Couves. 1971. "Experiences with a Sac-Type Artificial Heart." *Can Med Assoc J* 105(5):483–87.

Mosterd, A. and A. W. Hoes. 2007. "Clinical Epidemiology of Heart Failure." *Heart* 93(9):1137–46.

Mould, A. P., A. Komoriya, K. M. Yamada, and M. J. Humphries. 1991. "The CS5 Peptide Is a Second Site in the IIICS Region of Fibronectin Recognized by the Integrin A4β1: Inhibition of A4β1function by RGD Peptide Homologues." *Journal of Biological Chemistry* 266(6):3579–85.

Mouw, J. K., G. Ou, and V. M. Weaver. 2014. "Extracellular Matrix Assembly: A Multiscale Deconstruction." *Nature Reviews. Molecular Cell Biology* 15(12):771–85.

Müller-Ehmsen, J. et al. 2002. "Survival and Development of Neonatal Rat

Cardiomyocytes Transplanted into Adult Myocardium." *Journal of Molecular and Cellular Cardiology* 34(2):107–16.

Müller, P. et al. 2002. "Cardiomyocytes of Noncardiac Origin in Myocardial Biopsies of Human Transplanted Hearts." *Circulation* 106(1):31–35.

Mummery, C. 2003. "Differentiation of Human Embryonic Stem Cells to Cardiomyocytes: Role of Coculture With Visceral Endoderm-Like Cells." *Circulation* 107(>21):2733–40.

Muraoka, N. and M. Ieda. 2014. "Direct Reprogramming of Fibroblasts into Myocytes to Reverse Fibrosis." *Annual Review of Physiology*.

Murray, K. D., S. Hughes, D. Bearnson, and D. B. Olsen. 1983. "Infection in Total Artificial Heart Recipients." *Trans Am Soc Artif Intern Organs* 29:539–45.

Murry, C. E. et al. 2004. "Haematopoietic Stem Cells Do Not Transdifferentiate into Cardiac Myocytes in Myocardial Infarcts." *Nature* 428(6983):664–68.

Murry, C. E., R. W. Wiseman, S. M. Schwartz, and S. D. Hauschka. 1996. "Skeletal Myoblast Transplantation for Repair of Myocardial Necrosis." *Journal of Clinical Investigation* 98(11):2512–23.

Nakamura, M., M. Mie, H. Mihara, M. Nakamura, and E. Kobatake. 2008. "Construction of Multi-Functional Extracellular Matrix Proteins That Promote Tube Formation of Endothelial Cells." *Biomaterials* 29(20):2977–86.

Narmoneva, D. A. et al. 2005. "Self-Assembling Short Oligopeptides and the Promotion of Angiogenesis." *Biomaterials* 26(23):4837–46.

Naso, F. et al. 2010. "Differential Distribution of Structural Components and Hydration in Aortic and Pulmonary Heart Valve Conduits: Impact of Detergent-Based Cell Removal." *Acta Biomaterialia* 6(12):4675–88.

Naso, F. et al. 2017. "Alpha-Gal Inactivated Heart Valve Bioprostheses Exhibit an Anti-Calcification Propensity Similar to Knockout Tissues." *Tissue Engineering Part A* ten.tea.2016.0474.

Naso, F. and A. Gandaglia. 2017. "Different Approaches to Heart Valve Decellularization: A Comprehensive Overview of the Past 30 Years." *Xenotransplantation* (January):e12354.

Naso, F., A. Gandaglia, L. Iop, M. Spina, and G. Gerosa. 2011. "First Quantitative Assay of Alpha-Gal in Soft Tissues: Presence and Distribution of the Epitope before and after Cell Removal from Xenogeneic Heart Valves." *Acta Biomater* 7(4):1728–34.

National Museum of American History. 2018. "Dodrill GMR Heart." Retrieved July 29, 2018 (http://americanhistory.si.edu/collections/search/object/nmah_998420).

Netter, Frank. 2014. *Atlas of Human Anatomy.* 6th ed. Elsevier.

Nichols, W. K., D. Gospodarowicz, T. R. Kessler, and D. B. Olsen. 1981. "Increased Adherence of Vascular Endothelial Cells to Biomer Precoated with Extracellular Matrix." *Trans Am Soc Artif Intern Organs* 27:208–12.

Nilsson, B., K. N. Ekdahl, T. E. Mollnes, and J. D. Lambris. 2007. "The Role of Complement in Biomaterial-Induced Inflammation." *Molecular Immunology* 44(1–3):82–94.

Noiseux, N. et al. 2006. "Mesenchymal Stem Cells Overexpressing Akt Dramatically Repair Infarcted Myocardium and Improve Cardiac Function despite Infrequent Cellular Fusion or Differentiation." *Molecular Therapy* 14(6):840–50.

Norton, Gavin Robert et al. 1997. "Myocardial Stiffness Is Attributed to Alterations in Cross-Linked Collagen Rather than Total Collagen or Phenotypes in Spontaneously Hypertensive Rats." *Circulation* 96(6):1991–98.

Nosé, Y., K. Tajima, et al. 1971. "Artificial Heart Constructed with Biological Material." *Trans Am Soc Artif Intern Organs* 17:482–89.

Nosé, Y., Y. Imai, et al. 1971. "Cardiac Prosthesis Utilizing Biological Material." *J Thorac Cardiovasc Surg* 62(5):714–24.

Nosé, Y. 2007. "FDA Approval of Totally Implantable Permanent Total Artificial Heart for Humanitarian Use." *Artif Organs* 31(1):1–3.

Nosé, Y., H. Harasaki, and J. Murray. 1981. "Mineralization of Artificial Surfaces That Contact Blood." *Trans Am Soc Artif Intern Organs* 27:714–19.

Nosé, Y., P. Phillips, and W. J. Kolff. 1968. "Problems with Materials Used in

the Intrathoracic Artificial Heart." *Ann N Y Acad Sci* 146(1):271–88.

Noviani, M. et al. 2016. "Point-of-Care Rapid-Seeding Ventricular Assist Device with Blood-Derived Endothelial Cells to Create a Living Antithrombotic Coating." *ASAIO J* 62(4):447–53.

Nussbaum, J. et al. 2007. "Transplantation of Undifferentiated Murine Embryonic Stem Cells in the Heart: Teratoma Formation and Immune Response." *The FASEB Journal* 21(7):1345–57.

Nyilas, E. and R. S. Ward Jr. 1977. "Development of Blood-Compatible Elastomers. V. Surface Structure and Blood Compatibility of Avcothane Elastomers." *J Biomed Mater Res* 11(1):69–84.

O'Brien, F. J. 2011. "Biomaterials & Scaffolds for Tissue Engineering." *Materials Today* 14(3):88–95.

O'Reilly, M. S. et al. 1997. "Endostatin: An Endogenous Inhibitor of Angiogenesis and Tumor Growth." *Cell*.

Oberwallner, B. et al. 2014. "Preparation of Cardiac Extracellular Matrix Scaffolds by Decellularization of Human Myocardium." *Journal of Biomedical Materials Research - Part A* 102(9):3263–72.

Okamoto, O. and S. Fujiwara. 2006. "Dermatopontin, a Novel Player in the Biology of the Extracellular Matrix." *Connective Tissue Research* 47(4):177–89.

Oliver, James J., David J. Webb, and David E. Newby. 2005. "Stimulated Tissue Plasminogen Activator Release as a Marker of Endothelial Function in Humans." *Arteriosclerosis, Thrombosis, and Vascular Biology*.

Olsen, D. B. et al. 1975. "Thrombus Generation within the Artificial Heart." *J Thorac Cardiovasc Surg* 70(2):248–55.

Olsen, D. B. et al. 1977. "Implantation of the Total Artificial Heart by Lateral Thoracotomy." *Artif Organs* 1(2):92–98.

Olsson, A., F. Bredin, and A. Franco-Cereceda. 2005. "Echocardiographic Findings Using Tissue Velocity Imaging Following Passive Containment Surgery with the Acorn CorCap^{TM} Cardiac Support Device." *European Journal of Cardio-Thoracic Surgery*.

Ong, A. T. L., J. Aoki, M. J. Kutryk, and P. W. Serruys. 2005. "How to Accelerate the Endothelialization of Stents." *Archives Des Maladies Du Coeur et Des Vaisseaux* 98(2):123–26.

Orlic, D. et al. 2001. "Bone Marrow Cells Regenerate Infarcted Myocardium." *Nature* 410(6829):701–5.

Oswald, J. et al. 2004. "Mesenchymal Stem Cells Can Be Differentiated Into Endothelial Cells In Vitro." *Stem Cells* 22(3):377–84.

Ott, H. C. et al. 2008. "Perfusion-Decellularized Matrix: Using Nature's Platform to Engineer a Bioartificial Heart." *Nat Med* 14(2):213–21.

Ouzounian, Maral, Douglas S. Lee, and Peter P. Liu. 2008. "Diastolic Heart Failure: Mechanisms and Controversies." *Nature Clinical Practice Cardiovascular Medicine* 5(7):375–86.

Owen, D. R. and R. M. Zone. 1981. "Analysis of a Possible Mechanism of Surface Calcification on a Biomedical Elastomer." *Trans Am Soc Artif Intern Organs* 27:528–31.

Pangburn, M. K., D. C. Morrison, R. D. Schreiber, and H. J. Müller-Eberhard. 1980. "Activation of the Alternative Complement Pathway: Recognition of Surface Structures on Activators by Bound C3b." *The Journal of Immunology* 124(2):977–82.

Pangburn, M. K. and H. J. Müller-Eberhard. 1980. "Relation of Putative Thioester Bond in C3 to Activation of the Alternative Pathway and the Binding of C3b to Biological Targets of Complement." *The Journal of Experimental Medicine* 152(4):1102–14.

Pankov, R. 2002. "Fibronectin at a Glance." *Journal of Cell Science* 115(20):3861–63.

Pappas, J. J. and P. C. Yang. 2008. "Human ESC vs. IPSC-Pros and Cons." *Journal of Cardiovascular Translational Research* 1(2):96–99.

Parnis, S. et al. 1994. "Chronic in Vivo Evaluation of an Electrohydraulic Total Artificial Heart." *ASAIO J* (39):M386–91.

Pasumarthi, K. B. S. and L. J. Field. 2002. "Cardiomyocyte Cell Cycle Regulation." *Circulation Research* 90(10):1044–54.

Paul, R. G. and A. J. Bailey. 2003. "Chemical Stabilisation of Collagen as a Biomimetic." *TheScientificWorldJournal* 3:138–55.

Pawlowski, Kristin J., Stanley E. Rittgers, Steven P. Schmidt, and Gary L. Bowlin. 2004. "Endothelial Cell Seeding of Polymeric Vascular Grafts." *Frontiers in Bioscience : A Journal and Virtual Library* 9(1):1412–21.

Pena, A. M., T. Boulesteix, T. Dartigalongue, and M. C. Schanne-Klein. 2005. "Chiroptical Effects in the Second Harmonic Signal of Collagens I and IV." *J Am Chem Soc* 127(29):10314–22.

Perin, E. C. et al. 2003. "Transendocardial, Autologous Bone Marrow Cell Transplantation for Severe, Chronic Ischemic Heart Failure." *Circulation*.

Phillips, D. R., I. F. Charo, L. V Parise, and L. A. Fitzgerald. 1988. "The Platelet Membrane Glycoprotein IIb-IIIa Complex." *Blood* 71(4):831–43.

Picha, G. et al. 1976. "The Characterization of Intima Development in Left Ventricular Assist Device (LVAD) and Total Artificial Heart (TAH)." *Trans Am Soc Artif Intern Organs* 22:554–69.

Piepoli, M. 1999. "Diagnostic and Prognostic Indicators in Chronic Heart Failure." *Eur Heart J* 20(19):1367–69.

Pierce, W. S., J. H. Donachy, G. Rosenberg, and R. E. Baier. 1980. "Calcification inside Artificial Hearts: Inhibition by Warfarin-Sodium." *Science* 208(4444):601–3.

Pierschbacher, M. D. and E. Ruoslahti. 1984. "Cell Attachment Activity of Fibronectin Can Be Duplicated by Small Synthetic Fragments of the Molecule." *Nature* 309(5963):30–33.

Pinheiro, A., A. Cooley, J. Liao, R. Prabhu, and S. Elder. 2016. "Comparison of Natural Crosslinking Agents for the Stabilization of Xenogenic Articular Cartilage." *Journal of Orthopaedic Research* 34(6):1037–46.

Pislaru, Sorin V. et al. 2006. "Magnetic Forces Enable Rapid Endothelialization of Synthetic Vascular Grafts." *Circulation* 114(SUPPL. 1):I-314-I-318.

Poirer, N. C., L. C. Pelletier, M. Pellerin, and M. Carrier. 1998. "15-Year Experience with the Carpentier-Edwards Pericardial Bioprosthesis." *Ann Thorac Surg* 66(6 Suppl):S57-61.

Pouly, J. et al. 2008. "Cardiac Stem Cells in the Real World." *Journal of Thoracic and Cardiovascular Surgery* 135(3):673–78.

Pouzet, B. et al. 2000. "Intramyocardial Transplantation of Autologous Myoblasts: Can Tissue Processing Be Optimized?" *Circulation* 102(19 Suppl 3):III210-5.

Pretsch, T., I. Jakob, and W. Müller. 2009. "Hydrolytic Degradation and Functional Stability of a Segmented Shape Memory Poly(Ester Urethane)." *Polymer Degradation and Stability* 94(1):61–73.

Pries, A. R., T. W. Secomb, and P. Gaehtgens. 2000. "The Endothelial Surface Layer." *Pflugers Archiv European Journal of Physiology* 440(5):653–66.

Pytela, R., M. Pierschbacher, M. Ginsberg, E. Plow, and E. Ruoslahti. 1986. "Platelet Membrane Glycoprotein IIb/IIIa: Member of a Family of Arg-Gly-Asp--Specific Adhesion Receptors." *Science* 231(4745):1559–62.

Qian, H. et al. 2007. "Intracoronary Delivery of Autologous Bone Marrow Mononuclear Cells Radiolabeled by 18F-Fluoro-Deoxy-Glucose: Tissue Distribution and Impact on Post-Infarct Swine Hearts." *Journal of Cellular Biochemistry* 102(1):64–74.

Qian, L. et al. 2012. "In Vivo Reprogramming of Murine Cardiac Fibroblasts into Induced Cardiomyocytes." *Nature*.

Ramalanjaona, Georges, Richard F. Kempczinski, John E. Rosenman, E. Charles Douville, and Edward B. Silberstein. 1986. "The Effect of Fibronectin Coating on Endothial Cell Kinetics in Polytetrafluoroethylene Grafts." *Journal of Vascular Surgery* 3(2):264–72.

Ramzy, Danny et al. 2005. "Cardiac Allograft Vasculopathy: A Review." *Canadian Journal of Surgery. Journal Canadien de Chirurgie* 48(4):319–27.

Ratner, B. D. 1993. "The Blood Compatibility Catastrophe." *J Biomed Mater Res* 27(3):283–87.

Ratner, B. D. 2000. "Blood Compatibility--a Perspective." *J Biomater Sci Polym Ed* 11(11):1107–19.

Ratner, B. D. 2007. "The Catastrophe Revisited: Blood Compatibility in the 21st Century." *Biomaterials* 28(34):5144–47.

Ratner, B. D., A. S. Hoffman, F. J. Schoen, and J. E. Lemons. 2004. *Biomaterials Science: An Introduction to Materials in Medicine*. 2nd ed. Elsevier Academic Press.

Reed, A. M., J. Potter, and M. Szycher. 1994. "A Solution Grade Biostable Polyurethane Elastomer: ChronoFlex® AR." *Journal of Biomaterials Applications* 8(3):210–36.

Reinecke, H., G. H. MacDonald, S. D. Hauschka, and C. E. Murry. 2000. "Electromechanical Coupling between Skeletal and Cardiac Muscle: Implications for Infarct Repair." *Journal of Cell Biology* 149(3):731–40.

Reinecke, H., M. Zhang, T. Bartosek, and C. E. Murry. 1999. "Survival, Integration, and Differentiation of Cardiomyocyte Grafts: A Study in Normal and Injured Rat Hearts." *Circulation* 100(2):193–202.

Ren, Xiangkui et al. 2015. "Surface Modification and Endothelialization of Biomaterials as Potential Scaffolds for Vascular Tissue Engineering Applications." *Chemical Society Reviews* 44(15):5680–5742.

Rezakhaniha, R. et al. 2012. "Experimental Investigation of Collagen Waviness and Orientation in the Arterial Adventitia Using Confocal Laser Scanning Microscopy." *Biomech Model Mechanobiol* 11(3–4):461–73.

Rhodes, John M. and Michael Simons. 2007. "The Extracellular Matrix and Blood Vessel Formation: Not Just a Scaffold." *Journal of Cellular and Molecular Medicine* 11(2):176–205.

Richard Christ, F. et al. 1992. "A Comparative Evaluation of the Biostability of a Poly (Ether Urethane) in the Intraocular, Intramuscular, and Subcutaneous Environments." *Journal of Biomedical Materials Research* 26(5):607–29.

Richards-Kortum, R. and E. Sevick-Muraca. 1996. "Quantitative Optical Spectroscopy for Tissue Diagnosis." *Annu Rev Phys Chem* 47:555–606.

Rodriguez, E. Rene and Carmela D. Tan. 2017. "Structure and Anatomy of the Human Pericardium." *Progress in Cardiovascular Diseases* 59(4):327–40.

Rosenberg, Robert D. 1989. "Biochemistry of Heparin Antithrombin Interactions, and the Physiologic Role of This Natural Anticoagulant Mechanism." *The American Journal of Medicine* 87(3 SUPPL. 2):S2–9.

Ross, Michael H. and Wojciech Pawlina. 2010. *Histology: A Text and Atlas, with Correlated Cell and Molecular Biology.* 6th ed. Wolters Kluwer/Lippincott Williams & Wilkins Health.

Ruoslahti, E. 1996. "RGD and Other Recognition Sequences for Integrins." *Annual Review of Cell and Developmental Biology* 12(1):697–715.

Ruoslahti, E. and M. D. Pierschbacher. 1987. "New Perspectives in Cell Adhesion: RGD and Integrins." *Science* 238(4826):491–97.

Ruvinov, E., T. Dvir, J. Leor, and S. Cohen. 2008. "Myocardial Repair: From Salvage to Tissue Reconstruction." *Expert Review of Cardiovascular Therapy* 6(5):669–87.

Ryu, G., D. Han, Y. Kim, and B. Min. 1992. "Albumin Immobilized Polyurethane and Its Blood Compatibility." *ASAIO Journal* 38(3):M644-8.

Sadler, T. W. 2012. *Langman's Medical Embryology.* 12th ed. Philadelphia : Wolters Kluwer Health/Lippincott Williams & Wilkins, c2012.

Sage, D. 2018. "OrientationJ." Retrieved (http://bigwww.epfl.ch/demo/orientation/).

Salgaller, M. L. and P. K. Bajpai. 1985. "Immunogenicity of Glutaraldehyde-Treated Bovine Pericardial Tissue Xenografts in Rabbits." *Journal of Biomedical Materials Research* 19(1):1–12.

Sanchez, P. L. et al. 2016. "Data from Acellular Human Heart Matrix." *Data Brief* 8:211–19.

Sánchez, P. L. et al. 2015. "Acellular Human Heart Matrix: A Critical Step toward Whole Heart Grafts." *Biomaterials* 61:279–89.

Santos, L. L., T. B. Cavalcanti, and F. A. Bandeira. 2012. "Vascular Effects of Bisphosphonates-a Systematic Review." *Clin Med Insights Endocrinol Diabetes* 5:47–54.

Sarin, Virender K., Stephen B. H. Kent, James P. Tam, and R. B. Merrifield. 1981. "Quantitative Monitoring of Solid-Phase Peptide Synthesis by the Ninhydrin Reaction." *Analytical Biochemistry* 117(1):147–57.

Sartiani, L. et al. 2007. "Developmental Changes in Cardiomyocytes

Differentiated from Human Embryonic Stem Cells: A Molecular and Electrophysiological Approach." *Stem Cells* 25(5):1136–44.

Sawa, Y. et al. 2015. "Safety and Efficacy of Autologous Skeletal Myoblast Sheets (TCD-51073) for the Treatment of Severe Chronic Heart Failure Due to Ischemic Heart Disease." *Circulation Journal* 79(5):991–99.

Schenk, S. et al. 2007. "Monocyte Chemotactic Protein-3 Is a Myocardial Mesenchymal Stem Cell Homing Factor." *STEM CELLS* 25(1):245–51.

Schindelin, Johannes et al. 2012. "Fiji: An Open-Source Platform for Biological-Image Analysis." *Nature Methods* 9(7):676–82.

Schneider, Aviva et al. 1992. "An Improved Method for Endothelial Cell Seeding on Polytetrafluoroethylene Small Caliber Vascular Grafts." *Journal of Vascular Surgery* 15(4):649–56.

Schoen, Frederick J. and Robert J. Levy. 2005. "Calcification of Tissue Heart Valve Substitutes: Progress toward Understanding and Prevention." *Annals of Thoracic Surgery*.

Schuurman, H. J., J. Cheng, and T. Lam. 2003. "Pathology of Xenograft Rejection: A Commentary." *Xenotransplantation* 10(4):293–99.

Schwartz, A. et al. 2002. "Quantitating Fluorescence Intensity from Fluorophore: The Definition of MESF Assignment." *Journal of Research of the National Institute of Standards and Technology* 107(1):83–91.

Scimia, M. C., A. M. Gumpert, and W. J. Koch. 2014. "Cardiovascular Gene Therapy for Myocardial Infarction." *Expert Opinion on Biological Therapy* 14(2):183–95.

Scorsin, M. et al. 1996. "Can Grafted Cardiomyocytes Colonize Peri-Infarct Myocardial Areas?" *Circulation* 94(9 SUPPL.):II337-II340.

Scorsin, M. et al. 1997. "Does Transplantation of Cardiomyocytes Improve Function of Infarcted Myocardium?" *Circulation* 96(9 Suppl):II-188-93.

Scorsin, M. et al. 2000. "Comparison of the Effects of Fetal Cardiomyocyte and Skeletal Myoblast Transplantation on Postinfarction Left Ventricular Function." *Journal of Thoracic and Cardiovascular Surgery* 119(6):1169–75.

Seeger, James M. and Nina Klingman. 1988. "Improved in Vivo Endothelialization of Prosthetic Grafts by Surface Modification with Fibronectin." *Journal of Vascular Surgery* 8(4):476–82.

Sekine, H. et al. 2013. "In Vitro Fabrication of Functional Three-Dimensional Tissues with Perfusable Blood Vessels." *Nature Communications* 4(1):1399.

Sethi, Rishi and Chi Hang Lee. 2012. "Endothelial Progenitor Cell Capture Stent: Safety and Effectiveness." *Journal of Interventional Cardiology* 25(5):493–500.

Sevastianov, V. I. 2002. "Biocompatible Materials: Current Status and Future Perspectives." *Trends in Biomaterials & Artificial Organs* 15(2):20–30.

Sevastianov, V. I., I. V Drushlyak, R. C. Eberhart, and S. W. Kim. 1996. "Blood Compatible Biomaterials: Hydrophilicity vs. Hydrophobicity." *Macromolecular Symposia* 103(1):1–4.

Sewell, W. H. and W. W. L. Glenn. 1950. "Experimental Cardiac Surgery. I. Observation on the Action of a Pump Designed to Shunt the Venous Blood Past the Right Heart Directly into the Pulmonary Artery." *Surgery* 28(3):474–94.

Sharma, Kavita and David A. Kass. 2014. "Heart Failure with Preserved Ejection Fraction: Mechanisms, Clinical Features, and Therapies." *Circulation Research* 115(1):79–96.

Shi, C., Q. Li, W. Zhang, Y. Feng, and X. Ren. 2015. "REDV Peptide Conjugated Nanoparticles/PZNF580 Complexes for Actively Targeting Human Vascular Endothelial Cells." *ACS Applied Materials and Interfaces* 7(36):20389–99.

Shi, J., N. Dong, and Z. Sun. 2009. "Immobilization of Decellularized Valve Scaffolds with Arg-Gly-Asp- Containing Peptide to Promote Myofibroblast Adhesion." *Journal of Huazhong University of Science and Technology - Medical Science* 29(4):503–7.

Shields, K. J., D. Stolz, S. C. Watkins, and J. M. Ahearn. 2011. "Complement Proteins C3 and C4 Bind to Collagen and Elastin in the Vascular Wall: A Potential Role in Vascular Stiffness and Atherosclerosis." *Clinical and Translational Science* 4(3):146–52.

Shintani, S. et al. 2001. "Augmentation of Postnatal Neovascularization with Autologous Bone Marrow Transplantation." *Circulation* 103(6):897–903.

Shoulders, Matthew D. and Ronald T. Raines. 2009. "Collagen Structure and Stability." *Annual Review of Biochemistry* 78(1):929–58.

Sigma Aldrich. 2017. "Basic Steps in Solid Phase Peptide Synthesis Using Fmoc-Chemistry." Retrieved August 11, 2018 (https://www.sigmaaldrich.com/life-science/custom-oligos/custom-peptides/learning-center/solid-phase-synthesis.html).

Silva, Guilherme V. et al. 2005. "Mesenchymal Stem Cells Differentiate into an Endothelial Phenotype, Enhance Vascular Density, and Improve Heart Function in a Canine Chronic Ischemia Model." *Circulation* 111(2):150–56.

Siminiak, T. et al. 2005. "Percutaneous Trans-Coronary-Venous Transplantation of Autologous Skeletal Myoblasts in the Treatment of Post-Infarction Myocardial Contractility Impairment: The POZNAN Trial." *European Heart Journal* 26(12):1188–95.

Simionescu, D., R. V Iozzo, and N. A. Kefalides. 1989. "Bovine Pericardial Proteoglycan: Biochemical, Immunochemical and Ultrastructural Studies." *Matrix*.

Simionescu, N. (Nicolae) and Maya. Simionescu. 1988. *Endothelial Cell Biology in Health and Disease*. Plenum Press.

Singh, P. and J. E. Schwarzbauer. 2012. "Fibronectin and Stem Cell Differentiation - Lessons from Chondrogenesis." *Journal of Cell Science* 125(16):3703–12.

Sivaratnam, K. and J. M. Duggan. 2002. "Left Ventricular Assist Device Infections: Three Case Reports and a Review of the Literature." *ASAIO J* 48(1):2–7.

Slepian, M. J. et al. 2013. "The Syncardia^{TM} Total Artificial Heart: In Vivo, in Vitro, and Computational Modeling Studies." *Journal of Biomechanics* 46(2):266–75.

Smart, N. et al. 2007. "Thymosin B4 Induces Adult Epicardial Progenitor Mobilization and Neovascularization." *Nature* 445(7124):177–82.

Smith, J. W. and D. A. Cheresh. 1988. "The Arg-Gly-Asp Binding Domain of the Vitronectin Receptor." *J.Biol.Chem.* 263(35):18726–31.

Snyder, T. A. et al. 2007. "Preclinical Biocompatibility Assessment of the EVAHEART Ventricular Assist Device: Coating Comparison and Platelet Activation." *J Biomed Mater Res A* 81(1):85–92.

So, J. Y. et al. 2009. "Regeneration of Ischemic Heart Using Hyaluronic Acid-Based Injectable Hydrogel." *Journal of Biomedical Materials Research - Part B Applied Biomaterials*.

Souza, L. C. G. et al. 2002. "The Transplant of Cardiac Cells and Myoblast Skeletal Cells in Myocardial Infarction." *Revista Brasileira de Cirurgia Cardiovascular* 17(4):312–22.

Speer, Donald P., Milos Chvapil, C. D. Eskelson, and Judith Ulreich. 1980. "Biological Effects of Residual Glutaraldehyde in Glutaraldehyde-tanned Collagen Biomaterials." *Journal of Biomedical Materials Research* 14(6):753–64.

Spiliopoulos, K. et al. 2012. "Current Status of Mechanical Circulatory Support: A Systematic Review." *Cardiol Res Pract* 2012:574198.

Spina, M. et al. 2003. "Isolation of Intact Aortic Valve Scaffolds for Heart-Valve Bioprostheses: Extracellular Matrix Structure, Prevention from Calcification, and Cell Repopulation Features." *J Biomed Mater Res A* 67(4):1338–50.

Stachelek, S. J. et al. 2006. "Prevention of Oxidative Degradation of Polyurethane by Covalent Attachment of Di-Tert-Butylphenol Residues." *Journal of Biomedical Materials Research - Part A* 78(4):653–61.

Stankus, J. J., D. O. Freytes, S. F. Badylak, and W. R. Wagner. 2008. "Hybrid Nanofibrous Scaffolds from Electrospinning of a Synthetic Biodegradable Elastomer and Urinary Bladder Matrix." *Journal of Biomaterials Science, Polymer Edition* 19(5):635–52.

Stankus, J. J., J. Guan, and W. R. Wagner. 2004. "Fabrication of Biodegradable Elastomeric Scaffolds with Sub-Micron Morphologies." *Journal of Biomedical Materials Research - Part A* 70(4):603–14.

Starcher, Barry C. and Michael J. Galione. 1976. "Purification and Comparison of Elastins from Different Animal Species." *Analytical Biochemistry*.

Stawikowski, M. and G. B. Fields. 2002. "Introduction to Peptide Synthesis." *Current Protocols in Protein Science* Chapter 18:Unit 18.1.

Stephenson, Larry W., Agustin Arbulu, Joseph S. Bassett, Allen Silbergleit, and Calvin H. Hughes. 2002. "The Michigan Heart: The World's First Successful Open Heart Operation? Part I." *Journal of Cardiac Surgery* 17(3):238–46.

Stokes, K. B. 1988. "Polyether Polyurethanes: Biostable or Not?" *Journal of Biomaterials Applications* 3(2):228–59.

Stokes, K., P. Urbanski, and J. Upton. 1989. "The in Vivo Auto-Oxidation of Polyether Polyurethane By Metal Ions." *Journal of Biomaterials Science, Polymer Edition* 1(3):207–30.

Strauer, B. E. et al. 2002. "Repair of Infarcted Myocardium by Autologous Intracoronary Mononuclear Bone Marrow Cell Transplantation in Humans." *Circulation* 106(15):1913–18.

Strupler, M. et al. 2007. "Second Harmonic Imaging and Scoring of Collagen in Fibrotic Tissues." *Optics Express* 15(7):4054–65.

Swanson, Neil, Kai Hogrefe, Qamar Javed, and Anthony H. Gershlick. 2003. "In Vitro Evaluation of Vascular Endothelial Growth Factor (VEGF)-Eluting Stents." *International Journal of Cardiology* 92(2–3):247–51.

Swerlick, Robert A. and Thomas J. Lawley. 1993. "Role of Microvascular Endothelial Cells in Inflammation." *Journal of Investigative Dermatology* 100(1):S111–15.

Szycher, M. et al. 1980. "Integrally Textured Polymeric Surfaces for Permanently Implantable Cardiac Assist Devices." *Trans Am Soc Artif Intern Organs* 26:493–97.

Takahashi, K. et al. 2007. "Induction of Pluripotent Stem Cells from Adult Human Fibroblasts by Defined Factors." *Cell* 131(5):861–72.

Tallini, Y. N. et al. 2009. "C-Kit Expression Identifies Cardiovascular Precursors in the Neonatal Heart." *Proceedings of the National Academy of Sciences* 106(6):1808–13.

Tanai, Edit and Stefan Frantz. 2016. "Pathophysiology of Heart Failure." *Comprehensive Physiology* 6(1):187–214.

Tang, Dean G. and Claudio J. Conti. 2004. "Endothelial Cell Development, Vasculogenesis, Angiogenesis, and Tumor Neovascularization: An Update." *Seminars in Thrombosis and Hemostasis* 30(1):109–17.

Tang, X. L. et al. 2010. "Intracoronary Administration of Cardiac Progenitor Cells Alleviates Left Ventricular Dysfunction in Rats with a 30-Day-Old Infarction." *Circulation* 121(2):293–305.

Tanzi, M. C. et al. 1991. "Comparative Physical Tests on Segmented Polyurethanes for Cardiovascular Applications." *Clinical Materials* 8(1–2):57–64.

Tanzi, M. C., D. Mantovani, P. Petrini, R. Guidoin, and G. Laroche. 1997. "Chemical Stability of Polyether Urethanes versus Polycarbonate Urethanes." *Journal of Biomedical Materials Research* 36(4):550–59.

Tashiro, K. I. I. et al. 1991. "The RGD Containing Site of the Mouse Laminin A Chain Is Active for Cell Attachment, Spreading, Migration and Neurite Outgrowth." *Journal of Cellular Physiology* 146(3):451–59.

Taylor, D. A. et al. 1998. "Regenerating Functional Myocardium: Improved Performance after Skeletal Myoblast Transplantation." *Nature Medicine* 4(8):929–33.

The Eli Whitney Museum and Workshop. 2018. "Sewell's Pump." Retrieved (https://www.eliwhitney.org/7/gilbert/sewells-pump).

Thomson, J. A. 1998. "Embryonic Stem Cell Lines Derived from Human Blastocysts." *Science* 282(5391):1145–47.

Timms, Daniel. 2011. "A Review of Clinical Ventricular Assist Devices." *Med Eng Phys* 33(9):1041–47.

Toma, C., M. F. Pittenger, K. S. Cahill, B. J. Byrne, and P. D. Kessler. 2002. "Human Mesenchymal Stem Cells Differentiate to a Cardiomyocyte Phenotype in the Adult Murine Heart." *Circulation* 105(1):93–98.

Tomita, S. et al. 1999. "Autologous Transplantation of Bone Marrow Cells Improves Damaged Heart Function." *Circulation* 100(19 Suppl):II247-56.

Torregrossa, G. et al. 2014. "Results with SynCardia Total Artificial Heart beyond 1 Year." *ASAIO J* 60(6):626–34.

Turner, S. A. et al. 1982. "Calcification in Chronically-Implanted Blood Pumps: Experimental Results and Review of the Literature." *Tex Heart Inst J* 9(2):195–205.

Udelson, James E. 2011. "Heart Failure with Preserved Ejection Fraction." *Circulation* 124(21):e540-3.

Umashankar, PR R. et al. 2012. "Glutaraldehyde Treatment Elicits Toxic Response Compared to Decellularization in Bovine Pericardium." *Toxicol Int* 19(1):51–58.

UNOS. 2018. "United Network for Organ Sharing." Retrieved (https://unos.org).

Varda-Bloom, N. et al. 2000. "Cytotoxic T Lymphocytes Are Activated Following Myocardial Infarction and Can Recognize and Kill Healthy Myocytes in Vitro." *Journal of Molecular and Cellular Cardiology* 32(12):2141–49.

Vasku, J. and P. Urbanek. 1995. "Electron Microscopic Study of Driving Diaphragms in Long-Term Survival with a Total Artificial Heart." *Artif Organs* 19(4):344–54.

Verhamme, P. and M. F. Hoylaerts. 2006. "The Pivotal Role of the Endothelium in Haemostasis and Thrombosis." *Acta Clinica Belgica* 61(5):213–19.

Vicinanza, C. et al. 2017. "Adult Cardiac Stem Cells Are Multipotent and Robustly Myogenic: C-Kit Expression Is Necessary but Not Sufficient for Their Identification." *Cell Death and Differentiation* 24(12):2101–16.

Virchow, Rudolf. 1856. "Gesammelte Abhandlungen Zur Wissenschaftlichen Medicin." in *Meidinger Sohn & Comp.*

Visconti, R. P. et al. 2010. "Towards Organ Printing: Engineering an Intra-Organ Branched Vascular Tree." *Expert Opinion on Biological Therapy* 10(3):409–20.

Vossler, John D. et al. 2015. "CD133 Antibody Conjugation to Decellularized Human Heart Valves Intended for Circulating Cell Capture." *Biomedical Materials* 10(5):055001.

van Wachem, P. B. et al. 1987. "The Influence of Protein Adsorption on

Interactions of Cultured Human Endothelial Cells with Polymers." *Journal of Biomedical Materials Research* 21(6):701–18.

van Wachem, P. B., J. W. S. Stronck, R. Koers-Zuideveld, F. Dijk, and C. R. H. Wildevuur. 1990. "Vacuum Cell Seeding: A New Method for the Fast Application of an Evenly Distributed Cell Layer on Porous Vascular Grafts." *Biomaterials* 11(8):602–6.

Wainwright, J. M. et al. 2010. "Preparation of Cardiac Extracellular Matrix from an Intact Porcine Heart." *Tissue Eng Part C Methods* 16(3):525–32.

Wakitani, S., T. Saito, and A. I. Caplan. 1995. "Myogenic Cells Derived from Rat Bone Marrow Mesenchymal Stem Cells Exposed to 5-azacytidine." *Muscle & Nerve* 18(12):1417–26.

Walluscheck, Knut P., Gustav Steinhoff, and Axel Haverich. 1996. "Endothelial Cell Seeding of Native Vascular Surfaces." *European Journal of Vascular and Endovascular Surgery* 11(3):290–303.

Walter, Dirk H. et al. 2004. "Local Gene Transfer of PhVEGF-2 Plasmid by Gene-Eluting Stents: An Alternative Strategy for Inhibition of Restenosis." *Circulation* 110(1):36–45.

Wang, H., Y. Feng, J. Yang, J. Guo, and W. Zhang. 2015. "Targeting REDV Peptide Functionalized Polycationic Gene Carrier for Enhancing the Transfection and Migration Capability of Human Endothelial Cells." *Journal of Materials Chemistry B* 3(16):3379–91.

Ward, J., J. Kelly, W. Wang, D. I. Zeugolis, and A. Pandit. 2010. "Amine Functionalization of Collagen Matrices with Multifunctional Polyethylene Glycol Systems." *Biomacromolecules* 11(11):3093–3101.

Warren, Richard and Harry L. McCombs. 1965. "Morphologic Studies on Plastic Arterial Prostheses in Humans." *Annals of Surgery* 161(1):73–82.

Wei, Y. et al. 2013. "Surface Engineering of Cardiovascular Stent with Endothelial Cell Selectivity for in Vivo Re-Endothelialisation." *Biomaterials* 34(11):2588–99.

Wei, Y., Y. Ji, L. L. Xiao, Q. K. Lin, and J. Ji. 2011. "Different Complex Surfaces of Polyethyleneglycol (PEG) and REDV Ligand to Enhance the Endothelial Cells Selectivity over Smooth Muscle Cells." *Colloids and Surfaces B: Biointerfaces* 84(2):369–78.

Wenstrup, R. J. et al. 2004. "Type V Collagen Controls the Initiation of Collagen Fibril Assembly." *Journal of Biological Chemistry* 279(51):53331–37.

Wesolowski, S. A. et al. 1964. "Factors Contributing to Long-Term Failures in Human Vascular Prosthetic Grafts." *The Journal of Cardiovascular Surgery* 5:544–67.

Weymann, A., S. Loganathan, H. Takahashi, C. Schies, B. Claus, K. Hirschberg, P. Soos, et al. 2011. "Development and Evaluation of a Perfusion Decellularization Porcine Heart Model--Generation of 3-Dimensional Myocardial Neoscaffolds." *Circ J* 75(4):852–60.

Weymann, A., S. Loganathan, H. Takahashi, C. Schies, B. Claus, K. Hirschberg, P. Soós, et al. 2011. "Development and Evaluation of a Perfusion Decellularization Porcine Heart Model." *Circulation Journal* 75(4):852–60.

Weymann, A., N. P. Patil, A. Sabashnikov, P. Jungebluth, S. Korkmaz, S. Li, G. Veres, P. Soos, R. Ishtok, N. Chaimow, I. Patzold, et al. 2014. "Bioartificial Heart: A Human-Sized Porcine Model--the Way Ahead." *PLoS One* 9(11):e111591.

Weymann, A., N. P. Patil, A. Sabashnikov, P. Jungebluth, S. Korkmaz, S. Li, G. Veres, P. Soos, R. Ishtok, N. Chaimow, I. Pätzold, et al. 2014. "Bioartificial Heart: A Human-Sized Porcine Model - The Way Ahead." *PLoS ONE* 9(11):e111591.

Whalen, R. L., J. L. Snow, H. Harasaki, and Y. Nosé. 1980. "Mechanical Strain and Calcification in Blood Pumps." *Trans Am Soc Artif Intern Organs* 26:487–92.

Wiebe, D., J. Megerman, G. J. L'Italien, and W. M. Abbott. 1988. "Glutaraldehyde Release from Vascular Prostheses of Biologic Origin." *Surgery* 104(1):26–33.

Williams, C., K. P. Quinn, I. Georgakoudi, and L. D. Black. 2014. "Young Developmental Age Cardiac Extracellular Matrix Promotes the Expansion of Neonatal Cardiomyocytes in Vitro." *Acta Biomaterialia* 10(1):194–204.

Williams, J. Koudy et al. 2015. "Characterization of CD133 Antibody-Directed Recellularized Heart Valves." *Journal of Cardiovascular Translational Research* 8(7):411–20.

Wolf., M. F., Anderson J. M., and J. P. Boutrand. 2012. "Biocompatibility and Performance of Medical Devices." Pp. 158–206 in, edited by J. P. Boutrand. Woodhead Publishing.

Wong, M. L., J. L. Wong, K. A. Athanasiou, and L. G. Griffiths. 2013. "Stepwise Solubilization-Based Antigen Removal for Xenogeneic Scaffold Generation in Tissue Engineering." *Acta Biomaterialia*.

World Health Organization. 2018. "WHO." Retrieved (http://www.who.int/).

Wu, M.D, K. K. and P. Thiagarajan, M.D. 1996. "Role of Endothelium in Thormbosis and Hemostasis." *Annual Review of Medicine* 47(1):315–31.

Xu, C., S. Police, N. Rao, and M. K. Carpenter. 2002. "Characterization and Enrichment of Cardiomyocytes Derived from Human Embryonic Stem Cells." *Circulation Research* 91(6):501–8.

Xue, T. et al. 2005. "Functional Integration of Electrically Active Cardiac Derivatives from Genetically Engineered Human Embryonic Stem Cells with Quiescent Recipient Ventricular Cardiomyocytes: Insights into the Development of Cell-Based Pacemakers." *Circulation* 111(1):11–20.

Yamamoto, Kazuhiro et al. 2002. "Myocardial Stiffness Is Determined by Ventricular Fibrosis, but Not by Compensatory or Excessive Hypertrophy in Hypertensive Heart." *Cardiovascular Research* 55(1):76–82.

Yamauchi, M. and M. Sricholpech. 2012. "Lysine Post-Translational Modifications of Collagen." *Essays In Biochemistry* 52:113–33.

Yamazaki, K. et al. 1998. "An Implantable Centrifugal Blood Pump with a Recirculating Purge System (Cool-Seal System)." *Artif Organs* 22(6):466–74.

Yamazaki, K. et al. 2002. "EVAHEART: An Implantable Centrifugal Blood Pump for Long-Term Circulatory Support." *Jpn J Thorac Cardiovasc Surg* 50(11):461–65.

Yanagisawa, H., M. K. Schluterman, and R. A. Brekken. 2009. "Fibulin-5, an Integrin-Binding Matricellular Protein: Its Function in Development and Disease." *Journal of Cell Communication and Signaling* 3(3–4):337–47.

Yang, J. et al. 2015. "Antimicrobial Surfaces Grafted Random Copolymers with REDV Peptide Beneficial for Endothelialization." *Journal of Materials*

Chemistry B 3(39):7682–97.

Yang, M., Z. Zhang, C. Hahn, G. Laroche, et al. 1999. "Totally Implantable Artificial Hearts and Left Ventricular Assist Devices: Selecting Impermeable Polycarbonate Urethane to Manufacture Ventricles." *J Biomed Mater Res* 48(1):13–23.

Yang, M., Z. Zhang, C. Hahn, M. W. King, and R. Guidoin. 1999. "Assessing the Resistance to Calcification of Polyurethane Membranes Used in the Manufacture of Ventricles for a Totally Implantable Artificial Heart." *J Biomed Mater Res* 48(5):648–59.

Yao, L. T. et al. 2005. "Paracrine Action Enhances the Effects of Autologous Mesenchymal Stem Cell Transplantation on Vascular Regeneration in Rat Model of Myocardial Infarction." *Annals of Thoracic Surgery* 80(1):229–37.

Yoo, K. J. et al. 2000. "Heart Cell Transplantation Improves Heart Function in Dilated Cardiomyopathic Hamsters." *Circulation* 102(Supplement 3):III-204-III-209.

Yoshida, Y. and S. Yamanaka. 2011. "IPS Cells: A Source of Cardiac Regeneration." *Journal of Molecular and Cellular Cardiology* 50(2):327–32.

Yu, J. et al. 2009. "The Effect of Injected RGD Modified Alginate on Angiogenesis and Left Ventricular Function in a Chronic Rat Infarct Model." *Biomaterials*.

Yu, L. S. et al. 1993. "A Compact and Noise Free Electrohydraulic Total Artificial Heart." *ASAIO J* 39(3):M386-91.

Yu, S. et al. 2016. "Preparation of an Arg-Glu-Asp-Val Peptide Density Gradient on Hyaluronic Acid-Coated Poly(μ-Caprolactone) Film and Its Influence on the Selective Adhesion and Directional Migration of Endothelial Cells." *ACS Applied Materials and Interfaces* 8(43):29280–88.

Yurchenco, P. D. 2011. "Basement Membranes: Cell Scaffoldings and Signaling Platforms." *Cold Spring Harbor Perspectives in Biology* 3(2):1–27.

Zaferes, A. 2002. "The Complement System and Diving." 15–17.

Zangi, L. et al. 2013. "Modified MRNA Directs the Fate of Heart Progenitor

Cells and Induces Vascular Regeneration after Myocardial Infarction." *Nature Biotechnology* 31(10):898–907.

Zapanta, C. M. et al. 2006. "Microtextured Materials for Circulatory Support Devices: Preliminary Studies." *ASAIO J* 52(1):17–23.

Zaruba, M. M., M. Soonpaa, S. Reuter, and L. J. Field. 2010. "Cardiomyogenic Potential of C-Kit+-Expressing Cells Derived from Neonatal and Adult Mouse Hearts." *Circulation* 121(18):1992–2000.

Zdrahala, R. J. and I. J. Zdrahala. 1999. "Biomedical Applications of Polyurethanes: A Review of Past Promises, Present Realities, and a Vibrant Future." *J Biomater Appl* 14(1):67–90.

Zhang, Hong et al. 2013. "Dual-Delivery of VEGF and PDGF by Double-Layered Electrospun Membranes for Blood Vessel Regeneration." *Biomaterials* 34(9):2202–12.

Zhang, J. et al. 2009. "Functional Cardiomyocytes Derived from Human Induced Pluripotent Stem Cells." *Circulation Research* 104(4):e30–41.

Zhang, M. et al. 2001. "Cardiomyocyte Grafting for Cardiac Repair: Graft Cell Death and Anti-Death Strategies." *Journal of Molecular and Cellular Cardiology* 33(5):907–21.

Zhou, J. et al. 2015. "Promoting Endothelialization on Decellularized Porcine Aortic Valve by Immobilizing Branched Polyethylene Glycolmodified with Cyclic-RGD Peptide: An in Vitro Study." *Biomedical Materials (Bristol)* 10(6):065014.

Zhou, J. et al. 2016. "Promotion of Adhesion and Proliferation of Endothelial Progenitor Cells on Decellularized Valves by Covalent Incorporation of RGD Peptide and VEGF." *Journal of Materials Science: Materials in Medicine* 27(9):142.

Zhu, W. Z., K. D. Hauch, C. Xu, and M. A. Laflamme. 2009. "Human Embryonic Stem Cells and Cardiac Repair." *Transplantation Reviews* 23(1):53–68.

Zile, Michael R. et al. 2011. "Plasma Biomarkers That Reflect Determinants of Matrix Composition Identify the Presence of Left Ventricular Hypertrophy and Diastolic Heart Failure." *Circulation: Heart Failure* 4(3):246–56.

Zimmermann, W. H. et al. 2000. "Three-Dimensional Engineered Heart Tissue from Neonatal Rat Cardiac Myocytes." *Biotechnology and Bioengineering*.

Zimmermann, W. H., I. Melnychenko, and T. Eschenhagen. 2004. "Engineered Heart Tissue for Regeneration of Diseased Hearts." *Biomaterials* 25(9):1639–47.

Zohlnhöfer, D. et al. 2008. "Stem Cell Mobilization by Granulocyte Colony-Stimulating Factor for Myocardial Recovery After Acute Myocardial Infarction. A Meta-Analysis." *Journal of the American College of Cardiology* 51(15):1429–37.

Zoumi, A., A. Yeh, and B. J. Tromberg. 2002. "Imaging Cells and Extracellular Matrix in Vivo by Using Second-Harmonic Generation and Two-Photon Excited Fluorescence." *Proceedings of the National Academy of Sciences of the United States of America*.

Zwi, L. et al. 2009. "Cardiomyocyte Differentiation of Human Induced Pluripotent Stem Cells." *Circulation* 120(15):1513–23.

Acknowledgements

The research presented in this doctoral thesis has been carried out at the Cardiovascular Regenerative Medicine Laboratory, Department of Cardiac Thoracic and Vascular Sciences and Public Health, Università degli Studi di Padova, and at the Chemical Bioengineering Laboratory, Department of Industrial Engineering, Università degli Studi di Padova.

First, I would like to sincerely thank my tutor Prof. Gino Gerosa and supervisor Prof. Laura Iop for their constant guidance, advice and motivation during my Ph.D. studies. It has been a real privilege working with you and being part of the Cardiovascular Regenerative Medicine Laboratory. This Ph.D. would not have been achievable without your incredible support and enthusiasm.

I would like to thank Prof. Gaetano Thiene for believing in me and sharing his passion and dedication to Medicine and Science. You have been a great inspiration and example.

A heartfelt thank goes to Prof. Andrea Bagno for his suggestions, constant support and continued encouragement. I will always be grateful to you for sharing scientific knowledge and most of all for your humanity and friendship. Thank you for your collaboration in the work described in Chapter 2.

To Prof. Monica Dettin for the collaboration described in Chapter 3, thank you for the amazing opportunity to work with you at the Chemical Bioengineering Laboratory. I am really grateful for the fruitful discussions, your kindness and support. I thank also Annj Zamuner and Luca Stona for the time spent in teaching me with patience and dedication.

I would like to thank Prof. Fabio Di Lisa and Roberta Menabò of Cardiac Biochemistry Laboratory (Department of Biomedical Sciences, Università degli Studi di Padova) for their precious collaboration to the work presented in Chapter 4. Moreover, I thank the Proteomics Laboratory of Prof. Giorgio Arrigoni (Department of Biomedical Sciences, Università degli Studi di Padova) for the proteomic evaluation.

I am grateful to Prof. Michele Modesti and Dr. Carlo Boaretti of Polymer Engineering Laboratory (Department of Industrial Engineering, Università degli Studi di Padova) for the FTIR assessment and logistic help with the polymer casting.

As regards the TPM analyses, I would like to deeply thank Prof. Filippo Romanato and Andrea Filippi for their fundamental collaboration. Thank you Andrea for your patience, help, and unique irony.

I also would like to thank Prof. Laura Astolfi, Dr. Edi Simoni and Filippo Valente for their precious help and support. It has been always a pleasure working in the Bioacoustics Laboratory.

Words are not enough to thank all my colleagues of the Cardiovascular Regenerative Medicine Laboratory for their help and support. In particular, I would like to thank Sabra Zouhair, Catia Fidalgo, Sugat Tuladhar, and Paola Aguiari: you have been an exceptional example of true friendship and you made these years truly irreplaceable and unforgettable. It has been a real honor working with you.

During my Ph.D. I had the occasion to participate in the supervision of some excellent master students: Giulio Bolzonello, Guido Ascione, Valentina Zinelli, and Tea Lena. Thank you for your commitment, hard work and friendship. You have taught me more than I could ever hope to teach you.

Last but foremost, I am grateful to my family, Federico and close friends for their unconditional support, love and infinite patience throughout these years. All this work would not have been possible without you.